

LASER SPECTROSCOPIC STUDIES OF ACTIN-MYOSIN
INTERACTION IN ACTIVATED FROG MUSCLE

Julian Charles Eastwood

A Thesis Submitted for the Degree of PhD
at the
University of St Andrews



1987

Full metadata for this item is available in
St Andrews Research Repository
at:
<http://research-repository.st-andrews.ac.uk/>

Please use this identifier to cite or link to this item:
<http://hdl.handle.net/10023/14769>

This item is protected by original copyright

ST. ANDREWS

PhD Thesis by EASTWOOD J.C.

We have given the above thesis the Document
Supply Centre identification number:

D 80656

In your notification to Aslib please show this
number, so that it can be included in their
published Index to Theses with Abstracts.

JIC.

J P CHILLAG
Theses Officer

ProQuest Number: 10166381

All rights reserved

INFORMATION TO ALL USERS

The quality of this reproduction is dependent upon the quality of the copy submitted.

In the unlikely event that the author did not send a complete manuscript and there are missing pages, these will be noted. Also, if material had to be removed, a note will indicate the deletion.



ProQuest 10166381

Published by ProQuest LLC (2017). Copyright of the Dissertation is held by the Author.

All rights reserved.

This work is protected against unauthorized copying under Title 17, United States Code
Microform Edition © ProQuest LLC.

ProQuest LLC.
789 East Eisenhower Parkway
P.O. Box 1346
Ann Arbor, MI 48106 – 1346

LASER SPECTROSCOPIC STUDIES OF ACTIN-MYOSIN INTERACTION
IN ACTIVATED FROG MUSCLE.

A Thesis

Submitted to the University of St. Andrews
for the degree of Doctor of Philosophy.

by

JULIAN CHARLES EASTWOOD

Department of Physiology
University of St. Andrews

March 1987.



TR 1A 604

ACKNOWLEDGEMENTS

I would like to express my sincere thanks to my supervisor, Dr.F.W.Flitney, for his help and encouragement throughout this work.

I would also like to express my heartfelt thanks to all my friends and colleagues for their fellowship, ideas and for putting up with me; and my gratitude to Mr. Jim Honeyman and Miss. Karen Johnston for their expert technical help.

This work has been supported by: the Science and Engineering Research Council, the Medical Research Council and the Wellcome Trust.

DECLARATION

I, Julian Charles Eastwood hereby certify that this thesis has been composed by myself, that it is a record of my own work, and that it has not been accepted in partial or complete fulfilment of any other degree or professional qualification.

Julian Charles Eastwood.

30th. March 1987.

I was admitted to the Faculty of Science of the University of St. Andrews under Ordinance General No. 12 on 1st October 1980 and as a candidate for the degree of Ph.D. on 1st. October 1982.

Julian Charles Eastwood

30th. March 1987. .

I hereby certify that the candidate has fulfilled the conditions of the Resolution and Regulations appropriate to the Degree of Ph.D.

Frederick Werner Flitney

30th. March 1987.

In submitting this thesis to the University of St. Andrews I understand that I am giving permission for it to be made available for use in accordance with the regulations of the University Library for the time being in force, subject to any copyright vested in this work not being affected thereby. I also understand that the title and abstract will be published, and that a copy of the work may be made and supplied to any bona fide library or research worker.

ABSTRACT

Frog sartorius muscles were illuminated with laser light ($\lambda = 457.9 - 632.8\text{nm}$), stimulated electrically and stretched at the plateau of an isometric tetanus. An electro-optic system was used to rapidly ($\sim 7\text{kHz}$) switch the electric vector of the incident beam through $\pi/2$ radians (between $\varphi = 0^\circ$ and 90° , relative to the muscle long axis) and 'simultaneous' recordings of transmitted light intensity (I_a) were made at orthogonal beam orientations during single contractions, using a sample-hold device. Stretch causes I_a to fall: this is represented either as a decrease of transparency or an increase of turbidity (τ). The amplitudes of the optical transients vary in direct proportion to the tension increment generated by stretch (which is related to the extent of actin-myosin filament overlap) and are highly anisotropic with respect to both λ and φ . At any given λ the amplitude for $\varphi = 0^\circ > \varphi = 90^\circ$. Both 0° and 90° signals vary inversely with λ : the wavelength exponent for the former is -2.39 and for the latter, -3.87 . An attempt is made to analyse the changes in conservative dichroism ($= \Delta\tau_{0^\circ} - \Delta\tau_{90^\circ}$) using a model in which the scattering elements are forced to undergo a change of angular orientation ($\Delta\gamma$). The size of the scattering particles is estimated to be $\sim 17\text{nm}$ (long axis) and to occupy ~ 0.038 of the fibre volume. It is postulated that the dichroic signal is due to a change in cross-bridge head ($= S-1\text{HMM}$) orientation. The linear dimension of the actin-myosin interactive surface is estimated (from $\Delta\gamma$) to be $\sim 4.8\text{nm}$. The results are interpreted in terms of a multi-step force generating cycle, based on the Huxley-Simmons model in which each head progresses through as many as 5 to 7 discrete positions during its working stroke, each separated from its neighbour by a potential difference energy of $\sim 0.46 \times 10^{-20}\text{J}$.

'But what good came of it at last?'

Quoth little Peterkin:-

After Blenheim.

R. Southey.

CONTENTS

Chapter I

Introduction	1.1
Structural and mechanical properties of skeletal muscle	1.2
Optical characteristics of muscle	1.40
Background to work in this thesis	1.48

Transparency changes during stretch of active muscle

Chapter II

I. Experimental design and results of a preliminary study.	2.1
Materials and methods	2.4
Results	2.12
Discussion	2.25

Chapter III

II. Effect of changing the plane of polarisation of the incident laser beam.	3.1
Materials and methods	3.4
Results	3.10
Discussion	3.12

Chapter IV

III Simultaneous recordings of responses at orthogonal beam polarisations	4.1
Materials and methods	4.4
Results	4.11
Discussion	4.14

Chapter V

IV. Wavelength dependence	5.1
Materials and methods	5.6
Results	5.8
Discussion	5.13

Chapter VI

Time resolved changes in muscle conservative dichroism during stretch: a probe of cross-bridge orientation?	6.1
Materials and methods	6.7
Results	6.10
Discussion	6.15

Chapter VII

Some molecular and energetic aspects of actin-myosin interaction in living muscles.	7.1
I. Muscle tension, filament sliding and cross-bridge tilt	7.4
II. Work absorbed by cross-bridges during stretch	7.6

Chapter VIII

Discussion and scope for further study	
Summary	8.2
Discussion	8.5
Scope for further study	8.9
References	9.1

List of figures.

Fig	After page	Fig	After page
1.1	1.2	1.2	1.4
1.3	1.8	1.4	1.8
1.5	1.12	1.6	1.15
1.7	1.16	1.8	1.21
1.9	1.22	1.10	1.22
1.11	1.23	1.12	1.24
1.13	1.25	1.14	1.26
1.15	1.27	1.16	1.28
1.17	1.28	1.18	1.30
1.19	1.32	1.20	1.33
1.21	1.40	1.22	1.44
1.23	1.45	1.24	1.46
1.25	1.48	1.26	1.48
1.27	1.49	1.28	1.49
2.1	2.5	2.2	2.8
2.3	2.13	2.4	2.14
2.5	2.16	2.6	2.17
2.7	2.18	2.8	2.19
2.9	2.22	2.10	2.23
2.11	2.25		
3.1	3.5	3.2	3.10
3.3	3.10	3.4	3.11

List of figures (cont.)

Fig	After page	Fig	After page
4.1	4.4	4.2	4.6
4.3	4.6	4.4	4.7
4.5	4.7	4.6	4.9
4.7	4.11	4.8	4.11
4.9	4.11		
5.1	5.2	5.2	5.6
5.3	5.6	5.4	5.9
5.5	5.9	5.6	5.9
5.7	5.10	5.8	5.10
5.9	5.10	5.10	5.12
5.11	5.13		
6.1	6.3	6.2	6.10
6.3	6.11	6.4	6.12
6.5	6.17		
7.1	7.5	7.2	7.6
7.3	7.7	7.4	7.12
7.5	7.12		

List of tables.

Table	After page
4.1	4.11
5.1	5.9
5.2	5.10
6.1	6.15
6.2	6.17
7.1	7.8
7.2	7.8

CHAPTER I

INTRODUCTION

INTRODUCTION

One of the most remarkable biological tissues is skeletal or striated muscle, which is responsible for voluntary movement. The structure and properties of this tissue, in particular its ability to change its length or produce force very rapidly, has aroused the curiosity of many researchers, who have used a large number of techniques in an attempt to understand its structure and internal function.

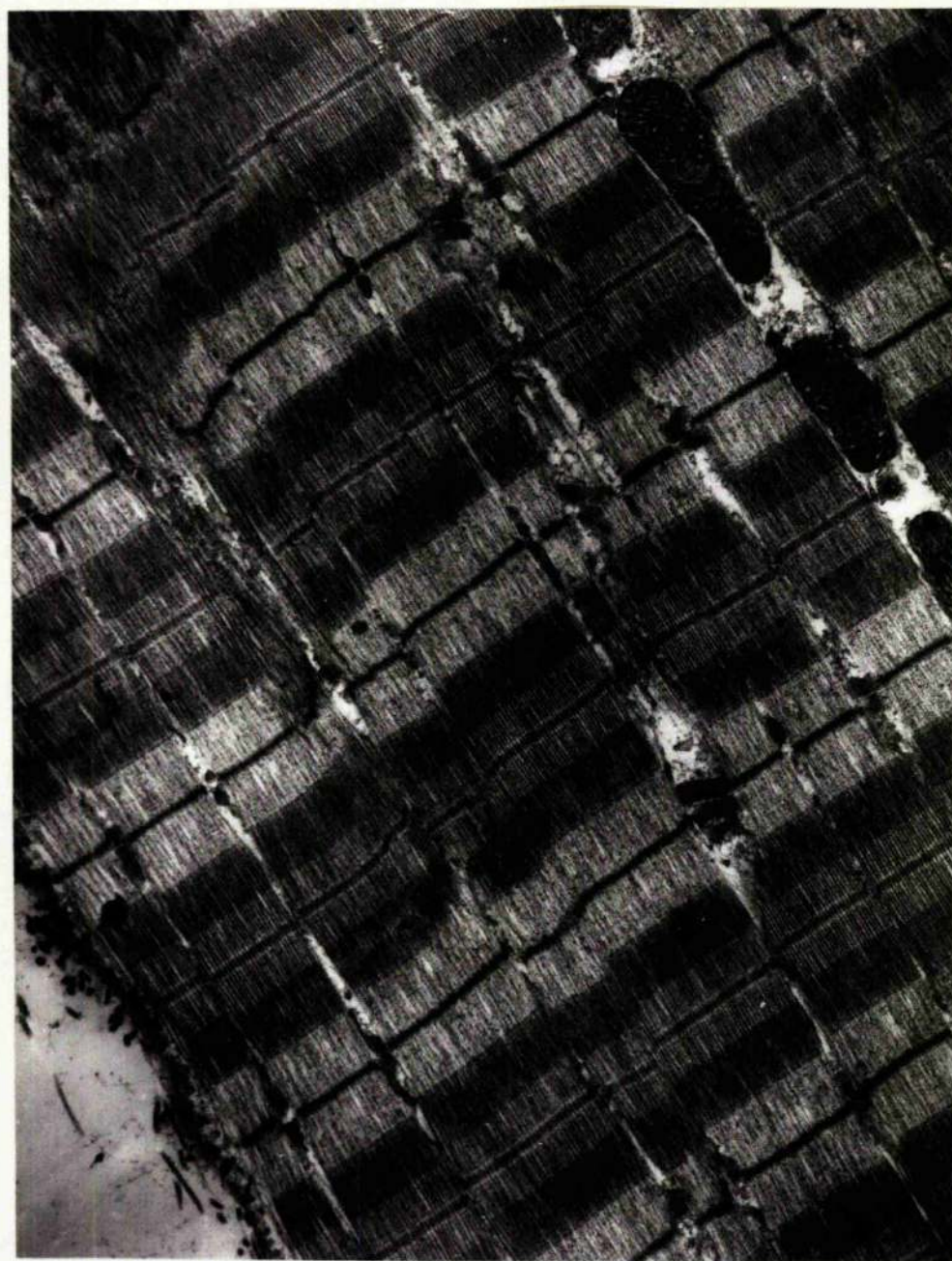
I. STRUCTURAL AND MECHANICAL PROPERTIES OF SKELETAL MUSCLE

Skeletal muscle fibres are cylindrical multinucleate cells, which vary from a few millimetres to several centimetres in length. They are formed by the end to end fusion of mononucleate cells called myoblasts, so that each muscle fibre comes to contain many nuclei which reside at the periphery of the cell. The membrane of the fibre is electrically excitable, and this with its basal lamina forms the sarcolemma. Each muscle fibre is innervated by a branch from a single motor neurone.

The interior of the cell or myoplasm is packed with columns of contractile material called myofibrils, which are surrounded by a system of membranous tubules called the sarcotubular system. The characteristic banding pattern of skeletal muscle is seen most clearly under the electron microscope. Fig 1.1 is a longitudinal section through a frog's skeletal muscle fibre. The myofibrils are made up of alternating light and dark staining bands. The narrow densely stained bands are the Z-discs, and the unit between two Z-

FIG. 1.1

Electron micrograph of Frog skeletal muscle (details in text.).



INTRODUCTION

discs is called the sarcomere. The central dark staining band is the A-band, and these alternate with lighter regions called I-bands. At high magnifications the A and I-bands are visible as long parallel threads known as myofilaments. These myofilaments are macromolecular assemblies of two proteins - actin and myosin - which are involved in the contraction process. The thicker myosin-containing filaments are confined to the A-band (Huxley, H.E., 1953b), where they form a regular hexagonal array. The thinner, actin containing filaments lie chiefly in the I-band, but they also penetrate the lateral regions of the A-band, creating a region of overlap. In this region each myosin filament is surrounded by six actin filaments, and each actin by three myosin filaments.

Early mechanical data suggested that skeletal muscle behaved as a cocked spring (Weber, 1846). This theory was complicated by evidence that muscle produced heat whilst contracting and this was dependent on force produced and the speed of shortening (Fenn, 1924; Hill, 1938). The idea that the contractile proteins were coils, which produced force by changing their pitch persisted (Hall Jakus, & Schmitt, 1946) for several years when doubts arose about these ideas.

In 1954 two papers were published together in 'Nature', one on observations of the striations of living fibres using interference microscopy (Huxley, A.F. & Neidergerke), and the other using phase contrast microscopy on isolated myofibrils in resting and active states (Huxley, H.E. & Hanson, 1954). These had shown that the length of the A-band region of the sarcomeres remains constant, and that changes in muscle

INTRODUCTION

length, produced either by contraction or by stretch, could all be accounted for by changes in the length of the I-band. These results coupled with earlier observations, using electron microscopy and X-ray diffraction of muscle in rigor which had shown the protein to be arranged in filaments (Huxley, H.E. 1953a+b), and selective extraction experiments which showed that myosin was confined to the A-band (Huxley, H.E. & Hanson 1954), led to the joint Nature 1954 papers proposing a new model for contraction. This model has become known as the "Sliding Filament Theory" and is now widely accepted.

The Sliding Filament Theory

The proteins are arranged in each sarcomere as two sets of interdigitating filaments, organized into hexagonal arrays. The myosin or thick filaments are located exclusively in the A-band whilst the actin or thin filaments are principally located in the I-band. Changes in the length of the muscle are brought about by a relative sliding of one set of filaments past the other, and the force is generated by a number of independent sites in the region where the two arrays overlap. Fig 1.2A taken from Aidely (1978) shows the manner in which the overlap of the two arrays changes with length.

If this theory is correct then muscle must possess two particular properties.

First, if a change in muscle length is caused by a relative sliding of the filament arrays, then the length of

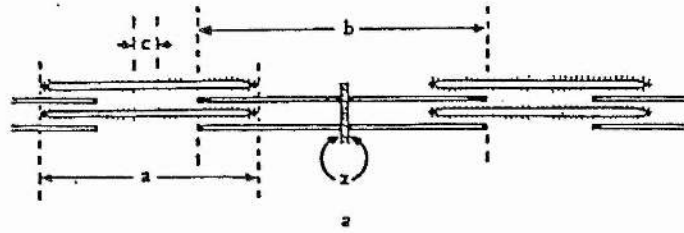
FIG. 1.2

A. The critical stages in the increase of filament overlap as sarcomere length increases.

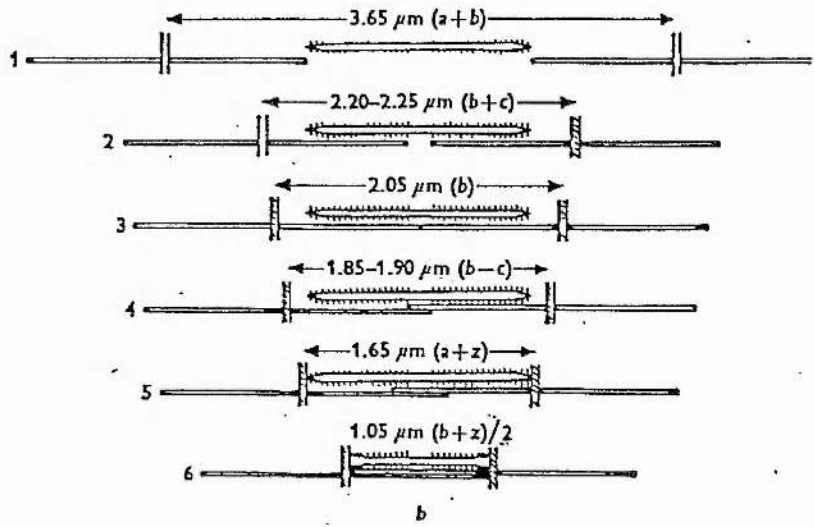
B. Length/Tension diagram from a single muscle fibre. The arrowed numbers correspond to the stages portrayed in fig. 1.2A.

(taken from Aidley, 1978)

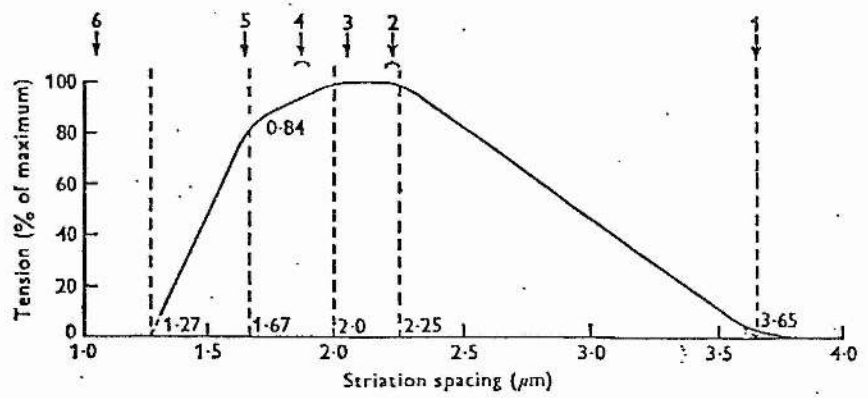
Fig 1.2



A



B



INTRODUCTION

the filaments should remain constant. Page (1964 & 1968) showed using electron microscopy on frog muscle, that the filaments in the A-band (myosin) are 1.6 μ m in length whilst the filaments in the I-band (actin) are 2.1 μ m long. Further, studies over a range of muscle lengths using low angle X-ray diffraction techniques show that on activation and at rest, the spacing of the subunits that make up the filaments remains constant (Huxley & Brown, 1967).

The second condition is that if force is produced by interaction of the two filament arrays at specific points in the region of overlap, then the amount of force per filament produced on activation should be proportional to the number of these sites, and hence on the degree of overlap. The inverse dependence of isometric force on muscle lengths greater than 2.45 μ m has been known for some time (Ramsay & Street, 1940) and then later more accurately when it was found that the inverse relationship started at 2.25 μ m (see fig 1.2B; Gordon, Huxley, & Julian 1966). The reason for this discrepancy between the two results can be simply explained. Ramsay and Street recorded the length of the muscle at rest, whereas Gordon et al. recorded the active sarcomere length, which removed the effects of internal shortening and transducer compliance.

As the techniques used in electron-microscopy improved, under certain conditions it was possible to see that physical linkages were formed between the thick and thin filaments in the region of overlap. This led A.F.Huxley (1957) to propose that force is generated by the formation of temporary linkages between the filaments. This is supported by

INTRODUCTION

biochemical evidence involving the interaction of the isolated contractile proteins in solution. Hasselbach(1952) showed that under physiological conditions the ATPase activity of myosin is very low, but that in the presence of actin it increases markedly. Later work showed that the ATPase activity was inhibited in the absence of calcium by troponin and tropomyosin which are regulatory proteins (Ebashi, 1963; Ebashi & Ebashi, 1966). It was later found that these regulatory proteins (Pepe, 1966; Ebashi, Endo, Nonomura, Masaki and Otsuki 1966) are associated with the thin filaments.

It would appear reasonable to assume that the region of the myosin molecule containing the ATPase activity is also the part that interacts with actin. Furthermore, as relatively large sliding movements of the filaments can occur, then it follows that each cross-bridge must be capable of performing repetitive cyclical movements. A further assumption is that each cycle is accompanied by the splitting of ATP which provides energy for the system.

Examination of negatively stained myosin preparations in the electron microscope, shows that the myosin filament is polarised, and that the orientation of the molecules in each half of the sarcomere is reversed (Huxley, H.E.; 1961, 1963). This arrangement means that relative sliding motion of the filaments is equal and opposite in each half of the sarcomere, and that the cross-bridges act in parallel.

X-ray diffraction studies have shown that the volume occupied by the filament lattice is constant at all physiological muscle lengths. It follows from this that the

INTRODUCTION

spacing of the filaments varies inversely with sarcomere length. Elliot(1964) found that the centre to centre spacing of the actin and myosin filaments in frog muscle varied between 19-26nm. The sum of the radii of the actin and myosin filaments is about 15nm.(Elliot, Lowy & Worthington, 1963), which means that the surface to surface separation can change from 4-11nm. over the physiological range of muscle lengths. This is an important observation, because the relationship between filament overlap and maximum isometric tension shows that a cross-bridge is equally effective at producing force regardless of the distance over which it must operate.

Structure and Characteristics of the Contractile Proteins

Kuhne(1864) prepared an extract from frog muscle which he called myosin. Kuhne's preparation was made by pulverizing frozen frogs muscle and then straining the homogenate, which he showed 'set' into a gel, but was soluble in strong sodium or potassium chloride solutions. Attempts were made to determine its molecular weight by observing its birefringence (von Muralt & Edsall, 1930). Later studies using extended extraction in high salt solutions, showed that this preparation had an ATPase activity (Engelhardt & Ljubimova, 1939). The addition of ATP caused a marked fall in both the birefringence and viscosity of the preparation (Needham J, Shen, Needham, & Lawrence; 1941), and these changes were reversed as the ATP became exhausted.

At about the same time as these experiments were made, it was becoming clear that the extract was not pure, and that there was not one but two proteins. Pure myosin could be

INTRODUCTION

extracted by using a concentrated salt solution for about twenty minutes, then from the residue a second protein, called actin, could be prepared (Banga & Szent-Gyorgyi, 1941-42; Straub 1942). Solutions of either protein were isotropic and of a low viscosity, but on mixing a highly viscous, birefringent solution resulted, which had the same properties as described by Needham et al. The conclusion made was that the proteins combine in solution, and that the changes that occur on the addition of ATP are caused by dissociation of the complex. The importance of this phenomenon was reinforced later, when it was shown that threads could be made by extruding actomyosin into a low ionic strength solution, and that these could be made to contract on the addition of ATP (Szentz-Gyorgyi, 1948).

Structure of Myosin Monomer

Myosin has three basic properties: first that under conditions of neutral pH the molecules aggregate to form bipolar filaments; secondly the protein binds to actin; and finally it exhibits ATPase activity.

Early electron microscope studies of isolated myosin suggested that the molecule was 150nm long, with a globular head of approx 5 by 20 nm.. Later studies using improved metal shadowing techniques, showed that the globular region at the end of the myosin rod comprises two apparently identical globular heads, connected to the rod by a flexible linkage (Slater & Lowey, 1967; Lowey, Slater, Weeds & Baker, 1969). Fig 1.3 shows the main features of the myosin molecule.

FIG. 1. 3

Schematic diagram of the myosin molecule. Binding sites for actin and ATP occur in the S_1 heads. (Aidley, 1978)

FIG. 1.4

Schematic illustration of the proteolytic cleavage of myosin (two globular heads with light chains on the end of a long rod) by trypsin and papain. (Squire, 1981)

Fig 1.3

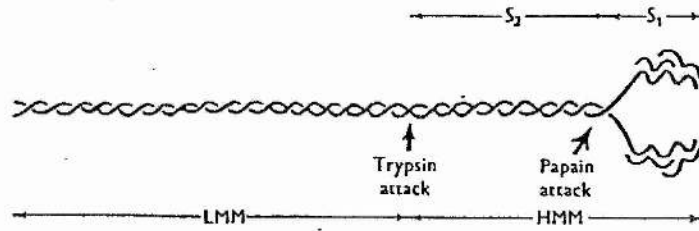
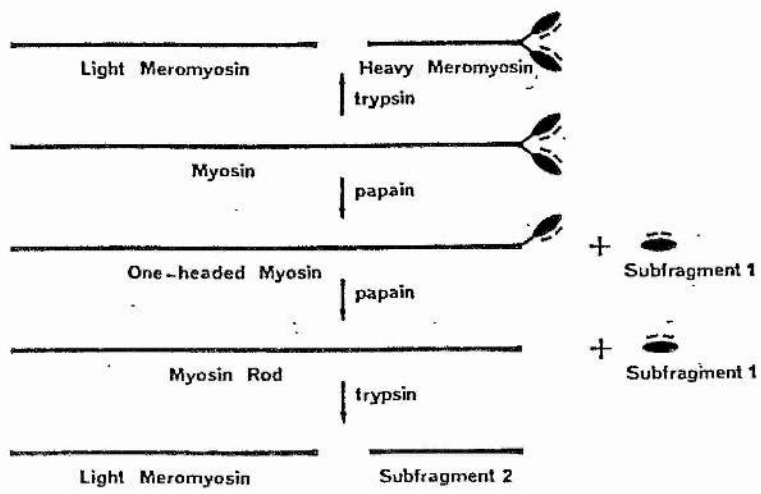


Fig 1.4



INTRODUCTION

The molecular weight of myosin molecule proved difficult to determine because of its tendency to aggregate, a range of molecular weights from 420-860k daltons being suggested. Work by Lowey (1971), which is now generally accepted, shows myosin to have a MW of 470kd and to be made up of two similar **heavy chains** (200k) which form an alpha helical coil for part of their length. Also, there are a number of **light chains** (20k) which are attached to the heavy chains that together make up the globular heads.

Myosin can be split by proteolytic enzymes into a number of well defined fragments (Szent-Gyorgyi, 1953b). Fig 1.4 shows the fragments produced by treatment with enzymes. Treatment with trypsin splits the molecule into two fragments: **light meromyosin (LMM)** and **heavy meromyosin (HMM)**. Only HMM behaves as an ATPase and binds to actin, and EM examination shows that HMM has the globular heads and a short tail (Slater & Lowey, 1967). LMM is the only fragment that has been shown to self aggregate (Lowey, Slater, Weeds, & Baker, 1969). By treatment with Papain, HMM can be split further to produce two fractions the S_1 and S_2 subunits. The S_2 subunit is a short length of the myosin rod, and S_1 the separated globular heads. Only the S_1 fraction behaves as an ATPase and binds to actin (Eisenberg & Moos, 1970). The S_2 fragment serves to link the S_1 's to LMM. A comparative study (Elliot, Offer & Burridge, 1976) shows that whilst myosins from different animals (vertebrate and invertebrate, embryonic and adult) have different chemical composition and properties, they all have similar molecular weights and size, which would indicate that it is their shape which is most important for the proper function of the molecule. This would

INTRODUCTION

suggest that two heads are needed for successful contraction, as there appears to be no evidence of naturally occurring single headed myosin, but a number of workers report that actomyosin, made by isolating actin and myosin, removing one head and then remixing will still produce force (Cooke & Franks, 1978).

The Flexibility of the Myosin Molecule

X-ray diffraction and electron microscope studies show that the myosin molecule is flexible. This is a requirement for many of the cross-bridge models discussed later, and also to cope with the change in inter-filamentary spacing with length. The flexibility of the myosin molecule has been inferred from EM studies (Slater & Lowey, 1967) and from electric birefringence studies (Kobayashi & Totsuka, 1975). An EM study which provided clear images of the shape of the head, also provided information on the position of the flexible links in the molecule (Elliot & Offer, 1978). Previously, it had been assumed that bending would occur at or around the sites in the molecule susceptible to enzyme action. Elliot and Offer found that the position of one head in relation to the other was not consistent, implying that the heads are flexibly attached to the rod. Another observation was that the rods of some molecules were bent back on themselves suggesting a 'second' flexible region, located at the LMM/HMM junction.

The lack of a consistent angular position between one head led Elliott and Offer (1978) to postulate that one myosin molecule could interact with two actin filaments, which was later found to be so in insect muscle (Freundlich & Squire,

1983).

Structure of Actin

The discovery of actin by Straub occurred shortly before it was shown that the raw myosin extract was actomyosin (Banga & Szent-Gyorgyi, 1941-42). Straub treated muscle first with acetone, then extracted the actin using solutions of low ionic strength. This soluble extract was G-actin with a number of impurities. By varying the extraction process two more proteins associated with the thin filaments, troponin and tropomyosin, can be extracted (Szent-Gyorgyi, 1951). At higher ionic strength, G-actin in the presence of ATP polymerises into F-actin filaments (Straub & Feuer, 1950; Asakura & Oosawa, 1960;). At low ionic strength actin exists as a single globular protein (hence G-actin) with a molecular weight of approx 42kd (Rees & Young, 1967).

As with myosin it is possible with negative staining to visualize the basic structure of the actin filament in the electron microscope (Hanson & Lowy, 1962 & 1963), where it can be seen that the thin filaments (F-actin) consist of two intertwined helical strands of G-actin. The pitch of the helix is $2 \times \sim 35\text{nm}$. and there are approximately 13 G-actin monomers per turn. The centre to centre spacing of the G-actin on each strand is about 5.5nm.

Actin has two important functions, first to activate the myosin ATPase; and second, to provide a site for the regulatory proteins to control the actin-myosin interaction.

INTRODUCTION

Structure of the Filaments

The Thick Filament.

H.E. Huxley's (Huxley, 1963) electron microscope study of isolated negatively stained myosin filaments showed that there were regular projections on the surface. Also that there was a zone between 0.15-0.2 μ m long in the centre of the filament where there were no projections, which he suggested corresponded to the M-zone of intact fibres.

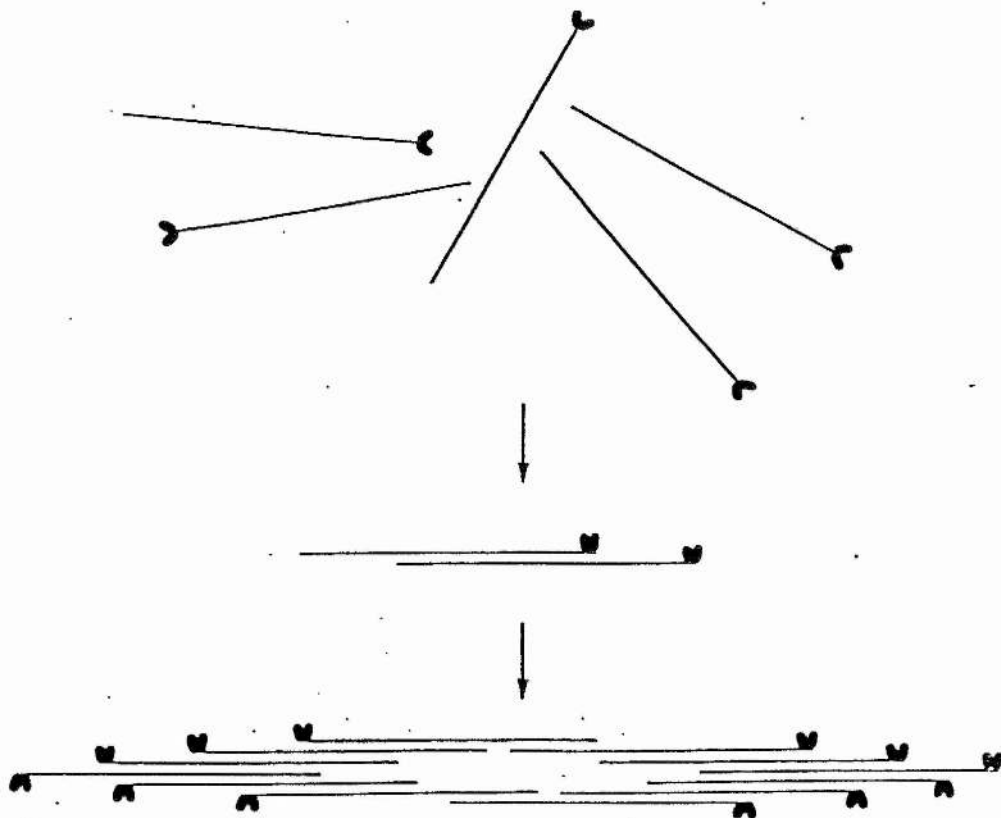
Huxley (1963) also found that under conditions of neutral pH myosin molecules aggregated into filaments. These were of varying lengths, but had the same general structure as isolated filaments. He suggested that the rods aggregate together to form the filament backbone with the heads projecting outwards (Fig 1.5). This arrangement also allows for the bare region in the middle and implies that the myosin molecules are reversed in the two halves of the filament.

In early X-ray diffraction experiments, using frog muscle in rigor (Huxley, H.E., 1953), it was possible to see reflections corresponding to a 42nm. axial repeat distance, and later 14.5 and 7.2nm. (Worthington, 1959). The latter reflections it was suggested were the third and sixth orders of a 43.5nm. repeat. These reflections did not correspond to those of actin and it was suggested that they arose from projections on the myosin filament (Worthington, 1959). Further work led to the suggestion that the projections emerge in pairs, from opposite sides of the filament, every 14.3nm, with an angle between pairs of 120 degrees,

FIG. 1.5

A schematic diagram to show how myosin molecules are arranged with opposite polarity in each half of the thick filament. The dimer is shown as a possible intermediate. (Companion of Biochemistry, 1974).

Fig 1.5



INTRODUCTION

generating a helical repeat of $3 \times 14.3\text{nm} = 42.9\text{nm}$ (Huxley & Brown, 1967). The width of the 14.3nm . meridional reflection was very small, suggesting a diffracting structure that was very large, and that the thick filaments are accurately arranged in a lateral register. In addition the off-meridional reflections of the myosin layer line are small, implying that there is a definite relationship in the rotational orientation of neighbouring filaments. This led Huxley and Brown (1967) to conclude that the filaments are arranged on a super lattice, in which each filament is surrounded by three filaments whose orientation is rotated through 120 degrees with respect to its own, and a further three orientated at 240 degrees. This further suggests that there must then be two populations of actin filaments, where half of them are opposite single myosin projections every 14.3nm and half opposite three projections every 42.9nm .

It was this rather strange arrangement that was contested by the suggestion that the myosin filament had three projections every 14.3nm ., instead of two (Squire, 1974). This can allow actin to receive a cross-bridge every 14.3nm (Squire, 1974). Other work concludes that there are four molecules every 14.3nm (Morimoto & Harrington, 1974). One possibility from this that would fit in with Huxley & Browns work is that two myosin molecules are involved with each cross-bridge, but it is difficult to see how this arrangement would work. The evidence for a three stranded model is good. Observations of transversely sectioned thick filaments display a clear three fold symmetry (Franzini-Armstrong & Porter, 1964), and disassembly of the filaments by Maw & Rowe (1980) shows that they can be disassembled into three sub-

INTRODUCTION

filaments. This does not necessarily show that the backbone is composed of three strands, it may just show that there are three cleavage lines. Cantino & Squire (1986) in a direct visualization of frog skeletal thick filaments, show that the myosin heads are arranged in progressively offset crowns of three, but no evidence of a discrete, three stranded backbone.

The Thin Filaments.

The main component of the thin filaments is F-actin, the polymerized form of G-actin. The basic structure of the native thin filament is shown in Fig 1.6. Early X-ray diffraction studies found that the monomers were arranged in a net like structure, or in the form of helices. Topologically a helix is the same as a cylinder, and the pitch of the helix was thought to be either 2×35 or $2 \times 40.6\text{nm}$. (13 or 15 G-actin monomers) (Selby & Bear, 1956). Later work showed that the helix was composed of two chains of F-actin monomers arranged in a double helix (Hanson & Lowy, 1963, 1964). Huxley & Brown (1967) found that the crossover was between 36-37nm. and that the number of monomers in each turn was not an integer. This was based on the following X-ray diffraction data. The main reflections in the actin X-ray diffraction pattern are a meridional one of 2.73nm. and two off meridional ones at 5.91 and 5.46nm. The meridional one represents the spacing between two successive actin monomers, whereas the off-meridional reflections indicate the pitches of the two left and right hand primitive helices. From this data the pitch of the non-primitive helix was estimated to be 72nm. with 13.54 monomers per turn.

INTRODUCTION

Each actin subunit is capable of interacting with one myosin head to form a stable complex, visible after negative staining in the electron microscope (Huxley, 1963). Actin filaments decorated with S_1 -HMM, appear as a string of arrow heads which all point in the same direction, which is reversed on either side of the Z-disc component.

The Position of the Regulatory Proteins in the Thin filament.

There are other reflections in the X-ray diffraction pattern that do not correspond to either actin or myosin. Worthington (1959) found a periodicity at 41nm., which it was later suggested (Huxley & Brown, 1967) was in fact two periodicities that were poorly resolved at 38.5 and 44.2nm. Periodicities corresponding to these distances are seen in EM of muscle, in both the A and I band. In the EM, the A band periodicity appears greater than that of the I band, and so the 44.2nm line was associated with the A-band proteins and the 38.5nm. to the I-band. Huxley & Brown (1967) suggested that the 38.5nm. repeat may be caused by troponin molecules decorating the tropomyosin molecule repeat along the thin filament. This was confirmed when glycerinated fibres were stained with an antibody to troponin and the 38.5nm repeat was greatly enhanced (Rome, Hirabayashi, & Perry, 1973). The ratio of actin to troponin to tropomyosin is 7:1:1, so if each tropomyosin molecule is attached to 7 actin monomers then the distance between molecules is 38.5nm. From this it has been suggested that the tropomyosin molecules lie end to end in the grooves of the actin helix and that each tropomyosin has a troponin molecule attached to it.

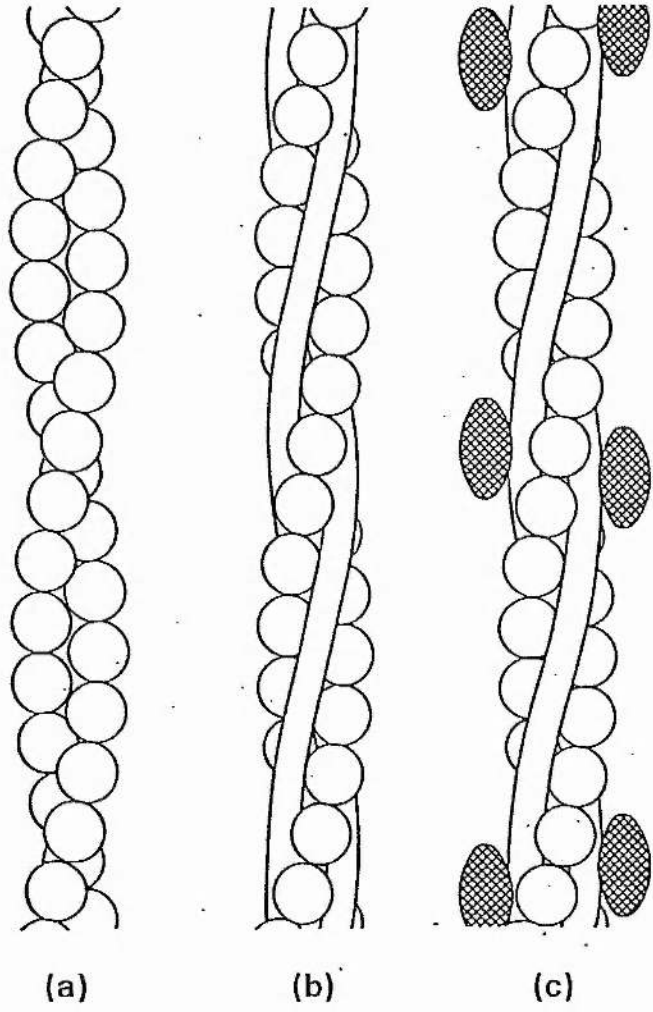
Ebashi and others (Ebashi, Endo, Ohtsuki, 1969)

FIG. 1.6

Diagram showing the components of the thin filament.

- (a) F-actin, showing the double helical arrangement of the subunits.
- (b) F-actin plus tropomyosin. The tropomyosin strands are drawn lying in the long pitch grooves of the actin helix.
- (c) F-actin plus tropomyosin plus troponin. The troponin is shown as hatched ellipsoids. (Companion of Biochemistry, 1974)

Fig 1.6



INTRODUCTION

established that the normally high actin-activated ATPase activity of semipurified actomyosin solution could be reduced to a low myosin ATPase level by lowering the calcium concentration from pCa_5 to pCa_7 and vice versa. Further, it was shown that when actin was removed, leaving only the regulatory proteins and myosin, the calcium dependency was lost. This suggested a reversible steric mechanism regulated by the calcium ion, and mediated by tropomyosin.

The steric mechanism by which tropomyosin regulates actomyosin ATPase, and so the actin cross-bridge interactions, has been put forward. By comparing the relative intensities of the thin filament X-ray diffraction lines, in relaxed and contracting vertebrate and molluscan muscle, they suggested that the myosin binding sites on the actin were modified, when the tropomyosin molecules moved deeper into the filament groove by a radial movement of 1.5nm. This model has been confirmed (Wakabayashi, Huxley, Amos, & Klug, 1975; Seymour & O'Brien, 1980), and a diagrammatic explanation is shown in Fig 1.7.

Direct Evidence for Interaction of Actin and Myosin in the Production of Force.

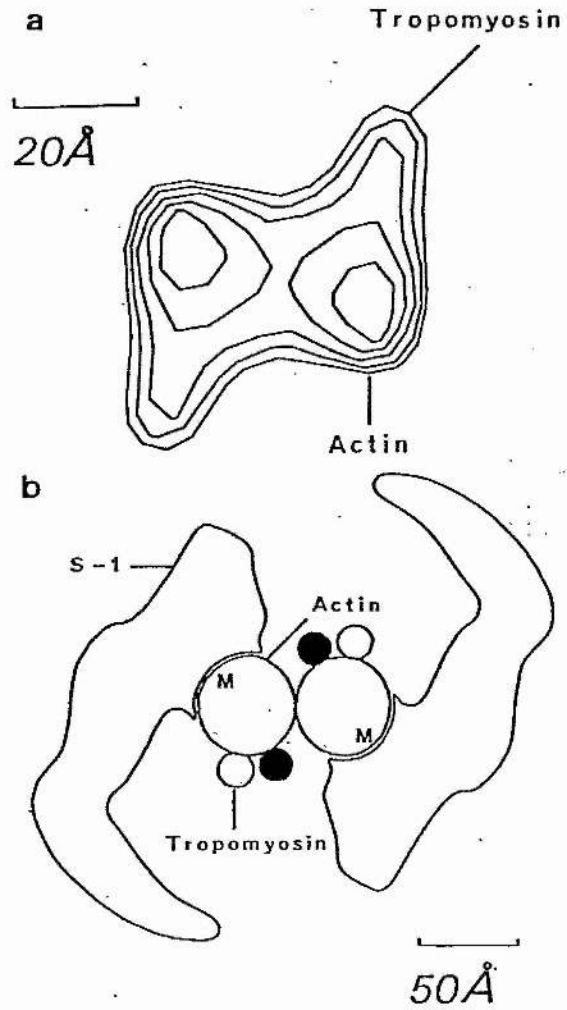
Huxley (1963) showed that when myosin is aggregated into filaments the LMM is buried in the filament backbone. This being the case, Trinick & Elliot (1979) produced evidence to suggest that almost the entire length of HMM is free to move about the surface of the filament. This also confirms what was thought to be the case from X-ray diffraction data on resting and active muscle.

FIG 1.7

- (a) A helical projection of the thin filament structure, corresponding to a view looking towards the Z-line.
- (b) A sketch of the view of the thin filament decorated with HMM-S₁. Note that the tropomyosin peaks in a are positioned top right and bottom left of the actin strands. In b the myosin (S₁) attachment sites (M) as drawn are at the top left and bottom right. The on, off positions of the tropomyosin are shown as closed and open circles respectively.

(Squire, 1981)

Fig 1.7



INTRODUCTION

It was noticed in glycerol extracted insect flight muscle, that there were differences between the X-ray diffraction patterns of the relaxed and rigor states (Reedy, Holmes & Tregear, 1965), and from this it was concluded that at rest the projections from the myosin filaments stick out at right angles, whereas in rigor they are attached to the actin filaments and move through an angle of 45 degrees, as if pulling the actin filaments to the centre of the sarcomere. Huxley & Brown (1967) also noted in living muscle that there was a change in the orientation of the cross-bridges between the resting and active states. They noticed that the off-meridional 42.9nm. reflection was only 30% of that in resting muscle and that there was a corresponding increase in 14.3nm. meridional reflection. This also implies that the repeating structures of the myosin filament become disarranged on activation. Further, as no new repeating structure appears, there is a movement of the cross-bridge heads towards the actin. This accords with the idea that the force is generated by independent sites which operate asynchronously. The asynchronous behaviour of the cross-bridges causes the biggest problem to unravelling their changes in orientation. The use of high intensity X-rays from synchrotron sources has resulted in an enormous reduction in the exposure time to produce a diffraction pattern; indeed it is now possible to record X-ray diffraction in 'real time'. This obviates the need for the complex arrangements of repetitive stimulation and an X-ray shutter (Elliot, Lowy, & Millman, 1965; Huxley, Brown, & Holmes, 1967). These improvements have also enabled changes in the myosin layer line on activation to be studied more fully.

INTRODUCTION

A study using synchrotron radiation on changes in the X-ray diffraction pattern on activation and relaxation (Huxley, Faruqi, Bordas, Koch, & Milch, 1980) using detectors with a 10ms. time resolution, confirmed earlier steady state studies (Elliott, Lowy, & Millman, 1967; Huxley, Brown & Holmes, 1967), which suggested that there was an increase in disorder of the myosin heads on activation. They ascribed the lack of myosin type labelled actin layer lines to the asynchronous behaviour of the crossbridges.

The cross-bridge model for muscle contraction entails the interaction of the myosin heads with actin in the region of filament overlap. X-ray equatorial diffraction patterns show that the heads are in the vicinity of the actin filaments but, structural evidence of actual attachment of myosin heads to actin during contraction has been elusive (Haselgrove & Huxley, 1973). Matsubara, Yagi, Miura, Ozeki, & Izumi (1984) provide strong evidence for this interaction. They show that during a contraction, the 5.9nm. layer line, arising from the genetic helix of actin (Selby & Bear, 1956), increases by up to 56% in frog skeletal muscle. During contraction the actin layer line is 30% more intense than at rest, and there is no apparent shift in the intensity peak along the layer line. In rigor, the intensity of the actin layer line is 55% greater than the resting pattern, and the radial position of the intensity peak lies closer to the meridian. Huxley & Brown (1967) attributed the intensification of the layer line and the inward shift of the intensity peak in rigor to the attachment of the myosin heads to actin. The absence of an inward shift of the intensity peak during contraction can be explained if the attachment of the myosin heads to actin in

INTRODUCTION

living muscle is at a variety of angles.

Later it became possible to observe changes in the diffraction pattern with much greater time resolution (lms.). On observing the effects of rapid changes in muscle length, Huxley, Simmons, Faruqi, Kress, Bordas, & Koch, (1981) were able to give support to earlier purely mechanical studies (Huxley, A.F. & Simmons, 1971; Ford, Huxley, A.F. & Simmons; 1977). Huxley et al. found that whilst the very small changes in the equatorial reflections and the 42.9nm. layer line on stretch or release did not give any definite indication as to the behaviour of the cross-bridges they were able to say that fast releases which reduced the tension to a quarter of the isometric force, did not move any of the cross-bridges back to their rest position away from the actin. Changes in the 14.3nm. meridional reflection, resulting from stretch or release, showed that there is a considerable change in the orientation of the cross-bridges, and that this change is caused by relative sliding movements of the filaments of less than 0.1nm. From these results Huxley et al. concluded that a large number of cross-bridges are attached to actin during an isometric tetanus, and that during a rapid release they undergo some longitudinal change which brings them to the end of their working stroke.

A carbodiimide zero-length crosslinking study (Mornet, Bertrand, Pantel, Audemard, & Kassab, 1981) shows that the 95K myosin head heavy chain enters into van der Waals contact with two neighbouring actin monomers; one is bound to the 50k domain and the other to the 20k domain of the myosin chain. In addition they suggest that each latitudinal pair of actin

INTRODUCTION

monomers acts as a functional unit specifically for the binding of the myosin head and the stimulation of its Mg-ATPase activity. A structural study of a rigor complex of thin filaments decorated with HMM-S₁ provides further evidence (Amos, Huxley, Holmes, Goody, & Taylor, 1982). A 3-D reconstruction of electron micrographs showed that the individual S₁ molecules do interact with both strands of the filament, straddling the regulatory proteins in the long pitch groove, which is in agreement with the cross-linking studies of Mornet et al.

Cross-Bridge Models

Hill (1938) produced a model to describe the behaviour of muscle as a "black box", relating the Fenn Effect (Fenn 1924) to mechanical behaviour, although the first serious attempt to describe the behaviour of individual molecules had to wait until 1957 (Huxley, A.F.; 1957).

Since that time a number of models have been proposed. The main models and their advantages, disadvantages and variations are discussed below.

A.F. Huxley's 1957 Model

This was the first attempt to try and account for the properties of muscle in the form of a cross-bridge model. Using force-velocity data obtained from Hill (Hill, 1938), he estimated the rate constants for the formation and detachment of cross-bridges. This involved a small rate constant for the formation of cross-bridges, which meant that the number formed at any one time is dependent on the rate of filament sliding. One consequence of this, which is observed experimentally, is that as the load on a muscle decreases so the shortening velocity increases. In addition he made one further assumption, that for each individual cross-bridge cycle one molecule of ATP is required.

The basis of the model is shown in fig 1.8, and the model proposes the following mechanism. At rest the actin and myosin molecules (A and M) are detached, and M is constantly oscillating about its equilibrium position (O) due to Brownian motion. If this movement results in M being brought close to

FIG. 1.8

Mechanism of contraction proposed by A.F.Huxley (1957). The part of the filaments shown is in the right half of the A-band. The myosin 'side piece' (M) is capable of binding to actin sites (A). O is the equilibrium position of M, where there is no net force in the elastic linkage. x is the displacement of A from O. (From Huxley, 1957).

INTRODUCTION

A, then it is possible for the two to combine. The resulting tension in the elastic linkage joining M to the myosin filament, is then transmitted to the actin filament. The result of this is either force or a relative sliding of the filaments. Fig 1.9 is the probability of a cross-bridge existing at different distances (X) from O, where f and g are rate constants for the formation and detachment of crossbridges. The interaction of myosin takes place to the right of O, and as the tension generated in the link causes the muscle to shorten, the actin-myosin combination moves towards O. When point O is passed, the probability of detachment (g) increases abruptly, and the link is broken. At high rates of shortening, it is possible for some of the links to remain attached long enough for a compressive force to be developed. The maximum speed of shortening (V_{max}) is reached when this force equals that generated on the other side of O, as a result the overall tension is zero. The force-velocity relation of this model is shown in fig 1.10. The different graphs show the ratio of A and M sites at different relative positions to the equilibrium site (O) for a range of velocities ($V=0$ (isometric tension) to V_{max}).

This model predicts the force velocity relationship, and with some modification, the liberation of energy under different loads and speeds, but it cannot account for the results of experiments involving rapid changes in load or length.

Huxley's 1957 theory assumes that tension in the link is generated by thermal agitation which is transmitted instantly to the actin filament whenever an AM combination occurs.

FIG. 1.9

Dependence of f and g on x , where f (broken line) is the rate constant for the formation of actin-myosin cross-links and g (solid line) is the rate constant for detachment. x is the distance A from O , the position where there is no net force in the elastic link. h represents the maximum value of x , at which attachment can occur. (Huxley, 1957)

Fig 1.9

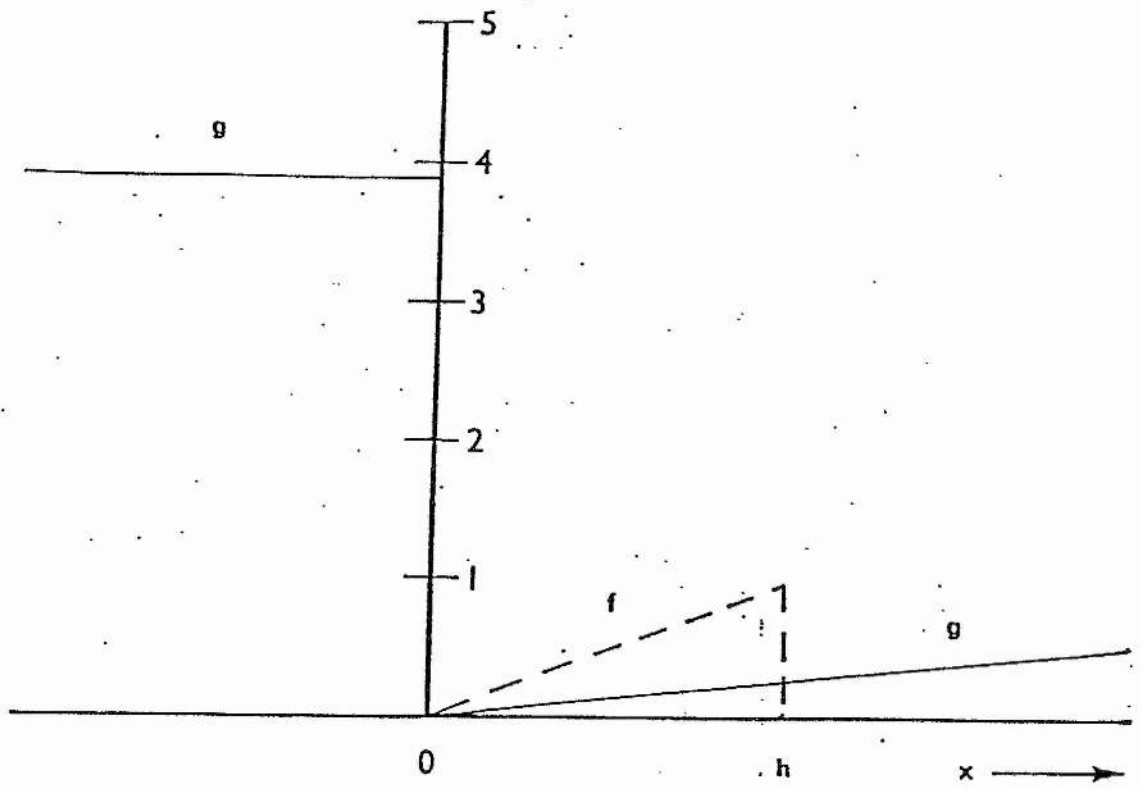
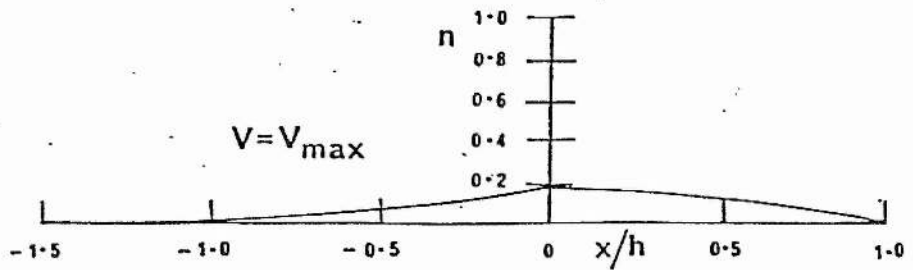
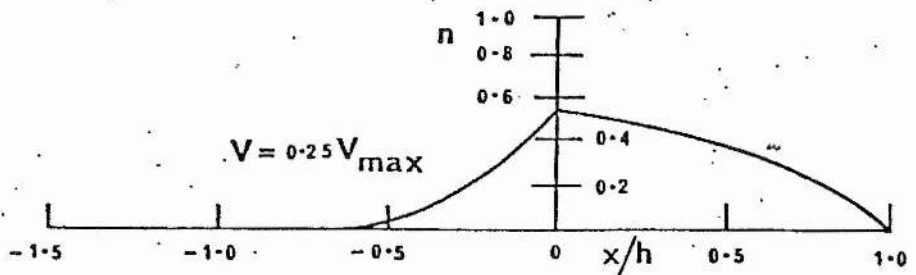
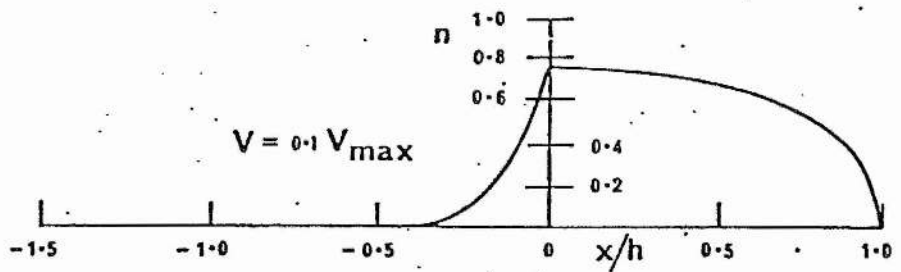
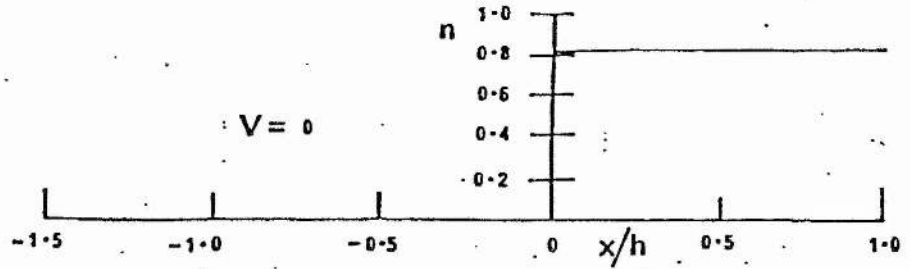


FIG. 1.10

Changes in n (proportion of sites where actin-myosin linkages can form), with x (position of A relative to the equilibrium position of M), for steady state velocities of shortening from 0 (isometric contraction) to V_{\max} (maximum speed of shortening in an unloaded, isotonic contraction). (Huxley, 1957)

Fig 1.10



INTRODUCTION

The effect of step changes in load on the tension response of contracting frog muscle fibres (Civan & Podolsky, 1966; Armstrong, Huxley, & Julian; 1966) are shown in fig 1.11a, where the changes in length upon step change to a fraction of P_0 are shown. The opposite type of experiment was performed by Huxley & Simmons (1970a, 1971a,b), where instead of varying the load, they applied step changes in length and recorded the resulting tension transients. Records from these experiments are shown in fig 1.11b, and the findings from the two kinds of experiments are summarized below.

- (a) During a length/tension step there is a simultaneous drop in tension/shortening.
- (b) This is followed over the next few milliseconds by a period of rapid tension recovery/rapid early shortening.
- (c) During the next 5-20ms. there follows an extreme reduction or reversal in the rate of tension recovery/shortening speed.
- (d) Gradual tension recovery to P_0 / steady shortening, occurs during the remainder of the response.

In addition to these effects Huxley & Simmons' (1971a) tension records show two other features. First that during the initial release tension drops to a value (T_1) that is dependent on the size of the step; and secondly, that the rapid tension recovery also varies with the size of the shortening step. The relationship of these two values with size of step is shown in fig 1.11a. The effect of a step increase in length is shown in the top part of fig 1.11b, and

FIG. 1.11

(a) Length responses to imposed 'step' reductions in loads of different amplitudes. The size of the initial instantaneous length change is shown by an arrow. The tension amplitudes after the applied 'load' step are:

A - $0.5 P_0$

B - $0.3 P_0$

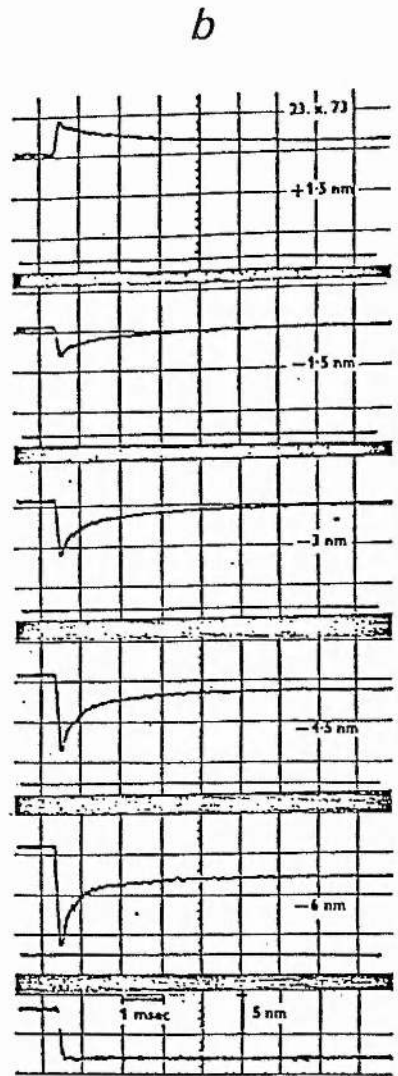
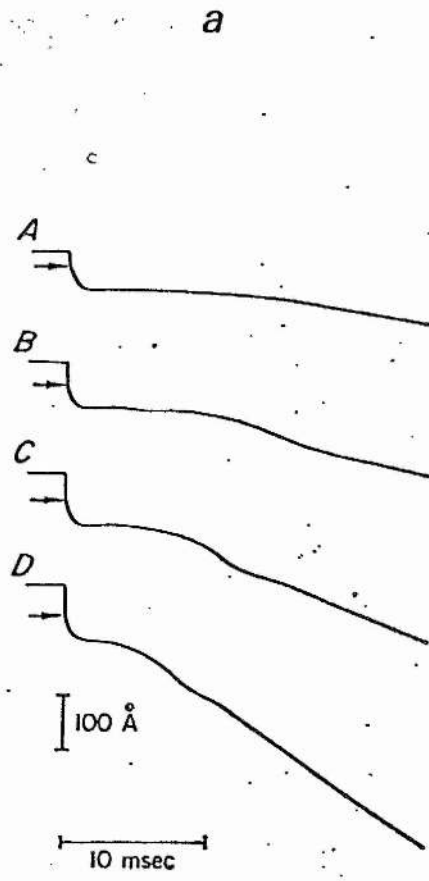
C - $0.15 P_0$

D - $0.01 P_0$

(from Julian et al., 1973)

(b) A group of tension transients produced by 'step' changes in length (Huxley, A.F., 1974). The figures to the right of each trace refer to the size of the length step.

Fig 1.11



INTRODUCTION

the values for T1 and T2 can be obtained in the same way as for releases. This kind of experiment yields the two curves in fig 1.12A which intersect at zero length change.

The first interpretation of these results was that the initial rapid drop in tension was caused by shortening of the filaments, and that the early rapid recovery was due to cross-bridges re-extending them. This change in actin filament length is unlikely as the actin filaments show no change in their length on activation (Huxley & Brown, 1967). This would then suggest an alternative that both features are properties of the cross-bridges, and this was confirmed later when experiments were carried out at longer muscle lengths. These experiments (Huxley & Simmons, 1971a) showed that at longer lengths, where there are fewer cross-bridges in the region of filament overlap, the slopes of T1 and T2 did not change. These results would suggest that the transient effects are due to the properties of the cross-bridges and that any compliance of the filaments or Z-lines is small enough to be ignored.

Explanation of the Tension Responses

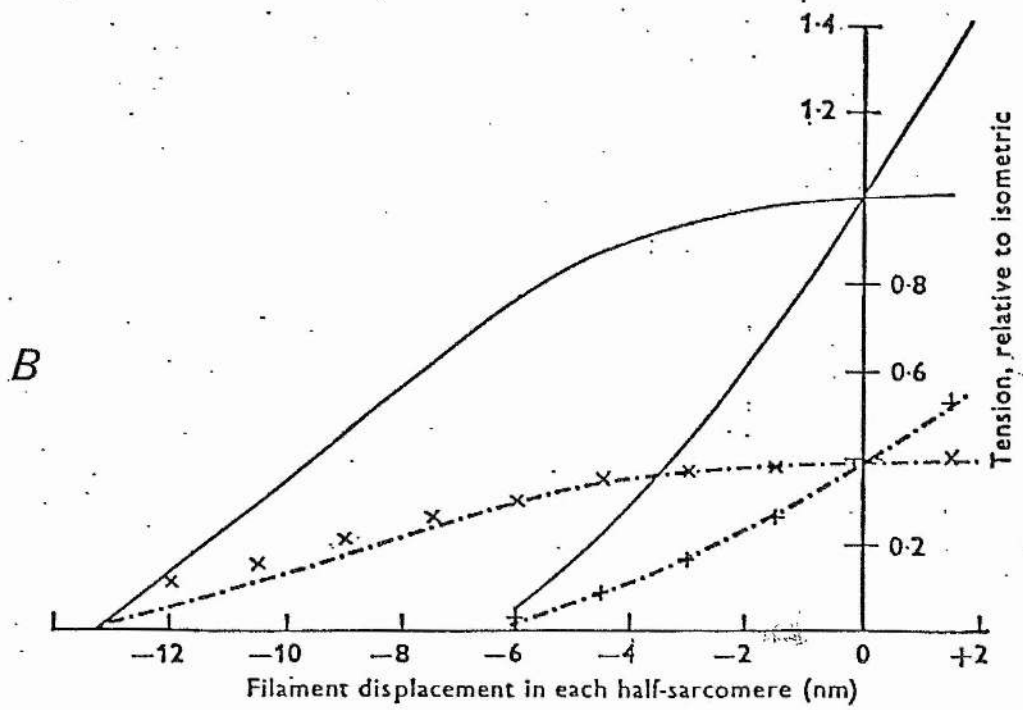
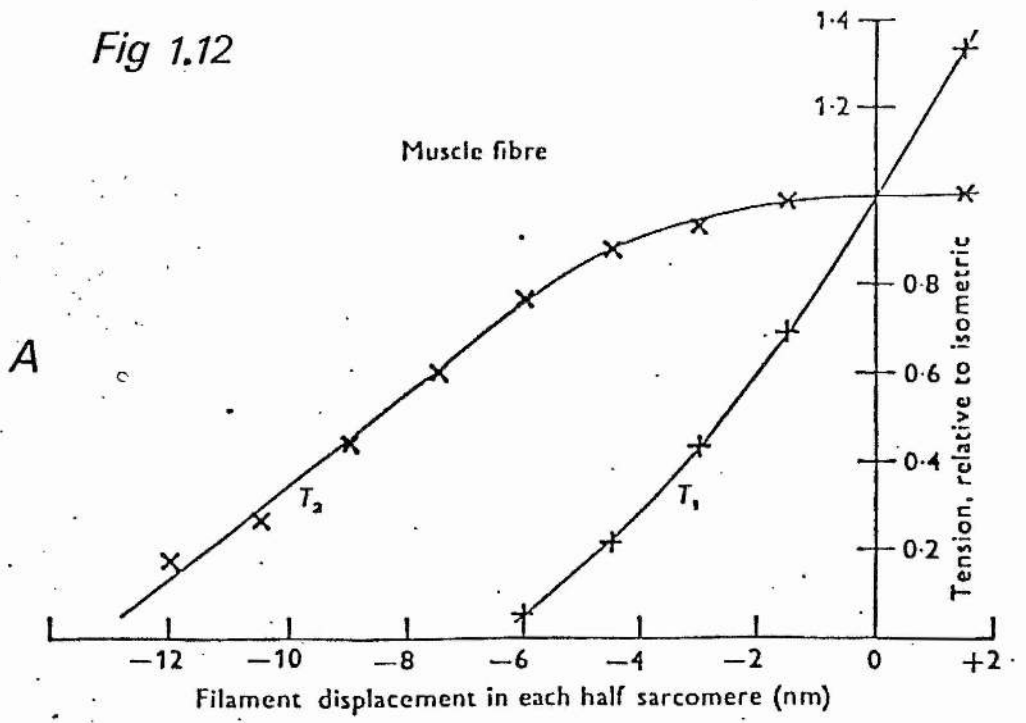
Stage 1.

The rapid fall in tension during this phase is caused by a change in length of an elastic component that forms part of each cross-bridge, and that because of the rapidity of the event there is no detachment or attachment of cross-bridges (i.e. the number of attached cross-bridges remains the same.). There ought in theory at this stage to be no change in the length of any other cross-bridge component, if the length change is abrupt enough, otherwise it will affect the next stage.

FIG. 1.12

- (a) T_1 and T_2 curves, constructed from a group of records such as those in fig. 1.11 (Huxley, 1974).
- (b) T_1 and T_2 curves obtained from the same muscle fibre at two different lengths. The solid line is the same as in 1.12A, where the sarcomere length was 2.2 μ m. The lower lines were obtained with the fibre stretched to a sarcomere length of 3.1 μ m. (Huxley, 1974)

Fig 1.12



Stage 2.

The stage of rapid early tension recovery is partially predicted by Huxley's 1957 model, as rapid shortening must result in the detachment of cross-bridges which have been displaced to the point where they exert 'negative' tension, that is to the left of 0 in fig 1.8. The 1957 model does not however account for the abrupt transition from the early rapid recovery to the gradual recovery or reversal seen later. As shown earlier, the amplitude of T1 & T2 is dependent on the size of the applied step. T1 has an almost linear dependence on the amplitude of the step, only deviating from linearity for large releases, where T1 approaches zero. Huxley and Simmons assume T1 to be linear under ideal experimental conditions. The T2 curve however, which shows the tension level during quick recovery, is concave downwards for releases and upwards for stretches, and when small length changes are applied, it is almost flat. Lastly the rate of rapid recovery is greater as the size of the release increases, but smaller with increasing size of stretch (fig 1.13).

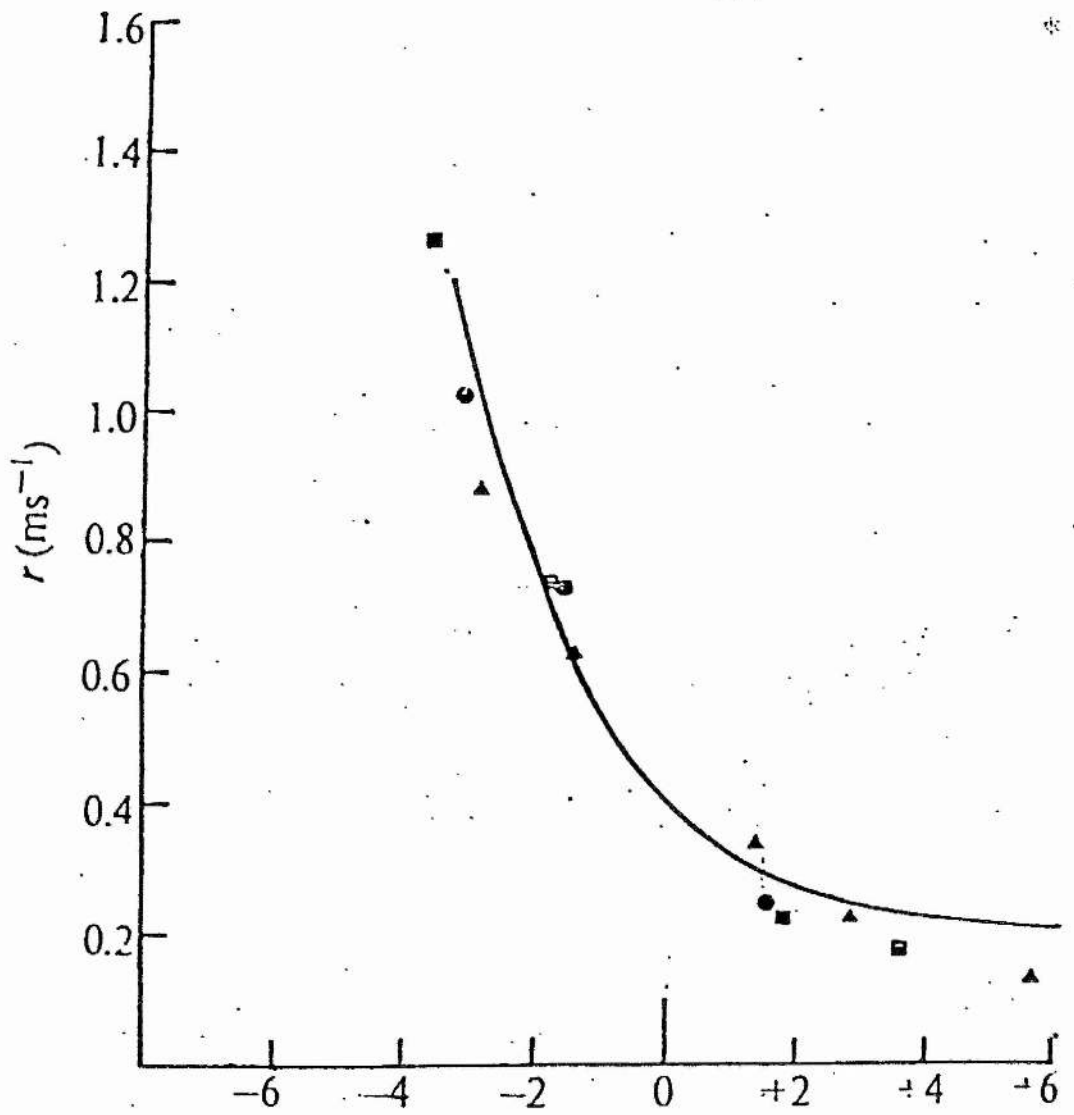
Stage 3.

This phase is difficult to explain without some modification in the values of the rate constants f and g from the 1957 model, but by doing this it is possible to predict a delayed fall in tension after a release. If the value of g increases after a shortening step, but f is unchanged, then there will be a net decrease in tension, therefore any influence which would delay cross-bridge reattachment would make itself more pronounced, before stage 4 occurs and tension returns to the isometric level.

FIG. 1.13

Changes in the rate constant for the quick recovery phase following 'step' changes in length of different size. The amplitude of the applied length changes (both stretches and releases) is given in nm per half sarcomere on the abscissa. (Huxley & Simmons, 1973)

Fig 1.13



Stage 4.

The cross-bridges recycle several times during this phase, reattaching each time further along the filament, and thus tension returns to the level prior to the length change.

Huxley and Simmons Cross-bridge Model

In this model two basic assumptions are made about cross-bridges.

First, that when an attached cross-bridge moves, it does so through a number of discrete steps, from one to the next of a series of stable positions which have progressively lower potential energy. Secondly, each cross-bridge contains an instantaneous elastic element, which enables the force generating element to move between stable positions, without simultaneously displacing the actin and myosin filaments relative to one another. These structures are thought to be in series with each other and so a relative movement of the filaments results in a change in the length of both elements.

A two component model of this kind is able to account for the nonlinear responses exhibited by living fibres (Huxley & Simmons, 1971b). The stable positions taken up by the force generating element can be represented in the form of a potential energy diagram (fig 1.14A). The effect of thermal agitation on the cross-bridge allows it to jump between one position and another. The amount of time it is allowed to spend in anyone position is dependent on the tension in the elastic link. When the time average of the potential energy is plotted against length the curve in fig 1.14B is obtained. The changes in the slope of this curve represent the length-tension characteristics of the force generating elements (fig

FIG. 1.14

A. Diagram of the potential energy in the force generating element (i), assuming three stable positions. The abscissa is the length of the element i, L_i .

B. Time average form of the potential energy curves shown in fig. 1.14A, plotted against the time average L_i .

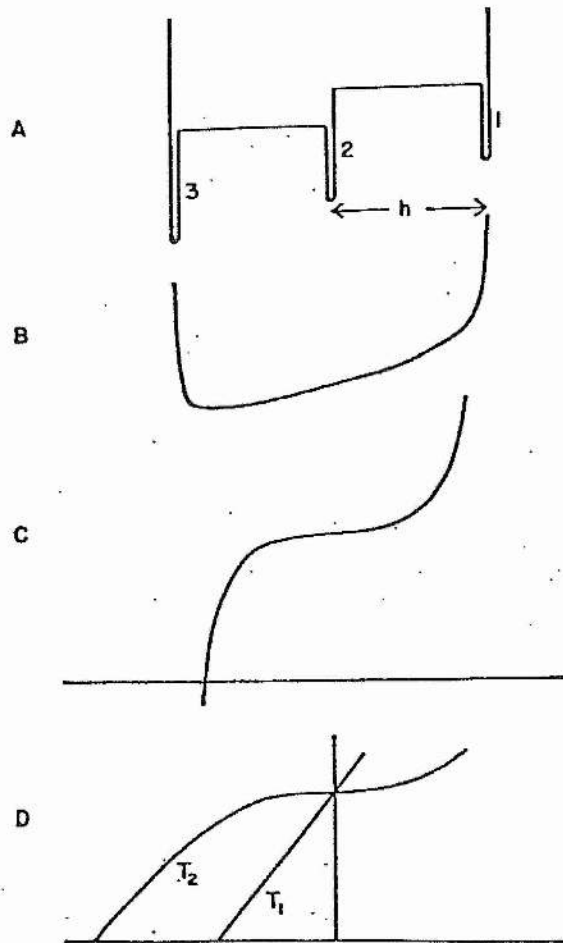
C. The slope of B, which represents the tension generated by the tendency of the element to spend more time in positions of lower potential energy.

D. T_1 , is the assumed linear, length/tension relation of the elastic element ii. T_2 , is the length/tension relation obtained by combining, in series the T_1 line and the curve

C.

(Huxley & Simmons, 1973.)

Fig 1.14



INTRODUCTION

1.14C). The length tension diagram for both the cross-bridge elements is shown by the curves T1 and T2 in fig 1.14D. These latter curves closely resemble those obtained experimentally.

Finally, the dependence of the rate constant for rapid recovery on the size of the length step can be explained by the model. In the stable states 1 and 2 the rate constant is proportional to the size of the potential energy step on going from state 1 to 2. Fig 1.15 shows that the size of this step is determined by the depth of the energy well which constitutes the stable position, and by the potential energy stored in the elastic link. The depth of the well is a fixed quantity, but the energy in the link is dependent on length. This means that the activation energy required to move from 2 to 1 is not affected by a length change, but that from 1 to 2 is decreased by a release and increased by a stretch. The model is therefore consistent with the properties of living fibres, in that a step decrease in length increases the rate of rapid recovery, whilst a step increase in length decreases it.

The Podolsky-Nolan Cross-bridge Model

Huxley's 1957 theory suggested that the rate constant for the attachment of cross-bridges (f) is relatively small; hence, as the speed of muscle shortening increases, a larger number of cross-bridges are unable to attach, and so cannot contribute to the overall tension. Podolsky (1960) and Civan & Podolsky (1966) showed that step reductions in force produced velocity transients which were similar to those of Armstrong, Huxley & Julian (1966) and this led Podolsky & Nolan (1971) to modify Huxley's 1957 model in an attempt to account for the

FIG. 1.15

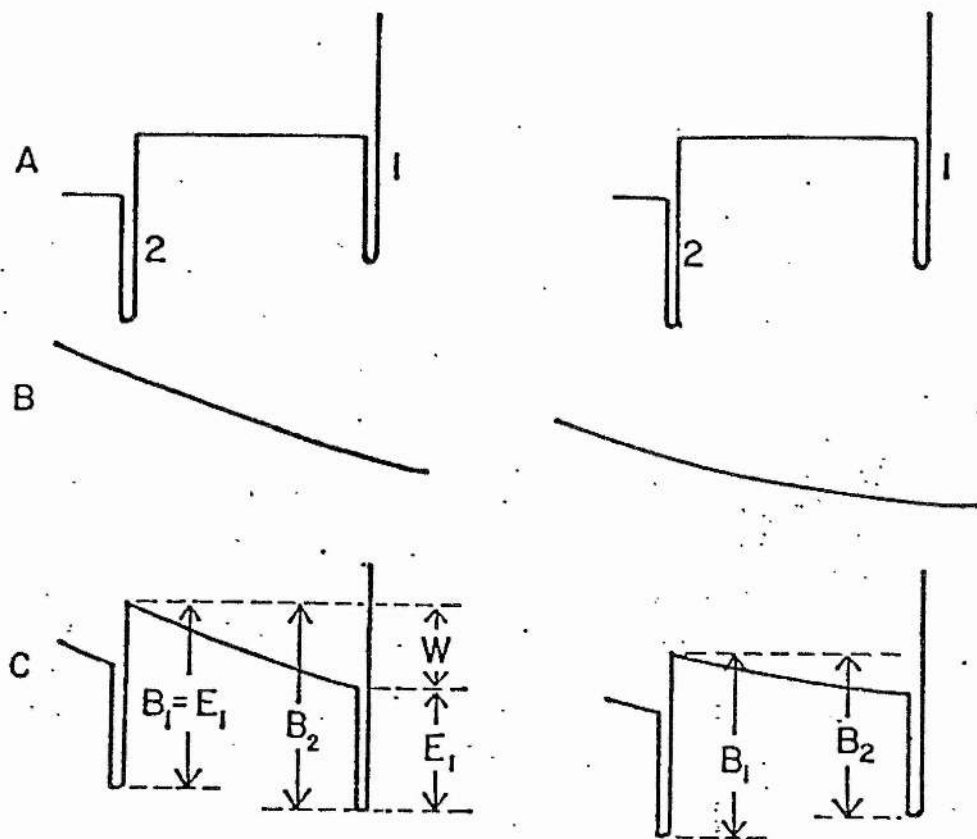
The dependence of the rate constant for early recovery on the size of the step.

A. Potential energy diagram for positions 1 and 2 of fig. 1.14A.

B. Potential energy/length diagram for the instantaneous elastic element.

C. Sum of A and B, giving the total potential energy in the cross-bridge as a function of L_i , (in the case where the total length of the cross-bridge is constant i.e. no relative movement of the filaments). B_1 and B_2 refer to the activation energies for the transition from position 2 to 1 and 1 to 2 respectively. W is the energy stored in the elastic element and E is the depth of the potential energy well, which constitutes a stable position. (Huxley & Simmons, 1973)

Fig 1.15



INTRODUCTION

transient behaviour.

This modification was made by adjusting the values f and g shown in fig 1.16a. Here g remains small for all positions of the site to the right of a point located 6.3nm to the left of O , beyond which it increases rapidly. This contrasts with Huxley's model where g rises to a high value at O . Podolsky and Nolan use this to explain the force-velocity relationship of muscle. Fig 1.16b shows the distribution of cross-bridge lengths predicted by this model, following step changes of load, simulating shortening at different speeds. At peak isometric tension, all the cross-bridges lie to the right of O , and therefore show positive tension. However, with increasing speed of shortening the cross-bridge population moves to the left, so that some are under negative tension, with the result that the net tension is zero. Finally, when the step reduces tension to zero, the contribution towards force of cross-bridges to the left of O is the same as to the right.

This model depends on the assumption that cross-bridge cycling is very rapid, regardless of the speed with which the filaments move past one another. This can then account for the high probability of a cross-bridge existing over a 6.3nm. range to the left of O , even at high velocities of filament movement.

There is a major difference between the explanation offered by Podolsky & Nolan and Huxley for the transient properties of muscle. The explanation offered by Podolsky & Nolan is summarized in fig 1.17. Prior to a length step the cross-bridge distribution is that in fig 1.17i. The application of a

FIG. 1.16

a

A. Diagram of Podolsky & Nolans' system, in which x and O are the same as in fig. 1.8.

B. Probability of making a bridge, f and breaking a bridge, g , for different values of x . Compare with Huxley's Fig 1.9.

C. Dependence of mean force (k) on x . The ordinate scales in B and C may be treated as arbitrary.

b

Variation in the distribution of cross-bridge lengths during contraction, for various force steps. Tension immediately after each step is given on the left. Areas enclosed by solid lines are the steady state distribution of cross-bridge lengths. Shaded areas should be ignored in this introduction. (Podolsky & Nolan, 1973).

Fig 1.16

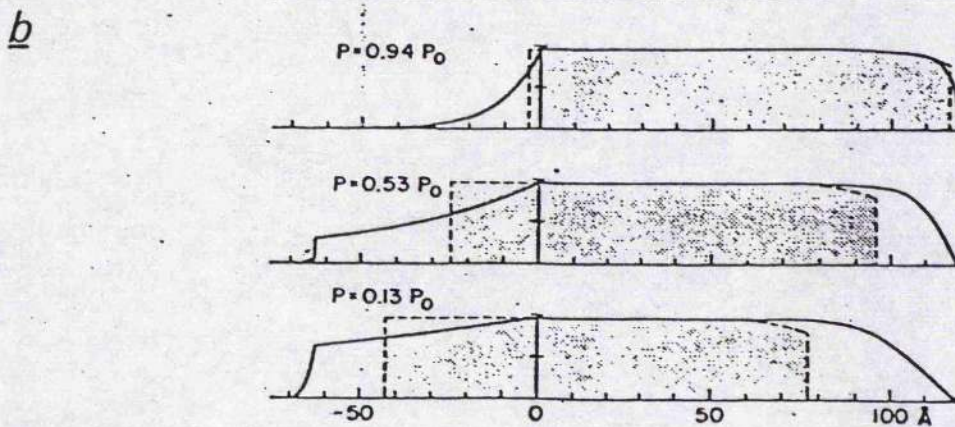
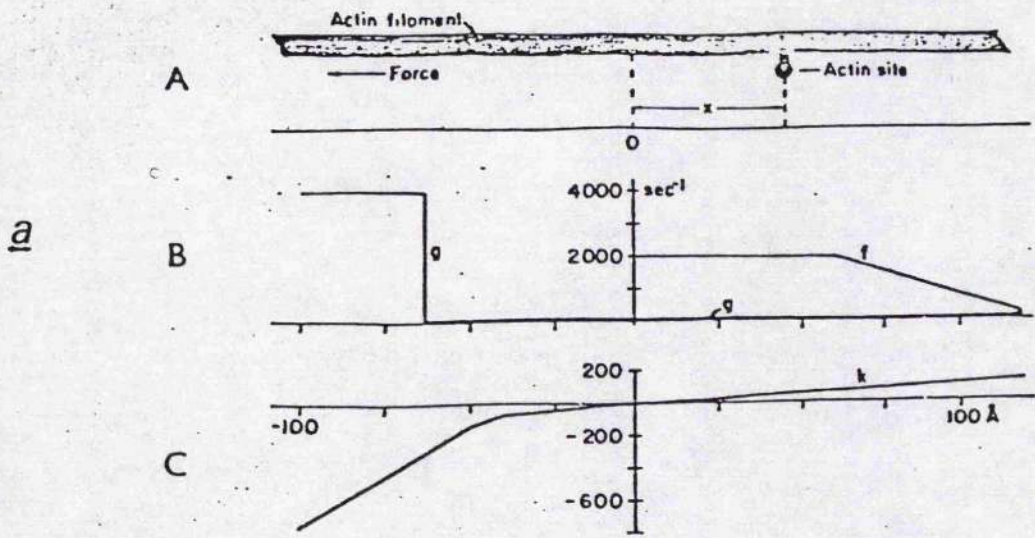


FIG. 1.17

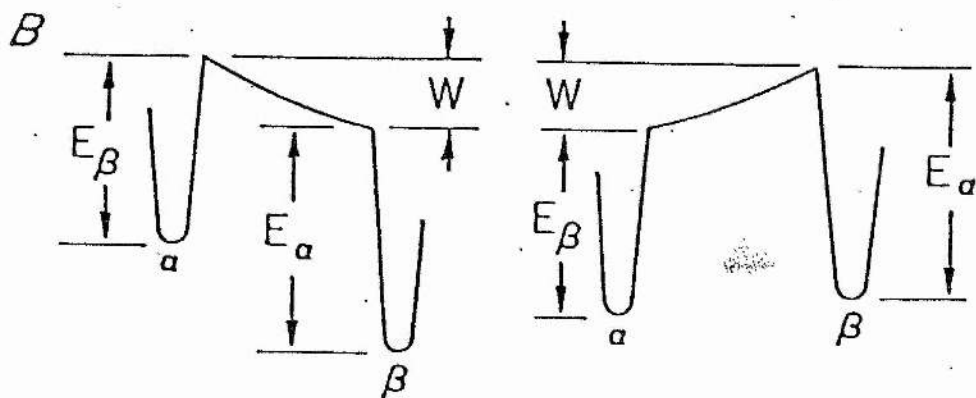
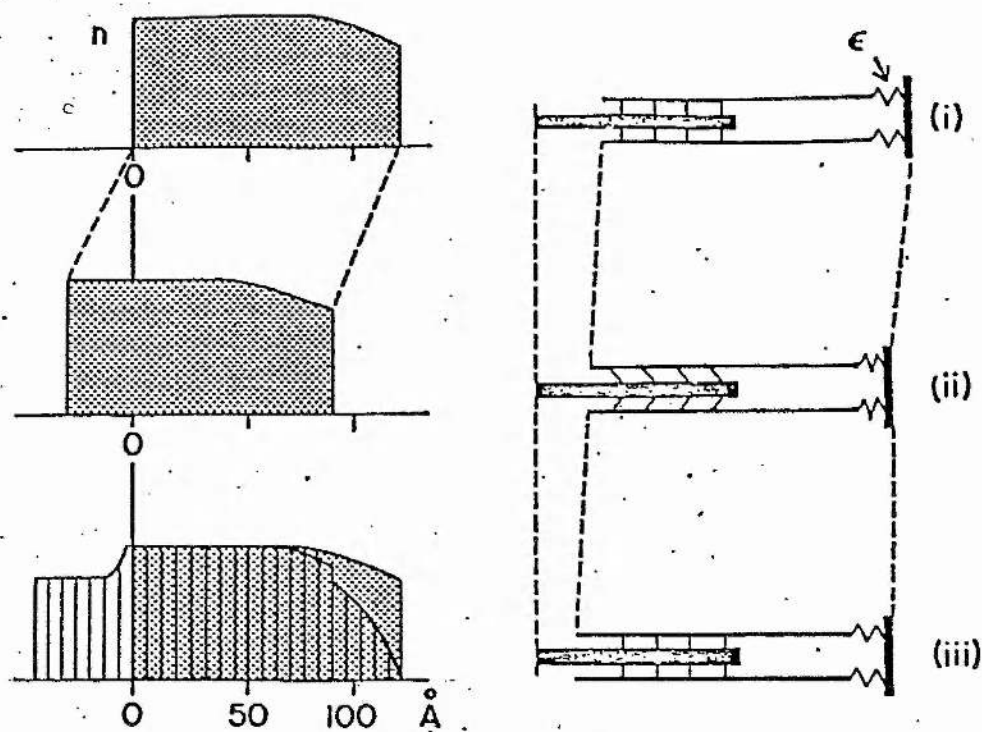
This figure shows a means of calculating tension redevelopment, following 'step' changes in length. Distribution functions (left, shaded areas) and filament configurations (right) at:

- i) the initial length, immediately before the tension step;
- ii) just after a tension step;
- iii) after tension has redeveloped; the lined area shows the distribution at a stage, intermediate between ii and iii, while tension redevelopment is occurring.

ϵ is a passive elastic element, lying in series with the filaments.

(Podolsky & Nolan, 1973).

Fig 1.17



INTRODUCTION

length step displaces the whole population to the left which causes a drop in tension (fig 1.17ii). Finally, cross-bridge cycling and the attachment of cross-bridges not previously attached brings about a redistribution of the cross-bridges and an increase in tension (fig 1.17iii).

Summary of the differences between the two models:-

First, a small shortening step causes the cross-bridges to change almost instantaneously, from their isometric position, where they exert considerable force, to one where they exert little force (T_1), either by shortening of the instantaneous element in the cross-bridge (Huxley & Simmons), or by a redistribution of the entire cross-bridge population to a new position, where the net force is greatly reduced (Podolsky & Nolan).

Secondly, immediately following the shortening step, tension is either regenerated by a stepwise movement of the cross-bridge head, which re-extends the instantaneous elastic element without detachment of the cross-bridges (Huxley & Simmons), or by redistribution of the whole cross-bridge population, by rapid cycling, to a position where net force is increased. This involves the attachment of cross-bridges that were previously unattached because of the lack of available actin sites.

This last suggestion by Podolsky & Nolan means that the number of attached cross-bridges ought to be increased following a release from peak isometric tension, and so the muscle should be stiffer. This is not the case, as shown by applying a quick release to a tetanised fibre, allowing rapid

INTRODUCTION

recovery to occur, then applying a step increase in length (Ford, Huxley, & Simmons 1974). The tension increment generated by stretch is then found to be marginally less than that produced by the same length change applied at the peak of an isometric tetanus. The conclusion then, is that there is no increase, and possibly a decrease, in the number of attached cross-bridges during the early recovery phase.

It is difficult, in the light of the last piece of evidence, to see how Podolsky & Nolan's model can apply to the early recovery phase. Even so, this does not mean that the model of Huxley & Simmons is the only explanation, or that one which allows some degree of cross-bridge cycling is necessarily discounted.

Cross-bridge Model of Julian, Sollins and Sollins

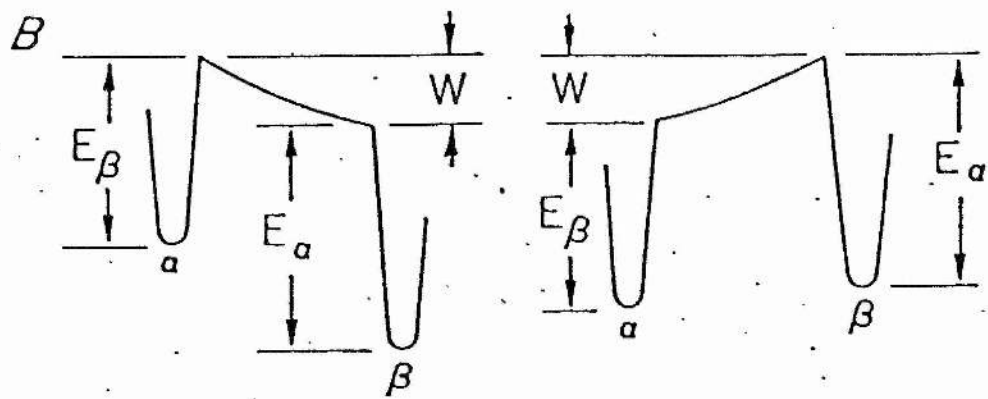
This is a modification of Huxley & Simmons (1971b) model proposed by Julian, Sollins & Sollins (1973). Its main feature is that the attachment step (a) is completely separate from the force generating step (b). It postulates that force is generated by a sudden 'flip' of the head after it has attached, into a second position, and that this second position is the only position from which the head can detach.

The dependence of the rate constant for rapid recovery is explained in a similar manner to that of Huxley & Simmons. The probability of a 'flip' from the unloaded state to the loaded state (a to b), is dependent on the activation energy for the step. This activation energy is determined by the sum of the depth of the energy well and a work term (W), which is the work required to extend the elastic link. Fig 1.18 shows that only when the energy required is positive, does the work term

FIG. 1.18

Potential energy diagram for the force generating elements, analogous to Fig. 1.15C, in the Huxley & Simmons scheme. The energy wells are labelled α and β , corresponding to the two stable states a and b proposed in this model. As in fig. 1.15C, the work term for extension of the elastic link is only effective, when it is positive, in opposing the 'flip' from a to b, and when it is negative, in opposing the 'flip' from b to a. (Julian, Sollins & Sollins; 1973)

Fig 1.18



INTRODUCTION

(W) have any effect on the activation energy for the step a to b. Conversely, only when it is negative does it affect the step from b to a. Thus, on stretch, when W is made more positive, the activation energy for moving from a to b is increased, but during a release, when W is made less positive, it is reduced. As the rate constant for the step a to b is inversely related to an exponential function of the activation energy, the rate constant for rapid recovery shows approximately the same dependence on step size as is found experimentally.

This model does not allow attached cross-bridges to remain in any position other than a or b, so that the distribution of crossbridges at the plateau of an isometric tetanus has two spikes: one where extension of the elastic link is zero (a), and the other, the force generating state, where the link is extended (b). If muscle length is changed, both spikes will in the case of a release be spread towards smaller link extensions, or in the case of a stretch, towards greater link extensions. The degree of spreading will depend on the speed of the length change and on the rate constants for the formation and detachment of cross-bridges.

The 'Structure' of Cross-bridges

As previously described, the myosin molecule is a rod shaped, two chain alpha helix, approximately 150nm. in length, with a globular region at one end (Lowey, Goldstein, Cohen & Luck, 1967; Lowey, Slater, Weeds, & Baker, 1969). The ability of the LMM sub-unit to self aggregate (Lowey, Slater, Weeds, & Baker, 1969), suggests that this forms the backbone of the myosin filament, leaving HMM free to hinge out towards the actin filament. X-ray diffraction experiments show that hinging is very likely as the relative intensities of the two principle equatorial reflections of the filament lattice reverse on activation, showing that there is a transfer of material from 1,0 to 1,1 lattice planes. The most likely explanation for this is that the S_2 HMM subunit hinges out towards the filament, allowing one or both of the S_1 heads to engage with actin. This type of mechanism enables the cross-bridge to form a link over a wide range of filament spacing and permits the S_1 units to 'mate' with actin at the required orientation.

The model proposed by H.E. Huxley(1969) proposes a cross-bridge with a flexible linkage, and that force is generated by the S_1 sub-unit changing its angle of attachment whilst still in contact with the actin filament. The force that results from this change in orientation, is transmitted via an inextensible S_2 linkage as in fig 1.19A.

Huxley & Simmons(1971a) proposed a modification of this idea so that it was compatible with their findings. First, that the limited number of stable positions required for the model corresponds to a number of different angular positions

FIG. 1.19

A. A model of the cross-bridge by H.E.Huxley (1969). Relative movement of the filaments results from a tendency for the S_1 subunit of HMM to undergo a change of orientation, while attached to the thin filament.

B. A diagram of the cross-bridge incorporating the features used by A.F.Huxley & Simmons (1971) as a structural basis for their theory. The myosin head (H) is connected to the thick filament by an undamped elastic link, AB. Solid lines show the head position with sites M_1A_1 and M_2A_2 attached; broken lines show the position with M_2A_2 and M_3A_3 attached.

INTRODUCTION

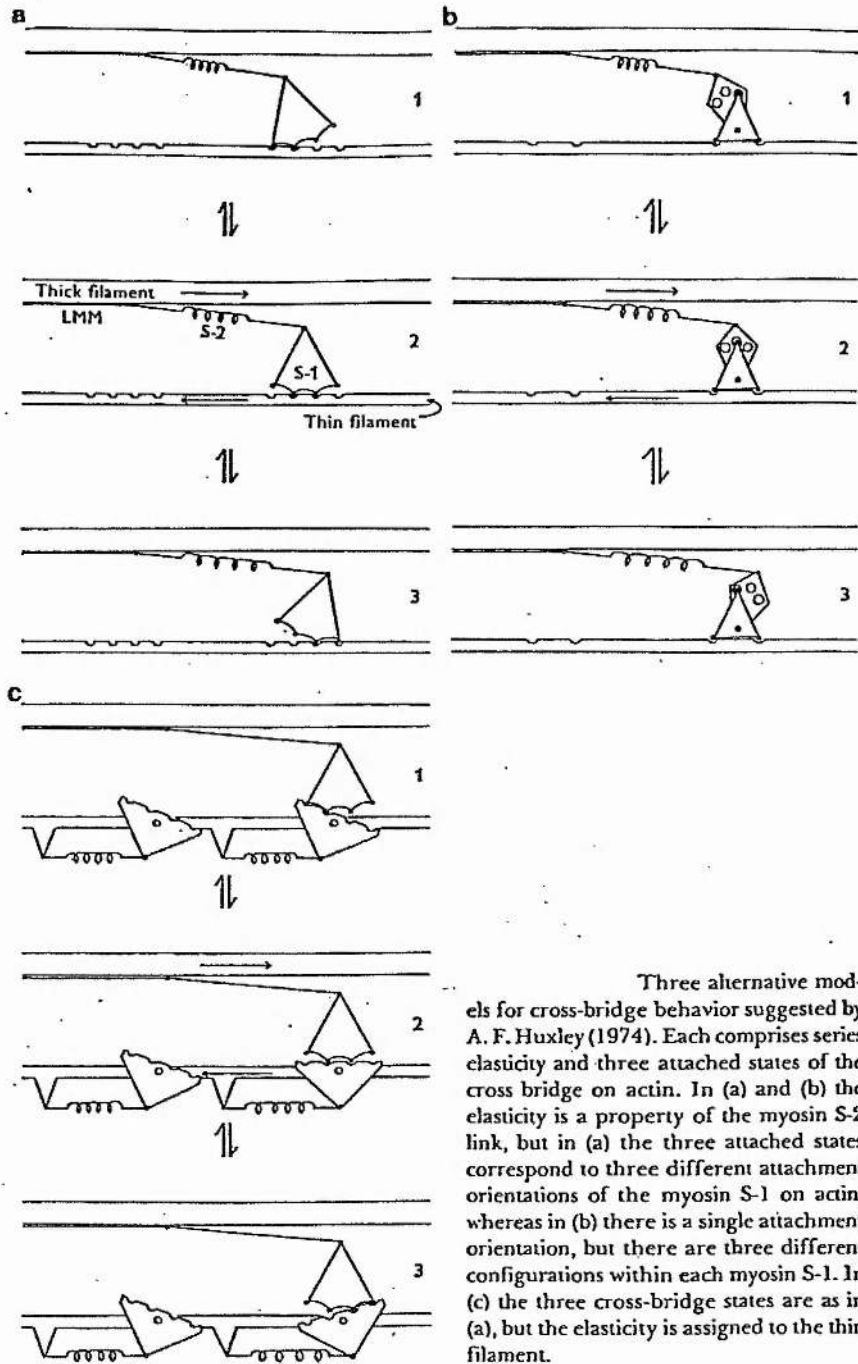
of the myosin head to the actin filament. Secondly that any two consecutive sites on the myosin head (M1,M2,M3,M4) when combined with two corresponding sites on the actin filament (A1,A2,A3,A4) constitutes a stable linkage. Finally, that the elastic element is most likely located in the S₂ linkage.

A diagram of their model is shown in fig 1.19B as are other logical variants in fig 1.20. Whilst it is thought most likely that the AB link in fig 1.19B is the instantaneous source of compliance, it is only one possibility. As fig 1.20 shows, it could equally well be located in the cross-bridge head or in the area of actomyosin interaction. By the same token, the site of the stepwise movement is also uncertain and could either be a property of the actin site or the cross-bridge head.

Cross-bridge Head Orientation.

Examination of muscle structure by EM and X-ray techniques led to the suggestion that force generation is the result of a change in the orientation of the cross-bridge heads attached to the actin filaments (Reedy, Holmes, & Tregear, 1965; Huxley H.E., 1969; Huxley A.F., 1974). This is further supported by the finding that myosin has the flexibility required for the rotation of the myosin heads (Mendelson, Morales, & Botts, 1973). Experiments on the polarisation fluorescence of tryptophan, which is located mainly in HMM-S₁ (dos Remedios, Millikan, Morales, 1972), showed that it depended on the physiological state of the muscle (Aaronson & Morales, 1969) and so gave some indication of the different mean orientations of the cross-bridges. Other methods have also been able to determine angles of heads, and give an indication of the

Fig 1.20



Three alternative models for cross-bridge behavior suggested by A. F. Huxley (1974). Each comprises series elasticity and three attached states of the cross bridge on actin. In (a) and (b) the elasticity is a property of the myosin S-2 link, but in (a) the three attached states correspond to three different attachment orientations of the myosin S-1 on actin, whereas in (b) there is a single attachment orientation, but there are three different configurations within each myosin S-1. In (c) the three cross-bridge states are as in (a), but the elasticity is assigned to the thin filament.

INTRODUCTION

number of cross-bridges in a particular state.

Resting Muscle.

Experiments using X-ray scattering on living fibres, indicate that the heads are highly disordered (Poulsen & Lowy, 1983), as the scattering is circularly symmetrical. This is also supported by electron paramagnetic resonance (EPR) spectroscopy studies of the orientation of spin labels, attached to a reactive sulfhydryl group on the myosin heads of glycerinated rabbit psoas muscle (Thomas & Cooke, 1980). A similar disorder has been seen in isolated myosin filaments (Thomas, Ishiwata, Seidel & Gergely, 1980) and in non-overlap regions of stretched fibres (Barnett & Thomas, 1982), indicating that in relaxed fibres the myosin heads are detached from the actin filaments.

The amplitude of the disorder and the angular movements of the head are difficult to determine, because the angle of the molecular probe to the myosin head is unknown. At 0°C there appears to be very little order on the probes attached to the myosin heads, but at 25°C there is a small increase in the order (Thomas & Cooke, 1980). This may correspond to a small population of attached heads, as has been suggested by studies of S_1 and actin in solution (Chalovich & Eisenberg, 1982), and by studies of resting tension (Hill, 1968).

There is further evidence that cross-bridges can form in resting muscle. Brenner, Schoenberg, Chalovich, Greene, & Eisenberg (1982) show that relaxed, glycerinated rabbit psoas muscle exhibits substantial stiffness when rapid stretches are applied at low ionic strength ($\mu=20\text{mM}$). This stiffness was

INTRODUCTION

shown to be proportional to filament overlap, and they suggest that it is caused by attached cross-bridges. Brenner et al. suggest that the cross-bridges are in rapid equilibrium, with actin, as at $u=20\text{mM}$ stiffness was only observed with very rapid stretches. Brenner et al. were unable to determine whether cross-bridges were formed at higher ionic strength ($u=170\text{mM}$) because there was no detectable stiffness. As the measured stiffness was found to depend on the speed of stretch applied, a decrease in stiffness could be explained by either an increase in the rates of cross-bridge attachment-detachment, or a decrease in the number of cross-bridges. A later study (Brenner, Leepo, & Podolsky, 1984) examined X-ray diffraction patterns from single skinned rabbit psoas fibres at various ionic strengths. At ionic strengths between 20-50mM, the intensity of the 1,1 reflection was close to that of rigor, whereas the 1,0 reflection was twice the rigor reflection. Using Fourier synthesis, Brenner et al. (1984) showed that substantial extra mass was associated with the thin filaments under these conditions. With increasing ionic strength, between 20 and 100mM, the 1,0 reflection increased and 1,1 decreased, indicating a net transfer of mass away from the thin filaments towards the thick. This showed that cross-bridges are formed in relaxed fibres at low ionic strength, but that as the ionic strength is increased, the number of cross-bridges decreases. Above $u=100\text{mM}$ both the 1,0 and 1,1 reflections decreased, indicating the onset of increasing disorder within the filament lattice.

The orientation of cross-bridges in relaxed frog skeletal muscle has been studied by Cantino and Squire (1986), who looked at freeze fractured sections of relaxed muscle rapidly

INTRODUCTION

frozen using a propane jet. By a combination of optical diffraction and computer enhancement, the details of the right handed, three stranded helix of myosin heads were revealed. These images clearly show the 43nm. and 14-15nm. repeats of the cross-bridge array and a filament backbone of 14-16nm. in diameter. Cantino & Squire conclude that both heads of each myosin molecule tilt in the same direction, at an angle of about 60° normal to the filament long axis, and are slewed so that they lie along side each other, their radially projected density lying along the three right handed helical tracks.

Rigor Muscle.

Muscle fibres in 'rigor' have almost all their cross-bridges attached to the actin filaments. In insect flight muscle, Holmes & Tregear (1965) concluded, that in rigor the myosin heads lie at an angle of 45° to the filament backbone. This orientation was confirmed by decorating isolated actin filaments with HMM-S₁, when an arrowhead structure was observed where all the heads are bound at an angle of 50° . A more sophisticated approach was adopted by Taylor, Reedy, Cordova, & Reedy (1984) using ultra thin 'myac' sections of insect flight muscle. By tilting these sections in the EM, it was possible to construct a three dimensional image of the cross-bridges in the filament lattice. Each double chevron which had been assumed to contain two pairs of cross-bridges, is clearly resolved into two elements. The 'lead' chevron of each pair is shorter by 1.5nm., and tilted at 50° to the thin filament. The 'rear' chevron is longer (17.5nm.), tilted at about 80 degrees to the thin filament, and appears to consist

INTRODUCTION

of only one myosin head. Thus it would seem that there are conformationally different populations of attached cross-bridges in the rigor state.

There are several reasons why this type of structure had not been predicted or observed by other methods. First, in X-ray studies only the case of single cross-bridge conformation had been considered. In decorated actin the S_1 angle is consistent with that of the 'lead' chevron; this angle is considered to be the preferred rigor orientation. There are geometrical constraints on the attachment of S_1 to the filament backbone, thus the second chevron may be forced to take up a second, energetically less favourable orientation.

Secondly, spin labelling techniques, where probes are attached rigidly to a specific region of S_1 , only reveal one rigor position. Taylor et al. note that the rear and lead chevrons have the same angle within 6-8nm. of the actin filament, so if the probe was bound to this region of S_1 it could not discriminate between the two orientations.

Although the cross-bridge theory suggests a change in orientation of cross-bridges, it does not suggest whether this is a change in the shape of the cross-bridge head or a change in the position of the head on the actin site (see figs 1.19 & 1.20). Experiments with spin labelling of muscle in rigor, show that when the muscle is stretched there is no change in the orientation of the labels, and therefore to the area of the molecule to which they are attached (Cooke, Crowder, Wendt, Barnett, & Thomas, 1984).

Isometrically Contracting Fibres

X-ray scattering experiments indicate that at the peak of an isometric tetanus, where there is little relative sliding of the filaments, the cross-bridge heads adopt a preferred orientation that is nearly perpendicular to the fibre long axis (Lowy & Poulsen, 1986). A different approach was used by Cooke et al (1984), who produced isometric force in glycerinated rabbit psoas fibres by the addition of ATP and calcium. The S_1 heads of these fibres had been spin labelled, and the relative orientation of these labels was studied using EPR spectroscopy. When 81% of the resting spectrum is subtracted from the active, the result is identical in shape to the rigor spectrum. This observation suggests that 19% of the myosin heads in active muscle have their probes orientated at the same angle as in rigor, whilst the remainder are highly disordered with a spectrum similar to that of a resting fibre. Additionally, there appear to be no new probe angles, other than those seen in rigor or at rest. The reason for probes in the rigor position could mean that the preparation was not properly perfused with ATP, but Cooke et al. showed that this was not so. Combining this study with an earlier saturation transfer EPR (ST-EPR) study, which is sensitive to rapid changes in orientation of the probes (Thomas, Ishiwata, Seidel & Gergely, 1980), Cooke et al. conclude that the myosin head in contracting muscle exists in two states: one in which the probes are immobile and highly orientated with respect to the fibre axis, and another in which the probes are highly mobile and disorientated. In rigor (at full filament overlap) all the probes are orientated and immobile, whilst in relaxed

INTRODUCTION

preparations all probes are mobile and disorientated.

II. OPTICAL CHARACTERISTICS OF SKELETAL MUSCLE.

If a well collimated beam of light is incident on a skeletal muscle preparation a diffraction pattern can be observed, an example of which is shown in fig 1.21. Like many other biological tissues there is light scattering from membranes and organelles etc., but the diffraction pattern is generated by the regular alternating arrays of the contractile proteins which have different refractive indices.

Ranviers' early work on the diffraction pattern (Ranvier, 1874) drew attention to the similarity between the diffraction patterns from skeletal muscle and those of a one dimensional diffraction grating, and he concluded that the cause of the pattern was the regular striations visible through the microscope. Later, Sandow(1936a) showed that muscle behaved as a series of one dimensional gratings and that the separation of the orders agreed with the grating equation:-

$$d = (n \cdot \lambda) / (\sin \theta)$$

where

n = diffracted order

λ = wavelength

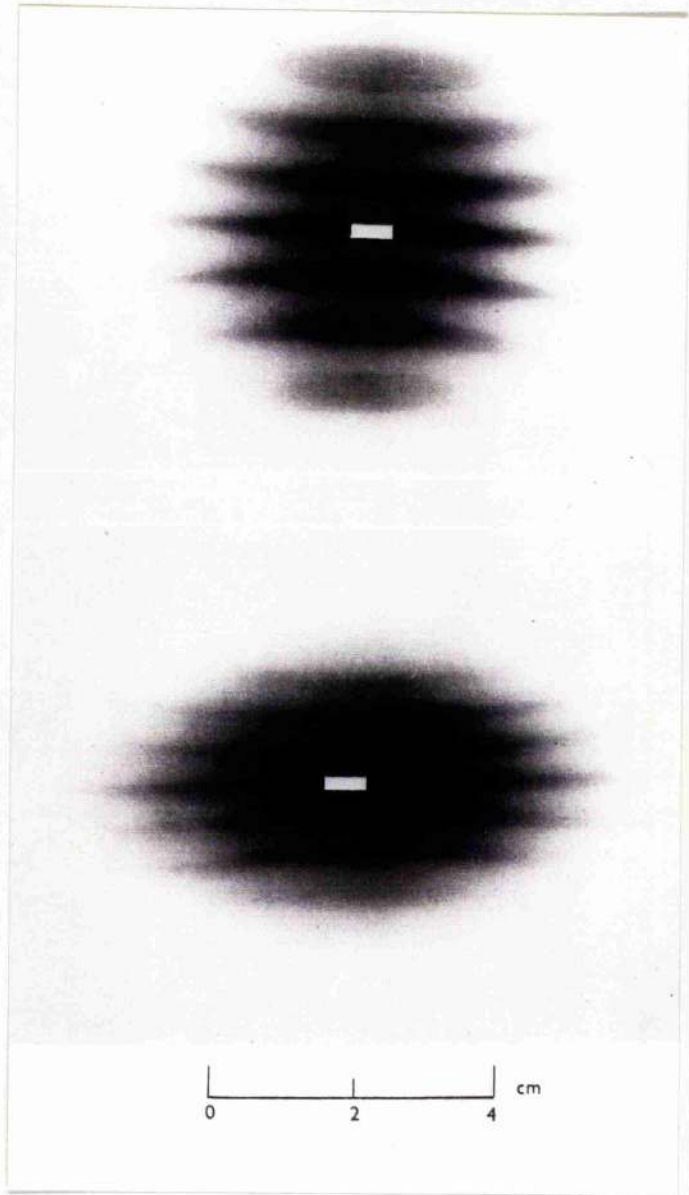
The Appearance of The Diffraction Pattern

The diffraction pattern consists of a number of lines arranged symmetrically about the zero order line. There is an inverse relationship between the spacing of the lines and muscle length (Zoth, 1890). These lines are arranged regularly in the meridional plane, and are spread out in the equatorial plane. Clearly visible in the orders are micro striations which have both meridional and equatorial components. By

FIG 1.21

Plate showing diffraction spectra from a frog sartorius muscle. Upper plate, muscle at l_0 (29mm). Lower plate, the same muscle at $l_0 + 11\text{mm}$. The white area illustrates the shape of the incident beam.

Plate taken from Hill (1953a).



INTRODUCTION

observing the movements of these microstructures it is possible to resolve changes in sarcomere length to a resolution of 0.5nm. (Cleworth & Edman, 1972; Haugen & Sten-Knudsen, 1976).

There is a great variation in the intensity and dispersion of the different orders, which in part is dependent on the preparation in use (Rudel & Zite-Ferenczy, 1979a)- the orders of a diffraction pattern from a single muscle fibre show large fluctuations in intensity, both equatorially and meridionally, whereas in whole muscle the intensity distribution is Gaussian.

There is now general agreement that the spacing in the orders of a diffraction pattern gives a reliable indication of the average sarcomere length in the illuminated area (e.g. Cleworth & Edman, 1972).

One notable difference between the diffraction pattern of a conventional transmission grating and the pattern arising from a muscle is that in the latter case, even though the incident beam is circular, the diffraction pattern appears as a series of lines. Various suggestions have been put forward to explain this. Cleworth & Edman(1972) suggest that the muscle fibres behave as a series of cylindrical lenses. Two other suggestions are that there are edge effects from the fibres, and that as the myofibrils are in the order of μm in diameter, they give rise to equatorial diffraction patterns(Baskin, Roos, & Yeh, 1979). This latter suggestion has further support. Work by Leung(1983) showed that in most fibres the transverse intensity of the diffracted orders decayed monotonically to zero. In some other fibres however

INTRODUCTION

there existed oscillations in the monotonic decay, and that these oscillations occurred where there was low dispersion in the diameter of the myofibrils. Whilst this suggests that the equatorial spread is caused by diffraction from the myofibrils, it does not rule out contributions from edge and lens effects. As will be described later, Rudel & Zite-Ferenczy (1979a) suggest that the cause of the equatorial spread is due to Bragg reflection.

The intensity of the higher order lines of the diffraction pattern is greater than one would expect from a simple grating, and Sandow(1936a) ascribed this to the multiple grating nature of skeletal muscle. A number of theoretical papers have appeared on the intensity of the diffracted orders. Using mathematics derived from X-ray diffraction, Fujime(1975) treated muscle as a one dimensional grating in which the primary scattering elements are the thick and thin filaments. By assigning a molecular scattering factor to the thick and thin filaments, Fujime predicted their relative contributions to the intensity of the diffracted orders at different sarcomere lengths. Another suggestion made by Fujime(1975) is that the decrease in first order intensity on activation is caused by random fluctuations in the relative positions of the thick filaments in the fibre.

Baskin, Roos, & Yeh (1979) on investigating the intensity profiles of single resting fibres suggest a 3-D model, where the basic scattering unit at rest is the whole fibre rather than the myofibril. On activation, however, they agree with Bonner & Carlson(1975) that the basic scattering unit is the myofibril. Yeh, Baskin, Lieber, & Roos (1980), in a

INTRODUCTION

modification of their earlier model, propose that the diffraction pattern arises from three sources: the regular repeating sarcomeres, the cylindrical nature of the myofibrils or fibres, and the lack of alignment, or staggering, of the myofibrils. This theory qualitatively predicts the intensity profiles of the resting and isometrically contracting fibres, but it does not explain the relatively high intensity of the second order lines that are found experimentally.

Explanation of the diffraction pattern using Bragg and Ewald formalism.

Rudel & Zite-Ferenczy (1979a) showed that the intensity of a given order is dependent on the angle of incidence of the light beam; in addition, they show that the intensity profile of the first order is not symmetrical, so that the left and right halves are not mirror images. Rudel & Zite-Ferenczy initially considered that if the myofibrils contain lattice planes which have different angles of tilt to the fibre axis, then there will be Bragg reflection (Bragg, 1913) of the incident beam according to the following formula:

$$2d \sin\theta = (k, \lambda) / nf \quad (1.2)$$

where d = the distance between the lattice planes.

nf = refractive index of the fibre

k = required order

λ = incident wavelength

Fig 1.22 shows a schematic representation of the Bragg reflection arising from one myofibril. Using this method the orders that are distributed about the zero order are caused by different myofibrillar lattice planes having opposite tilt

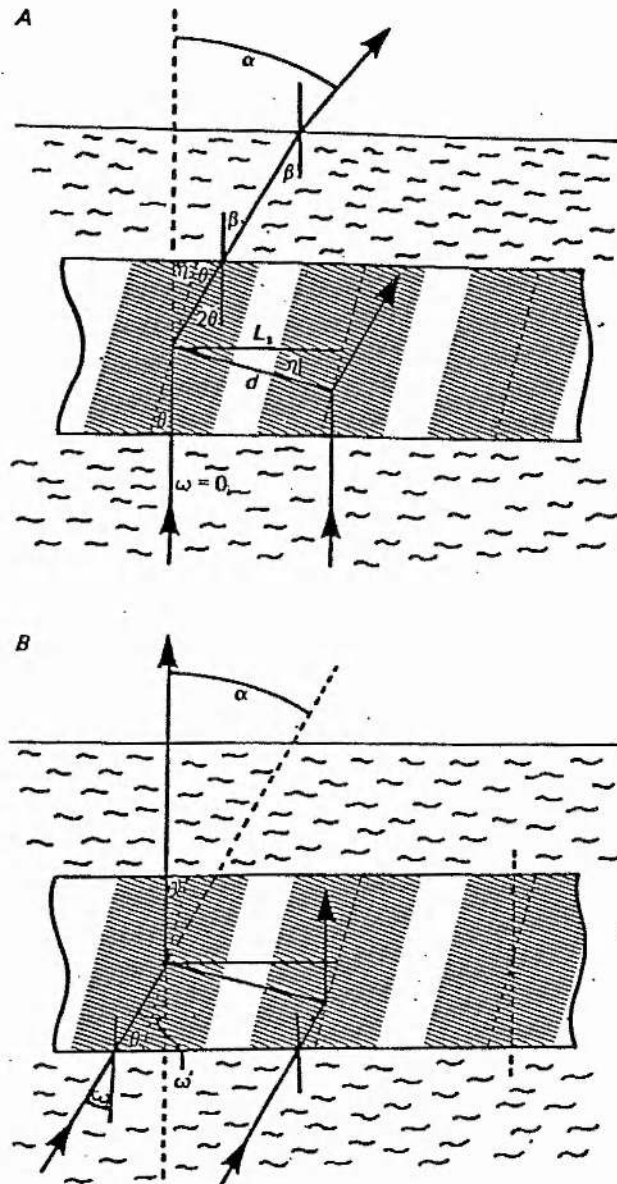
INTRODUCTION

with respect to the fibre axis. The different intensities of the corresponding orders is due to distinct myofibrillar populations having different degrees of tilt. In fig 1.22A the beam incident on the muscle is normal to the preparation, but is inclined at angle ω to the lattice plane. Therefore Bragg reflection will occur to the right of the incident beam if ω is equal to the Bragg angle θ . In the lower part of fig 1.22 (fig 1.22B) reflection occurs to the left of the incident beam, when the angle ω' between the refracted incident beam and the lattice plane is equal to twice the Bragg angle ($\omega' = 2\theta$). For normal incidence of the beam on the muscle fibre the Bragg equation can be shown to be similar to the grating equation.

The equatorial spread of the diffraction pattern can be explained using this method, on the basis of the tilt of the myofibrillar lattice planes about the axis of the incident beam. Therefore Bragg reflection also accomodates the appearance of the orders as lines rather than spots which would be seen from a simple grating.

The Bragg theory enables one to explain many of the features of the diffraction pattern, but it has shortcomings as it was originally conceived to apply to an infinitely thick diffractor. In this sense, the Bragg model is the opposite of the simple grating equation which holds for the case of an infinitely thin diffractor. Zite-Ferenczy, Haberle, Rudel & Wilke (1986) present a method of explaining the phenomena seen in the diffraction patterns called "Ewald's construction". This formalism enables all the geometrical aspects of the diffraction pattern to be explained, making only plausible

Fig1.22



Schematic representation of scattering by Bragg reflection. In (A), the incident light is normal to the surface of the muscle fiber. In (B), the light is incident at angle ω (α) Angle of reflection with respect to the path of the incident beam; (θ) Bragg angle; (L_s) sarcomere length; (d) = shortest distance between lattice planes; (η) angle of tilt of lattice planes with respect to fiber axis. From Rüdél and Zite-Ferency (1979a).

INTRODUCTION

assumptions about the structure of the muscle, which can be tested using light or electron microscopy.

Ewald's construction.

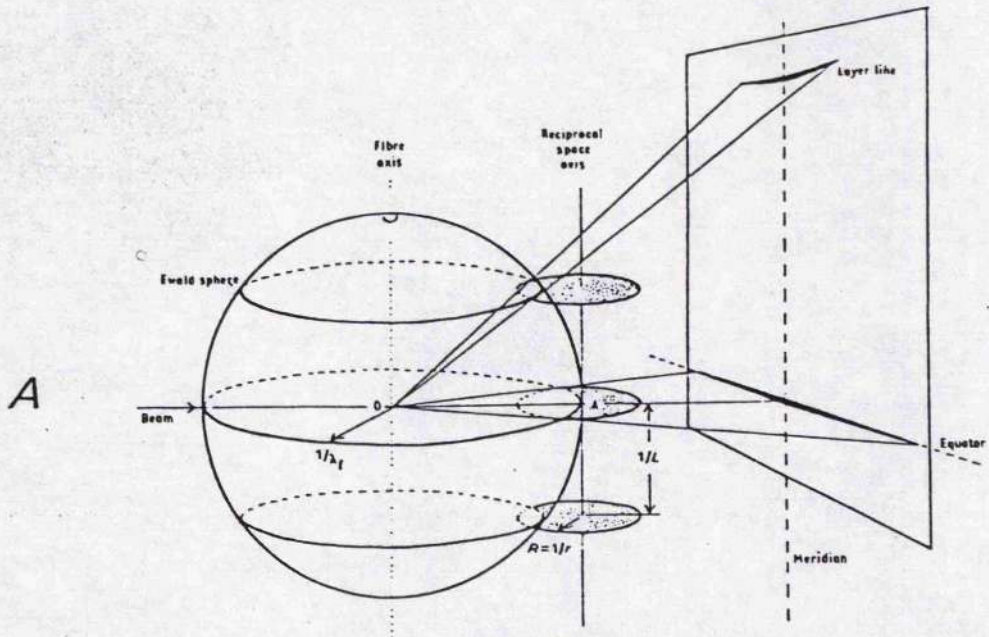
This is a method to construct the diffraction pattern of a periodic diffractor using the wavelength of the incident light within the diffractor, its periodicities and radii in reciprocal space. A single myofibril or a muscle fibre with all its myofibrils in register is a good approximation to this type of diffractor. A diagram of the method is shown in fig 1.23A

Using this technique it is possible to determine the number of orders that are present in the diffraction pattern, the diffraction angles in the meridional plane and the extent of the layer lines.

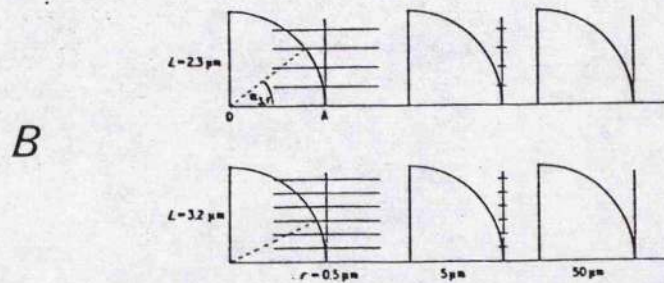
Fig 1.23B shows two side views of Ewald's construction for two sarcomere lengths and three sizes of diffractors. The incident beam is perpendicular to the fibre axis, and the Ewald sphere is the reciprocal of the He-Ne laser line ($\lambda=632.8\text{nm}$). If the diffractor is taken to be the size of a myofibril ($r=0.5\mu\text{m}$) then (depending on sarcomere length) 4-6 orders will be expected, falling to three or less at the whole fibre level. Notice how the diffractor in reciprocal space becomes smaller as the diffraction volume becomes bigger. If the wavelength is reduced then the size of the diffractor in reciprocal space remains constant, but the Ewald sphere (which varies in size as the reciprocal of the wavelength) becomes larger.

Ewald's construction explains why the intensity profile of

Fig 1.23



Ewald's construction for a cylindrical diffractor of radius r , consisting of homogeneous layers of alternating density, creating diffracting planes perpendicular to the diffractor axis with a periodicity L . The incident beam axis is perpendicular to the diffractor axis. The stippled discs are a representation of the diffractor in reciprocal space.



Lateral views of Ewald constructions made to scale for three diffractors as in Fig. 1 with radius $r = 0.5 \mu\text{m}$ (myofibril), $5 \mu\text{m}$ ('column' of myofibrils) and $50 \mu\text{m}$ (fibre) with periodicity $L = 2.3 \mu\text{m}$ (upper) and $L = 3.2 \mu\text{m}$ (lower). The radius of Ewald's sphere is based on the condition for He-Ne laser light of $0.633 \mu\text{m}$ wavelength divided by the refractive index $n_i = 1.38$ of a muscle fibre. Intersections of the discs in reciprocal space with Ewald's sphere indicate possible orders of diffraction and diffraction angles within the diffractor.

INTRODUCTION

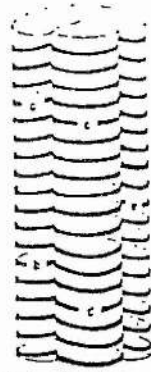
the respective halves of the diffracted orders are not identical. When a diffractor is tilted, so is its transform in reciprocal space. By tilting the diffractor in the meridional plane (ω -scan) the intensity of the layer line is reduced. The maximum intensity occurs when the tilt angle ω equals the Bragg angle. Under other conditions there may be skew of the diffracted planes, this leaves the periodicity unaltered, but when the diffractors are transformed into reciprocal space their axes are not parallel with the fibre axis and so may not intersect Ewald's sphere symmetrically, giving rise to layer lines in one half of a diffracted order but not in the other. This phenomenon is demonstrated in fig 1.24, where a hypothetical muscle fibre with the units a-e containing areas of well defined tilt and skew, is shown in fig 1.24A. Fig 1.24B shows the transform of this fibre. Notice the resulting layer lines in fig 1.24Bb and how they only appear if the diffractors intersect or are enclosed by Ewald's sphere.

To summarise simply the diffractors - single or bundles of myofibrils will because of their size, tilt and skew occupy different positions in the reciprocal space axis. If a diffractor is partially or completely enclosed by the Ewald sphere (whose size is inversely related to wavelength) then it will give rise to a layer line. The extent of the layer line will depend on the amount by which the diffractor lies within the Ewald sphere, and the intensity of a given order will depend on the extent to which the diffractors are in register.

Zite-Ferenczy et al make several suggestions to help overcome the problems caused by uneven first order profiles when determining the sarcomere length of single muscle fibres.

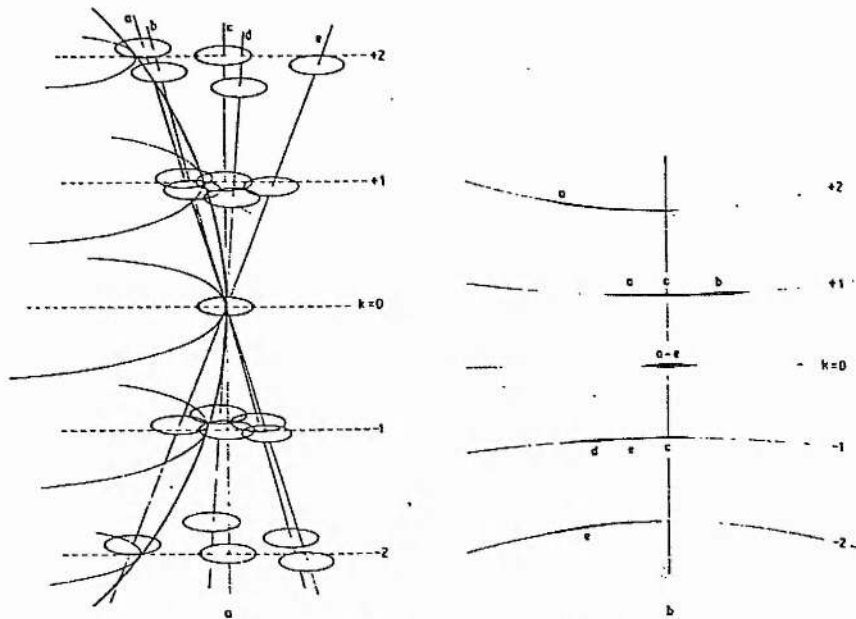
Fig 1.24

A



Hypothetical structure of a muscle fibre. 'Columns' (a-e) of myofibrils contain regions with well-defined regular diffracting planes differing in their skew angles from their surroundings. These regions act as diffracting units. We assume that within a diffracting unit the periodicity is nearly constant over many sarcomeres, whereas in the 'transition zones' the sarcomere length is not uniform. This model is in agreement with observations by light and electron microscopy.

B



(a) Representation in the reciprocal space of a diffractor composed of five diffracting units (a-e) having identical periodicity but differing in the skew angles of their diffracting planes. The axes of all diffracting units are parallel to the fibre axis and perpendicular to the incident beam. (b) The diffraction pattern created by such a composite diffractor does not display homogeneous layer lines but layer-lines composed of 'streaks' which are contributions to the diffraction intensity of units which fulfil the diffraction condition. Layer lines of different diffracting orders have a different streak structure.

INTRODUCTION

- 1.) that a large diameter ($>1\text{mm}$) laser beam should be used.
- 2.) The separation of the orders should be measured at the meridian of the diffraction pattern.
- 3.) That the diffraction pattern should not be compressed meridionally with lenses.

An alternative method is proposed by Goldman & Simmons (1979). Most experiments are carried out with the incoming beam having normal incidence on the fibre, which is not necessarily the Bragg angle. The method Goldman & Simmons use is to allow for variable angles of incidence, by directing the beam onto a rapidly oscillating mirror. Using this system it is possible to change the angle of incidence but not the position of illumination on the fibre.

III. BACKGROUND TO THE WORK DESCRIBED IN THIS THESIS

Hill (1953a) investigated the optical properties of resting striated muscle subjected to rapid stretch. Using 'white' light he reported that if a rapid stretch was applied to resting muscle there was a transient decrease in transmitted light intensity (see fig 1.25A), and that this was due to a change in the light scattering power of the muscle, rather than a change in its diffracting power. This was shown by moving the detector away from the centre of the zero-order and recording the lateral intensity of the zero-order. If the optical transient was caused by a change in diffracting power, rather than light scattering, then no matter where the intensity was recorded it should fall; but if it was a change in light scattering the transient should reverse, which was the case (see fig 1.25B).

Later, Hill (1968) showed that the resting tension exerted by a relaxed muscle was generated by a small number of 'active' cross-bridges which form relatively stable linkages between the actin and myosin filaments, giving the muscle short-range elastic properties. He referred to these collectively as the short range elastic component, or SREC. Flitney (1975) recorded the tension and optical transients that occurred when a frog sartorius muscle was subjected to ramp and hold stretches of up to 1.5% of the rest length. Examples of the transient responses are shown in fig 1.26. The results showed a triphasic response. First, during the early part of the stretch there is a rise in the resting tension during which time transparency falls. Then there is an abrupt

FIG. 1.25

A. Two examples of the transient change in the zero order direct intensity during and after a stretch applied to resting muscle.

B. Two examples of the transient change in the zero order lateral intensity during stretch of resting muscle.

(all traces from Hill, D.K.; 1953a)

Fig 1.25

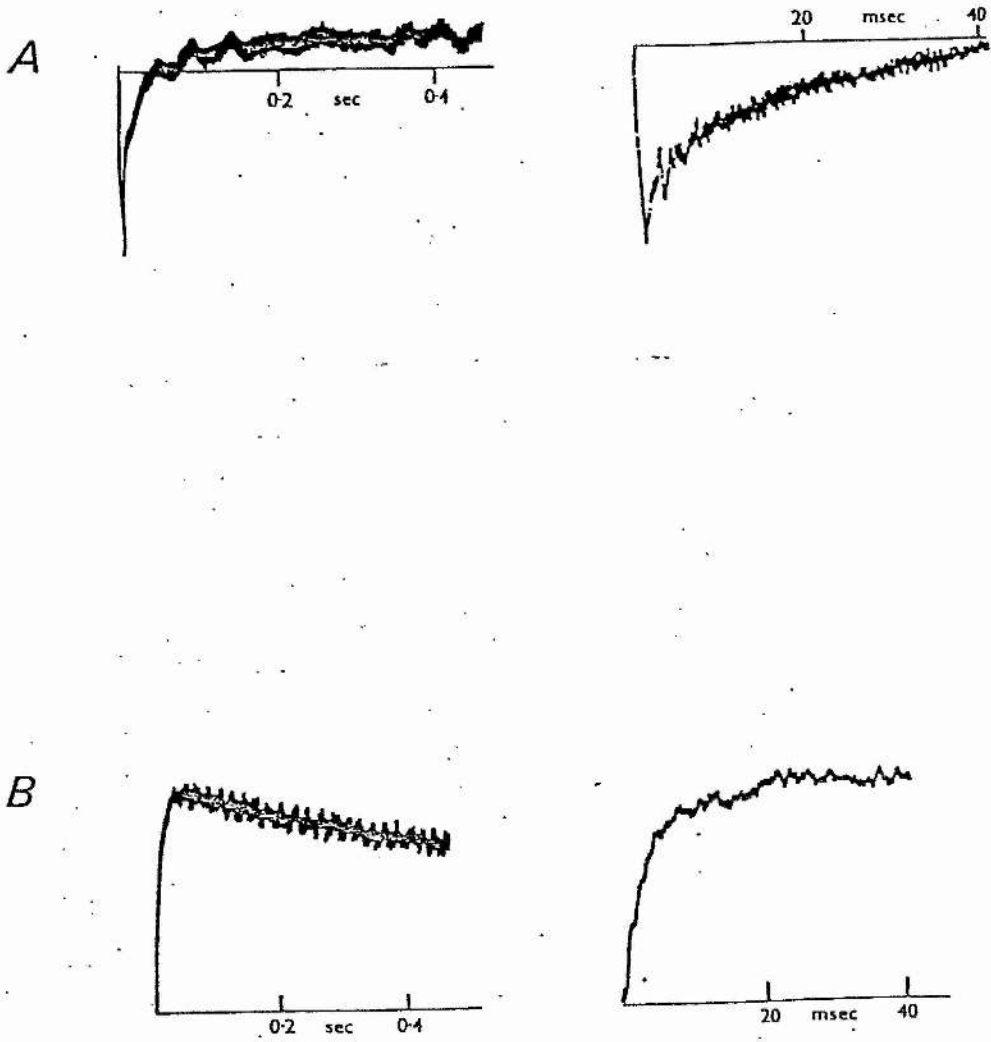
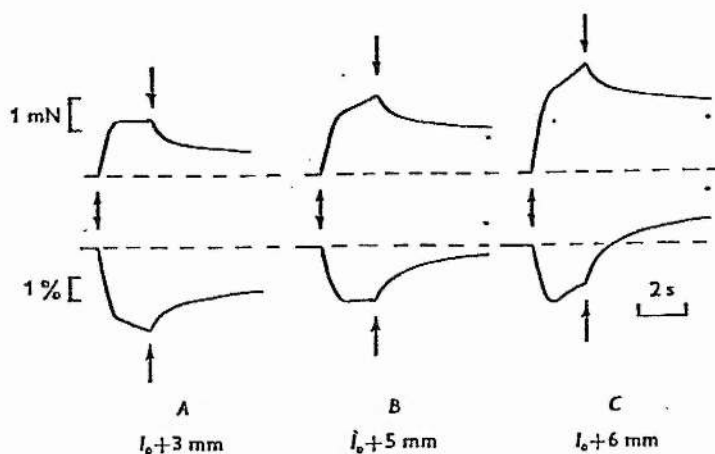


Fig 1.26



Tension (upper trace) and transparency changes (lower trace) resulting from stretch ($207 \mu\text{m}$, velocity, $100 \mu\text{s}^{-1}$) at three different muscle lengths. Light guide, zero, direct. Temp. 0°C . Osmotic strength, $1.65 \times \text{NR}$. Vertical arrows, onset and end of stretch. Records traced from original chart recordings.

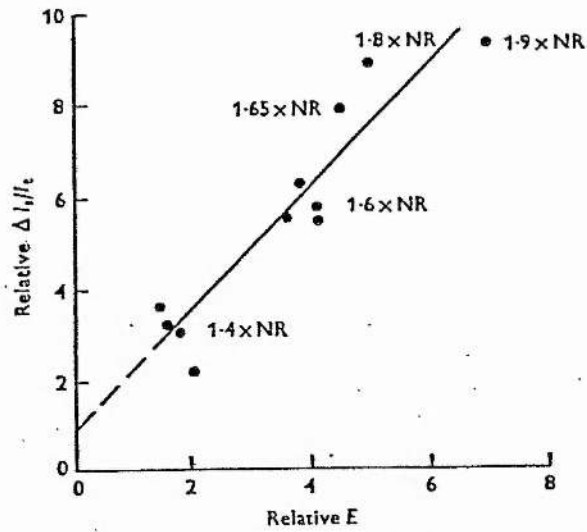
From Flitney (1975)

INTRODUCTION

change in slope in both the tension and the optical signals where, depending on the length of the muscle, the transparency and tension may decrease, increase or remain constant until the end of the stretch (see fig 1.26). At the end of the stretch both the tension and optical signals 'decay' to new steady state levels. Interestingly, the light and tension transients are reversed on release. The elastic limit of the SREC is at the junction between the first two phases and corresponds to a relative sliding movement of the filaments of 3.4nm. By varying the osmotic strength of the Ringer solution bathing the muscle low levels of activation were possible, which potentiated the SREC and Flitney shows that the optical transient is proportional to the amplitude of the SREC and therefore to the number of attached cross-bridges (see fig 1.27).

This thesis explores the possibility of a similar optical transient when a muscle is stretched at the plateau of a tetanus. The changes in tension and in the sarcomere length when stretch of 7-10% of the muscle rest length is applied at the plateau of a tetanus were investigated by Flitney and Hirst. The movement of the sarcomere diffraction pattern was recorded using cine film. The changes in sarcomere length and tension were examined during a single ramp and hold stretch (Flitney & Hirst, 1978a; fig 1.28) and during cyclical stretches (Flitney & Hirst, 1978b; fig 1.28). First in the case of single ramp and hold stretches the sarcomeres were seen to 'give' when sufficient stretch to displace the filaments by 11-12 nm had been given. Secondly, the stiffness of the sarcomeres during active stretch varied inversely with length at sarcomere lengths greater than 2.4um. From these

Fig 1.27



Effect of hypertonicity on E and $\Delta I_i/I_t$. Normalized values of both parameters increase progressively as the osmotic strength is raised. Osmotic strength of solutions marked near points. Continuous line fitted by regression analysis.

From Flitney (1975)

FIG 1.28

A. Example of sarcomere movements during a ramp and hold stretch applied at the plateau of a tetanus.

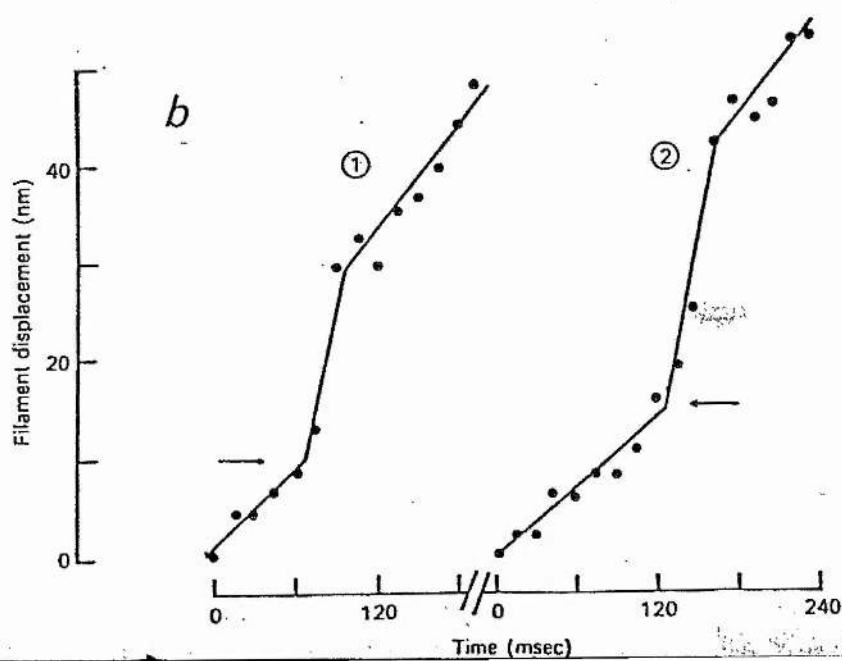
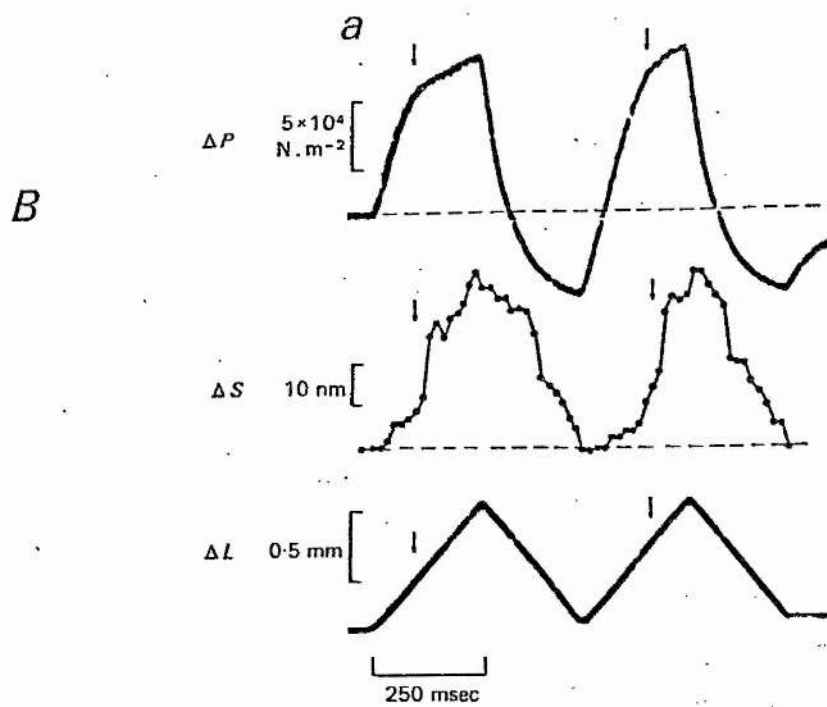
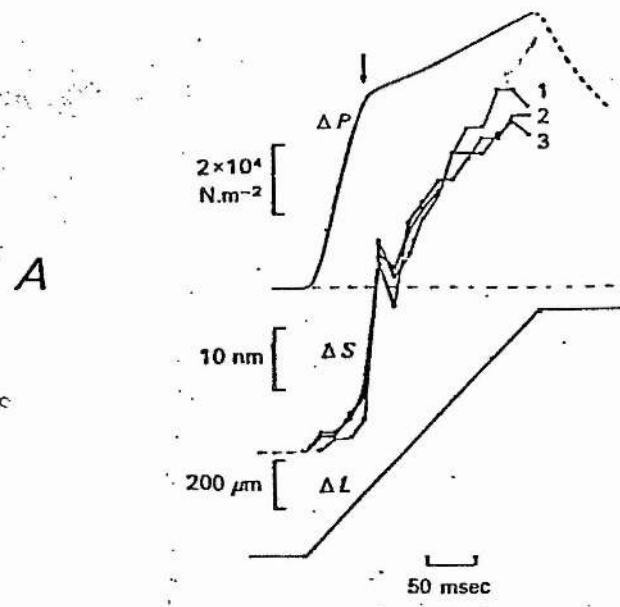
(Flitney & Hirst, 1978a)

B. Example of a stretch then release and re-stretch. Notice how during re-stretch the filament sliding before sarcomere 'yielding' is greater than in the preceding stretch.

Bb. This shows on an expanded scale the sarcomere movements during a first stretch (1) and re-stretch (2).

(Flitney & Hirst, 1978b)

Fig 1.28



INTRODUCTION

results Flitney and Hirst were able to give evidence favouring a range of movement for cross-bridge actin interaction of approximately 12nm. They also showed that the strength of a cross-bridge is independent of the surface-surface distance between the filaments. Using single fibres Edman, Elzinga, & Noble(1978) did not find 'give' of the sarcomeres. Flitney and Hirst(1978a) ascribe this to the much greater series compliance in whole muscle. In a personal communication to Edman (Edman, 1978) Flitney observes that the effect is seen if a series compliance is introduced in a single fibre preparation.

In a later paper Flitney & Hirst studied sarcomere movements that occur when cycles of stretches are applied at the plateau of a tetanus (Flitney & Hirst, 1978b; fig 1.29). This paper provides evidence for a second force producing site. This suggestion is made because the relative sliding distance required to induce sarcomere 'give' is 11-12nm when a single stretch is applied at the plateau of a tetanus but, if a release is given prior to stretch, then this distance increases to 18nm.. Both papers are discussed more fully in later chapters dealing with the optical changes during stretch.

CHAPTER II

CHAPTER II

TRANSPARENCY CHANGES DURING STRETCH OF ACTIVE MUSCLE

o

I. EXPERIMENTAL DESIGN AND RESULTS OF A PRELIMINARY STUDY

INTRODUCTION

The background to the present investigation can be directly traced to the studies of resting muscle by Hill (1949, 1953a, 1968) and Flitney (1975), reviewed earlier. In the first of these, Hill (1949) showed that stretch caused a transient decrease in transparency and he went on to demonstrate (Hill, 1953a) that this was due to an increase in the light scattering power of the muscle. Then, in a seemingly unrelated study (Hill, 1968), he showed that resting muscles exhibit an unusual form of short range elasticity, which he attributed to a small population of myosin projections forming long lasting connections with neighbouring actin filaments. The possibility that the scattering effect might be caused by the deformation of Hill's 'resting' cross-bridges, was later taken up by Flitney (1975), who made simultaneous recordings of muscle transparency and tension during stretch. These experiments revealed a striking similarity between the form of the tension transient and that of the associated transparency change. Moreover, a component of the optical signal, identified as being a change in light scattering, was seen to vary in the same sense as the mechanical stiffness of the short range elasticity, when this was made to change by altering the experimental conditions.

These observations pointed the way for the present study. It was recognised at the time that a similar approach might offer a novel means for studying structural changes in the force generating elements of actively contracting muscles. The myosin

CHAPTER II

projections are thought to interact with actin by undergoing repeated cycles of attachment, tilting and detachment, so as to generate a relative sliding motion between two sets of filaments. Each cross-bridge acts independently of the others and this asynchronous behaviour has made it difficult to investigate the details of the force generating process. This problem can be overcome, to some extent, by subjecting isometrically contracting muscles to controlled (ramp) stretches: the sliding motion of the filaments constrains the cross-bridges to move in one direction and it forces them to do so in a synchronised fashion. This idea is the basis of the experiments described here.

The work was carried out during 1978-1985. The essential features of the experimental design remained the same throughout this period, although it became necessary to make certain modifications to both apparatus and the experimental protocol from time to time, in light of the results. The investigation is therefore presented chronologically, so that the nature of these changes and the reasons for making them can appear in their proper context in subsequent chapters.

This chapter outlines the apparatus and methods used in the earliest experiments, made during 1981. Some aspects of this work have already been published (Flitney & Eastwood, 1982).

MATERIALS AND METHODS

I. EXPERIMENTAL MATERIAL

Animals. The experiments were made using isolated sartorius muscles of the Common frog, Rana temporaria. The animals were imported from Eire (The Frog Farm, Kells, Co.Meath.) and kept in shallow tanks at 4°C until required. The tanks were cleaned daily and frogs that showed any sign of disease were removed. No attempt was made to feed the animals and they were generally used within 2-3 weeks of delivery.

Dissection procedure. The animals were stunned by a blow to the head and killed by inserting a probe down the vertebral canal to destroy the spinal cord. The procedure for removing the muscles was as follows. First, an incision was made through the skin and continued round the body at the level of the mid-abdomen. The leg musculature was exposed by stripping away the skin covering the lower half of the body. The legs were separated from the body by a transverse cut and pinned out on to a cork board at an angle of 180°. The sartorii were identified and the in situ length (l_0) measured using a pair of dividers. A blunt needle was used to make a space between the tibial tendon and the underlying bone. The tendon was then secured by a double knot formed from four parallel strands of cotton thread. A small stainless steel hook was tied to the knot to provide a means of mounting the preparation in the muscle chamber. The tibial tendon was then severed and the sartorius freed from neighbouring muscles by gently pulling on the thread and teasing away adhering connective tissue fascia with a pair of fine dissecting scissors. The process was

CHAPTER II

continued in the anterior direction towards the pelvic tendon, taking care to avoid any damage to the muscle, especially in the region close to the pelvic tendon where the fibres spread out laterally. Once the muscle had been separated along its entire length, it was removed by sectioning the pelvic bone, along the plane of the pubic symphysis, using a sharp razor blade. The small piece of bone remaining attached to the muscle served to help secure it in the apparatus.

II. APPARATUS

A. Mechanical systems

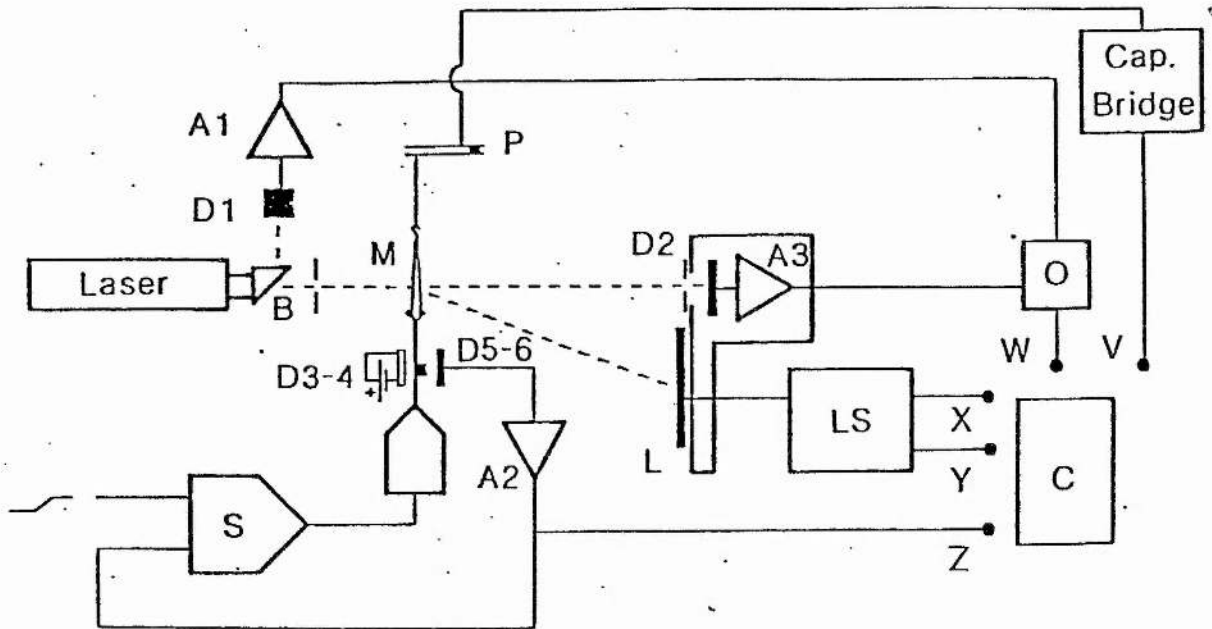
The apparatus is shown diagrammatically in fig 2.1. The muscle (M) was suspended vertically in a glass walled chamber with its tibial end uppermost, and superfused with Ringer's solution (NaCl, 115 KCL, 5; CaCl₂, 2; buffered to pH 6.9 with sodium phosphates, 5 (mM)) in a closed circuit system. The solution was gravity fed to the base of the chamber from a reservoir (cap. 1.5l) surrounded by a glycol-water jacket. The temperature of the jacket was thermostatically controlled using a heater cooler system (Grant Ltd., type FH115 and FC20 units, respectively) capable of providing chamber temperatures down to -1°C. The circulation was maintained by a peristaltic pump (Watson-Marlow Ltd., type MHRE 200) which returned the solution to the reservoir from an outlet located at the top of the chamber. The volume of the chamber was ca. 30ml. and the flow rate ca. 200ml.min⁻¹. The temperature within the chamber could be maintained to within ±0.5°.

Tension Transducer. The muscle was attached to the tension transducer (P) via the stainless steel hook and a short length

FIG. 2.1

Diagram of the apparatus used in the experiments presented in this chapter.

Fig2.1



A1-3, current-voltage converters; B, beam splitter; C, storage oscilloscope; D1-6, photodiodes; P, tension recorder; L, position sensitive photodiode; M, muscle; O, source-ratioing system; V-Z, oscilloscope input, tension, zero-order intensity, first order position, first order intensity and stretcher position, respectively; S, waveform generator.

CHAPTER II

of fine silver chain. The transducer was a variable capacitance gauge, similar in design to that described by Huxley & Simmons (1968) for use with single fibres, but of a more robust construction to enable it to record the greater forces produced by whole muscles. It had a compliance of $100\mu\text{m}\cdot\text{N}^{-1}$ and a resonant frequency of 1.8kHz. The voltage output varied linearly ($\pm 2\%$) with load over the range 0-1.5N, and long term stability was better than $50\text{mN}\cdot\text{hr}^{-1}$.

Stretcher System. The pelvic (lower) end of the muscle was secured by a stirrup formed at the upper part of a platinum rod, approximately 7cm. in length. The rod passed through a water-tight seal in the base of the chamber and its tip was inserted into the chuck of a moving coil electromagnetic puller (Ling-Altec, type 201). This was used to apply ramp stretches/releases to the muscle. It was powered by a 130 watt amplifier (DC-100kHz) and a Servomex (type LF 141) waveform generator (not shown) provided the command signal.

The movement of the armature was servo-controlled using the system described by Flitney & Hirst (1975) but with infra-red (rather than visible) light emitting and recording photodiodes. The motion of a flag attached to the shaft of the platinum rod was used to modulate the light from IR emitting diodes D3 and D4, and the change in intensity was detected using matched IR photodetectors D5 and D6. The comparator circuit was also modified to avoid the possibility of corrupting the position signal by the command waveform.

Stimulator. The muscles were stimulated through broad platinum electrodes fitted to the inner surface of the chamber. A custom built stimulator was used, designed to

generate square pulses (.01-100ms duration) at frequencies ranging from 0.1Hz-5kHz. Its output was variable, from 0-20V @ 4A, and could be set to give either +ve., -ve. or alternately polarised pulses. The stimulator was triggered from an external source or operated manually, in either single shot or pulse train modes.

B. Optical system

Light source. A helium-neon laser (Scientifica & Cooke Ltd., type SLH 15) illuminated the muscle. This produced a narrow (ca. 1mm) beam of light at a wavelength (λ) of 632.8nm. The beam was linearly polarised (polarisation ratio >100:1) and arranged such that its electric vector was parallel to the long axis of the muscle.

Fluctuations in the output intensity of the laser beam were measured and found to be ~1% random noise and 4% rectified 50Hz ripple from the power supply. Preliminary experiments showed that these noise levels were unacceptable and steps were therefore taken to improve matters by means of a source ratioing system. The design was similar to that used by Anson & Bayley(1976). The laser beam was made to pass through a glass coverslip (B) inclined at 45° to the optical axis. This caused a small percentage (ca.1-2%) of the light to be deflected on to a reference photodiode (D1; RS type 303-719). The output of D1 was passed through a current to voltage converter (A1) and thence to the denominator of an analogue divider (O; Burr Brown Inc., type 4192). The output of the photodiode used to record the intensity of the zero order transmitted light (D2, see below) was fed to the numerator and the divider performed the function $(10.N)/D$. Care was taken

CHAPTER II

when operating the system to ensure that both the reference and zero order detectors functioned linearly over the range of intensities encountered during an experiment. It was sometimes necessary to attenuate the laser beam in order to meet this requirement and this was done using Wratten neutral density filters (Ilford Ltd.). The signal to noise ratio was substantially improved using this means; under optimal operating conditions common mode noise was attenuated by ca. 39dB (ca. 90-fold reduction).

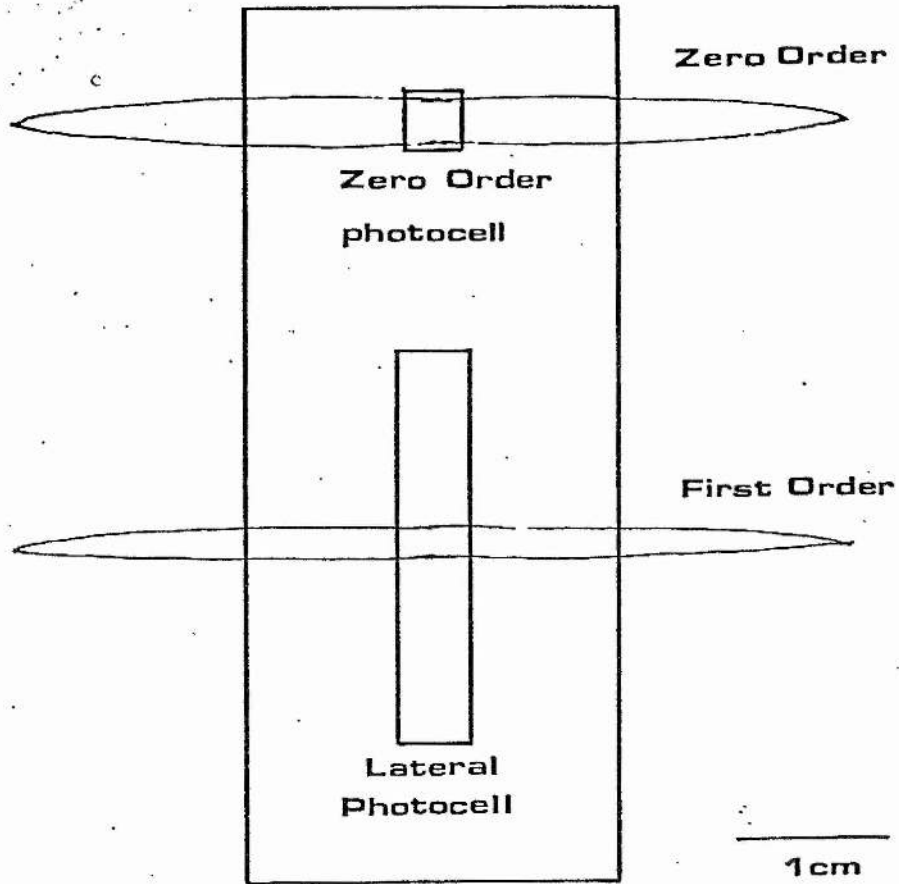
Zero-order recording photodiode. The intensity of light transmitted in the direction of the incident beam was measured using photodiode D2 (RS, type 303-719). This has an active area of 100mm^2 and was operated photoconductively using a JFET operational amplifier as a current-voltage converter. It was mounted on an aluminium plate located in the vertical plane parallel to and 10cm. away from the muscle long axis. Light entering the detector was collimated by means of a 4mm. x 4mm. square aperture giving an acceptance angle of 2.3° .

Position sensitive photodiode for measuring sarcomere lengths. A position sensitive photodiode (Silicon Detector Corp., type SD116-21-11-391) measured the separation of the zero and first order diffraction maxima and this was used to calculate resting sarcomere lengths. The device was mounted on the aluminium plate, vertically below the zero order photodetector (fig 2.2). It was operated photoconductively and the output from each half of the diode fed to its own current to voltage convertor. The sum of the two outputs (A+B) passed to the denominator of an analogue divider (Burr Brown Inc., type DIV100) and their difference (A-B) to the numerator. The

FIG 2.2

This diagram shows the manner in which the diffraction pattern fell on the detector plate.

Fig 2.2



CHAPTER II

output voltage of the device varied linearly with the position of the first order maxima and experiments showed that its performance was not affected by changes in the first order intensity over a 30-fold range.

III. PROTOCOL

Freshly dissected muscles were mounted in the chamber and perfused with Ringer's solution at temperatures ranging from 2-8°C. The muscle was adjusted to its in situ length by raising/lowering the tension transducer assembly on a screw mount. The laser beam was directed into the chamber and on to a region of muscle located 5-10mm from the pelvic tendon. Here, the fibres form a relatively thin sheet (5-6 fibre thick) and it is therefore possible to generate reasonably clear diffraction spectra. The zero-order detector was aligned on the optical axis by moving the detector plate in both X and Y directions, using a two-dimensional, micrometer-actuated stage, until the transmitted light intensity was maximal. The sarcomere spacing at rest was then measured using the position sensitive photodiode. Sarcomere lengths were calculated from the relation:

$$s = \lambda / \sin \theta \quad (2.1)$$

where θ = angle subtended at the muscle between the zero and first order beams, λ = wavelength of the incident light (632.8nm), and s = sarcomere length (um.)

The angle θ is given by:

$$\theta = \tan^{-1}(a/b) \quad (2.2)$$

where b = distance between the detector plate and the muscle (=10cm.)

CHAPTER II

a = vertical separation of the zero and first order spectra measured in the plane of the detector plate.

The zero to first order distance, a, is given by:

$$a = d - (v.s) \quad (2.3)$$

where d = centre-centre spacing of the zero and first order detectors.

v = output voltage of the divider

s = position sensitivity (mm.V^{-1}) of the photodiode.

The values which were obtained for muscles held at their in situ length ranged from 2.35-2.45 μm .

Optimal conditions for stimulating the muscles were determined by setting the stimulator to deliver single pulses (0.2ms duration) and gradually increasing the voltage output to give a maximal twitch (Rudel & Taylor, 1969). The stimulus intensity was then set to 1.5 times this value (generally 7-12V) and the stimulator changed to the pulse train mode. The frequency of stimulation was progressively increased to determine the minimum value that would produce a fused tetanus (usually 15-25Hz).

At the start of each experiment the width, W, of the muscle was measured at the level of the region illuminated by the laser beam. When the experiment finished, the muscle was taken from the chamber and the pelvic bone fragment and stainless steel hook were removed. The muscle was gently blotted on filter paper and its mass, M_0 , determined by weighing on a microbalance. The density of the muscle was taken as unity. The cross-sectional area, A, could then be calculated from the following relation:

CHAPTER II

$$A = M_o/l_o \quad (2.4)$$

For some purposes an estimate of the muscle thickness was required. The pelvic region of the sartorius appears roughly elliptical in transversely sectioned material (Hill, 1953a) and its thickness, T , can therefore be calculated from the relationship between cross-sectional area and the dimensions of the major and minor axes (a and b respectively):

$$A = \pi \cdot a \cdot b \quad (2.5)$$

where a = the half width ($W/2$) of the muscle

b = the half thickness of the muscle

therefore:

$$T = 2b = 2(A/\pi \cdot a) \quad (2.6)$$

RESULTS

The pilot experiments established a basis for asserting that a component of the transparency change produced by stretching active muscle is generated by structural changes in the force generating mechanism, the cross-bridges and/or filaments. These results are described below, but first, some consideration is given to measurements of muscle transparency made on resting and activated muscles held at constant length (steady state transparency), since these have an important bearing on the method used for analysing the complex optical transients (dynamic responses) produced by stretching active muscles.

I. Measurements of muscle transparency at rest and during activation.

Dependence on sarcomere length

The steady state transparency of both resting and activated muscles was measured as follows. The intensity of the incident beam, I_0 , was determined by first attenuating the beam, using a Wratten neutral density filter, and then displacing it laterally so that it bypassed the muscle and travelled directly to the zero order detector. The output voltage (V) of the detector was recorded on a storage oscilloscope (Tektronix type 5103N/D13) and used to calculate I_0 ($=V \times N$, where N is the attenuation factor of the filter). The laser beam was then redirected on to the muscle and the filter removed. The transmitted intensity in the centre of the zero order was then measured, first at rest (I_r) and afterwards during a tetanus (I_a). The rest length of the muscle was then increased and the procedure repeated for sarcomere

lengths ranging from 1.9-3.1um..

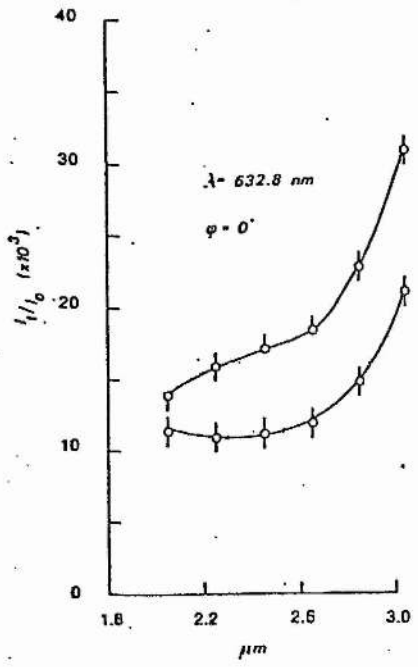
Resting muscles. Fig 2.3 (lower curve) shows the fraction, f_r , of the incident beam transmitted by resting muscles ($f_r = I_r/I_o$) over the range of sarcomere lengths 1.95-3.05um.. The data are mean values (\pm SE means) for 23 muscles. The results show that most of the light entering a muscle (>95%) is either scattered or diffracted by the fibres and relatively little passes through undeviated: at l_o for example, the mean value for f_r (23 muscles) was found to be 11.179×10^{-3} (\pm S.E. 1.090×10^{-3}). Increasing the rest length of the muscles had little effect on their transparency in the range 1.95-2.65um.. This portion of the curve is relatively flat, with a slight upward concavity. However the situation is different at lengths >2.6um.. Here, f_r rises steeply with further increases in muscle length, so that over the whole range studied it increased approximately 2-fold, from 11 to 21×10^{-3} .

Activated muscles. The transition from the resting to the fully activated state caused the transmitted light intensity to increase. This was true for all lengths, but muscles stimulated at intermediate lengths showed the largest increases. The curve relating $f_a (=I_a/I_o)$ to sarcomere length (fig 2.3, upper curve) appears sigmoidal, rising most steeply at both short and long lengths. The region inbetween, from 2.25 to 2.65um., shows an almost linear dependence on sarcomere length with a slope of $6.2 \times 10^{-3} \cdot \text{um}^{-1}$ extension. This last point is referred to again in connection with the procedure used to analyse the dynamic responses (below).

FIG 2.3

Transmitted light intensity (0.6328nm; $\phi = 0^\circ$) for resting and active states (lower and upper traces respectively), plotted against resting sarcomere length.

Fig 2.3



II. Tension and transparency changes produced by stretching active muscle.

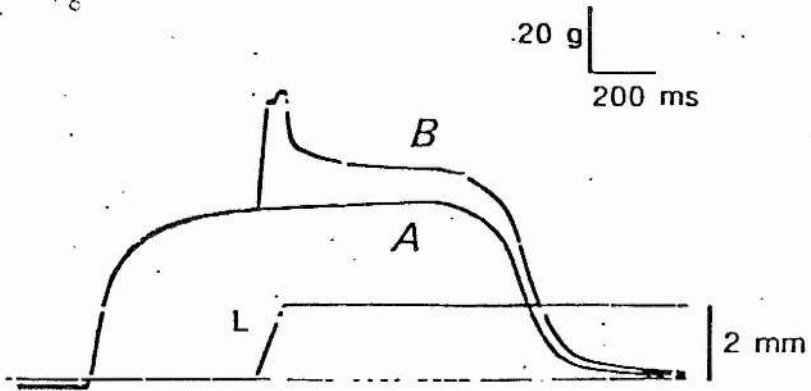
Most of the experiments are concerned with changes in transparency resulting from the stretch of active muscles. In these, muscles were stimulated repetitively for 1-2s using pulses of alternating polarity. Then, at a preset time during the plateau phase of the resulting tetanus, a ramp and hold stretch (amplitude: $0.05-0.1 \times l_0$) was applied to the muscle. Muscle tension, length and zero order light intensity were recorded simultaneously, using a storage oscilloscope and a single channel transient recorder (Datalab Ltd., type DL901) connected to an X-Y/t plotter (J.J.Instruments Ltd., type PL4). The flow of Ringer's solution was halted temporarily during each run, 10-15s prior to the onset of stimulation. This was a precaution against movement artifacts caused by the passage of the Ringer. The muscle was returned to its rest length five seconds after stimulation ceased and the flow of Ringer's solution resumed some ten seconds later. Two coupled Digitimers (Digitimer Ltd., type 3290) controlled the timing of events and the collection of data. The experiments were run on a ten minute cycle time, to allow the muscle to recover between successive contractions.

Tension transients. The form of the tension response produced by stretching an active muscle is illustrated in fig 2.4. This is an oscilloscope recording from an early experiment showing two consecutive tetani. Trace A is an undisturbed tetanus and the superimposed trace B shows the effect produced by a stretch during the plateau phase. The amplitude of the stretch was 2mm and the velocity $24 \text{mm} (=l_0) \cdot \text{s}^{-1}$.

FIG 2.4

Figure showing A. a normal unstretched tetanus. B. the effect of applying a ramp and hold stretch at the plateau of a tetanus.

Fig 2.4



CHAPTER II

The tension transient comprises three distinct phases: an early phase (I) during which tension rises steeply and approximately linearly with muscle length; a second phase (II) when the muscle slope stiffness is substantially reduced, as compared to the first; and a third phase (III), commencing at the end of stretch, when tension decays smoothly towards a new steady state level which is invariably greater than that existing before stretch.

Flitney & Hirst (1978a) showed that the reduction in muscle slope stiffness, marking the transition between phases (I) and (II), is accompanied by an abrupt lengthening of the sarcomeres. Cine film recordings of the diffraction spectra throughout the period of the stretch revealed that sarcomere yielding occurred for a relative displacement of the actin and myosin filaments of around 10-12nm. They postulated that this was caused by the forcible detachment of the cross-bridges linking the filaments together. Their experiments also showed that the exact form of the tension response depends on the length of the muscle prior to stimulation. The transition between phases (I) and (II) is most clearly seen at short sarcomere lengths ($<2.4\mu\text{m}$), where the slope stiffness may decrease to zero or even become negative. It is much less obvious at longer lengths and this is due to the intervention of inert parallel elastic elements, found around and in the fibres (e.g. collagen fibrils, sarcolemmal membranes and possibly longitudinal membranes of the saroplasmic reticulum). Tension generated in these components continues to rise throughout the period of the stretch and adds to that developed in the contractile system, so that the responses take on a more rounded (less angular) appearance.

CHAPTER II

Form of the transparency change generated by stretching active muscles. Fig 2.5 is an early chart recording of the tension response (A) and transparency change (B) produced by stretching an active muscle. Trace B is the displacement signal from the photodetector in the servo-system.

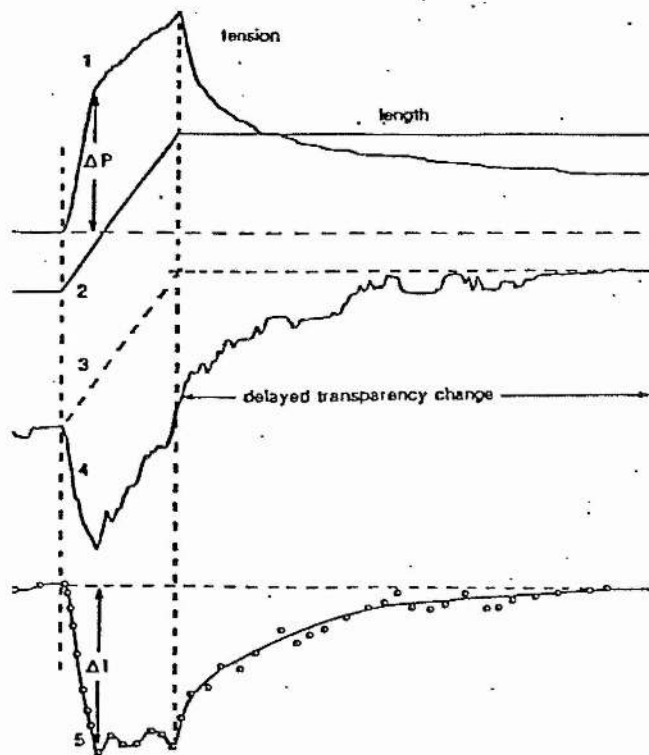
The recording shows that stretch causes a transient decrease in muscle transparency. This is qualitatively similar to that shown by a resting muscle (see, e.g., fig 2.A taken from Flitney, 1975) although its amplitude is much greater. The shape of the signal closely resembles that of the tension transient. It comprises three, easily discernible phases, each of which corresponds to one of the phases of the tension record. The first of these (i), an early decrease in transparency, coincides with the initial steep increase in muscle force; it commences with the stretch, but ends before it is over, at (or close to) the point at which the sarcomeres 'yield'. This event marks the onset of the second (ii) phase where the transparency change reverses direction and begins to increase. Phase iii the delayed transparency change, begins at the end of the stretch. The transmitted light intensity increases during this time, towards a steady state level which is greater than that existing immediately before stretch. This phase parallels closely the decay of tension in the post-stretch period.

The precise form of the transparency change, like that of the tension transient, is strongly influenced by the length of the muscle prior to stimulation. Muscle transparency generally decreases initially, throughout phase i, but there is considerable variability in what happens next. The transparency may continue to fall, beyond the point of sarcomere 'yielding',

FIG 2.5

Procedure used to analyse a transparency change. 1, tension response; 2, length change; 3. time course of the length dependent transparency change; 4, recorded optical signal; 5, tension-dependent component of the optical signal, obtained by subtracting curve 4 from curve 3.

Fig 2.5



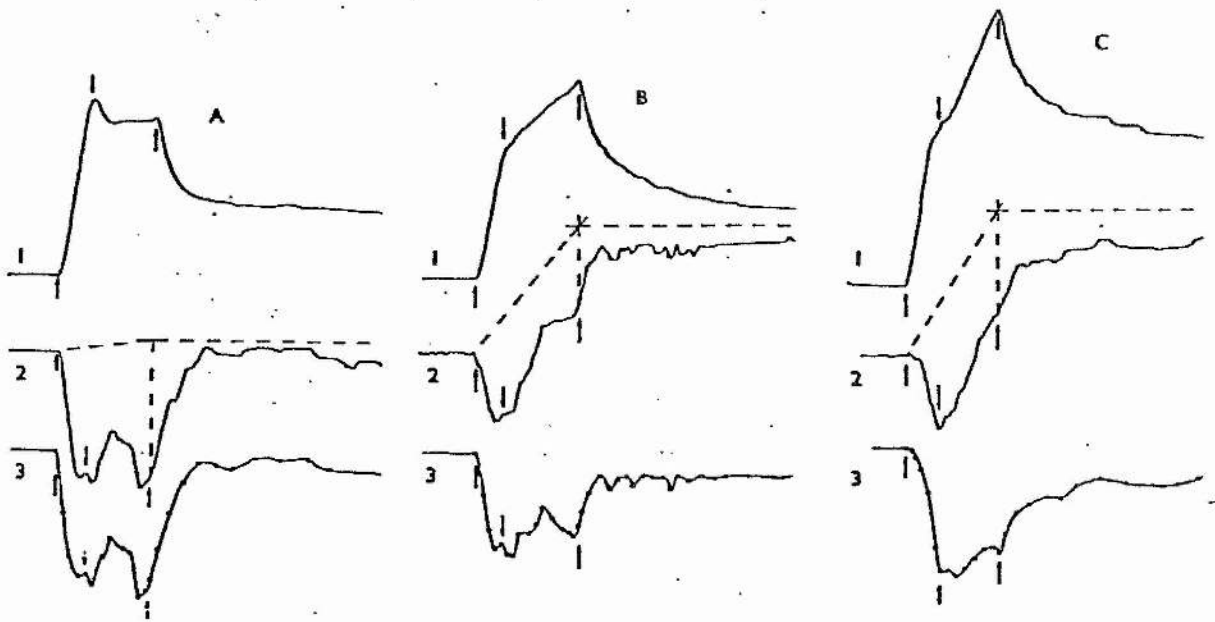
but at a slower rate compared to the first phase; it may remain more or less constant during this time; or, alternatively, it may increase. The increase in light intensity during the delayed transparency change, (phase iii), may result in a final steady state level which is less than, equal to or greater than that existing immediately prior to stretch. These points are illustrated by reference to fig 2.6, where responses recorded at starting sarcomere lengths of 2.15 μ m. (A), 2.25 μ m. (B), and 2.45 μ m. (C) are shown (middle traces). Notice in particular that the sign of the transparency change reverses at the point of sarcomere yielding in records B & C, but not in A. Responses B & C also illustrate that the delayed transparency change can (and indeed generally does) result in a net increase in muscle transparency compared to that before stretch.

III. Quantitative analysis of tension transients and optical signals

The striking similarity in the shape of the optical signals and the tension transients raises the interesting possibility that both phenomena may be caused by the same underlying structural event. The cross-bridges account for most of the compliance in an activated muscle (Huxley & Simmons, 1971; Flitney & Hirst, 1978a) and the form of the tension response is largely determined by their stress-strain properties. It follows from this that the transparency change may be generated, at least in part, by deformation of the cross-bridges.

This idea is amenable to testing, by recording the change in muscle transparency at different degrees of actin-myosin filament overlap: if the hypothesis is correct, then the amplitude of the

Fig 2.6



Three recordings of the tension response and transparency change produced by stretching a muscle at different rest lengths (A, 2.15; B, 2.25; C, 2.45 μm). Lower curves = 'corrected' optical recordings, obtained as described in the text

optical signals should be inversely related to sarcomere length, tending towards zero at around 3.5-3.6 μ m.. In practice, the results of such an experiment are not easy to interpret. This is because the overall shape of the optical signals changes markedly with muscle length, as has been previously shown, and this makes it difficult to decide which feature of the response should be measured. The way in which this problem is resolved, enabling the signals to be studied quantitatively, is discussed below.

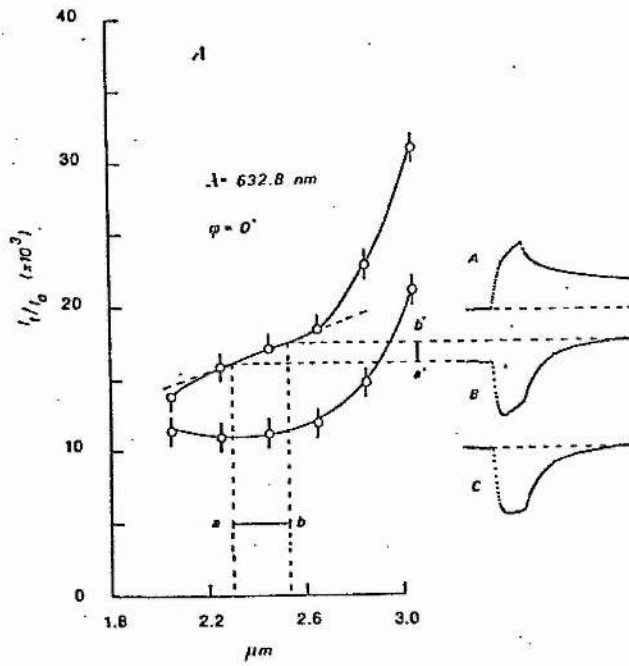
First when a muscle is stretched it becomes thinner, and for this reason alone, its transparency increases. However, the optical recordings almost always show an initial effect of opposite sign: a muscle becomes less, and not more, transparent when stretched. It follows from this that the observed change in muscle transparency must be the resultant of two components of opposite sign: a positive going one, related to muscle length, and a negative going effect related to muscle tension. The form of the response will then depend on the relative amplitudes of these two components.

This can be understood by reference to fig 2.7, where the steady-state measurements of active muscle transparency at different sarcomere lengths are replotted, using data from fig 2.3 (upper curve). Consider what happens on stretching a muscle from a to b. The length change alone would cause the base line to increase, from a' to b'. The centre recording in the righthand panel illustrates how this influences the form of the response. It can be seen that the amplitude of the initial downward deflection will be underestimated if the change in baseline is not taken into account. The situation will be exacerbated at longer muscle lengths, where a stretch of similar amplitude would

FIG 2.7

Active and resting transmitted light intensities plotted against sarcomere length. Shown is an experimental record before and after correction. See text p2.18 for details.

Fig 2.7



generate a much greater offset. Moreover, any component of a signal arising from the cross-bridges would be smaller at longer muscle lengths, in proportion to the decreased amount of filament overlap, and this would make it even more difficult to obtain a reliable estimate of its amplitude.

These considerations highlight the need to make an allowance for the baseline shift, especially so when comparing optical signals recorded at different muscle lengths. There is another, related point to consider in this context. Reference was made earlier to the way in which the tension transients are affected by muscle length. The contribution from inert parallel elastic elements increases steeply with muscle length, giving responses a more rounded appearance, and making it more difficult to estimate the tension borne by the muscle at the point where the slope stiffness falls.

The procedures used for analysing the recordings of tension and transparency in order to compensate for these length dependent effects are described below, and illustrated diagrammatically in fig 2.8.

Tension responses. The contribution from parallel elastic elements is small at short muscle lengths and its effects were generally ignored, except in those experiments that dealt specifically with the way in which the tension responses and optical signals change with muscle length. In these, stretches were first applied to resting muscles. The tension recordings obtained (B, fig 2.8) were then subtracted from those produced by stretching active muscles (A, fig 2.8). The force generated at the point of sarcomere 'yielding' (ΔP) was measured from corrected records (C, fig 2.8). It is expressed throughout in

FIG 2.8

A diagrammatic explanation of the length correction method illustrated for short and long muscle lengths.

A. Raw tension record.

B. Resting tension.

C. Active tension with resting component removed.

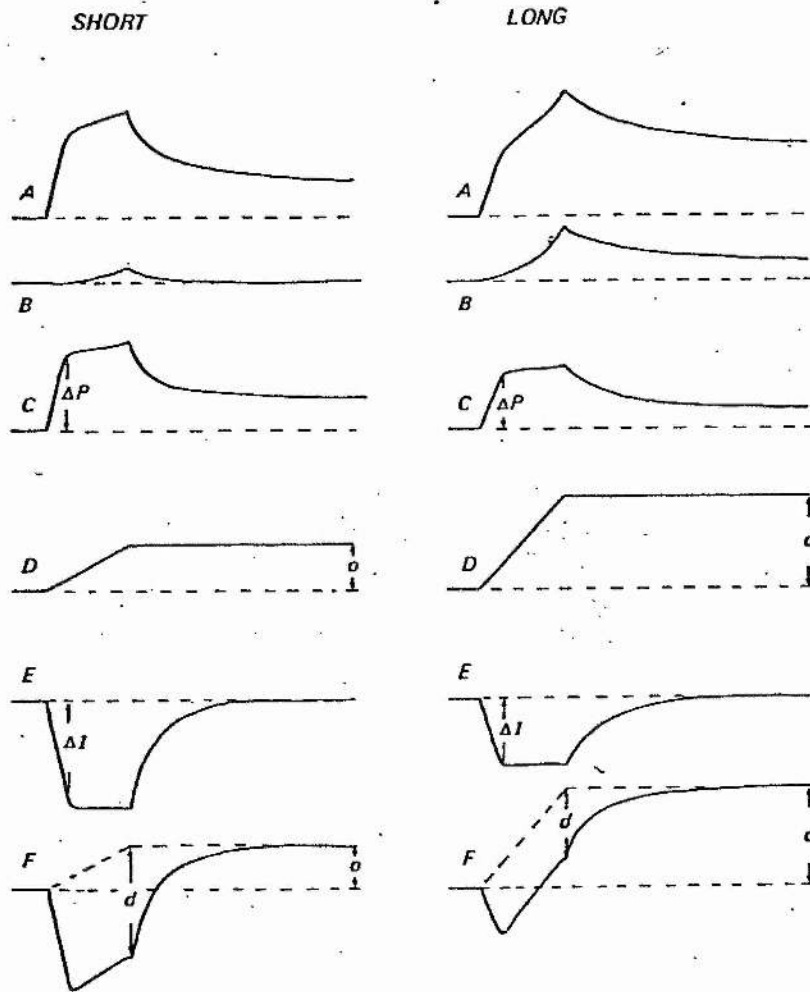
D. Optical length dependent component.

E. Optical tension dependent component.

F. Optical record composed of both length and tension dependent components.

Full details given in text p2.19

Fig 2.8



terms of unit cross-sectional area ($N.m^{-2}$) to facilitate comparisons between muscles of different size.

Optical responses. The procedure for analysing the optical signals involves two further assumptions about the nature of the transparency change:

First, it is assumed that the amplitude of the tension-related component of the response increases during the early part of the stretch and attains its maximum value at the onset of sarcomere 'yielding'. It remains at this high level during the rest of the stretch and then reverses when the new muscle length is reached. The process of reversal is thought to correspond with the delayed transparency change (phase iii), since the amplitude of the latter is almost identical to that of the initial decrease in transparency (phase i) for recordings made at short muscle lengths, where the baseline shift makes only a small contribution.

Secondly, it is assumed that the baseline changes instantaneously and varies linearly with stretch. Although the relationship between muscle transparency and sarcomere length in fig 2.3 appears curvilinear when viewed over the whole range of lengths, small segments of this curve, corresponding to stretches $< 0.1 \times l_0$, approximate to a straight line. This is evidently so for the region between 2.2-2.5 μm . (where most experiments were conducted) and it is very nearly the case for stretches made at longer lengths.

Having regard to all these factors, the procedure adopted for removing the length-related contribution from the optical signals is as follows. First, the light-intensity level reached on

completion of the delayed transparency change (iii) is determined. This value is extrapolated backwards in time to the point where the stretch ends (horizontal dashed lines in fig 2.8,F) where it is joined by another straight line (see assumption (2) above) to the value existing immediately prior to the stretch. The contribution from the tension related component alone is then obtained by subtracting the actual signal from that given by the dashed lines (see, for example, curves C & D in fig: 2.5). The amplitude of the tension-related transparency change, measured from corrected records (E, fig 2.8), is defined as $\Delta I/I_a$ where ΔI is the change in light intensity recorded at the point of sarcomere 'yielding', and I_a is the transmitted light intensity at the onset of stretch.

IV. The relationship between ΔP and $\Delta I/I_a$ under different experimental conditions.

The suggestion was made earlier that a component of the transparency change might be caused by deformation of the cross-bridges and it was pointed out that this hypothesis could be tested simply by comparing responses made at different amounts of actin-myosin filament overlap. It was not feasible to monitor sarcomere lengths in these experiments and for this reason $\Delta I/I_a$ could not be related to filament overlap directly (Flitney & Hirst, 1978a). The relationship between ΔP and $\Delta I/I_a$ was therefore studied instead.

It is worth noting here that if the hypothesis is correct, then any procedure which alters ΔP should produce a corresponding change in $\Delta I/I_a$. In view of this, two different methods for changing ΔP were used:

First by altering the muscle length (amount of actin-myosin filament overlap) prior to stimulation, keeping both the amplitude and velocity of stretch constant.

Secondly, by changing the velocity of stretch, this time keeping the starting length of the muscle and the stretch amplitude constant.

The second of these approaches requires some explanation. Flitney, Hirst & Jones (1976) showed that ΔP increases steeply with speed of stretch until a certain critical velocity, V_c , is reached, above which it shows no further increase. The critical velocity was found to have a positive temperature coefficient and comparative studies, using frog, toad and mouse muscles, showed that it was related to the intrinsic speed of contraction. These observations, taken together, suggest that V_c is related to the speed of cross-bridge cycling. Hence sarcomere stiffness (and so ΔP) will be maximal for velocities which are sufficiently high ($>V_c$) to effectively preclude cross-bridge cycling, but will be reduced at velocities $<V_c$ where some cross-bridges will still have time to complete their cycle and detach. The latter clearly cannot contribute to muscle stiffness, nor to any optical signal arising from cross-bridge deformation.

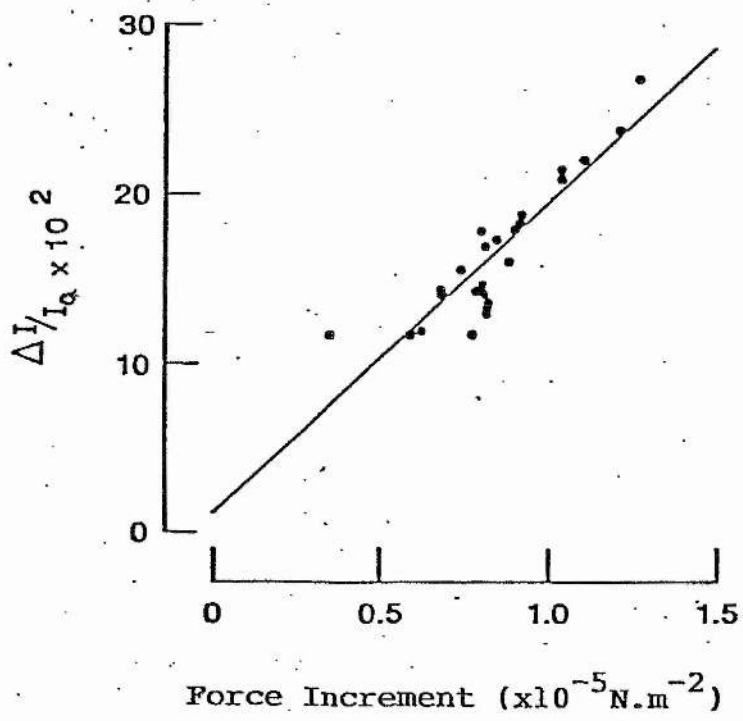
Effect of changing muscle length (actin-myosin overlap) on ΔP and $\Delta I/I_a$.

The results obtained for three muscles (26 recordings) set up at initial sarcomere lengths ranging from 2.1-2.9 μ m. are shown in fig 2.9. The stretch amplitude (2mm) and its duration (50ms.) were kept constant so that the velocity was always 40mm.s⁻¹. The tension transients and optical responses were all corrected for baseline shifts prior to measuring ΔP and $\Delta I/I_a$ as described

FIG 2.9

Active tension increment (varied by changing muscle length) plotted against corrected optical transient at the 'give' point.

Fig 2.9



above.

As can be seen, changing the length of a muscle causes both parameters to change in a parallel fashion. The data show a 14-15 fold increase in both over the range of lengths studied: ΔP varied from $0.1-1.5 \times 10^5 \text{ N.m}^{-2}$ and $\Delta I/I_a$ from 0.02-0.28. The maximum recorded values for ΔP and $\Delta I/I_a$ were obtained when the muscle rest length was set to 2.3-2.4 μm . The sarcomeres shorten during the onset of a tetanus, by as much as 10-15% (Flitney & Hirst, 1978a), so that the real (active) sarcomere length at which both ΔP and $\Delta I/I_a$ are maximal must actually lie close to the theoretical value at which the actin and myosin filaments are fully overlapped, around 2.1-2.2 μm . (Gordon, Huxley & Julian, 1966). The linear regression analysis of the data presented in fig 2.9 gives a value for the slope of the solid line $[(\Delta I/I_a) \cdot (10^5 \text{ N.m}^{-2})^{-1}]$ of 0.18 (correlation coefficient: 0.89).

Effect of changing the velocity of stretch on $\Delta I/I_a$ and ΔP . In these experiments, constant amplitude stretches (1.8mm) were applied to muscles at velocities ranging from 2-36 mm.s^{-1} . The muscles were set up at an initial sarcomere length of 2.3 μm , giving maximal filament overlap in the activated state. The results are shown in fig 2.10 A, B.

Fig 2.10A shows the way in which ΔP and $\Delta I/I_a$ change with speed of stretch, here expressed in terms of relative sliding velocity of the actin and myosin filaments (nm.ms^{-1}). The results are for one of the three muscles used in these experiments. As can be seen, increasing the velocity of stretch up to ca. 1 nm.ms^{-1} produced parallel increases in both parameters. Above 1 nm.ms^{-1} neither ΔP nor $\Delta I/I_a$ showed any appreciable increase.

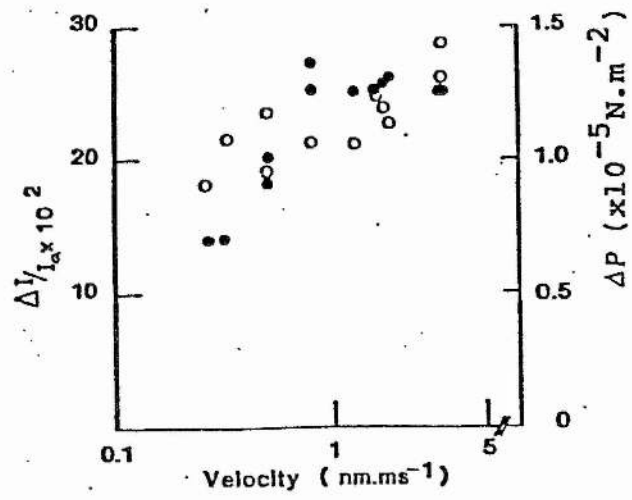
FIG 2.10

A. In this diagram the corrected optical transient and the tension increment are plotted against velocity of stretch. Open circles - optical transient, closed circles - tension increment.

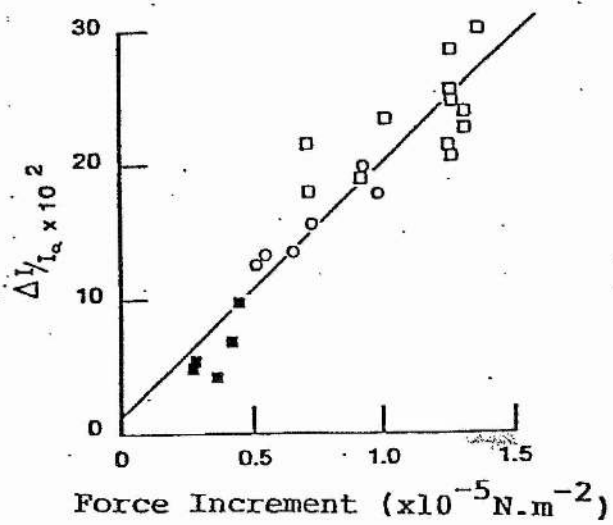
B. Corrected optical transient plotted against tension increment for three muscles. The tension was altered by varying the velocity of stretch.

Fig 2.10

A



B



CHAPTER II

The data for all three muscles used in this experiment (=23 recordings) are shown in Fig 2.10 B, this time with $\Delta I/I_a$ plotted as a function of ΔP . The two parameters are linearly related and the slope of the solid line $(\Delta I/I_a \cdot (10^5 \text{ N.m}^{-2})^{-1}) = 0.188$, which is not appreciably different from that obtained in the preceding experiments where ΔP was varied by changing the muscle rest length.

DISCUSSION

The elastic properties of the cross-bridges determine the principal features of the tension response to stretch (Huxley & Simmons, 1971; Flitney & Hirst, 1978a). The sliding motion of the filaments deforms the linkages, generating extra force, and ultimately causing them to detach. This event is responsible for the onset of sarcomere yielding and for the abrupt fall in muscle slope stiffness. The results of the experiments described here suggest that a component of the transparency change resulting from stretch is also caused by cross-bridge deformation.

This hypothesis is based, first, on the marked similarity in the form of the optical and tension recordings mentioned earlier. It is especially significant that the transition between phases i and ii invariably coincides with the change in slope stiffness (Fig 2.11), because this shows that the early part of the transparency change is influenced by an optical process that parallels cross-bridge deformation, and which is terminated at the point where the linkages reach their elastic limit.

The argument is reinforced by the proven quantitative association of a component of the optical signal with tension developed at the point of sarcomere 'yielding': the results show that $\Delta I/I_a$ changes in parallel with ΔP , when muscle stiffness is varied experimentally, either by altering the extent of actin-myosin filament overlap (Fig 2.9) or by changing the velocity of stretch (Fig 2.10).

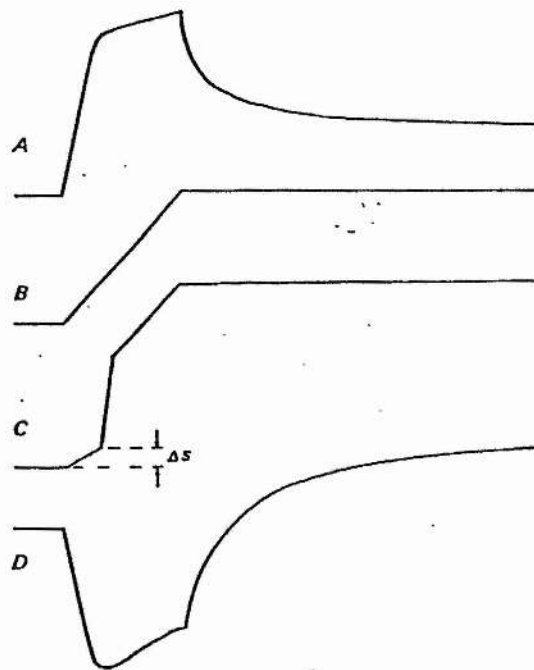
The strength of the previous argument depends on the validity

FIG 2.11

A diagrammatic representation of:

- A. Tension transient.
- B. length change.
- C. Sarcomere movement (increasing length upwards).
- D Optical transient.

Fig 2.11



CHAPTER II

of the method used to analyse the optical signals and there are two aspects of this which require some comment. The first concerns the baseline shift. The origin of this has not been investigated, although it is probable from what was said earlier that changes in the diffracting power of the muscle, as well as changes in its thickness, must make a contribution. Whatever the cause, the steady state measurements of muscle transparency clearly show that the underlying optical processes together combine to make the transmitted light intensity increase with increasing length (Fig 2.3). Moreover it will be seen later that estimates of the amplitude of the offsets, calculated from muscle transparency-length curves like that of Fig 2.3, are in excellent agreement with measurements of actual recordings of dynamic stretches.

The second point concerning the analysis relates to the assumption that the delayed transparency change (phase iii) actually represents a reversal of the process responsible for the initial decrease in muscle transparency (phase i). The argument here has centred on the observation that the two phases are comparable in size for recordings made at short muscle lengths, where any baseline shift is small. At longer lengths, the amplitude of the delayed phase is greater than that of the initial decrease in transparency, because the latter is more strongly attenuated by the baseline shift, which becomes steeper at longer muscle lengths. However, after analysis has been made, the transparency is seen to remain more or less constant through out phase ii and this is so for recordings made at all muscle lengths. It is easy to see that this would not be the case if the delayed transparency change were not equal in amplitude and opposite in sign to phase i. This result is therefore consistent

with the original assumption, though it does not prove it to be true: it could be that another, quite different process begins at the end of the stretch and that this happens (by chance) to be equal and opposite in sign to the first phase. This does not seem at all likely.

The tension transients generated by the stretch of resting muscles are also thought to be due to the flexural rigidity of myosin projections that form long lasting connections with neighbouring actin filaments (Hill, 1968; Flitney, 1975). The properties of the cross-bridges of active muscle differ from Hill's resting cross-bridges in two important respects: first, in being able to accommodate a larger range of filament sliding before reaching their elastic limit; and secondly, in having a much shorter lifetime. How do the present results compare with those reported by Flitney (1975) for resting muscles?

The mechanical stiffness of a muscle is increased as the result of stimulation. Flitney & Hirst (1978a) showed that the elastic limit of the cross-bridges in active muscle is reached for a relative sliding movement of ca. 10nm. The tension increment resulting from stretch at maximum filament overlap amounts to 10^5 N.m^{-2} and so sarcomere stiffness ($\Delta P / \Delta S$) is around $10^4 \text{ N.m}^{-2} \cdot \text{nm}^{-1}$ extension. The corresponding value for resting muscle can be calculated from the data in Figs 2A and 7 of Flitney's (1975) paper. His fig 2A shows tension generated by stretching a muscle in Ringer's solution made hypertonic (1.65 x normal osmolarity) by the addition of sucrose. This procedure enhances the stiffness by a factor of ca. 5x compared to its value in isotonic solution. The force increment was 10mN, which would therefore be equivalent to around 2mN in isotonic solution.

The cross-sectional area of the muscle was 2mm^2 (Flitney, personal communication) so that ΔP is equivalent to 10^3N.m^{-2} . The elastic limit was reached for a relative sliding movement of 3.4nm and so the stiffness amounted to $3 \times 10^2\text{N.m}^{-2}.\text{nm}^{-1}$ extension. Stimulation, then, increases muscle stiffness by a factor of $10^4/3 \times 10^2 = 33$ times. The corresponding transparency changes ($\Delta I/I_{(a,r)}^c$) were 0.18 for active muscle (for $\Delta P = 10^5\text{N.m}^{-2}$, see figs 2.9 and 2.10B), or $0.018.\text{nm}^{-1}$ extension, and 0.002 for resting muscle (for $\Delta P = 10^3\text{N.m}^{-2}$; Flitney's Fig 2A and correcting for the increases in hypertonic solution) or 0.0006nm^{-1} extension. The values for active muscle therefore exceed those for resting muscle by a factor of $0.018/0.0006 = 30$ times. In other words, for a given amount of filament sliding the transparency change and the tension increment increase by about the same factor on going from the resting to the fully activated state.

This result is of some interest but it needs to be interpreted cautiously for two reasons. First, Flitney's experiments were made with a randomly polarised white light source, whereas the present observations were made with a linearly polarised, monochromatic laser source to illuminate the muscles. It will be seen later that $\Delta I/I_a$ is strongly dependent on the wavelength of the incident beam and upon its plane of polarisation relative to the muscle long axis. The degree of agreement noted above may therefore be fortuitous. This matter is taken up again in a later chapter.

Secondly, the velocities of stretch were very different. The resting muscle used in the experiment for Flitney's Fig 2A was stretched at a velocity of 1.6mm.s^{-1} , whereas the experiments

with active muscles used stretch velocities of $40\text{mm}\cdot\text{s}^{-1}$. In fact, it can be shown that this difference is unlikely to affect the outcome of the calculation significantly, because the elastic modulus of resting muscle is extremely insensitive to changes in the velocity of stretch. Reference to Hill's (1968) Fig 6 shows that it is increased 2-3 times for a 10,000 fold increase in stretch speed. Again, arguing on the basis of the proven association between ΔP and $\Delta I/I_a$ one would not expect to see much of a change in the amplitude of the transparency signals with stretch velocity either. This conclusion is borne out by Flitney's observations: his experiments showed that $\Delta I/I_r$ changed only 2.5 times for a 750 fold range of stretch velocities.

CHAPTER III

CHAPTER III

TRANSPARENCY CHANGES DURING STRETCH OF ACTIVE MUSCLE

II.EFFECT OF CHANGING THE PLANE OF POLARISATION OF THE INCIDENT
LASER BEAM

CHAPTER III

INTRODUCTION

Hill (1953) showed that the transparency change produced by stretching a resting muscle is due to an increase of light scattering: this causes more of the light to be deviated by the muscle with the result that less is transmitted in the direction of the incident beam. Flitney's (1975) experiments later established that the scattering change was temporally associated with tension development in Hill's resting cross-bridges. The identification of the underlying process as one of light scattering was based upon comparisons of recordings taken from different regions of the optical field. This technique was not used here, but the way in which the transparency change depends upon the wavelength of the incident light (detailed in a later chapter) suggests that a change of light scattering may also be responsible for the optical signals produced by stretching active muscles.

The phenomenon of scattering is caused by the re-radiation of light from charged particles which are made to oscillate by the fluctuating electric component of the incoming light. The intensity of the light deviated in this way is proportional to the amplitude of the incoming oscillations. This is dependent upon the dipole moment of the scattering centres, and in the case of assymetric scatterers illuminated by a plane polarised source, on their orientation in relation to the electric vector of the incident light. The scattering intensity depends too upon the dimensions of the particles relative to the wavelength of the light source.

Two kinds of structural change could affect the scattering

CHAPTER III

properties of a muscle under these conditions of illumination: changes in the dipole moment of the scatterers, as might result from stretch of compliant structures within the fibres; and changes in the angular orientation of scattering dipoles in relation to the electric vector (E-vector) of the polarised beam, as might result, for example, from tilting of attached cross-bridge heads. The identification of a signal that could be attributed to the second of these processes would be an important result, because an analysis of its form is potentially able to give information on the angular range over which a cross-bridge operates during its power stroke.

The experiments now described are concerned with the effect on the optical signals of changing the angle (ϕ) between the E-vector of the laser beam and the muscle long axis. Recordings made at $\phi=0^\circ$ - that is, with the E-vector parallel to the long axis of the fibre, as in the experiments described in the previous chapter - were compared with those obtained for $\phi=90^\circ$. The results will show that the amplitude of the transparency change ($\Delta I/I_a$) and its form are both dependent upon ϕ .

MATERIALS AND METHODS

The apparatus differed in two respects from that used in preceding experiments.

A. Optical System

The light emerged from the laser with its E-vector vibrating in the vertical plane and this configuration was the one used for the experiments described in the previous chapter. The present experiments had a requirement for light with its E-vector orientated at right angles to this direction ($\phi=90^\circ$). This could have been achieved simply, by rotating the laser head through 90° but this was not a practical solution. An optical device, called a half-wave retarder, was used instead. This is made from a material which is optically anisotropic, that is to say, its optical properties are not the same in all directions within the material. An optically anisotropic material is said to exhibit birefringence, or double refraction, if its refractive index, n , depends on the direction of propagation of the light in relation to the optical axes. Mica is one such material. It is a biaxial material that can be cleaved easily to form sheets in which the two principal optic axes lie almost parallel to the cleavage plane. The E-vector of a plane polarised wave normally incident on a mica sheet is resolved into two orthogonal components which propagate through the crystal at different velocities. This introduces a relative phase shift, $\Delta\theta$, between the two waves, given by:

$$\Delta\theta = (2\pi/\lambda_0)d(|n_o - n_e|) \quad (3.1)$$

Where

λ_0 = wavelength in vacuo

n_o & n_e = refractive indices of the

orthogonal components.

d = thickness of the mica sheet.

The birefringence of the material is defined as $(|n_o - n_e|)$, and the retardation of the plate is $d(|n_o - n_e|)$. The thickness of the sheet can then be selected such that:

$$d(|n_o - n_e|) = (2m + 1)\lambda_o/2 \quad (3.2)$$

where $m = 0, 1, 2, 3 \dots$

and its retardation $(=(m + 1)\lambda_o)$ is then equivalent to a relative phase shift of half a wavelength. Thus for $m=1$ the equation (3.2) becomes:

$$d(|n_o - n_e|) = 3\lambda_o/2 \quad (3.3)$$

and from the equation (3.1), $\Delta\theta = 3\pi$ rads.

Such a device is called a 'half wave' (or $\lambda/2$) plate. The important property of a $\lambda/2$ plate for this present study is that it causes the plane of polarisation of the incident light to be rotated: if the E-vector entering the plate makes an angle θ with one of the principle optical axes, then it emerges having been rotated through 2θ . Moreover, the beam remains linearly polarised.

The arrangement used in the present experiments was as follows. A sheet of mica $\sim 2\text{cm.} \times 2\text{cm.} \times 60\mu\text{m.}$ thick was glued to an aluminium turret which was fitted to the laser head by means of a threaded mount. The turret could be rotated about the optical axis so the the E-vector was either parallel to ($\varphi=0^\circ$) or at right angles to ($\varphi=90^\circ$) the long axis of the fibres.

B. Microcomputer system

A microcomputer and its associated hardware was used to control the experiments and to collect and process the data. This is

FIG. 3.1

Diagram of the computer and transient recorder system.

A., B. Dual channel transient recorders, a-d analogue inputs.

C. Digital plotter.

D. Dual disc drive.

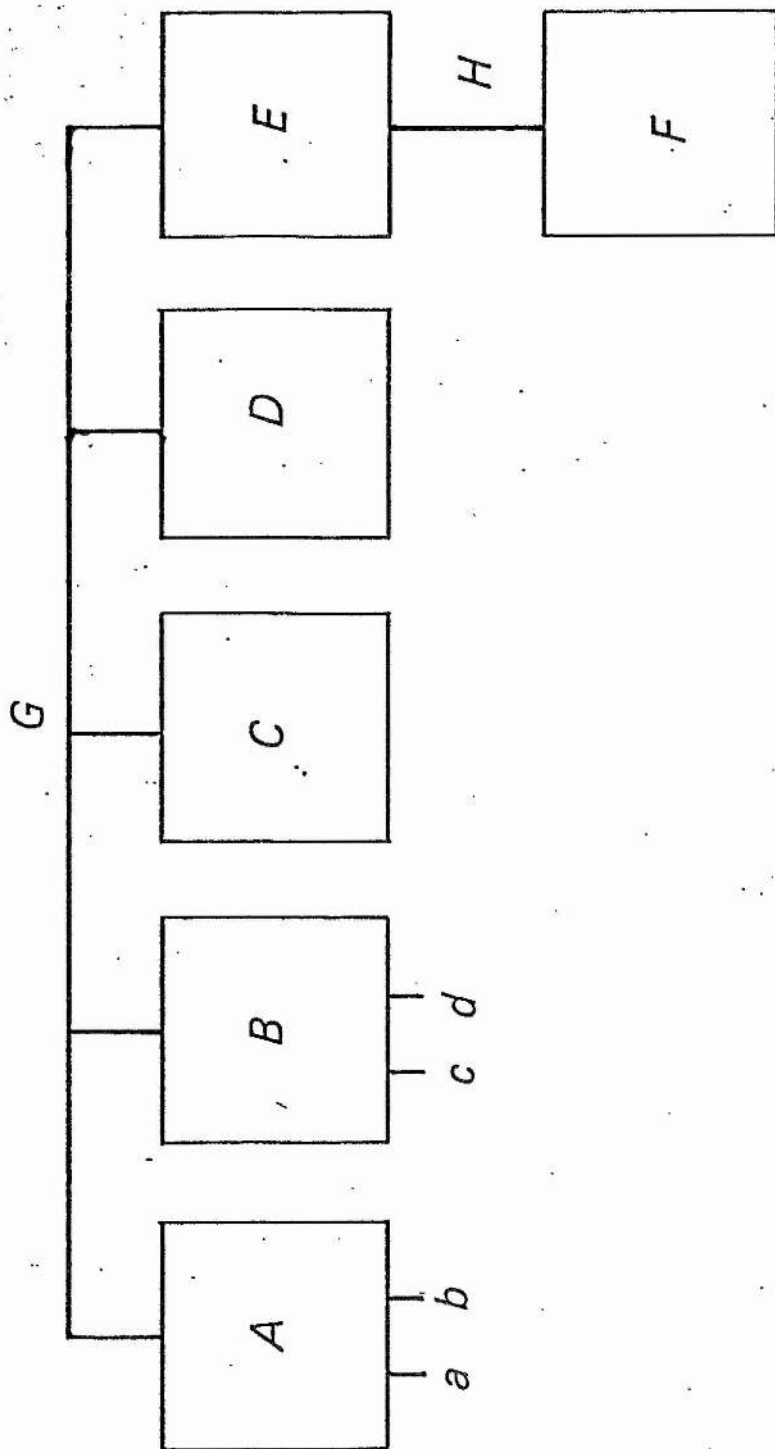
E. H.P. 85 micro-computer.

F. Kratos Digital 'Linkon', serial to parallel converter.

G. IEE-488 interface bus.

H. 20mA serial interface (1200 baud).

Fig 3.1



CHAPTER III

shown diagrammatically in Fig 3.1.

Transient recorders. Two dual channel transient recorders (Datalab, type DL902) were used to capture data from the tension transducer, stretcher position sensor and the zero order photodiode. They each had a capacity of 2kB points per channel, the input sensitivity range was 0.1-5V and they were equipped with 8 bit A/D convertors (resolution 1:256). The sample rate could be adjusted from 1 μ s to 50ms.

Disc Storage Systems. Data from the transient recorders was fed to the computer (via an IEEE-488 interface) and then to a dual floppy disc drive (Hewlett-Packard, type HP8290M) for storage. The device uses 5.25" single sided discs with a capacity of 270k per drive. One disc was sufficient to hold ~30 experimental runs.

Plotter. A Hewlett-Packard flatbed digital plotter (type 7255B) was used to produce A4-sized hard copies from the computer.

Computer. A Hewlett-Packard HP85 microcomputer was used to control the timing of events throughout an experiment and for processing the stored data afterwards. This has 32kB RAM (Random Access Memory) and a full set of HP supporting software ROMs (Read Only Memory). It was interfaced to the transient recorders, disc drives and plotter through an IEEE-488 interface and to the monitor oscilloscope, stretcher, stimulator and solenoid valve through a serial current interface via a serial to parallel convertor (Kratos Ltd., type Digital Linkon.).

C. Experimental Protocol.

Sartorius muscles were dissected and mounted in the chamber, as described previously. Optimal stimulation parameters were

CHAPTER III

determined (18-25Hz., 0.2ms pulses, 10-12 volts) and the temperature set to -4°C . The computer was programmed to deliver a one second tetanus. The transient recorders were triggered to collect data over a two second period, commencing at the time of the first stimulus. A ramp and hold stretch (amplitude, $0.075 \times l_0$; duration, 50ms.) was applied to the muscle 500ms after the onset of stimulation, by which time the isometric tension had fully developed and the muscle was in a steady state. The sample rate was lms and each input contained 2kB data points. The contents of the transient recorders were fed to the computer and then on to the disc drives for storage and later processing.

Aligning the E-vector of the incident laser beam. The plane of polarisation was set at either 0° or 90° with respect to the fibre axis. The method for doing this was as follows. First an analyser made from a dichroic sheet (Polariod film) was placed in front of the muscle, with its fast axis orientated either parallel or perpendicular to the fibre long axis. The $\lambda/2$ plate was then rotated slowly until the emergent light was completely extinguished by the analyser. Hence, with the fast axis of the analyser at 0° the angle $\phi=90^{\circ}$, and vice versa. This process was repeated between tetani such that recordings of the transparency change were made at alternate E-vector orientations on consecutive contractions.

D. Analysing data

The information was stored as character strings so as to economise on archive disc space. Data was taken into the computer and a character-number conversion performed. The data was truncated, so that only the 512 points, containing a period

starting 12ms before and ending 450ms after the stretch (=512 points) was used in the subsequent analysis.

Tension responses. Any contribution from the parallel elastic elements was removed by subtracting the response of a resting muscle from that produced by stretch of an active muscle. The maximum isometric force (P_0) just prior to the stretch was found by computing the mean value of the first 12 data points in the array. The array was then normalised to this mean ($=P/P_0$).

Optical responses: baseline correction. The data from the zero order photodiode and the position sensitive photodiode in the stretcher servo-system were brought into the computer, converted from character to number arrays, and truncated to 512 points as before. The light intensity immediately prior to the stretch ($=I_a$) was computed by taking the mean of the first 12 data points and the array normalised to 100% using this value. The final light intensity reached after the delayed transparency change (I_f) had ended was then computed by averaging points 503-512. The amplitude of the baseline offset is therefore:

$$(I_f - I_a) = (I_f - 100) \quad (3.4)$$

The change in the baseline during stretch was compensated for by normalising the data from the stretcher position sensitive photodiode, such that its maximum amplitude was unity, and then multiplying each data point by the factor $(I_f - 100)$, thereby scaling it to the same amplitude as the offset. The position array was then subtracted from the array containing the normalised light intensity. The results were displayed graphically on the computer screen and a moveable cursor was positioned at the point which coincided with the change in muscle slope stiffness. The values for ΔP and $\Delta I/I_a$ were then computed

CHAPTER III

and printed out. Hard copies of the analysed records were produced on the plotter as required.

RESULTS

I. Steady state measurements of muscle transparency at rest and during activity.

The fraction of light transmitted by muscles at rest ($f_r = I_r/I_o$) and during stimulation ($f_a = I_a/I_o$) at different sarcomere lengths is shown in Fig 3.2 for light polarised at right angles to the muscle long axis ($\phi=90^\circ$). The results for $\phi=90^\circ$ are analagous to those presented earlier (Fig 2.3), but there are some quantitative differences which require comment. First, muscles are more transparent to light polarised at 90° than 0° . This applies to muscles in both the resting and active states. Secondly, the change in f_a over the range 2.0-2.7 μ m is greater for $\phi=90^\circ$ than for $\phi=0^\circ$: the slope of this fraction of the curve is $8.22 \times 10^{-3} \cdot \mu\text{m}^{-1}$ extension, as compared to $6.2 \times 10^{-3} \cdot \mu\text{m}^{-1}$ for $\phi=0^\circ$, with the result that the baseline shift is invariably greater for $\phi=90^\circ$ than for $\phi=0^\circ$.

II. Transparency changes generated by stretching active muscles recorded at orthogonal beam orientations.

Transparency changes resulting from stretch of active muscles were recorded at different sarcomere lengths using alternate (orthogonal) beam orientations. These experiments showed that the response to stretch is highly anisotropic with respect to ϕ . First at any given sarcomere length, $\Delta I/I_a$ was found to be ~ 2 x greater for $\phi=0^\circ$ than for $\phi=90^\circ$. The results for 6 muscles (n = 44 recordings), covering the range of sarcomere lengths from 2.0-3.2 μ m, are shown in Fig 3.3. Here, $\Delta I/I_a$ is shown plotted as a function of ΔP (cf. Figs 2.9, 2.10A,B). The results again show an

FIG 3.2

The resting and active (lower and upper traces respectively) transmitted light intensities (632.8nm) plotted against resting sarcomere length.

Fig 3.2

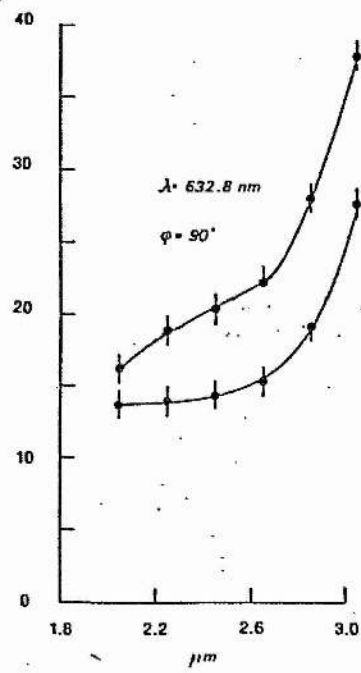
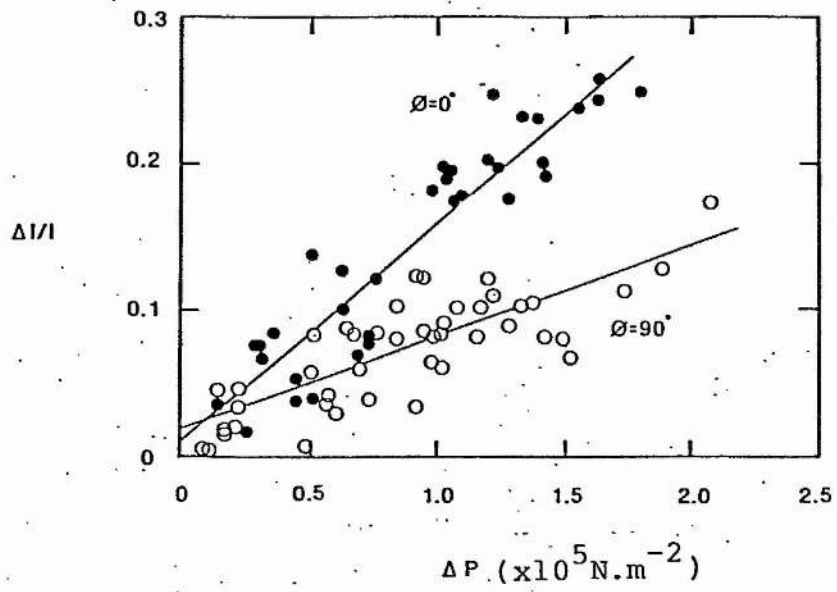


FIG 3.3

Tension increment at the 'yield' point plotted against ΔI .

Open circles $\varphi = 90^\circ$ and closed circles $\varphi = 0^\circ$.

Fig 3.3



CHAPTER III

approximately linear relation between the two parameters, but with different slopes for light at the two beam orientations: thus for $\phi=0^\circ$ the slope of the line $((\Delta I/I_a)/(\Delta P))$ from a least squares analysis equals $0.148.(10^5 \text{N.m}^{-2})^{-1}$ and for $\phi=90^\circ$ the slope equals $0.063.(10^5 \text{N.m}^{-2})^{-1}$.

Secondly, comparison of recordings at the two beam orientations under similar conditions, that is to say, recordings made on consecutive tetani at the same sarcomere length, reveal qualitative differences. Examples of consecutive recordings from two muscles (A,B), specially selected for the comparison because the tension responses (lower traces) were nearly superimposable, are shown in Fig 3.4A. The upper traces show the optical transients, after having made the appropriate baseline correction. In each case, the two signals begin to diverge at (or close to) the point where the muscle slope stiffness declines: the 0° intensity signal continues to fall, whereas the 90° signal increases. This is most clearly seen in the responses from muscle B. The differences between 0° and 90° recordings, obtained by subtracting the 90° from the 0° , are shown in Fig 3.4B. These results are from two other muscles, stimulated at a starting length of 2.3 μm . The traces (upper) show that the difference between the two signals increases during the early part of the stretch, and rises to a maximum value immediately after the sudden decrease in muscle stiffness.

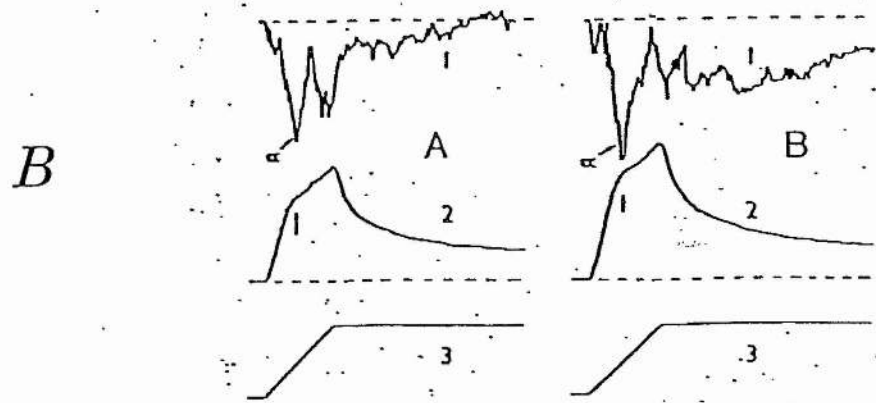
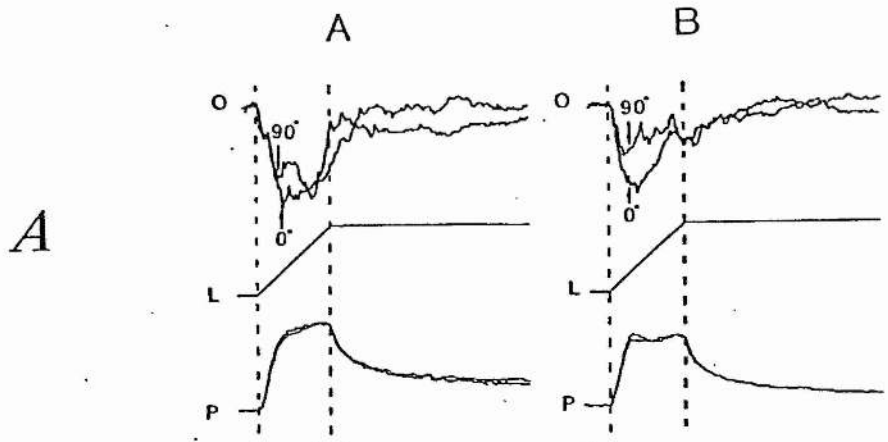
FIG 3.4

A. The upper figure shows consecutive corrected transparency recordings for $\phi = 0^\circ$ and 90° .

- O. - optical records
- L. - muscle length
- P. - tension increment.

B. 'Difference' traces made by subtracting records obtained with $\phi = 90^\circ$ from those recorded using $\phi = 0^\circ$. Note that the difference reaches a maximum just after the decrease in muscle stiffness.

Fig 3.4



DISCUSSION

The experiments described in the preceding chapter provided evidence that a specific component of the transparency change produced by stretching an activated muscle arises as the result of structural changes in the force generating elements. This conclusion was based on two lines of evidence: first the similarity in the form of the tension response and the transparency change; and secondly, the observed relationship between ΔP and $\Delta I/I_a$ at different sarcomere lengths, which implied that $\Delta I/I_a$ varies in direct proportion to the extent of actin-myosin filament overlap. There can be no doubt that the filaments slide past one another during a stretch (Flitney & Hirst, 1978a; Edman, Elzinga & Noble, 1981) and therefore the cross-bridges linking them together must be deformed. This could involve a change in their angular orientation relative to the muscle long axis, and/or a change in the length of either the S_1 or S_2 -HMM sub-units, or both. The filaments themselves are by comparison much less compliant structures (Huxley & Brown, 1967; Huxley & Simmons, 1971) but they transmit the extra force generated by the stretch and presumably become strained, if only by a relatively small amount. Since large particles (relative to λ) scatter light more strongly than small ones, and because the combined mass of the filaments constitutes a greater fraction of the muscle than the cross-bridges, it follows that they could make a significant contribution to the transparency change.

It was pointed out earlier that the intensity of the light scattered by asymmetric particles which are illuminated by a plane polarised source will depend upon the orientation of the

scatterers in relation to the E-vector of the incident beam: the scattering will be maximal when the dipole axes coincide with the plane of vibration of the electric field. A study of the way in which the optical signals vary with ϕ is therefore potentially able to provide information on the nature of the structures responsible for the transparency change. This is because the effect of a stretch on the cross-bridges and on the filaments will be different: the filaments do not change their orientation (with respect to ϕ) since stress is applied in the direction which is parallel to their long axis. In contrast, the orientation of the cross-bridges will undergo a change, and this will have opposing effects on the scattering of light polarised in the two orthogonal directions.

The results presented here show that the transparency change is highly anisotropic with respect to ϕ : the amplitudes of the tension related components of the signals are seen to differ by a factor of more than two times, and moreover, the shapes of the signals appear to be different. It would be premature to draw any firm conclusion from the results at this stage because the comparisons are based on observations which were of necessity made on different contractions: even when the sarcomere length and plane of polarisation of the light remain constant, there is always some variability between results obtained from different contractions, particularly with regard to the precise form of the optical transients, and so while there can be little doubt that the amplitudes of the two signals are significantly different, the same degree of reliance cannot be placed on the differences in their shape. Indeed, this particular problem can only be resolved by making 'simultaneous' recordings of transparency changes at orthogonal beam polarisations. The experiments to be

CHAPTER III

described in the following chapter were designed to enable this to be done.

CHAPTER IV

TRANSPARENCY CHANGES DURING STRETCH OF ACTIVE MUSCLE

III. SIMULTANEOUS RECORDINGS OF RESPONSES AT ORTHOGONAL BEAM
POLARISATIONS.

INTRODUCTION

A.F.Huxley & Simmons' (1973) experiments led to them conclude that each cross-bridge is a 'jointed' structure, made up of two functionally distinct elements connected in series: a force generating element, the myosin 'heads', and an instantaneous elastic element, tentatively identified as being the S2-HMM sub unit. Their hypothesis is that the force required to propel the filaments is generated by a stepwise movement of the attached heads, along the active sites on the actin filament. In their simplest model, the stepping motion is permitted by rotation about the junction between the myosin heads and the instantaneous elastic elements. Flitney & Hirst's (1978a) experiments led them to postulate that most of the sliding movement required to induce sarcomere 'yielding' (~10-12 nm) during a stretch is actually associated with backward rotation of the heads whilst they remain attached to the actin and that only a relatively small amount is taken up by the extension of elastic cross-bridge elements. These considerations mean that several structural events may be involved in generating the transparency change: longitudinal strain in the filaments themselves; longitudinal strain in the elastic elements of the cross-bridge; shearing strain in the attached heads, on the assumption that they may not be entirely rigid; and finally, changes in the angular orientation of the attached heads, relative to the long axis.

From what has been said, it is reasonable to assume that the

relative contribution to any scattering change made by each of those events will depend on ϕ . In particular, changes in the angular orientation of the heads is likely to be important because they would have opposite effects on light polarised at 0° and 90° .

It follows that a careful and detailed comparison of the form of the two signals is required. This could not be made satisfactorily with the experimental arrangement used in preceding chapters, for reasons outlined earlier. Instead, it was necessary to devise a system that would permit optical signals to be recorded at orthogonal beam orientations simultaneously: that is to say during a single tetanus. This was achieved by rapidly switching the plane of polarisation of the incident laser beam electro-optically, using a device called a 'Pockels cell'. Additionally, in previous experiments muscles had been suspended vertically (see fig 2.1) and stretched from the pelvic end, close to the region illuminated by the laser beam. This was considered undesirable for the present experiments because it meant that the area of muscle sampled by the laser shifted appreciably during the stretch: indeed, since the stretches were 1.5-3mm and the beam diameter was ~1mm, by the time the stretch had ended the laser beam was illuminating an entirely different region of the muscle. This difficulty could not be overcome simply by illuminating the tibial end of the muscle, because this is much thicker and optically unsuitable. The problem was therefore solved by mounting the muscle horizontally and attaching the stretcher armature to the tibial (rather than pelvic) end.

MATERIALS & METHODS.

I. APPARATUS.

The modified form of the apparatus is shown in fig 4.1.

A. Mechanical Components

The muscle chamber, stretcher (S) and tension transducer (P) were mounted in the horizontal plane on a common mechanical ground (MG1). It was not possible to incorporate the variable capacitance transducer in the new configuration and so this was replaced with a more conventional device. This comprised a stainless steel bar (3 x 1 x 12mm) onto which two foil strain gauges (RS., type 308-102) were mounted. The compliance of the bar was $\sim 100 \mu\text{N}^{-1}$ and its resonant frequency 2.1kHz. The output of the bridge circuit and amplifier varied linearly (to within $\pm 1\%$) with applied load in the range 0-1.5N.

B. Optical system.

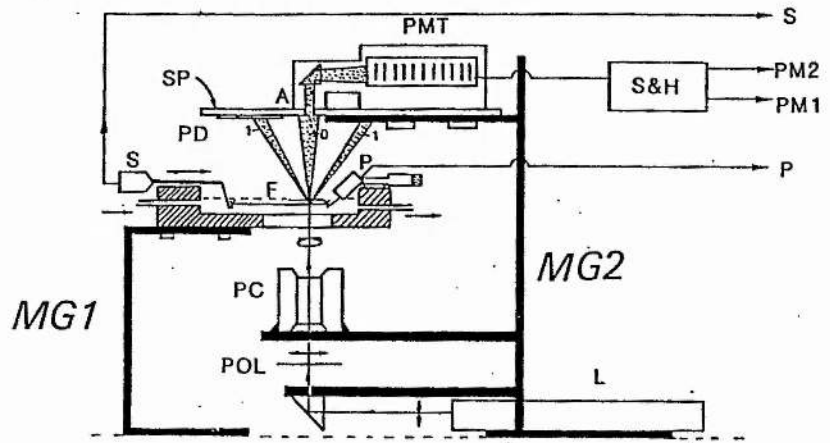
The optical system - comprising the laser (L), Pockels cell (PC) and photomultiplier tube (PMT) housing - was mounted on a moveable mechanical ground (MG2) which was isolated from that supporting the muscle chamber (MG1). This arrangement meant that the position of the laser beam (on or off the muscle) could be changed easily without the need to realign the individual optical components on the optic axis afterwards.

Light source. The laser used in previous experiments was replaced with a Spectra-Physics Stablite model 124B He-Ne laser. This produced $\sim 25\text{-}30\text{mW}$ at 632.8nm. Its output stability was much

FIG. 4.1

Diagram of the apparatus used in the experiments in this chapter (see p4.4 for explanation).

Fig 4.1



CHAPTER IV

greater than that for the Scientifica-Cook laser and the source ratioing system was no longer required.

Pockels cell. Some classes of crystal exhibit an electro-optic phenomenon known as the 'Pockels' effect. The birefringence of such a crystal can be made to change by placing it in an electric field. The induced birefringence is directly proportional to the applied voltage and so the retardation, θ , can be varied as required:

$$\Delta\theta = 2\pi \cdot n_o^3 \cdot r \cdot V / \lambda_o \quad (4.1)$$

where n_o = ordinary refractive index.
 V = applied voltage.
 λ_o = wavelength of light in vacuo.
 r = electro-optic constant.

The response time of crystals which show the Pockels effect is extremely short, typically < 1 ns, and so the orientation of the E-vector of a linearly polarised beam can be rapidly switched by oscillating the applied voltage.

Fig 4.1 illustrates the arrangement used in these experiments. The laser beam was first deflected vertically by means of a prism. This caused some depolarisation of the light and so the beam was passed through a polariser (P), arranged with its fast axis parallel to the long axis of the muscle, before entering the Pockels cell (Electro-Optic Developments, Basildon, Essex, U.K., type PC105-4T). The voltage applied to the cell was generated by a high voltage linear amplifier (Electro-Optic Developments, type LDA50), critically adjusted so as to oscillate the E-vector of the beam through $\pi/2$ radians, between $\phi = 0^\circ$ & 90° , at a frequency of 7.4kHz (see II. Protocol for details). The switched beam then passed vertically

through the muscle and into the photomultiplier housing.

Photomultiplier tube and sample-hold system. The intensity of the zero-order (transmitted) light was recorded using a photomultiplier tube (EMI, type 9558C). This is a 14 stage device which was used with only 10 of its plates connected. The voltage across the tube was 1kV and the anode was connected to earth via a $1k\Omega$ resistor so as to increase its frequency response. The output of the PMT was fed alternately to one of two sample hold ic's (RS, type LF-398). The switching of the Pockels cell and the sampling of the PMT output voltage was synchronised by a clock signal from the de-multiplexor. A schematic diagram of the device and its operational logic pulses is shown in fig 4.2. When the command signal to the Pockels cell changes polarity, it directs the PMT output voltage to one of the sample-hold ic's. After a delay 50us, The PMT voltage is sampled for 10us. The resulting signal is fed to an output amplifier with an adjustable low pass filter (1-4khz) and from there to one of the transient recorder channels. At the next change of polarity, the PMT output is passed to the second sample hold ic, then to an output amplifier and finally to the second channel of the transient recorder. The result is to generate two DC signals each of which registers the intensity of the light transmitted by the muscle at one of the orthogonal orientations.

Performance characteristics of the Pockels cell-sample hold system. Three different experiments were designed to test the performance characteristics of the system.

Expt. I. The optical arrangement is shown in fig 4.3A. A 1khz square wave (50% duty cycle) was applied to the Pockels cell and

FIG 4.2

A. Schematic diagram of the Pockels cell controller and demultiplexor.

B. Waveform diagram of the Pockels cell controller and demultiplexor.

Fig 4.2

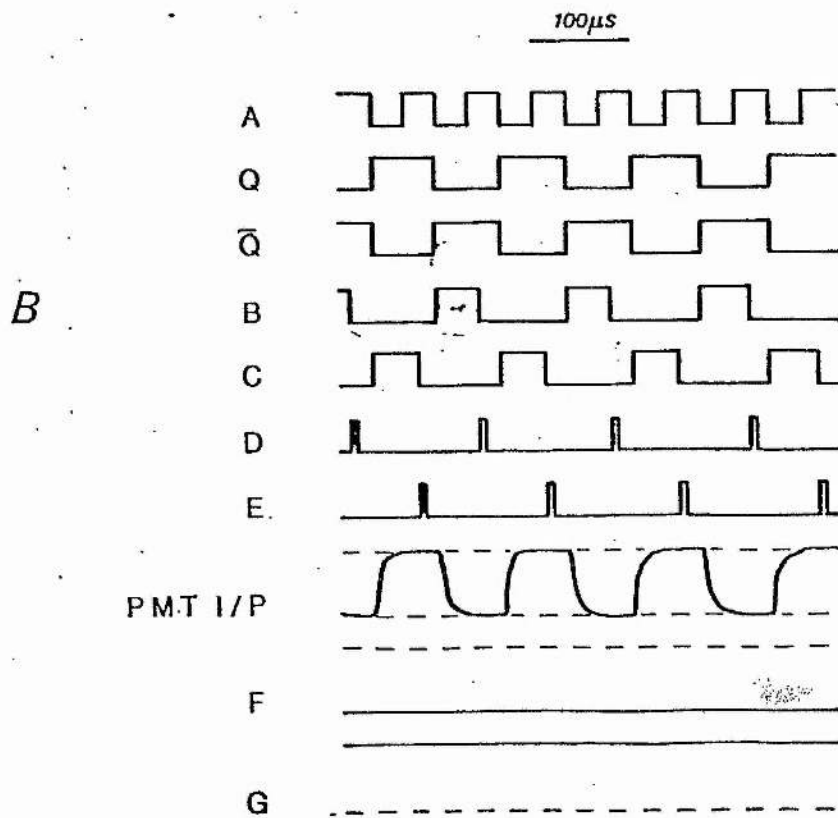
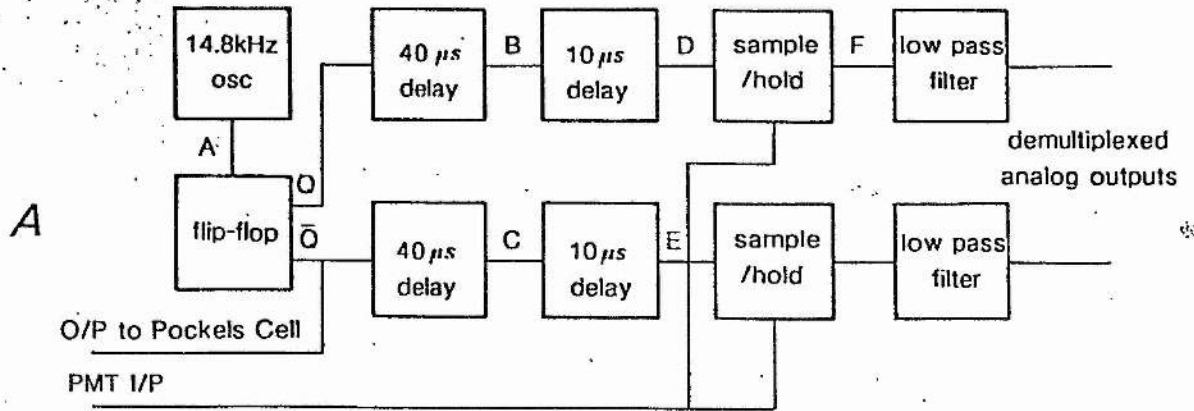
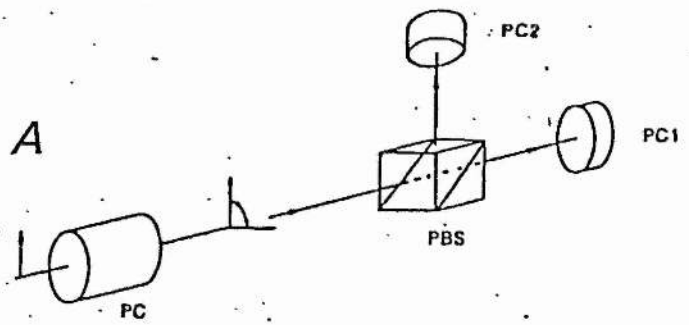


FIG 4.3

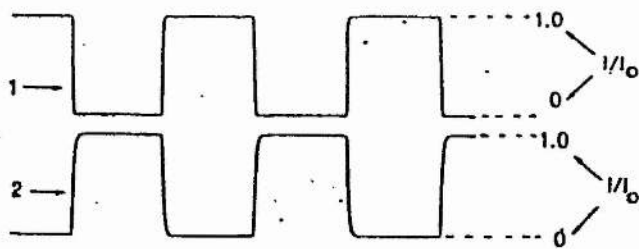
A. Optical arrangement used in Expt. 1 to test the Pockels cell.

B. Waveforms obtained during this test:

Fig 4.3



B



the optical field of the emergent beam resolved into its orthogonal components using a polarising beam splitter (PBS). The change in the intensity of each beam was recorded separately using a pair of matched photodiodes (PC1, PC2). The two signals obtained (fig 4.3B) are of equal amplitude and exactly out of phase, showing that the E-vector is being switched through $\pi/2$ radians.

Expt. II. The optical arrangement is shown in fig 4.4A. Here the switched beam is passed through an analyser (A) arranged with its fast axis parallel to one of the orthogonal directions. The clock frequency was set this time at 8kHz and the intensity of the light transmitted by the analyser was recorded using the photomultiplier tube. The intensity of the transmitted light, I_t

is given by $I_t = I_o \cos^2 \theta$, where θ = angle of polarization of the beam relative to the analyser's fast axis: thus $I_t = I_o$ at $\theta = 0^\circ$, and $I_t = 0$ (complete extinction) at $\theta = 90^\circ$. The recorded waveform from the PMT shows that the rise time (I_t/I_o from 0.1 - 0.9) is $\sim 16\mu\text{s}$, equivalent to a mean optical field slew rate of $5.8 \times 10^4 \text{ rad.s}^{-1}$. 'Complete' transmission/extinction occurs after a settling period of $\sim 45\text{-}50\mu\text{s}$. (The horizontal lines labelled 1-6 indicate the times in the cycle when the sample-hold ic's are normally operational).

Expt. III. The linearity of the switched beams and the efficacy of the sample-hold system was examined using the apparatus shown in fig 4.4A. The analyser was rotated through 180° in steps of 10° and the steady outputs from the two sample-hold amplifiers were recorded on separate digital volt meters. Fig 4.5 is a polar diagram, comparing the theoretical lines ($I_t = I_o \cos^2 \theta$) with the experimental data for the orthogonal polarisations. The

FIG 4.4

A. Optical arrangement used to test the Pockels cell in Expt.

2.

B. Example of the waveform obtained.

Fig 4.4

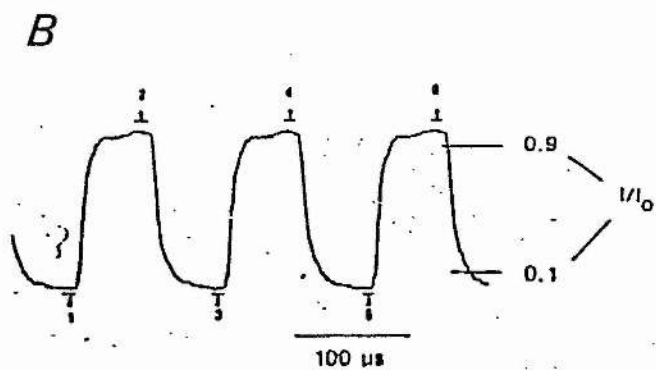
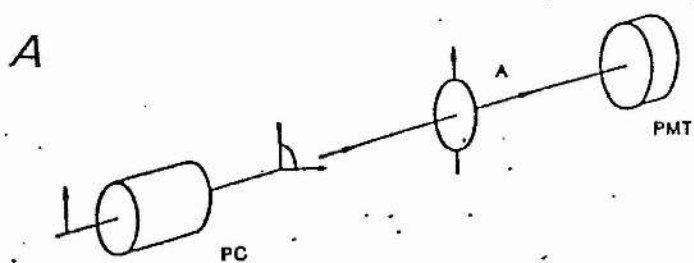
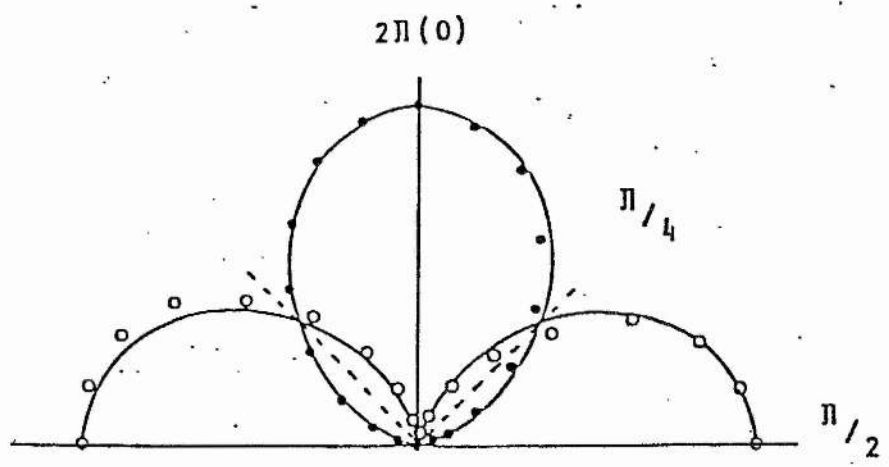


FIG 4.5

Polar diagram obtained in testing the Pockels cell in Expt. 3. The solid lines indicate the theoretical line, whilst the solid and filled circles indicate the results for the orthogonal polarisations.

Fig 4.5



observed values lie close to the solid lines and demonstrate (a) that the linearity is not significantly affected by the switching and (b) that the sample-hold system is operating satisfactorily. Notice, in particular, that the beam intensity is either maximal or extinct when the fast axis of the analyser is aligned in the direction of one of the orthogonal components.

C. Modifications to the data capture system.

The transient recorders were 8 bit devices and were therefore able to quantize the input signals into 256 levels. The optical transients were typically <20% of the light intensity immediately prior to stretch and this meant that they were not always well resolved. The apparatus was therefore modified so that each of the data input lines first passed through a digital backoff device. The 'DC' component could therefore be removed and the input sensitivity of the transient recorders increased so that the signals resulting from stretch filled as much of the available 'window' (256 levels) as possible. The backoffs were designed around RS type 303-040 ic's. The value of the subtracted DC component was fed to the computer for storage via the Kratos 'Linkon' interface.

II. Experimental Protocol.

Muscles were dissected in the usual manner and mounted horizontally in the chamber. They were attached to the tension recorder via the pelvic bone and to the stretcher by the hook attached to the tibial tendon. The laser beam was made to illuminate a region of muscle close to the pelvic end. Sarcomere lengths were measured at rest, using a precalibrated graticule mounted on the front face of the detector plate supporting the

CHAPTER IV

PMT. Stimulation parameters were determined as previously described.

The procedure for aligning the E-vectors of the switched laser beam relative to the muscle long axis was as follows. First, the entire optical system was moved so that the laser beam bypassed the muscle and entered the aperture of the PMT housing directly. This was done by moving MG2 laterally. The PMT was protected at this time by a x1000 neutral density filter and the Pockels cell was removed from the system. An analyser was placed on top of the muscle chamber with its fast axis precisely at right angles to the long axis of the fibres. The polariser on top of the prism was carefully aligned so that the PMT output fell to zero. This polariser attenuated any depolarised component of the beam and ensured that the E-vector was aligned parallel to the muscle long axis before entering the Pockels cell. The latter was then replaced in the optical system and the demultiplexor switched on. The voltage from the Pockels cell amplifier was then adjusted so that the intensity varied from zero (beam extinguished) to its maximal value (full transmission). The analyser was then rotated through 90° and the PMT output checked to ensure complete switching. After critically adjusting the Pockels cell amplifier (see below and fig 4.6) the analyser was removed from the system and MG2 returned to its original position so that the laser beam passed through the muscle.

The output of the PMT is shown in fig 4.6, A-C. Fig 4.6B shows the waveform generated when the Pockels cell is correctly adjusted. Figs 4.6A & C show the waveforms produced when the retardation is less than (A) or greater than (C) that required

FIG 4.6

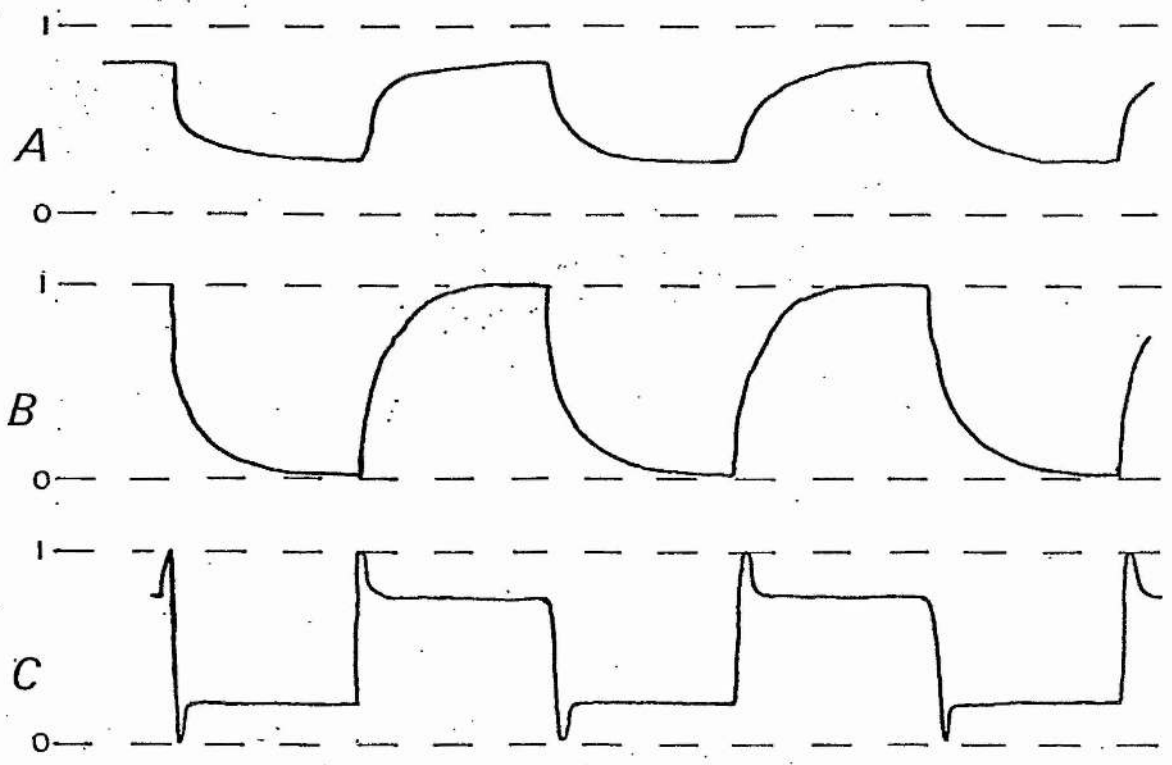
Examples of the waveform obtained from the photomultiplier under the conditions on page 4.9 if:

A. The voltage applied to the cell is too small.

B. Correct

C. Too large, notice the overshoot as the polarisation of the beam passes beyond an orthogonal polarisation.

Fig 4.6



$50\mu s$

CHAPTER IV

to rotate the E- vector through $\pi/2$ radians.

CHAPTER IV

RESULTS

The results for this series of experiments are presented in figs 4.7, 4.8, and 4.9, and in table 4.1. Simultaneous recordings of the transparency signals at orthogonal beam orientations ($\varphi=0^\circ$ & $\varphi=90^\circ$), obtained using the Pockels cell - sample and hold system, are shown in fig 4.7 A - C. The amplitude of stretch was adjusted to be $\sim 0.11_0$ and the duration set to either 50ms (A), 75ms (B) or 100ms (C). Each of the three recordings shown is an average response from 2 - 5 different muscles, including 4 - 30 different individual records (see legend to fig 4.7 for details and also Table 4.1). The optical signals (lower traces) have been corrected to eliminate the baseline shift and their amplitudes scaled to be a fraction (see scale bar) of the light intensity existing immediately prior to the stretch. The 0° and 90° responses are displayed in such a way that the starting light intensities are superimposed. These results clearly confirm that the transparency signal is highly anisotropic with respect to φ . The most obvious difference between the two kinds of recording relates to the amplitude of the responses, though there are important differences in their form also. In confirmation of what was said in the preceding chapter, the data show that $\Delta I/I_a$ for incident light orientated with φ at 0° (referred hereafter as $\Delta I/I_a(0^\circ)$) invariably exceeds that obtained for light polarised in the orthogonal direction ($\Delta I/I_a(90^\circ)$): in this particular series of experiments, by a factor of 1.67 - 2.14 times. Fig 4.8 A-C show the differences in amplitude (A) between the orthogonal responses, computed according to the following expression:

Table 4.1

File Name:-

AV841129

AV850109S

PUBAVE

Parameters	Units	AV841129	AV850109S	PUBAVE
Muscle length	mm	28.75	26.0	30
Peak tension	$\times 10^5 \text{N.m}^{-2}$	1.8 ± 0.056	1.859 ± 0.228	1.77 ± 0.06
Extra tension at 'yield' point	$\times 10^5 \text{N.m}^{-2}$	0.79	0.138	0.853
Stretch amplitude (x)	mm	2.704	2.48	2.88
	\times / l_0	0.094	0.0953	0.096
Stretch duration	ms	50.00	75.00	100.00
Stretch velocity	mm.s^{-1}	54.1	33.1	28.8
	$\Delta l_0 \cdot \text{s}^{-1}$	1.862	1.273	0.96
Δl to 'yield' point	$\Delta l / l_0$	0.0382	0.0364	0.0268
Amplitude of trans. sig.	$\Delta I / I_{a, 90^\circ}$	0.1094	0.1313	0.0906
	$\Delta I / I_{a, 0^\circ}$	0.234	0.219	0.184
normalised trans. sig.	$(\Delta I / I_{a, 90^\circ}) \cdot (10^5 \text{N.m}^{-2})^{-1}$	0.1385	0.1154	0.1062
	$(\Delta I / I_{a, 0^\circ}) \cdot (10^5 \text{N.m}^{-2})^{-1}$	0.297	0.1924	0.2162
Differences between	D^* (eqn 4.2)	0.0864	0.0536	0.0536
$0^\circ - 90^\circ$	D_y^*	0.363	0.250	0.342
No. of records	n	=4	=9	=30

* D^* using the non-normalised values for $\Delta I / I_{a, 0^\circ}$ & 90°

FIG 4.7

Examples of averaged optical transients obtained using the Pockels cell.

A. 50ms - (n = 4, 2 muscles).

B. 75ms - (n = 9, 3 muscles).

C. 100ms - (n = 30, 5 muscles).

Fig 4.7

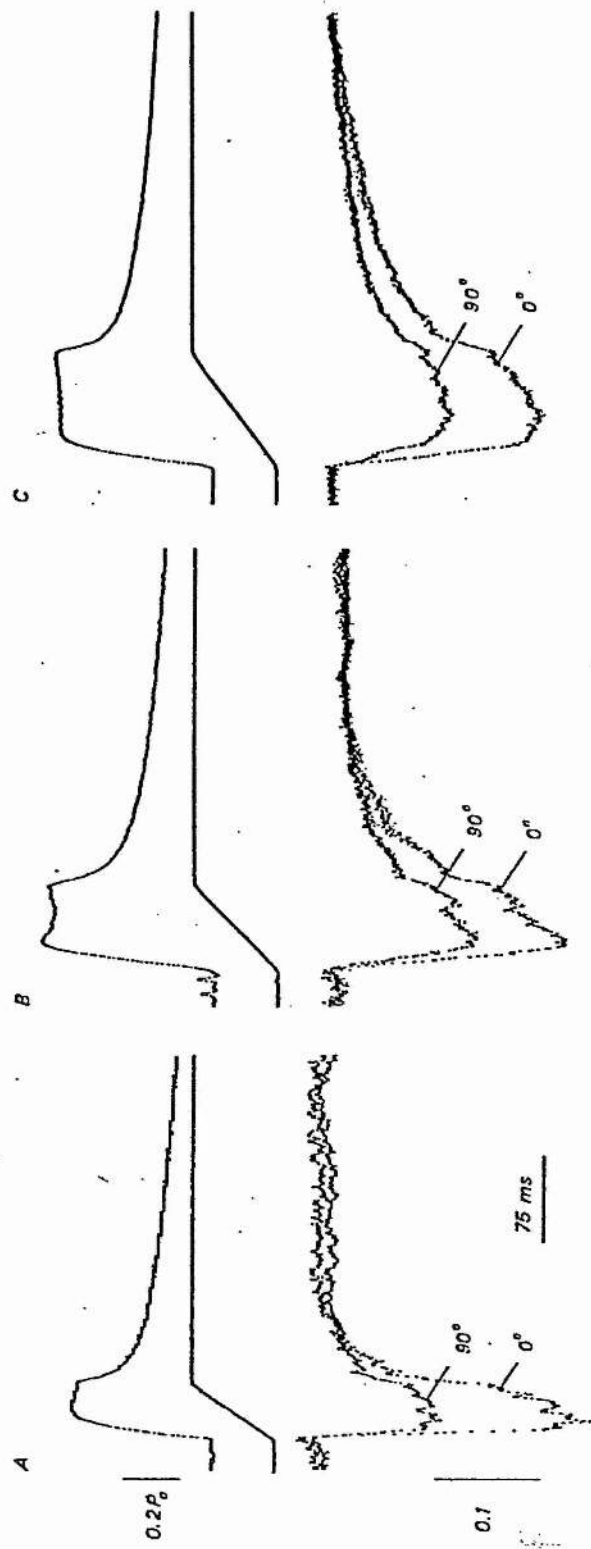


FIG 4.8

Diagram showing the differences traces for the optical data in fig 4.7.

A. 50ms.

B. 75ms.

C. 100ms.

Fig 4.8

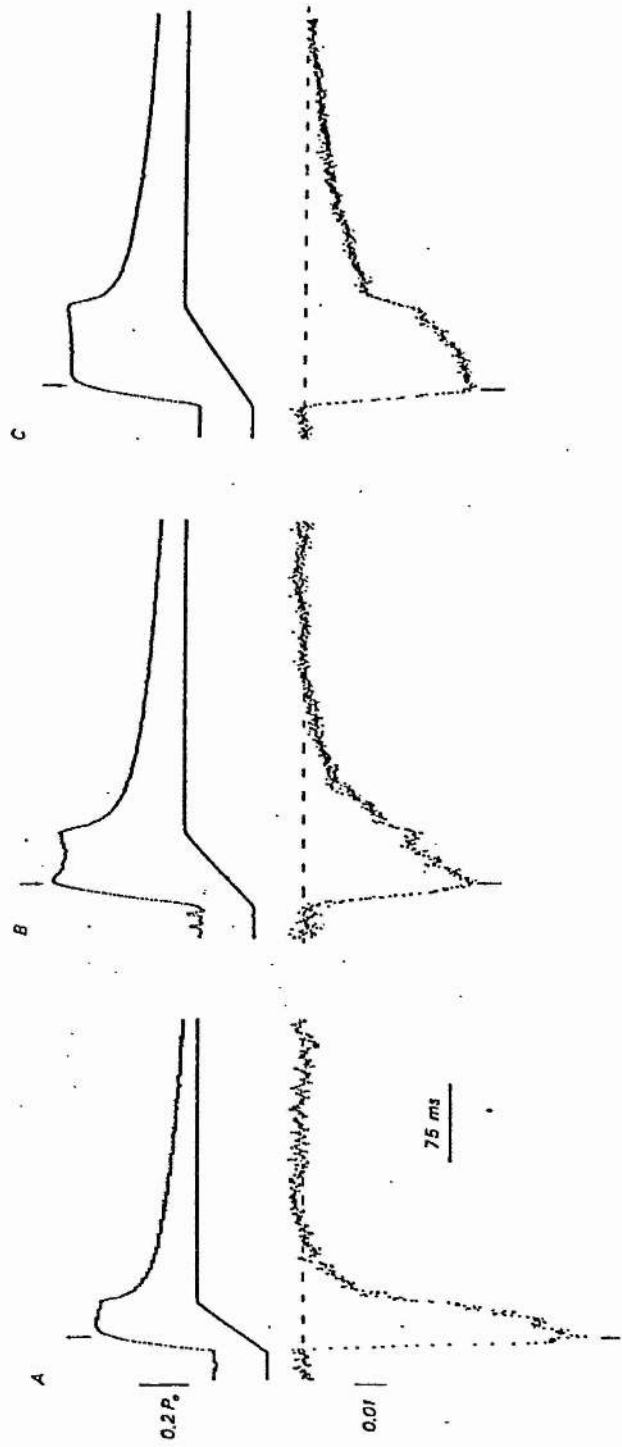


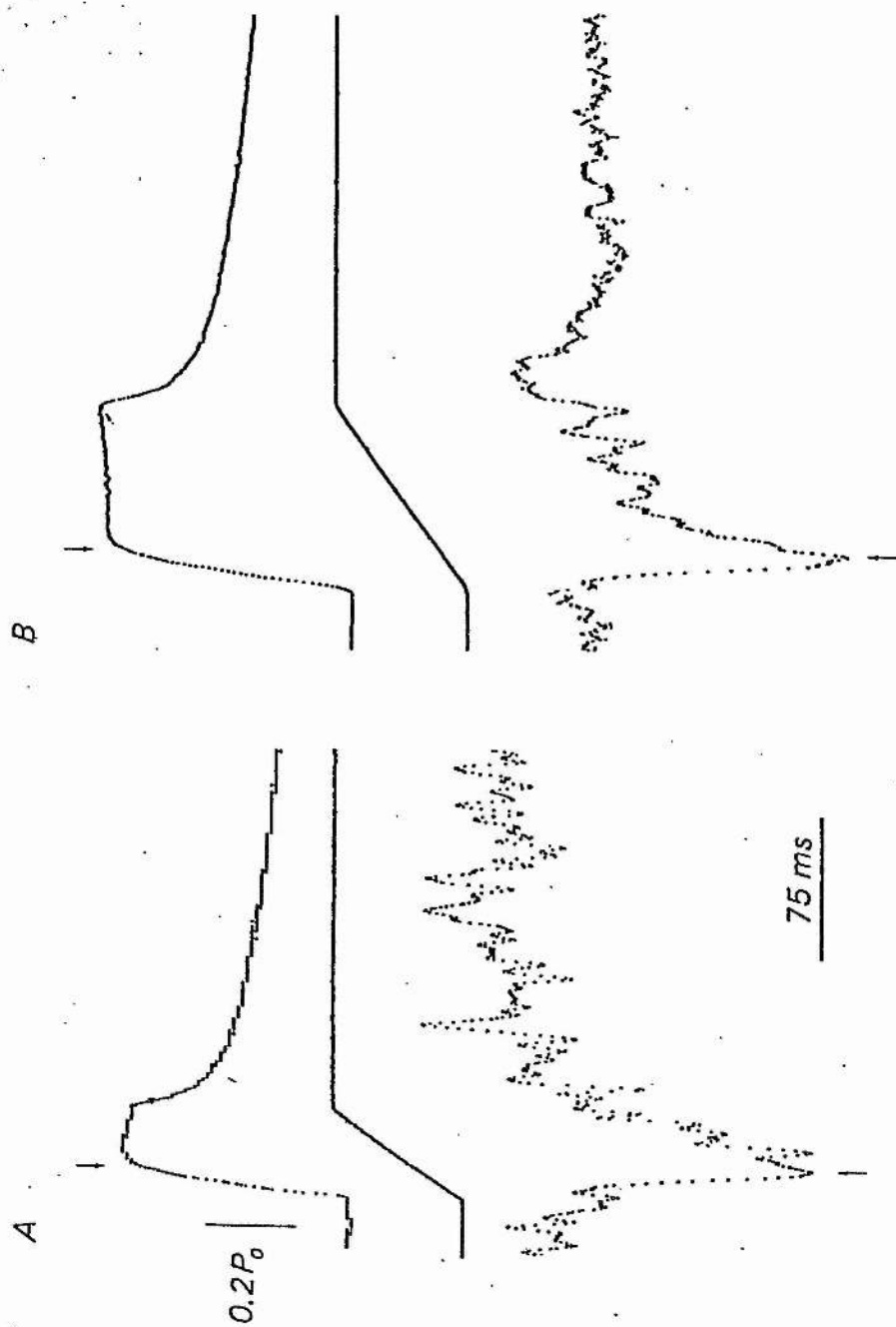
FIG 4.9

This diagram shows the differences obtained using eqn. 4.4
for the averaged 50 & 100ms transients.

A. 50ms.

B. 100ms.

Fig 4.9



CHAPTER IV

$$A = [(I_{0^{\circ}} - I_{90^{\circ}})] / [(I_{0^{\circ}} + I_{90^{\circ}})] \quad (4.2)$$

where: I = the intensity of the light transmitted in the forward direction.

This method of computing the difference has the advantage of eliminating any 'noise' which is common to both recordings. The resulting traces show that the signal anisotropy increases steeply during the early part of the stretch and reaches its maximum value at (or close to) the point at which the muscle slope stiffness falls abruptly. The value of A falls slightly during the remainder of the stretch, but after the new muscle length is reached, it then decays rapidly towards zero.

The procedure used to obtain the difference traces, summarised by eq. 4.2, requires some explanation, because it uses values for the transmitted light intensities (I_a) to compute the values for A, whereas what is of more interest is the differences in the amount of light deviated by the muscle at the two beam polarisations. There is a practical reason why it is not feasible to compute the latter directly: this is because the denominator in eqn 4.2 can be zero, which means that A then becomes infinitely large. This problem is most often encountered in the initial stages of a stretch because the two signals are comparable with the 'noise' associated with each, and of course, this is a period which is potentially of some interest. It is possible, nevertheless, to compute the amplitude of the differences between the amounts of light deviated by a muscle at the point where cross-bridges are forcibly detached ($=A_y$). This is given by:

$$A_y = [(\Delta I/I_{a,0^{\circ}}) - (\Delta I/I_{a,90^{\circ}})] / [(\Delta I/I_{a,0^{\circ}}) + (\Delta I/I_{a,90^{\circ}})] \quad (4.3)$$

CHAPTER IV

Table 4.1 shows that this calculation returns values for A_y ranging from 0.25 - 0.36 (for the muscles used in obtaining the data for figs 4.7 & 4.8) indicating a high degree of asymmetry.

Inspection of fig 4.8 A - C shows that the shapes of the differences traces resemble those of the original recordings of fig 4.7 A - C rather closely and this raises the important question: are the 90° signals merely scaled down versions of the 0° signals, or are there subtle differences in their shape? The traces shown in fig 4.9 A and B are the result of performing another kind of analysis, designed this time to highlight differences in the form of the transparency signals. Here, the amplitude of the 90° response measured at the end of the stretch is scaled upwards so that it is the same as the corresponding data point in the array for the 0° signal. The other data points in the 90° signal are scaled upwards by the same factor and the computer performs the following subtraction:

$$S = [(I_{a, 0^\circ}) - (I'_{a, 90^\circ})] \quad (4.4)$$

where $I'_{a, 90^\circ} = F \cdot (I_{a, 90^\circ})$ and F is the scaling factor.

This method of analysis emphasises the differences in the shape of the responses during the period of the stretch. It is easy to see that if the scaled 90° responses were identical to the 0° responses, then S would be zero throughout, within the limits imposed by the 'noise' associated with each trace. Instead, as fig 4.9 A and B show, it deviates significantly from zero, beginning during the early part of the stretch and again reaching its maximum value at the time which coincides with the sudden reduction in muscle slope stiffness (vertical arrows).

DISCUSSION

There are significant improvements to the design of these experiments when compared to that used in the earlier studies: first, the stretches were applied to the end of the muscle which is remote from the area illuminated by the laser, so that the possibility of optical artifacts arising from translational motion of the muscle through the beam is substantially reduced; and secondly, the Pockels cell - sample and hold system permits recordings of muscle transparency to be obtained at orthogonal beam orientations during the same tetanus, thereby effectively avoiding any spurious differences arising from variations in muscle performance. For these reasons, the data which has been obtained is considered to be more reliable than that described in previous chapters.

The results which are presented here support the main conclusion to emerge from chapter III: the optical signals are indeed highly anisotropic with respect to ϕ , both in regard to their amplitude and shape. The anisotropy is shown to develop early on in a stretch; to increase progressively throughout the period when the muscle slope stiffness is high; and to reach a maximum value at the point where the cross-bridges become forcibly detached. It can therefore be inferred that the time course of the signal anisotropy parallels cross-bridge deformation.

The results of experiments in which muscles are subjected to cycles of stretch-release and restretch (chapter VI) reinforce this view and further discussion of this important conclusion is

therefore deferred until these data have been presented. Meantime, it is worth drawing attention to the similarity which exists between the signal asymmetry reported here and the optical anisotropy shown by suspensions of anisometric particles which become orientated by flow or by the application of electric or magnetic fields. Heller (1959) has shown that the scattering of a linearly polarised light beam under these conditions varies with the orientation of the electric vector of the beam relative to the preferred direction of alignment of the particles: for rod-shaped particles it is maximal when the plane of polarisation is parallel to the preferred direction and minimal for the orthogonal direction. This is termed 'dityndallism'. The amount of light transmitted by such a system may likewise depend upon the direction of the electric vector: the turbidity (τ) is greatest when the plane of polarisation is parallel to the direction of alignment ($\tau_{0^{\circ}}$) and least when at right angles to this direction ($\tau_{90^{\circ}}$). This phenomenon is referred to as 'conservative dichroism'. It is quite distinct from true dichroism, which is the dependence of the extinction (or absorption) coefficient on the direction of polarisation. It is given by:

$$D = (\tau_{0^{\circ}} - \tau_{90^{\circ}}) \quad (4.5)$$

where $\tau_{0^{\circ}}$ and $\tau_{90^{\circ}}$ are the turbidities for light polarised in the orthogonal directions. The conservative dichroism may be finite even in a system not subject to any orienting force, if for example, there is some intrinsic structural order, as in a muscle fibre, and so a better expression is:

$$\Delta D = (\tau'_{0^{\circ}} - \tau''_{0^{\circ}}) - (\tau'_{90^{\circ}} - \tau''_{90^{\circ}}) \quad (4.6)$$

$$= (\Delta\tau_{0^{\circ}} - \Delta\tau_{90^{\circ}}) \quad (4.7)$$

CHAPTER IV

where the superscripts ' and " refer to the turbidities when subject to an orienting force and when not (respectively) and where ΔD is the change in conservative dichroism. The following normalised form of equation 4.7:

$$\Delta D_n = (\Delta\tau_0 - \Delta\tau_{90^\circ}) / (\Delta\tau_0 + \Delta\tau_{90^\circ}) \quad (4.8)$$

is similar in form to equation 4.2, and to continue the analogy, where muscle stretch provides the orienting force.

This analysis will be pursued further later, but meantime, it should be emphasised that the experiments presented thus far do not give any insight into the optical process/es underlying the transparency signals: are they due to a change of light scattering, or diffraction or absorption, or perhaps a combination of all three? It is necessary to give some consideration to this question at this time, because the physical nature of the dominant optical process will govern the kind of information contained within the signals. This is the subject of the experiments described in the following chapter.

CHAPTER V

TRANSPARENCY CHANGES DURING STRETCH OF ACTIVE MUSCLE:

IV. WAVELENGTH DEPENDENCE.

INTRODUCTION

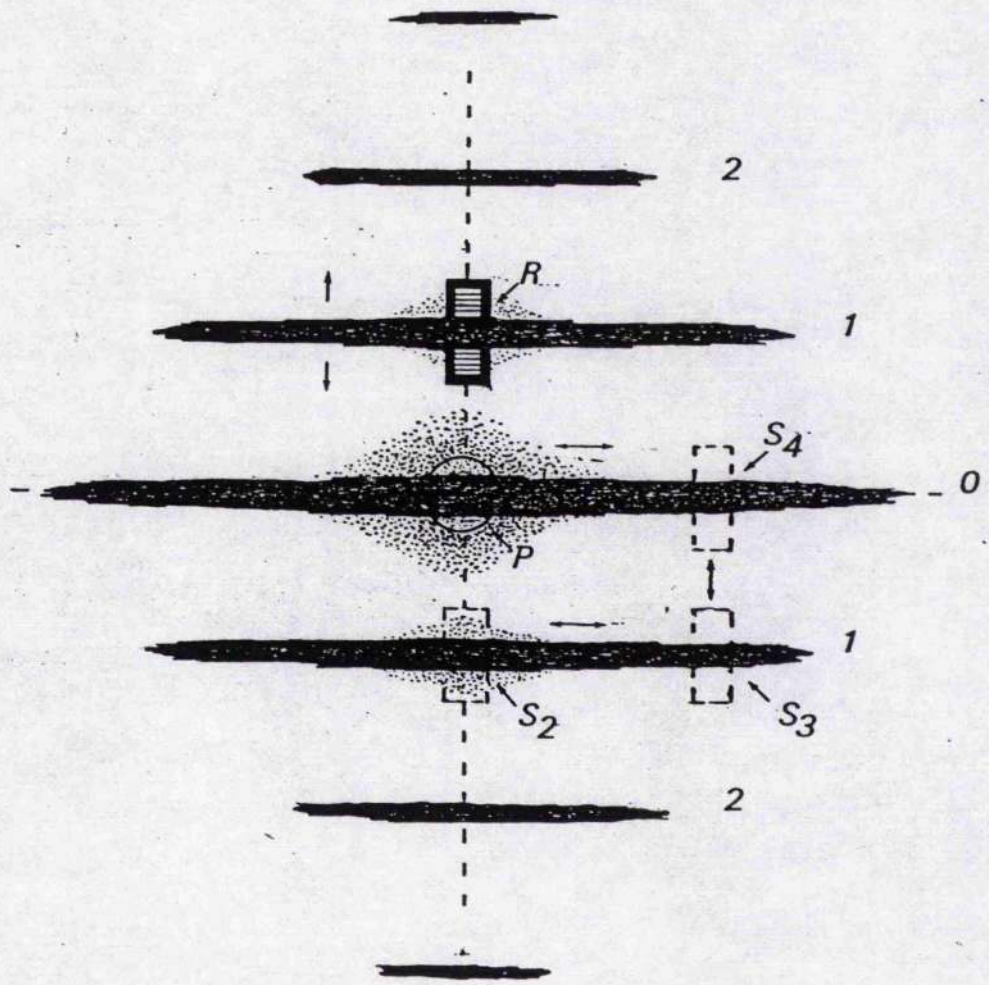
It is important to identify the optical process/es which give rise to the transparency change, in order to interpret the optical signals correctly, in terms of the structural changes occurring within the muscle. We have seen that only a small fraction (<5%) of the light entering the muscle passes through directly (figs 2.3 & 3.2); the remainder is deviated by scattering or diffraction, or else it is lost through absorption. In fact, there is very little true absorption by the muscle in the visible region of the spectrum (Hill, 1959) and so this process cannot be the principal one. On the other hand, the intensity distribution of light emerging from the muscle is evidently dominated by diffraction effects, because the parallel spectra are the most prominent feature of the optical field. In addition, there is some diffuse light distributed about the central zero order region and this also extends outwards, to occupy the spaces between the diffracted orders.

The contribution that each of the above physical processes makes to the transparency signals can be determined experimentally, in principle, by a technique known as 'directional' recording (Hill, 1953a). The method involves making optical recordings from different regions of the optical field. Consider fig 5.1, which is a diagrammatic representation of the intensity distribution of light emerging from a muscle. The zero order line together with the first and second diffracted orders are illustrated. The distinction between changes in light scattering, diffraction and absorption is achieved by making simultaneous recordings from the central region of the zero order

FIG. 5.1

Diagrammatic representation of the diffraction pattern,
further details in text p5.2.

Fig 5.1



(with the primary photocell, P) and from one of the following other positions: S2, on the central, first-order line; S3, on the first-order line, but with the photocell displaced laterally from the meridian; S4, on the zero-order line, but again displaced laterally from the meridian; and S5, (not illustrated), located at various 'between order' positions. The analysis is as follows. The observed decrease in transparency could be due to an increase in absorption, scattering or diffraction. The polarity of signals arising from scattering or diffraction alone will show reversal when the output of the secondary cells is compared to that of the primary photocell, whereas signals due to absorption alone will not. A pure scattering signal will show reversal at S3, S4 & S5, but not at S2, while a pure diffraction signal will reverse at S2 & S3 but not at S4. It is therefore possible, in principle, to distinguish between the three kinds of optical change; it is even possible (see Flitney, 1975) to 'dissect' complex responses which contain contributions from all three, because one phase of the signal may show reversal at a particular location while others do not.

Using this analysis, Flitney (1975) was able to show unequivocally that a component of the transparency signal generated by stretching a resting muscle is caused by an increase in light scattering. The amplitude of the scattering change was shown to be directly proportional to the tension generated in the so called 'short range elastic component' of resting muscle; since the latter is thought to be due to the flexural rigidity of long lasting cross-bridges (Hill, 1968) it was concluded that the scattering effect arose as a direct result of the deformation of actin-myosin linkages.

CHAPTER V

The form of the optical signals and of the tension increment generated by stretching active muscle is quite similar to that produced by stretching resting muscles; and qualitatively, we saw earlier that the amplitudes of the optical signals, expressed as the fractional change in transmitted light intensity per unit tension developed, are also similar. This, then, suggests that the same physical process underlies both kinds of transparency signal (i.e. both resting and active).

The technique of directional recording has not been used in this present study. There were practical difficulties in making the necessary recordings and so a different approach was used instead. This involved making optical recordings using incident light of different wavelengths. Lord Raleigh (Kerker, 1969) first showed that the scattering of light by isometric particles which are small in comparison to the wavelength of the incident beam varies in direct proportion to the fourth power of the driving frequency: thus, the amount of light scattered increases as the wavelength is decreased.

This form of scattering is referred to as Rayleigh scattering and it is best seen in rarefied gases. It is also shown by liquids and even by some solids but the effect is relatively weak due to the greater degree of structural order in these states. Conceptually, muscle can be thought of as lying somewhere between a solid and a liquid containing a relatively high concentration of large molecular weight solutes. In such a condensed system the effects of multiple scattering - that is to say, the interaction of an already scattered wavelet with a second, third, or nth. scattering particle - is certain to complicate the interpretation of the results obtained by varying the wavelength.

CHAPTER V

Nevertheless, it was considered worthwhile to attempt this kind of experiment and the opportunity to do so arose in the summer of 1985, when a tunable Argon ion laser (on loan from Mr.W.Burke, of Burke Electronics Ltd., Glasgow.) was being evaluated in the laboratory for use in connection with another project. Simultaneous recordings of transparency signals were made at orthogonal polarisations using four different laser lines, spanning the range 632.8 - 457.9nm. The results obtained will show that both 0° and 90° signals vary inversely with wavelength, although not to the same degree: the 90° signal has a wavelength dependence which approximates to that of a Rayleigh scatterer ($\lambda^{-3.9}$), whereas the change in the 0° signal has a significantly smaller wavelength exponent, varying as $\lambda^{-2.3}$.

MATERIALS AND METHODS.

I. Apparatus

The apparatus was in most respects the same as that used for the experiments described in the preceding chapter, but with the addition of a second laser source. This was a tunable Argon ion laser (Spectra-Physics Ltd., type 162A-07) capable of generating three usable lines, at 514.5nm (21mW), 488nm (15mW) and 457.9nm (3mW), selected by means of an adjustable prism monochromator. The device was mounted with the tube axis in the horizontal plane, immediately above the He-Ne laser (which provided the 632.8nm line). The two output beams were made co-axial by a system comprising a prism (P) and half silvered mirror (M) as diagrammatically shown in fig 5.2.

II. Experimental Protocol,

Sartorius muscles were dissected and mounted in the usual manner. The resting sarcomere length (at l_0) was measured using the He-Ne laser since this gave the greatest spatial separation of the diffracted orders. The voltage required to switch ϕ through $\pi/2$ radians (between 0° & 90°) is dependent upon λ (see equ. 4.1) and so the procedure for critically adjusting the Pockels cell amplifier was followed after each change of wavelength. The voltage output from the photomultiplier tube, representing the transmitted intensities for the two orthogonal incident beams, were recorded separately, using the sample-hold device.

Recordings of the steady-state transparency at rest and during

FIG 5.2

Diagram showing the method of making two laser beams co-axial.

M. half silvered mirror.

P. Prism.

Fig 5.2

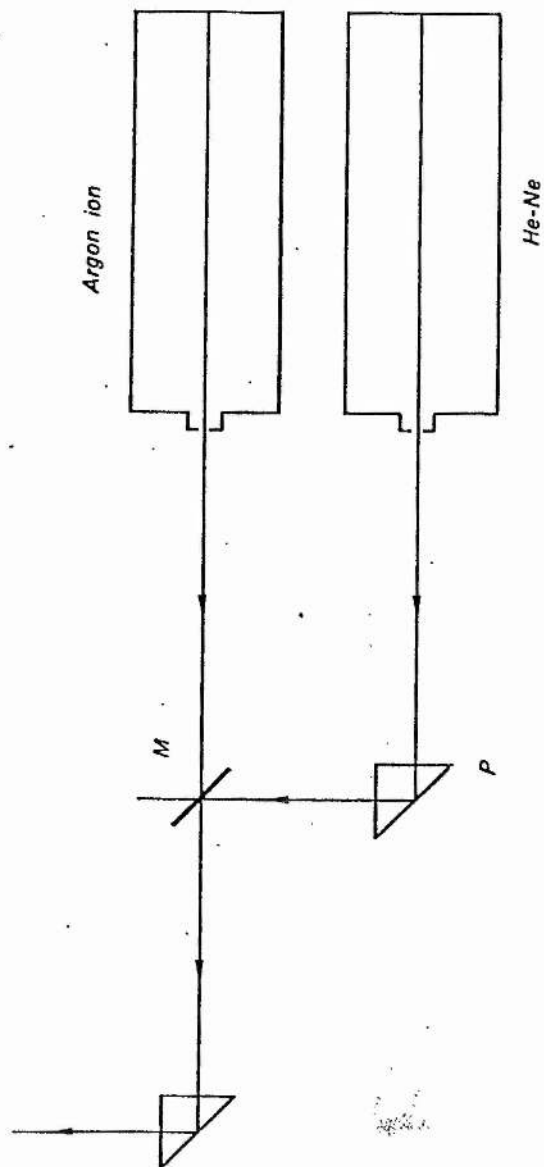


FIG 5.3

Resting turbidity plotted against sarcomere length for the following wavelengths (closed circles $\phi = 0^\circ$ open circles $\phi = 90^\circ$):

A. 632.8nm.

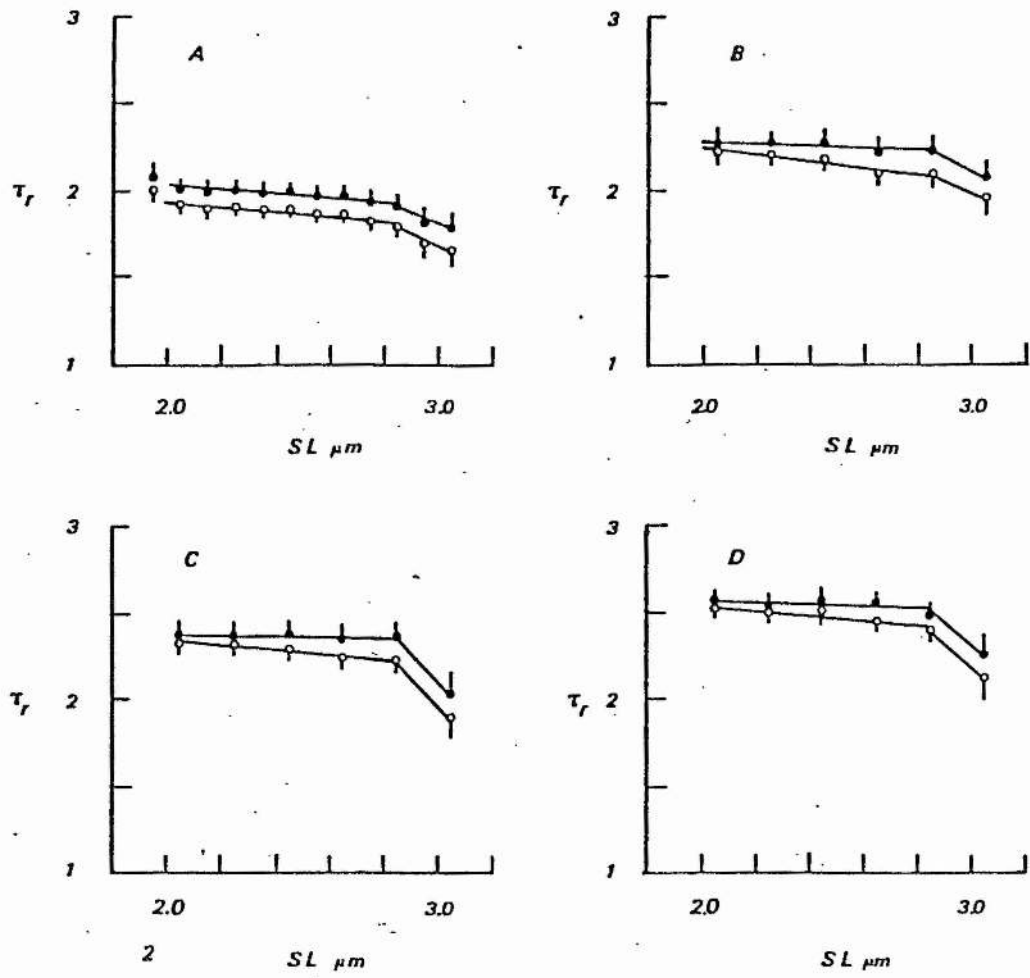
B. 514.5nm.

C. 488nm.

D. 457.9nm.

All points plotted \pm S.E.

Fig 5.3



CHAPTER V

activation were made over a range of sarcomere lengths (2.05 - 3.05 μ m). Dynamic responses, produced by applying stretches ($\sim 0.1 \times l_0$, 100ms duration) to active muscles were all recorded using muscles set up at an initial (resting) sarcomere length of 2.3-2.4 μ m.

RESULTS**I. Steady state turbidity measurements of resting and activated muscles at different sarcomere lengths: wavelength dependence.**

Measurements of incident light intensity, I_o , and zero order transmitted light intensity, I_t were made in the range of sarcomere lengths 1.95 - 3.05 μm ; for $\phi = 0^\circ$ and 90° ; for λ 's = 632.8nm, 514.5nm, 488nm and 457.9nm; and for both resting and active states.

A. Resting muscles. The results obtained for resting muscles ($n=34$ muscles) are shown in fig 5.3., where τ_r , the resting muscle turbidity, given by:

$$\tau_r = \log_{10} (I_o/I_{t(r)}) \quad (5.1)$$

is plotted against sarcomere length. The observations can be summarised as follows:

1. $\tau_r(0^\circ)$ is invariably greater than $\tau_r(90^\circ)$. This is true at all sarcomere lengths and all wavelengths studied.
2. τ_r is inversely related to sarcomere length. The change is comparatively small (and approximately linear) over the range 2.0 - 2.8 μm and is greater for $\phi = 90^\circ$ than for $\phi = 0^\circ$ (see table 5.1, columns marked 'b'). Beyond 2.8 μm , τ_r decreases more steeply with muscle length.
3. τ_r is inversely related to λ . The greater dependence of $\tau_r(90^\circ)$ upon sarcomere length relative to $\tau_r(0^\circ)$ means that the conservative dichroism of resting muscle, D_r , given by:

$$D_r = (\tau_r(0^\circ) - \tau_r(90^\circ)) \quad (5.2)$$

is always (a) positive and (b) increases with increasing sarcomere

length. These points are illustrated by the data presented in fig 5.4, where D_r is plotted against sarcomere length for the four wavelengths studied.

B. Activated muscles. Stimulation invariably causes the zero-order transmitted light intensity to increase. This was found to be so at all sarcomere lengths and wavelengths studied, and it applied to observations made with $\phi = 0^\circ$ and 90° . Consequently, the steady state turbidity for active muscles, τ_a , is less than that for resting muscles. The results, depicted in fig 5.5, can be summarised as follows:

1. Stimulation causes muscle turbidity to fall, so that $\tau_a < \tau_r$
2. τ_a decreases with increasing muscle length. This effect is greatest at $\lambda = 632.8\text{nm}$, and it decreases in the order $632.8 > 514.5 > 488 > 457.9\text{nm}$ (table 5.1, columns 'b').

The conservative dichroism of active muscle, D_a , given by:

$$D_a = (\tau_a(0^\circ) - \tau_a(90^\circ)) \quad (5.3)$$

remains positive for all wavelengths studied. For $\lambda = 632.8\text{nm}$, 514.5nm and 488nm , D_a increases with increasing sarcomere length (fig 5.6). The trend for $\lambda = 457.9\text{nm}$ is less clear: the variability in D_a at any one sarcomere length is much greater than for any other wavelength.

C. The effect of stimulation on the conservative dichroism of muscle. The change in conservative dichroism on activation, ΔD , defined as:

FIG 5.4

The conservative dichroism of resting muscle plotted against sarcomere length for the following wavelengths:

A. 632.8nm.

B. 514.5nm.

C. 488nm.

D. 457.9nm.

All points plotted \pm S.E.

Fig 5.4

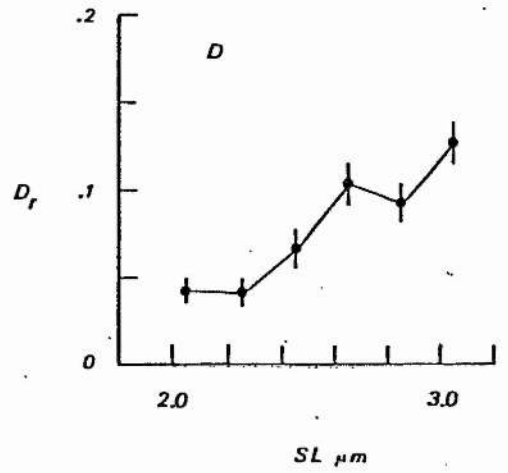
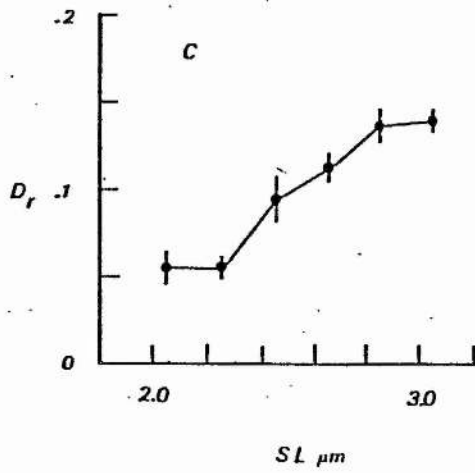
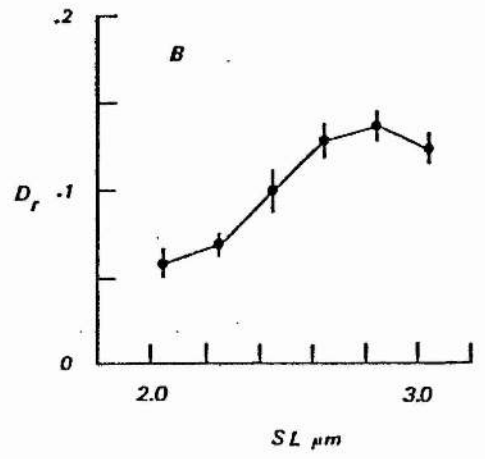
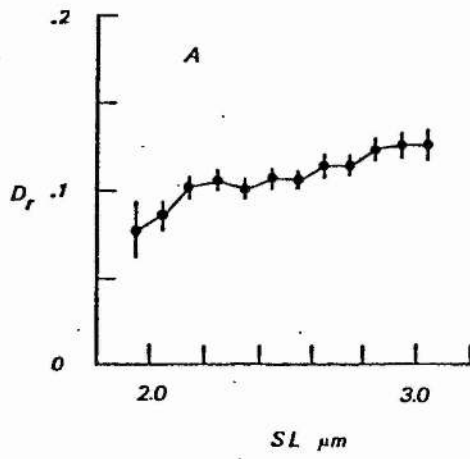


FIG 5.5

Active turbidity plotted against sarcomere length for the following wavelengths (closed circles $\varphi = 0^\circ$ open circles $\varphi = 90^\circ$):

A. 632.8nm.

B. 514.5nm.

C. 488nm.

D. 457.9nm.

All points plotted \pm S.E.

Fig 5.5

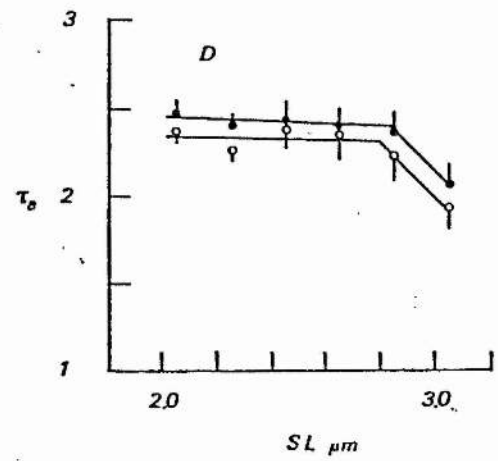
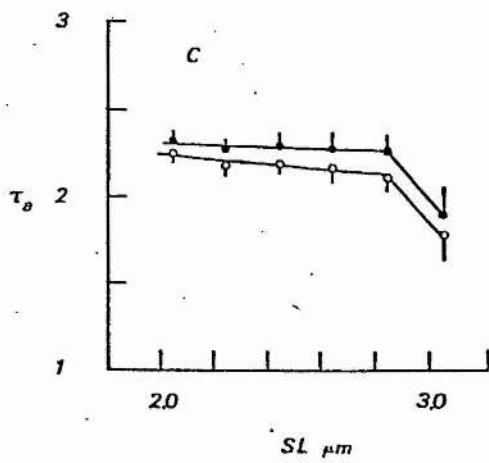
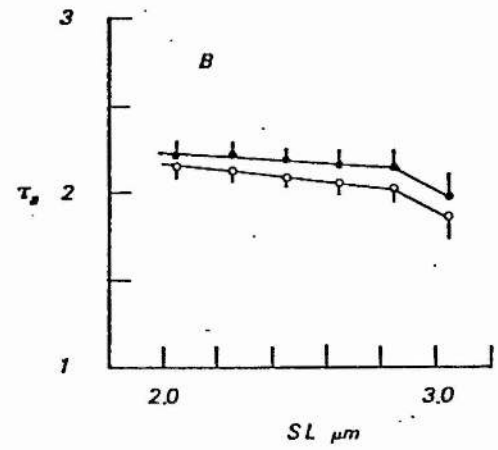
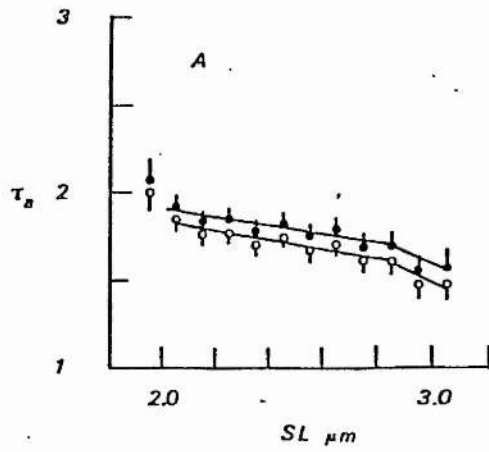


FIG 5.6

The conservative dichroism of active muscle plotted against sarcomere length for the following wavelengths:

A. 632.8nm.

B. 514.5nm.

C. 488nm.

D. 457.9nm.

All points plotted \pm S.E.

Fig 5.6

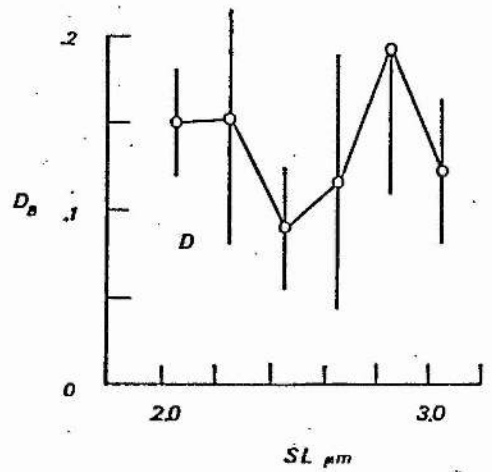
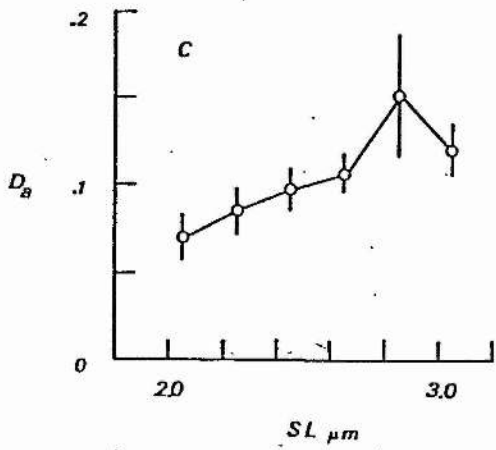
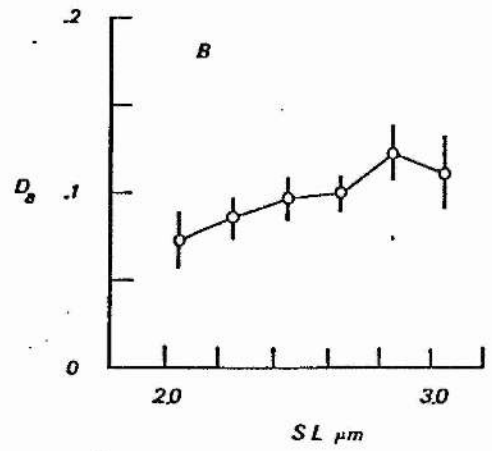
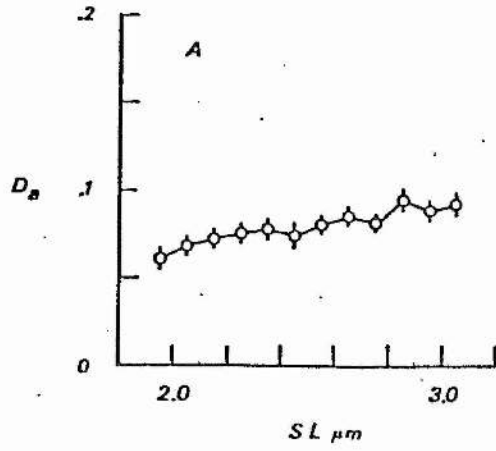


Table 5.1

Linear regression analysis* of τ_r and τ_a verses sarcomere length.

		$\lambda(nm)$					
		632.8	514.5	488	457.9		
	φ	b	r^2	b	r^2	b	r^2
τ_r	0°	-0.106	0.820	-0.064	0.661	-0.029	0.463
	90°	-0.141	0.887	-0.171	0.893	-0.141	0.937
τ_a	0°	0.228	0.830	-0.102	0.980	-0.053	0.556
	90°	-0.255	0.870	-0.161	0.996	-0.145	0.861
						-0.085	0.157

* to equation of the form $y = a + bx$, where the slope (b), the intercept (a) and the coefficient of determination (r^2) are given by the following:

$$a = \left[\frac{\sum y_i}{n} - b \frac{\sum x_i}{n} \right]$$

$$b = \frac{\sum x_i y_i - \frac{\sum x_i \sum y_i}{n}}{\sum x_i^2 - \frac{(\sum x_i)^2}{n}}$$

$$r^2 = \frac{\left[\sum x_i y_i - \frac{\sum x_i \sum y_i}{n} \right]^2}{\left[\sum x_i^2 - \frac{(\sum x_i)^2}{n} \right] \left[\sum y_i^2 - \frac{(\sum y_i)^2}{n} \right]}$$

$$\begin{aligned}\Delta D &= D_a - D_r \\ &= (\tau_a(0^\circ) - \tau_a(90^\circ)) - (\tau_r(0^\circ) - \tau_r(90^\circ))\end{aligned}\quad (5.4)$$

is shown in fig 5.7. For $\lambda = 632.8$, ΔD is always negative, in other words, stimulation causes muscle conservative dichroism to decrease. For $\lambda = 514.5\text{nm}$ and 488nm , ΔD is positive at short sarcomere lengths ($<$ or $=$ to $2.5\mu\text{m}$) but is either negative at longer lengths (514.5nm) or unchanged (488nm). At $\lambda = 457.9\text{nm}$, ΔD is positive at shorter sarcomere lengths ($<$ or $=$ to $2.6\mu\text{m}$). In summary, then, the conservative dichroism decreases on activation at the longer lengths, but there is a tendency for it to increase at shorter wavelengths and especially at short sarcomere spacings.

II. Wavelength dependence of transparency changes produced by stretching active muscles.

Dynamic responses, generated by stretching active muscles are shown in fig 5.8 A - D, for the four wavelengths under investigation. Each recording shows muscle tension (upper trace), length (mid = trace) and transparency (lower trace). The change in muscle transparency is represented as the fractional change of the light intensity level immediately before the stretch, and the recordings are corrected for the baseline offset. Each trace is an averaged response from several muscles (in all, 246 recordings from 13 muscles are included in the analysis) and in order to compare their amplitudes directly they are scaled to give the value $\Delta I/I_a$ (at the 'yield' point) for a ΔP of 10^5N.m^{-2} (see figs 5.9 A & B). The data obtained is shown in table 5.2. The results can be summarised as follows:

FIG 5.7

The change in conservative dichroism upon stimulation.

● 632.8nm.

○ 514.5nm.

△ 488nm.

□ 457.9nm.

Fig 5.7

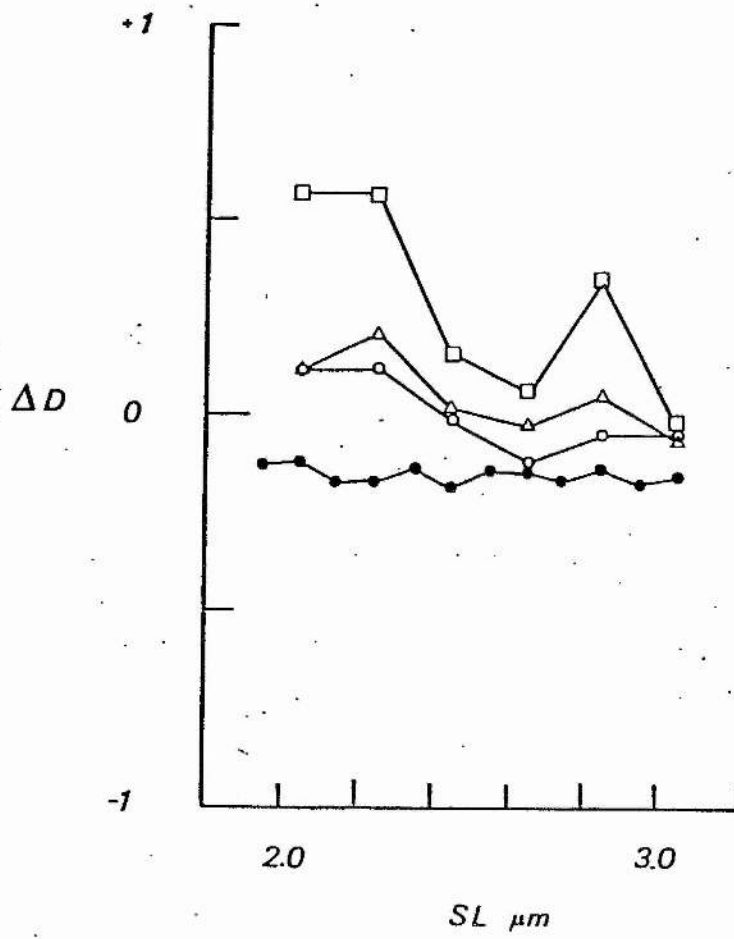


FIG 5.8

The dynamic responses, generated by stretching active muscles, for the following wavelengths:

A. 632.8nm.

B. 514.5nm.

C. 488nm.

D. 457.9nm.

Scale bars:

Tension:- 0.25P
o'

Optical:- 0.1 x I_a.

Fig 5.8

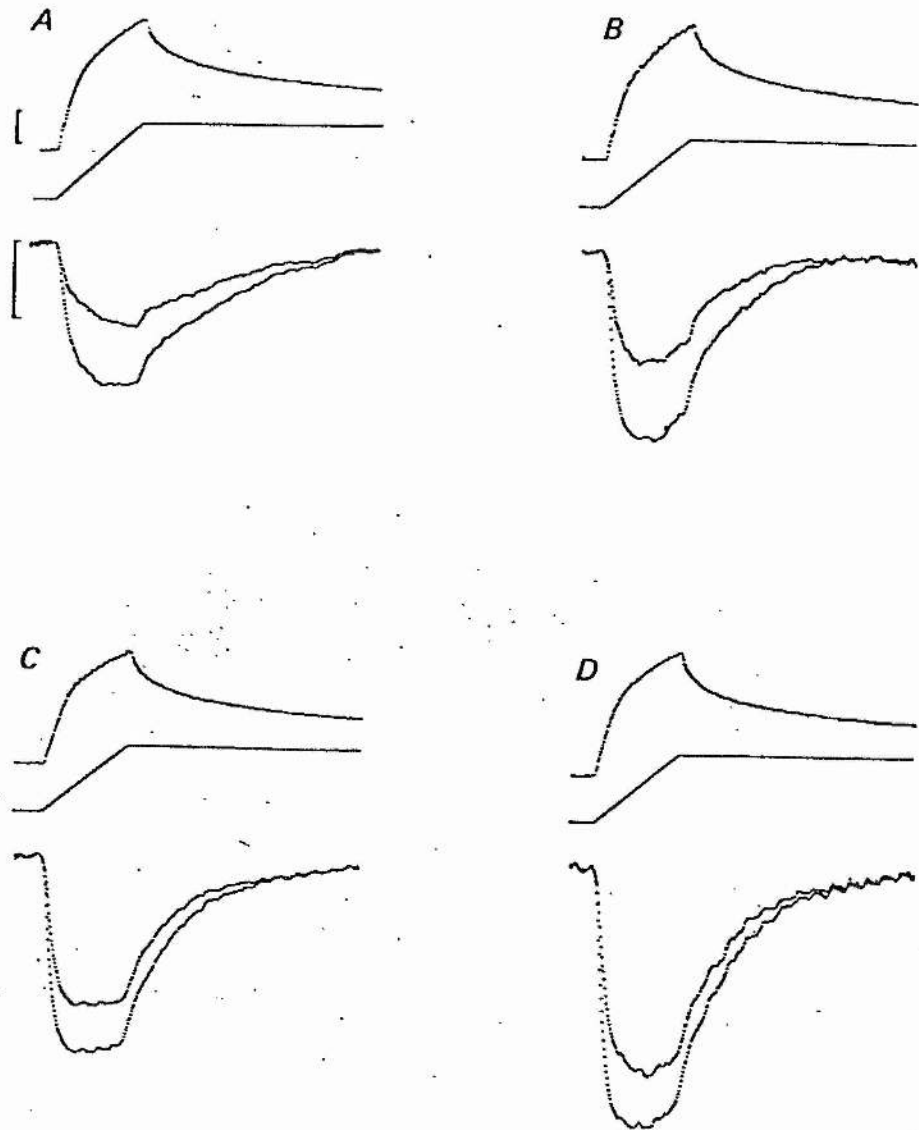


FIG 5.9

Figure showing:

A., B. corrected 0° and 90° transients respectively.

C. as A.

D. Here the 90° transients have all been scaled by the same factor that is required to bring the 90° (632.8nm) response to the same level as the 0° (632.8nm) response at the yield point.

Fig 5.9

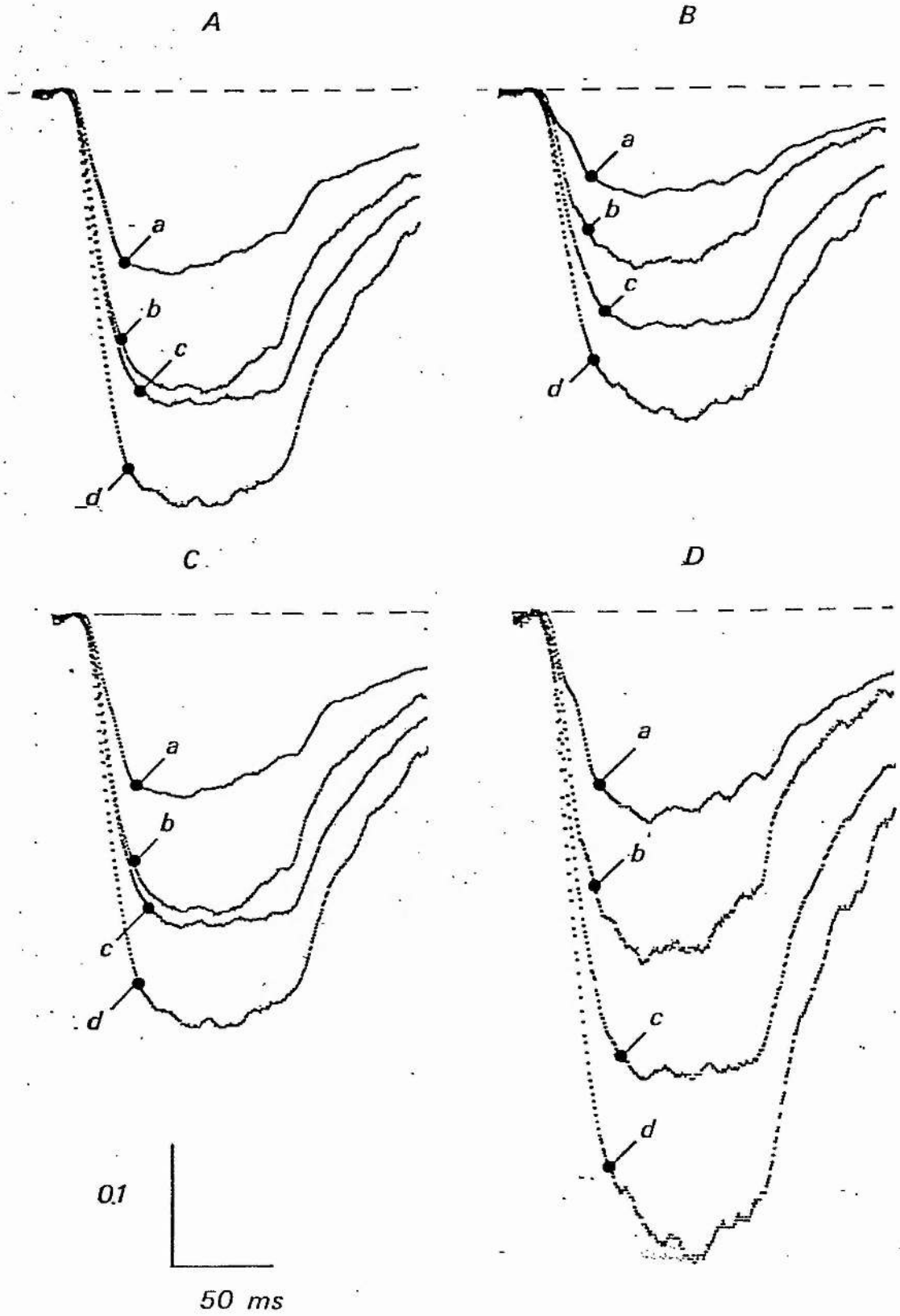


Table 5.2

λ (nm)	$\Delta I/I_{\alpha}^*$		No. of muscles, responses	
	$\Phi = 0^\circ$	$\Phi = 90^\circ$		
632.8	0.143 ± 0.007	0.073 ± 0.006	7	47
514.5	0.209 ± 0.013	0.116 ± 0.014	1	10
488.0	0.259 ± 0.018	0.191 ± 0.009	5	31
457.9	0.310 ± 0.013	0.227 ± 0.012	8	40
Wavelength dependence (λ^b)	$b = -2.39$	$n = -3.87$		
Linear regr. coefficients	$r^2 = 0.972$	$r^2 = 0.923$		

Mean values \pm SE's tabulated. Note that 90° signal displays a greater inverse dependence on λ than 0° signal. * $\Delta I/I$ scaled to ΔP of $1 \text{ kg}\cdot\text{cm}^{-2}$.

1. $\Delta I/I_a$ is greater for $\varphi = 0^\circ$ than for $\varphi = 90^\circ$ at all wavelengths.
2. $\Delta I/I_a$ is inversely related to λ . The change in $\Delta I/I_a$ with λ is greater for $\varphi = 90^\circ$ than for $\varphi = 0^\circ$; as a result, the ratio of the two signals ($= \Delta I/I_{a(0^\circ)} / \Delta I/I_{a(90^\circ)}$) decreases with λ (632.8 = 1.96, 514.5 = 1.80, 488 = 1.36, and 557.9 = 1.37).

Point 2 is illustrated by reference to fig 5.9A,B where the 0° (A) and 90° (B) responses are superimposed: $\Delta I/I_{a(90^\circ)}$ increases 3.1-fold whereas $\Delta I/I_{a(0^\circ)}$ increases by only 2.17 times. This difference is highlighted in fig 5.9, C and D. Panel C is the same as panel A. In panel D, the amplitude of the 90° responses at $\lambda = 632.8\text{nm}$ (measured at the 'yield' point) is scaled to have the same value as that for the corresponding 0° response, and the 90° response for each one of the remaining wavelengths is increased by the same scaling factor. As can be seen, the relative increase in the 90° signal is considerably greater than for the 0° signal.

The wavelength exponent describing the variation of $\Delta I/I_a$ with λ for both 0° and 90° recordings were estimated from a least squares fit to an equation of the form:

$$y = a \cdot x^b \quad (5.5)$$

where the wavelength exponent (b) is estimated by:

$$b = \frac{\sum(\ln x_i)(\ln y_i) - \frac{(\sum \ln x_i)(\sum \ln y_i)}{n}}{\sum(\ln x_i)^2 - \frac{(\sum \ln x_i)^2}{n}} \quad (5.6)$$

and a by:

$$a = \exp \left[\frac{\sum \ln y_i}{n} - b \frac{\sum \ln x_i}{n} \right] \quad (5.7)$$

The coefficient of determination, r^2 , given by:

$$r^2 = \frac{\left[\sum(\ln x_i)(\ln y_i) - \frac{(\sum \ln x_i)(\sum \ln y_i)}{n} \right]^2}{\left[\sum(\ln x_i)^2 - \frac{(\sum \ln x_i)^2}{n} \right] \left[\sum(\ln y_i)^2 - \frac{(\sum \ln y_i)^2}{n} \right]} \quad (5.8)$$

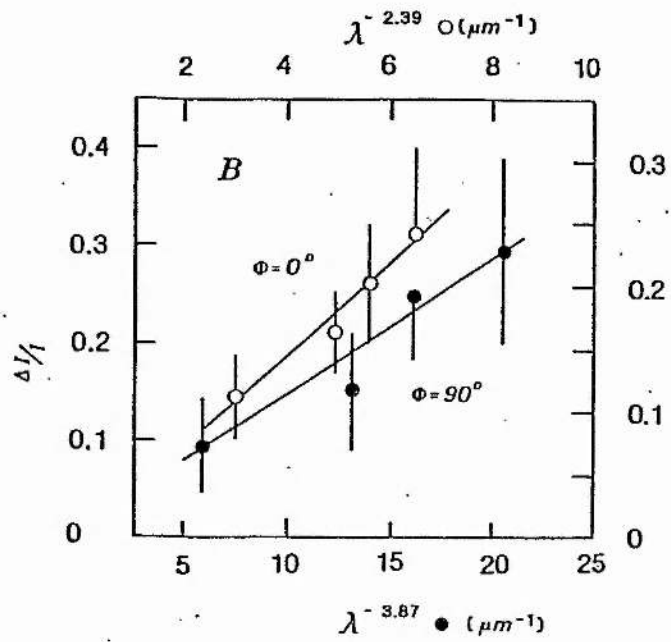
indicates the quality of fit achieved by the regression: a value approaching unity indicates a better fit than one tending towards zero. The analysis, performed using the original recordings (246 in all, from 21 muscles), returned values for $b = -2.39$ and -3.87 for 0° and 90° signals respectively (see table 5.2, rows 5 and 6) Fig 5.10 is a linearised plot of this data where the signal amplitudes (mean \pm S.D.) are plotted as a function of λ raised to the appropriate power (abscissa).

FIG 5.10

Linearised plots of wavelength raised to the appropriate power against modulation. Closed circles, and the lower and right hand axes refer to $\varphi = 90^\circ$. Open circles, and the upper and left hand axes refer to $\varphi = 0^\circ$.

All points plotted \pm S.E.

Fig 5.10



DISCUSSION

There are two points of theoretical importance which must be considered before discussing the present results. The first concerns the method used to quantify the transparency change. The change in transmitted light intensity, ΔI , can be expressed in one of two ways: either as a fraction of I_0 , the incident light intensity, or as a fraction of I_a , the transmitted light intensity immediately prior to stretch. It can be shown that the latter ($= \Delta I/I_a$) is the appropriate parameter to use. The reasoning is as follows. It is assumed that as the laser beam traverses the muscle it suffers scattering due to various optical inhomogeneities which are of no interest (component 1) and also by structural elements of the contractile system, such as the cross-bridges (component 2). It is justifiable to treat this situation as if the light were affected by each component sequentially, rather than simultaneously, as is actually the case. This is depicted diagrammatically in fig 5.11. If the scattering power of component 1 is much greater than that of component 2, as it presumably is since it represents everything other than the cross-bridges, then the difference between I_0 and I_2 will be much greater than between I_2 and I_a . In fact, one can consider $I_2 \approx I_a$. Therefore it follows that the wavelength exponent of $\Delta I/I_a$ (and not $\Delta I/I_0$) should be determined, and this is the parameter which has been estimated here.

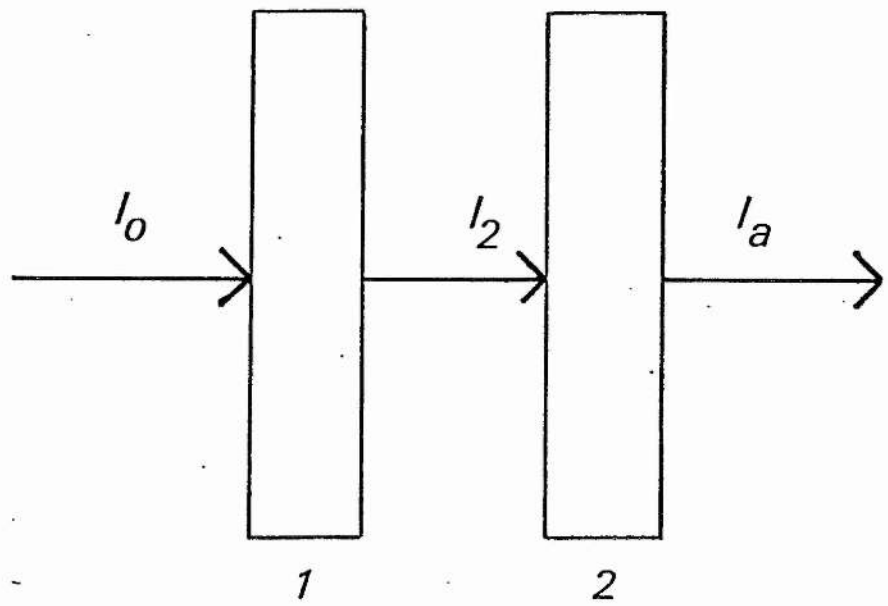
The second point to consider is the way in which the scattering of light by isometric and anisometric particles is influenced by the wavelength of the incident light. Lord Rayleigh



FIG 5.11

Diagrammatic model of the manner by which a muscle scatters light. See p5.13 for details.

Fig 5.11



used a simple dimensional argument to show that the light scattered by a system of small, isometric particles varies inversely as the fourth power of the wavelength. He reasoned as follows. First, it is evident that the scattered light intensity, I_s , will be proportional to the incident light intensity, I_o . Rayleigh then assumed that the other determinants of I_s would be the volume, V , of the particles; the distance, r to the point of observation; the wavelength, λ , of the incident light; and the refractive indices (n_1 and n_2) of the particles and the medium, respectively. Thus, for non-absorbing spheres and media whose refractive indices are not complex:

$$I_s = f(V, \lambda, r, n_1, n_2) \cdot I_o \quad (5.9)$$

Since the induced dipole radiates light in all directions, I must vary as $1/r^2$. The field of the dipole is proportional to the dipole moment, which is in turn proportional to V , but since the intensity is equal to the square of the field, I_s will vary as V^2 . Finally, the dipole moment is inversely related to the square of the driving frequency ($1/\omega^2$) and because $\omega = \lambda^{-1}$, it follows that I_s will vary as ω^4 or $1/\lambda^4$. We therefore have that:

$$I_s = (n_1, n_2) \cdot (V^2/r^2 \cdot \lambda^4) \cdot I_o \dots \quad (5.10)$$

The derivation is more complex for anisometric particles, but for a dielectric cylinder whose diameter is $\ll \lambda$, it can be shown (Kerker, 1969) that I_s varies as $1/\lambda^3$.

The most significant result to emerge from this study is the observation that the wavelength dependence is not the same for the orthogonally polarised beams: $\Delta I/I_a$ varies as $\lambda^{-3.87}$ for $\varphi = 90^\circ$ and as $\lambda^{-2.39}$ for $\varphi = 0^\circ$. Presumably, both signals are made up of contributions from large and small particles, but the

exponent for the 90° signal is close to the theoretical value of λ^{-4} , characteristic of particles which are 'small' relative to λ . The term 'small' in this context is generally taken to mean around $\lambda/20$, so that the oscillators within the particles are all subject to the same electric field strength. The cross-bridges fall into this category: the wavelength used varied from 632.8 - 457.9nm, and taking the largest dimension of the cross-bridge heads (= S1-HMM sub-units) as ~ 19 nm, then they range in size from $\lambda/33.3$ - $\lambda/24.1$. The fact that the heads project radially from the myosin filament axis - and that their angle of attachment to neighbouring actin filaments changes continuously during stretch - is another important reason why they would be expected to influence the 90° component of the light intensity more than the 0° . In contrast, the actin and myosin filaments are 'large' relative to λ , and they are aligned parallel to both the direction of stretch and the 0° component of the light. Moreover, unlike the cross-bridges their orientation is unaffected by stretch. As a result, they would be expected to contribute relatively more to the 0° than 90° signal. The wavelength exponent of -2.39 is significantly less than that expected for 'small' particles and closer to that characteristic of cylindrical scatterers with diameters $\ll \lambda$.

These considerations make it seem likely that a change in the light scattering properties of the muscle makes a major contribution to the transparency signals, although this conclusion needs some qualification. Strictly speaking, a muscle does not fulfill the conditions for a Raleigh scatterer. It is probable, for example, that multiple scattering occurs, because the interior of the muscle fibre is a relatively condensed system, and no allowance has been made for this. The degree of

CHAPTER V

agreement between theoretical values for the wavelength exponents and those observed experimentally cannot therefore be regarded as unequivocal proof that the major underlying effect is one of light scattering; on the other hand, it is not easy to see why a change of absorption, for example, would return the values obtained here purely by chance. The evidence one way or the other could have been strengthened by making 'directional' recordings of the signals, but this was not practicable.

CHAPTER VI

TIME RESOLVED CHANGES IN MUSCLE CONSERVATIVE DICHROISM DURING
STRETCH.

A PROBE OF CROSS-BRIDGE ORIENTATION ?

INTRODUCTION

The results of experiments presented in chapters III & IV showed that changes in muscle transparency accompanying stretch are highly anisotropic with respect to ϕ : both the form and the amplitudes of the optical signals were found to depend on the direction of the E-vector of the laser beam in relation to the muscle long axis. It was inferred (p 4.11) that the time course of the difference between recordings made at the two orthogonal polarisations (see, for example, fig 4.8, lower traces) actually parallels cross-bridge deformation, on the basis of the observation that the signal anisotropy increases steeply during the early part of the stretch (when the muscle stiffness is high) and rises to its maximum value at the point where the cross-bridges are eventually broken. It should therefore be possible to probe changes in the orientation of the cross-bridges during stretch, by analysing the waveform of the difference signal. This is the purpose of the present chapter.

I. Presentation of experimental data.

It was pointed out earlier (see Discussion, chapter IV) that the scattering of a linearly polarised beam of light by a system of anisometric particles subject to an orientating force (e.g. flow, electric or magnetic fields) is dependent on the direction of the E-vector in relation to the preferred direction of alignment of the dipoles: in a system of rod-shaped particles the scattering will be maximal when the E-vector is parallel to the dipole axis and minimal when it is orientated in the orthogonal direction. It follows directly from this that the

transmitted light intensity will also depend upon the plane of polarisation of the incident beam. The term conservative dichroism is used to describe the dependence of the turbidity, τ , of a system on the direction of the E-vector (Heller, 1959). For orthogonally polarised beams, the conservative dichroism, D , is given by $(\tau_{0^\circ} - \tau_{90^\circ})$ and the change in conservative dichroism, ΔD , resulting from the orientating force by $(\Delta\tau_{0^\circ} - \Delta\tau_{90^\circ})$. In what follows, then, the optical recordings are represented as changes of turbidity (rather than transparency), where $\Delta\tau$ is defined as:

$$\Delta\tau_{(0^\circ, 90^\circ)} = \log_{10} (I_a / \Delta I)_{0^\circ, 90^\circ} \quad (6.1)$$

and what will be referred to hereafter as the dichroic signal is defined as:

$$D = (\Delta\tau_{0^\circ} - \Delta\tau_{90^\circ}) \quad (6.2).$$

2. Optical theory

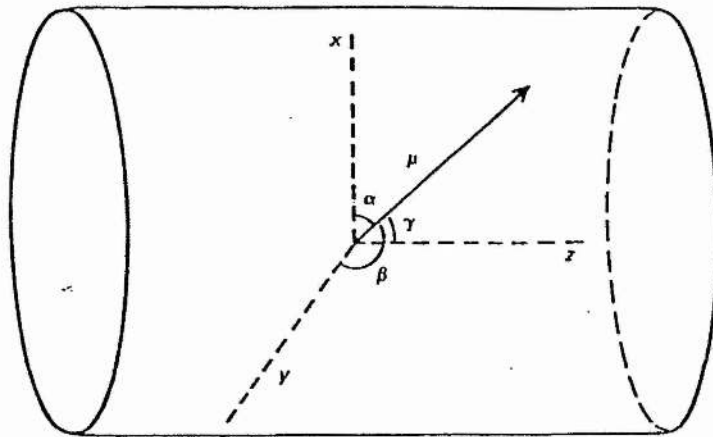
We require to derive an expression which describes the waveform of the dichroic signal in terms of the change in angle of attachment of cross-bridges. The following is adapted from Baylor, Chandler & Marshall (1982), who developed a theoretical basis for investigating the effects of re-orientating dye molecules on the absorbance of orthogonally polarised light beams by muscle fibres injected with Ca^{2+} -sensitive dyes.

Fig 6.1 shows the geometry of a muscle fibre and the co-ordinate system used to describe the spatial orientation of a single scattering element within the fibre. The z axis corresponds to the long axis of the fibre and lies in the plane

FIG. 6.1

Diagram showing the geometry of a muscle and illustrating the terms used in this chapter. μ is the dipole moment (taken from Baylor, Chandler & Marshall; 1982).

Fig 6.1



of the paper. The x and y axes point radially with the x axis in the plane of the paper and the y axis orthogonal to it. The dipole axis makes angles α , β and γ with the x, y, and z axes.

The convention for describing the turbidity, τ' , due to a single dipole is:

τ'_x - the turbidity when light is directed along the y axis with its E-vector in the x direction (= 90° light)

τ'_y - the turbidity when the light is directed along the x axis with its E-vector in the y direction.

τ'_z - the turbidity when light is directed along the y axis with its E-vector in the z direction (= 0° light).

Since the above terms vary as the square of the cosine of the angle between the dipole and the E-vector, we can write that:

$$\tau'_x = 3\tau \cdot \cos^2 \alpha \quad (6.3)$$

$$\tau'_y = 3\tau \cdot \cos^2 \beta \quad (6.4)$$

$$\tau'_z = 3\tau \cdot \cos^2 \gamma \quad (6.5)$$

The proportionality constant 3 is equal to the turbidity which would result if the dipole axis were orientated parallel to the E-vector. Regardless of orientation, the trigonometrical identity:

$$\cos^2 \alpha + \cos^2 \beta + \cos^2 \gamma = 1 \quad (6.6)$$

gives:

$$3\tau' = \tau'_x + \tau'_y + \tau'_z \quad (6.7)$$

If the scattering system is thought of as containing N identical dipoles, unconstrained with regard to their spatial orientations, then the turbidities τ_x , τ_y and τ_z can be defined in the same way as τ'_x , τ'_y and τ'_z . The turbidity for either 90° or 0° light is additive and so τ_x is the sum of all the individual τ'_x 's, therefore:

$$\tau_x = \sum^N \tau'_x \quad (6.8)$$

Similarly

$$\tau_y = \sum^N \tau'_y \quad (6.9)$$

and

$$\tau_z = \sum^N \tau'_z \quad (6.10)$$

Equations 6.3 - 6.5, 6.7 and 6.8 - 6.10 can be combined to give

$$\tau_x = 3 \overline{\cos^2 \alpha} \quad (6.11)$$

$$\tau_y = 3 \overline{\cos^2 \beta} \quad (6.12)$$

$$\tau_z = 3 \overline{\cos^2 \gamma} \quad (6.13)$$

and

$$3\tau = \tau_x + \tau_y + \tau_z \quad (6.14)$$

where $\tau = N \cdot \tau'$ and the horizontal bars denote the average values of the \cos^2 terms. For non-randomly orientated dipoles the radial symmetry of the fibres means that on average $\overline{\cos^2 \alpha} = \overline{\cos^2 \beta}$, giving $\tau_x = \tau_y$. Since $\tau_{0^\circ} = \tau_z$ the dichroic waveform is given by:

$$D = (\Delta\tau_z - \Delta\tau_x)$$

so that

CHAPTER VI

$$D \propto (\overline{\cos^2 \gamma} - \overline{\cos^2 \alpha}) \quad (6.15)$$

Expressing $\overline{\cos^2 \alpha}$ in terms of the angle γ (from equation 6.6 and making use of the fact that $\overline{\cos^2 \alpha} = \overline{\cos^2 \beta}$) we finally obtain:

$$D \propto \overline{\cos^2 \gamma} - ((1 - \overline{\cos^2 \gamma})/2) \quad (6.16)$$

CHAPTER VI

MATERIALS & METHODS

Protocol

The analysis to be undertaken is based in part on the results of experiments presented in the previous chapter, using data obtained for $\lambda = 632.8\text{nm}$, 514.5nm , 488nm and 457.9nm . In addition, series of experiments was performed in which muscles were subjected to a more complex pattern of length perturbation, comprising (1) stretch from the plateau of a tetanus, followed by (2) release from the high tension state existing at the end of a stretch and finally (3) a restretch, without delay, from the low tension state reached at the end of the release. For brevity, the latter will be referred to as 'double stretch' experiments, and the former as 'single stretch' experiments.

The rationale for studying optical signals generated by double stretches is to be found in an earlier paper by Flitney & Hirst (1978b). These authors measured sarcomere length changes during single stretches, commencing from the plateau of a tetanus, and also during stretch from a low tension state, immediately following a previous release. Since their observations have a direct bearing on the design of the present experiments they are summarised briefly below, before presenting the results.

Flitney & Hirst's interpretation of tension responses and sarcomere length changes in 'double stretch' experiments

Fig 1A in Flitney & Hirst's paper (fig 1.28B in this thesis) shows the tension response (upper trace), sarcomere length

changes (middle traces) and the pattern of applied length change. Their findings based upon recordings of this type can be summarised as follows:

1. The level of tension reached at the point where muscle slope stiffness falls abruptly, associated with sarcomere 'yielding', is approximately the same ($=1.4P_0$) for first and second stretches.

2. The muscle slope stiffness, $\Delta P/\Delta L$, where ΔP has its usual meaning and ΔL is the external length change, is approximately the same for first and second stretches.

3. The amount of filament sliding required to cause sarcomere 'yielding' is substantially greater for a second stretch as compared to a first: 18-20nm, compared with only 10-12nm respectively.

4. Sarcomere stiffness, $\Delta P/\Delta S$, where ΔS is the change in sarcomere length, is approximately the same for first and second stretches ($\sim 5-6 \times 10^{12} \text{N.m}^{-2} \cdot \text{m}^{-1}$).

On the basis of these observations, Flitney & Hirst concluded (a) that the number of cross-bridges linking the filaments is nearly the same for first stretches and second stretches (following from points 1, 2 & 4 above) and (b) that the difference in the amount of filament sliding required to precipitate sarcomere 'give' arises because the myosin heads adopt different preferred orientations in the isometric steady state and after a release (point 3).

The results were interpreted in terms of the Huxley-Simmons model, in which force production by attached cross-bridges results from stepwise movement between different attached

CHAPTER VI

states. Measurements of the amount of work absorbed by the sarcomeres during first and second stretches showed that the two preferred attachment states are separated by a potential energy difference of around 2×10^{-20} J per cross-bridge.

Returning to the present investigation, it seemed probable that differences in cross-bridge orientation, as between first and second stretches, might be reflected in the dichroic signal, and this proved to be so. It will be seen that an analysis of the two different waveforms provides a basis for drawing some important inferences about the nature of the interaction between actin and myosin at the molecular level.

RESULTS

1. Observations

Single stretch experiments. Fig 6.2A-D is the same experimental data as appeared previously in fig 5.8 A-D, but here changes in muscle turbidity are depicted (upper trace) for orthogonally polarised beams at four different wavelengths. Hence, the decrease in transparency generated by the stretch now appears as an increase of turbidity. The amplitude of the change is greater for $\phi=0^\circ$ than for $\phi=90^\circ$, and both of the signals increase in size with decreasing wavelength, as expected.

The dichroic signals ($=(\Delta\tau_{0^\circ}-\Delta\tau_{90^\circ})$) appear as the bottom row of traces in fig 6.2(D). The following points should be emphasised.

First, stretch causes muscle dichroism to increase. This is indicative of a tendency for material to become more closely aligned with the filament long axis.

Secondly, as was noted for the 'difference' traces described previously (fig 4.8 A-C), the dichroic signals rise steeply during the early part of the stretch and reach their maximum amplitude near to the point of sarcomere 'yielding'. They remain more or less constant throughout the remainder of the stretch (or show a small decrease) but decay away rapidly in the period following stretch. It is the time course of the initial part of the dichroic signal, up to the 'yield' point, which is analysed later to provide information on the angular orientation of the attached cross-bridge heads.

FIG 6.2

Optical transients for 4 different wavelengths. The same data as fig 5.8A - D except the optical traces are plotted as turbidity:

A. 632.8nm.

B. 514.5nm.

C. 488nm.

D. 457.9nm.

Scale bars:

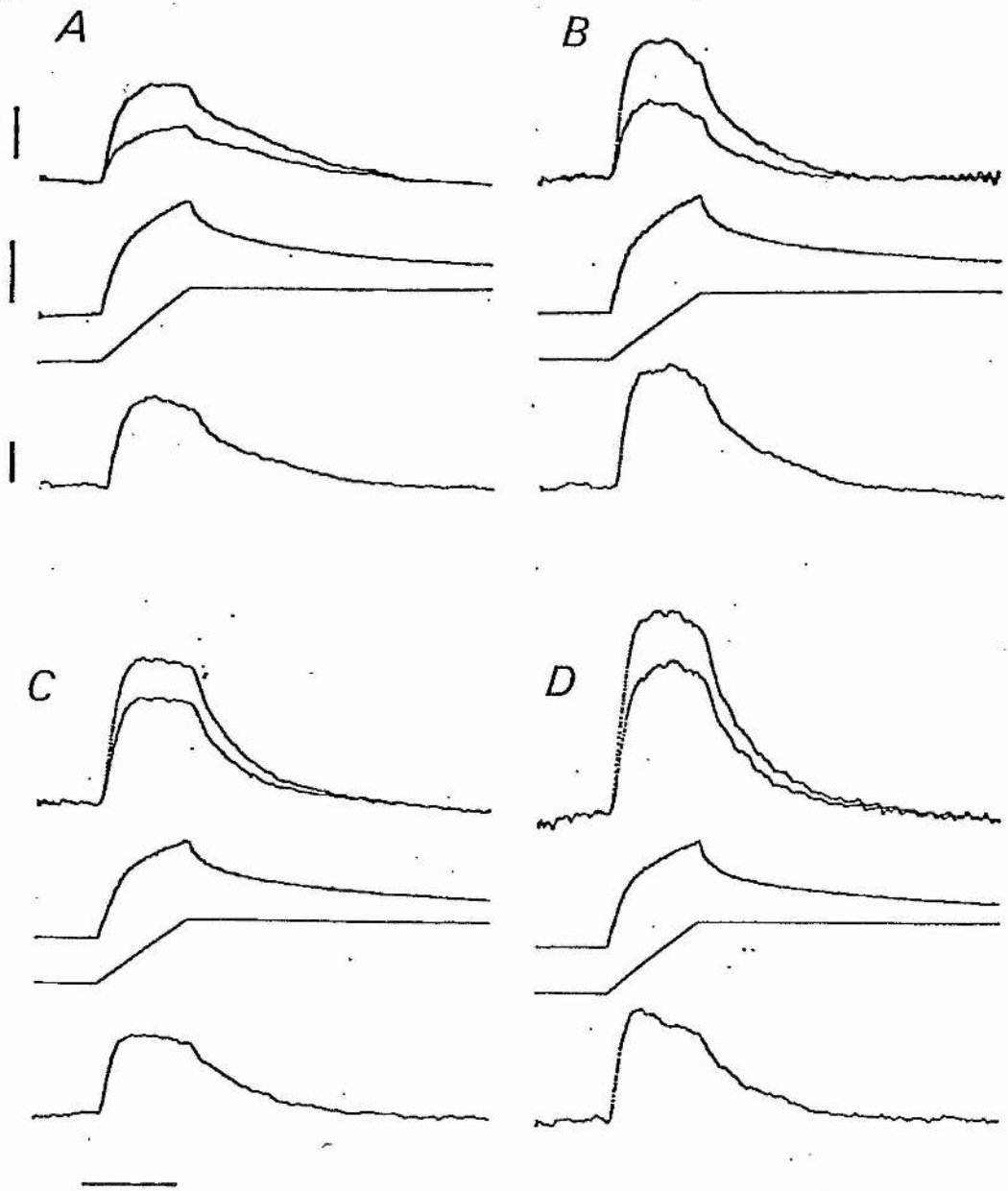
Turbidity - 0.05

Tension - 10^5N.m^{-2}

Dichroism - 0.02

Time - 100ms.

Fig 6.2



CHAPTER VI

Third, the amplitude of the dichroic signal does not change appreciably with wavelength, at least, not in any systematic way. This is in contrast to the original turbidity recordings, from which the dichroic data is derived, both of which display a marked inverse dependence on λ , as documented in the preceding chapter. This last observation suggests that the dichroic component is generated by changes in the orientation of scattering elements, rather than changes in their scattering properties.

Double stretch experiments. Fig 6.3 is a computer averaged response showing the 0° and 90° turbidities recorded during a double stretch experiment. The data are from six muscles and include 37 different recordings. The amplitude of the stretch was $0.1 \times l_0$ and the overall duration (stretch, release and restretch) was ~ 300 ms. The wavelength chosen was 457.9nm, since this generates the largest signals.

The tension response (A) resembles that in Flitney & Hirst's Fig 1A, but because the velocity of the length changes was greater, the second stretch begins from a lower tension level ($\sim 0.4P_0$ as compared to $0.7P_0$). The conditions were chosen carefully so that the second stretch would start from the lowest tension level possible - commensurate with achieving approximately the same force levels at the point of sarcomere give and with approximately the same slope stiffness - since this then maximises the chance of forcing the largest possible number of cross-bridge heads into a different preferred orientation.

The changes in τ_{0° and τ_{90° are shown in C_1 and C_2 . In C_1 the turbidities are normalised to the value existing immediately

FIG 6.3

A. computer averaged response of the effect on tension and turbidity to double stretch (37 recordings, 6 muscles).

A. Tension

B. Length change

C. Turbidity

D. Dichroism

Scale bars:

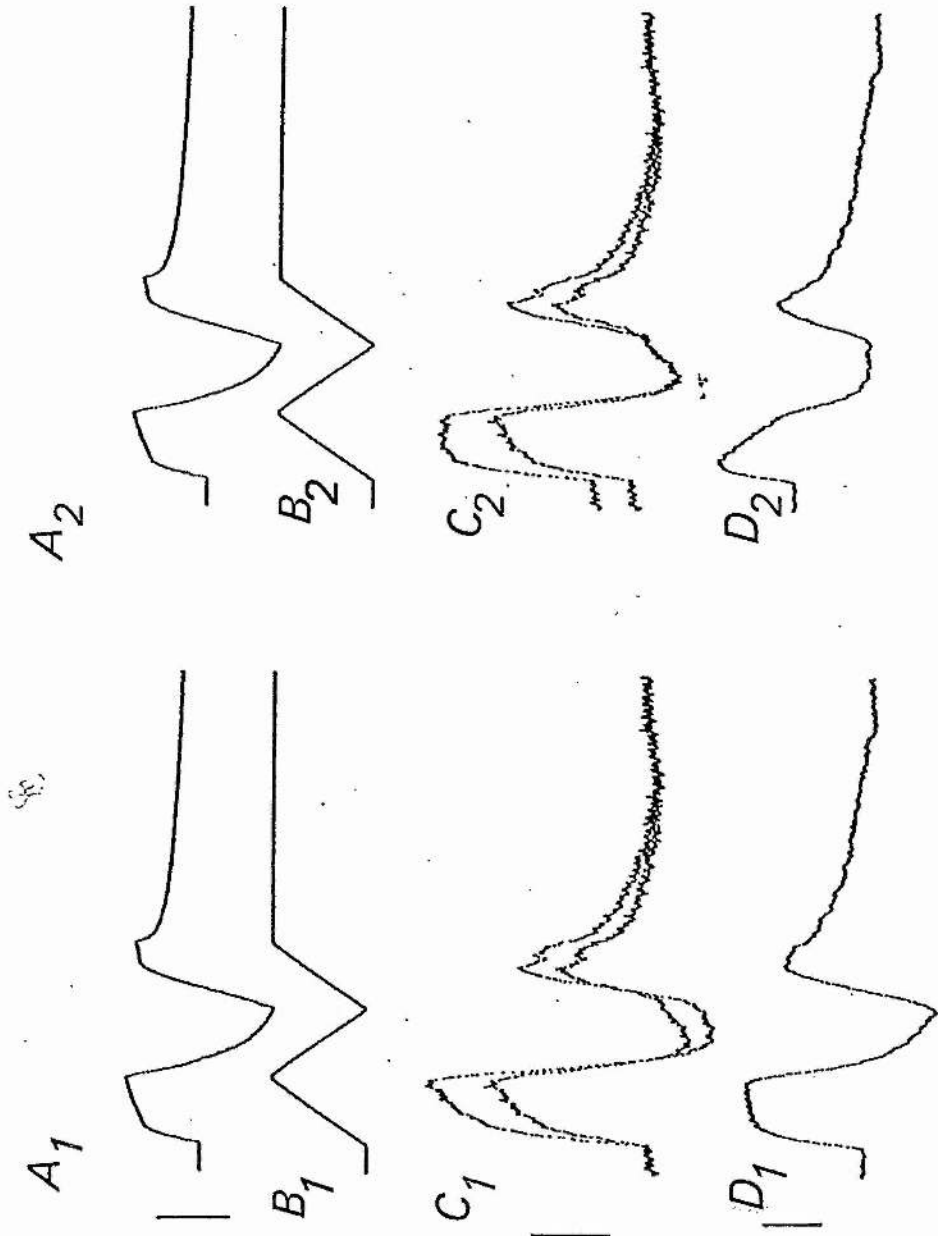
Tension - 10^5N.m^{-2}

Turbidity - 0.05

Dichroism - 0.02

Time - 100ms.

Fig 6.3



prior to the first stretch before making the baseline correction, whereas in C_2 the offset is removed after normalising both recordings to the value immediately prior to the second stretch. The dichroic signals D_1 and D_2 are derived from C_1 and C_2 in the usual way.

The portion of D_2 recorded during the second stretch and that of D_1 , recorded during the first stretch are shown superimposed in fig 6.4 (top traces), in order to facilitate the comparison between the two. The following points should be noted. First, D_1 and D_2 attain their peak amplitudes at different times, that is, after different amounts of muscle extension. In both cases, these values are reached at the time of sarcomere yielding. The maximum values for D_1 and D_2 are comparable. Secondly, the shapes of the two signals are quite different. D_2 is sigmoidal, concave upwards initially but concave downwards later on in the stretch, whereas by contrast D_1 rises monotonically from the onset of stretch. This difference in shape is to be expected if the orientation of the cross-bridge heads is not the same at the peak of a tetanus and at the end of a release.

2. Analysis of the dichroic signal waveform.

The waveform of the dichroic signals can be analysed to provide information on the angular orientation of the scattering dipoles. The latter are assumed to be attached cross-bridge heads and for the purpose of analysis they are taken to be infinitely thin, rigid rods.

It was shown earlier that the change in dichroism should follow eqn. 6.16;

FIG 6.4

The effects of first and second stretches on tension and dichroism are superimposed.

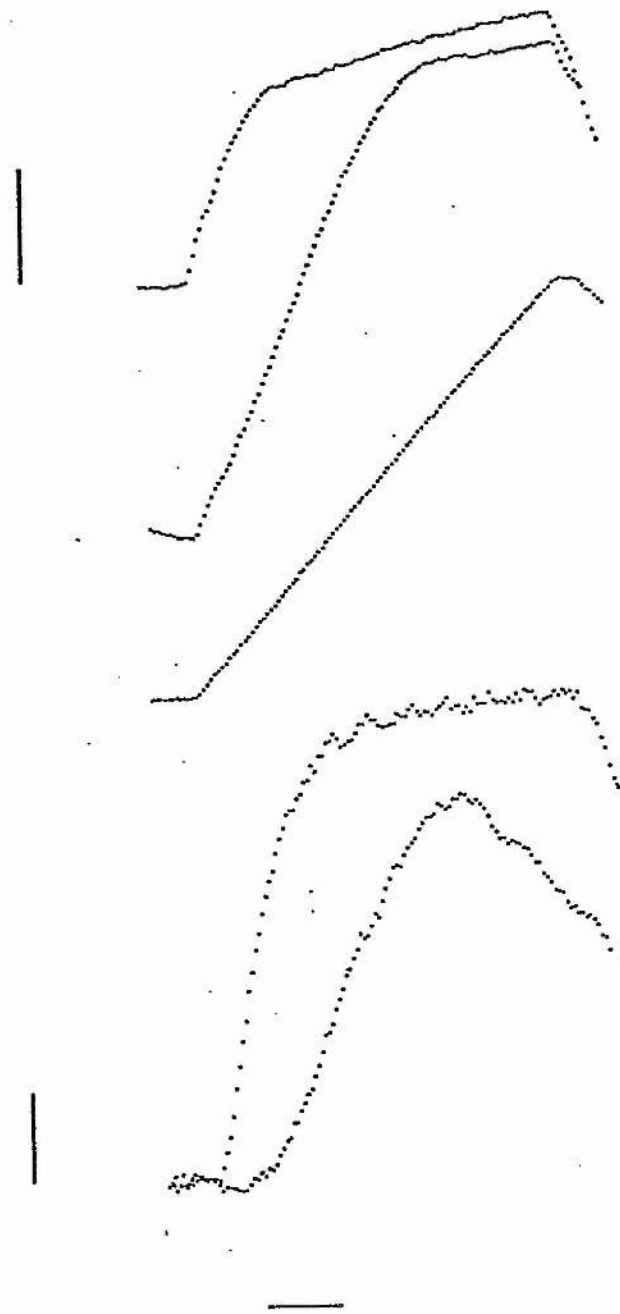
Scale bars:

Tension $0.5 \times 10^5 \text{ N.m}^{-2}$

Dichroism - 0.01

Time - 20ms

Fig 6.4



$$\Delta D \propto \overline{\cos^2 \mathcal{V}} - \Delta((1 - \overline{\cos^2 \mathcal{V}})/2)$$

where \mathcal{V} , defined in fig 6.1, is the axial tilt of the scatterers relative to the long axis of the filaments.

The procedure for fitting the experimental waveform to the above equation, so as to obtain values of start and finish angles (\mathcal{V}_1 and \mathcal{V}_2), was as follows.

First, the data array containing the dichroic signals was truncated, so that only those points collected from the beginning of the stretch to the yield point (determined from the tension record) were included in the subsequent analysis. The number of points selected in this was defined as N.

Next, values for the start angle, \mathcal{V}_1 , and the finishing angle, \mathcal{V}_2 , were selected and equation 6.16 evaluated for $(\mathcal{V}_2 - \mathcal{V}_1)/N$ intermediate angles. The theoretical values for D obtained in this way were compared statistically to the actual values obtained experimentally, after first scaling the theoretical values by the same factor required to make the maximum amplitude for the theoretical D equal to the experimental one. A least squares regression analysis (see eqn.5.5-5.8) was then performed on the two sets of data points. In practise, a repetitive program was devised to increment \mathcal{V}_1 and the difference between \mathcal{V}_2 and \mathcal{V}_1 ($\Delta\mathcal{V}$, the span covered) automatically, initially in 5° or 10° intervals and covering the range of \mathcal{V}_1 and $\Delta\mathcal{V} = 0-180^\circ$. The tabulated data was then inspected and the values of \mathcal{V}_1 and $\Delta\mathcal{V}$ giving the maximum value for r^2 , a measure of the goodness of fit, were determined. The procedure was then repeated, covering a more restricted range of \mathcal{V}_1 and $\Delta\mathcal{V}$ values, generally, $\pm 20^\circ$ of the first estimate, but this time increasing

the angular resolution by incrementing both parameters by 1° .

The results of this analysis are presented in table 6.1 for dichroic signals derived from both single and double stretch experiments. The mean values obtained for the single stretch data, from the recordings of fig 6.3, covering λ 's ranging from 514.5 to 457.9nm, were $\mathcal{V}_1 = 106 \pm \text{S.E. } 4.04^\circ$ and $\mathcal{V}_2 = 172.7 \pm \text{S.E. } 1.33^\circ$, which means that from the start of the stretch to the onset of sarcomere 'give', the angular range of movement of the scatterers ($\mathcal{V}_2 - \mathcal{V}_1$) is $66.7 \pm \text{S.E. } 4.26^\circ$.

The corresponding values obtained for the first stretch in the double stretch data compare closely with these: $\mathcal{V}_1 = 105^\circ$ and $\mathcal{V}_2 = 171^\circ$, with $\Delta\mathcal{V} = 66^\circ$. In contrast, the analysis of the dichroic signal recorded during the second stretch returned different values for \mathcal{V}_1 and $\Delta\mathcal{V}$, but a similar value for \mathcal{V}_2 : $\mathcal{V}_1 = 87^\circ$, $\mathcal{V}_2 = 179^\circ$ and with an increased range of movement ($\Delta\mathcal{V}$) of 92° .

DISCUSSION

It has been tacitly assumed that the dichroic signals arise from scattering elements which are forced to change their axial alignment as a result of the relative sliding motion of the filaments, and that such elements probably represent attached cross-bridge heads. The evidence in support of this hypothesis is outlined below, before considering some of the implications of the results presented in this chapter:

1. The values of r^2 (listed in table 6.1) measure the quality of fit of the experimental data to the theoretical waveforms derived from eqn. 6.16: values approaching unity indicate a good fit, and conversely, values tending towards zero indicate a poor fit. Those listed in table 6.1 all lie within 0.2% of unity (>0.998) and this suggests that the theoretical framework, upon which eqn. 6.16 is based, provides a realistic description of the process/es which generates the dichroic signal. It will be recalled that the model assumes that the signals are due to scattering dipoles which are made to undergo axial tilting as a result of the stretch.
2. The amplitudes of the dichroic signals do not vary in any systematic way with the wavelength of the incident light, whereas the turbidity signals, from which they are derived, display a marked dependence on λ . Moreover, estimates of \mathcal{V}_1 and \mathcal{V}_2 are similar for different λ 's, indicating that the waveform is also independent of wavelength.

Points 1 & 2 are consistent with the idea that the dichroic signals are the result of changes in the orientation of

Table 6.1

Analysis of the dichroic signals.

λ	γ_1	γ_2	$\Delta\gamma$	r^2	b	a	n_m	n_r	n_p
514.5	106	170	64	0.998023	0.98558	0.0012	1	10	31
488	113	174	61	0.998399	0.98892	0.0009	5	31	41
457.9 ₁	99	174	75	0.999232	0.99754	0.0006	8	40	33
$\bar{x} \pm \text{S.E.}$	106 ± 4.04	172 ± 1.33	66.26 ± 4.3						
457.9 ₁	105	171	66	0.999097	1.00853	0.0002	6	37	19
457.9 ₂	87	179	92	0.998371	1.00003	0.0004	6	37	63

* suffixes indicate first and second stretches.

n_m , n_r & n_p = numbers of muscles, records and data points used for curve fit analysis

r^2 = coefficient of determination, a = intercept and b = slope.

scattering elements, although neither gives any clue as to the identity of the scatterers. However, the following lines of evidence support the view that changes in the axial tilt of attached cross-bridges generate the dichroic signal.

3. The change in the dichroism varies with filament overlap. This can be inferred from fig 3.3: the two regression lines, relating $\Delta I/I_a$ to ΔP , the tension increment generated by stretch, converge at low ΔP values (= small filament overlap), and this means that the difference between the two (= dichroic signal) decreases with increasing sarcomere length.

4. It is possible to estimate the linear dimension of the scattering elements, d , and show that the result compares favourably with the length of the S_1 -HMM subunit. The amount of filament sliding required to induce sarcomere 'give' ΔS , was measured directly by Flitney & Hirst (1978a,b) and found to be 12.3 ± 0.9 nm for a first stretch and 18.3 ± 1.0 nm for a second stretch. From fig 6.5 it can be seen that:

$$\Delta S = d \cdot \cos \nu_2 - d \cdot \cos \nu_1 \quad (6.17)$$

$$= d(\cos \nu_2 - \cos \nu_1) \quad (6.18)$$

so that

$$d = \Delta S / (\cos \nu_2 - \cos \nu_1) \quad (6.19)$$

Table 6.2 shows that d , calculated from eqn. 6.19 and using values for ν_1 and ν_2 listed in table 6.1, ranges from 14.6 - 20.3 nm, with a mean value (\pm S.E.) of 17.33 ± 1.815 nm. This estimate falls within the range of published values for the long dimension of the S_1 -HMM subunit (Squire, 1981).

Dimensions of the actin-myosin interface.

Flitney & Hirst (1978a,b) reasoned that nearly all of the filament sliding required to induce sarcomere 'give' is associated with a change in the angle of attachment of the cross-bridge heads: indeed, they postulated that the relative motion of the myosin heads over the actin filament surface might actually represent a reversal of the structural events normally involved in the force generating process. In other words, in terms of the Huxley-Simmons model, the heads are constrained by stretch to move up (rather than down) a series of potential energy barriers, until the linkages are finally broken.

With this hypothesis in mind, the values obtained for \mathcal{V}_1 and \mathcal{V}_2 (and, hence, $\Delta\mathcal{V}$) can be used to make some estimate of the dimension of the actin-myosin interactive surface. The S_1 -HMM sub-unit is thought to be club-shaped, approximately 19nm in length, expanding towards its distal tip to ~6nm at its widest point.

Elliot & Offer (1978) have represented this by a model comprising a rod ~2nm in diameter and 13nm long, terminating in a 6nm diameter sphere (fig 6.5). Using this model, the linear dimension of the interactive surface between the S_1 tip and the actin filament is given by:

$$l = (\mathcal{V}_2 - \mathcal{V}_1) \cdot 2\pi \cdot r / 360 \quad (6.20)$$

Since $r = 3\text{nm}$ eqn. 6.20 reduces to:

$$l = (\mathcal{V}_2 - \mathcal{V}_1) \cdot \pi / 60 \quad (6.21)$$

Values for l calculated from the values for \mathcal{V}_1 and \mathcal{V}_2 in table 6.1 are shown in table 6.2, column 3. They range from 3.2 - 3.9nm for a first stretch, to 4.82nm for a second stretch. These figures imply that the relative motion between each S_1

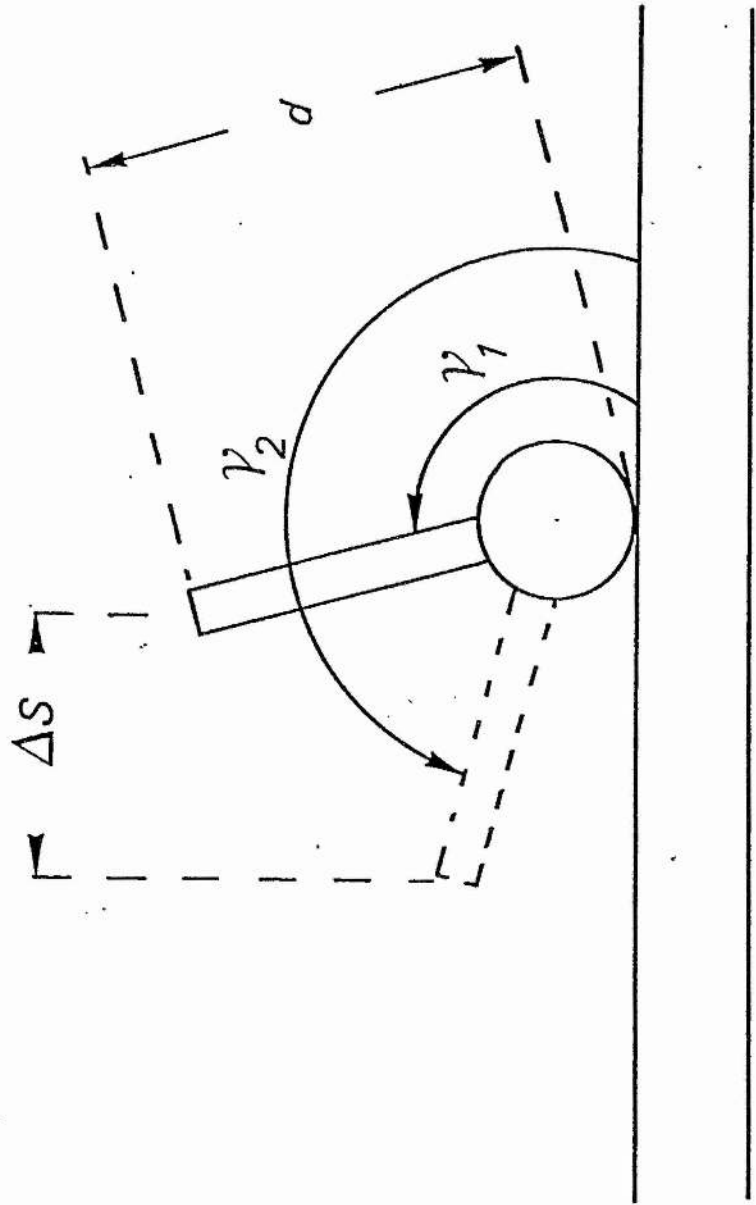
Table 6.2

λ (nm)	d (nm)	t (nm)	$\gamma_2 - \gamma_1$ ($^\circ$)
514.5	17.34	3.35	64
488	20.37	3.19	61
457.9 ₁	14.68	3.93	75
457.9 ₁	16.87	3.46	66
457.9 ₂	17.39	4.82	92
$x =$	17.33 \pm SE	1.81	

FIG 6.5

Diagram showing the cross-bridge head model and terminology used in this chapter.

Fig 6.5



CHAPTER VI

sub-unit and the actin filament is small enough to be accommodated on the surface of a single actin monomer. This conclusion is based on the assumption that the extreme tip of the myosin head is the only region which interacts with the actin filament, whereas this may not be so. There is some evidence (Mornet, Bertrand, Pantel, Audemard & Kassab; 1981) to show that more than one region of the head is involved in making the link and it is possible that two neighbouring (latitudinal) actin monomers become connected to each S_1 -HMM subunit.

CHAPTER VII

CHAPTER VII

SOME MOLECULAR AND ENERGETIC ASPECTS OF ACTIN-MYOSIN INTERACTION
IN LIVING MUSCLES.

CHAPTER VII

INTRODUCTION

The information gleaned from the foregoing analysis of the dichroic signals, relating to the axial tilt of the attached cross-bridges and the changes that occur on stretch, is potentially of value in helping to provide a clearer picture of the molecular events at the actin myosin interface and of the energetics of the force generating process.

The relationship between changes in cross-bridge orientation and the tension increment generated by stretch are here explored in some detail. The results obtained can be readily interpreted within the framework of the Huxley-Simmons model.

The analysis that follows makes one important assumption - that changes in the axial tilt of cross-bridges during stretch actually represent a reversal of the sequence of events which would normally take place during the cross-bridge working stroke. Stretch is therefore the agent which drives the fundamental contractile event, the molecular interactions between the actin-myosin complex, in reverse. There can be no direct proof that this assumption is justified, as will be seen, although some of the consequences of having made it lead to conclusions which are consistent with ideas based upon independent evidence, gathered using entirely different experimental approaches.

The analysis is divided into two sections: the first deals with the relationship between muscle tension, filament sliding and cross-bridge tilt, and provides evidence for the existence of sub-populations of cross-bridges having different attached

CHAPTER VII

configurations; and the second is concerned with calculations of the amount of work done on the cross-bridges during stretch. The latter enables an estimate to be made of the potential energy difference between different attached states. In both sections, comparisons are drawn between first and second stretches and this is crucial to the interpretation of the data.

I. Muscle tension, filament sliding and cross-bridge tilt:
evidence for different attached states.

A. Amount of filament sliding required to cause cross-bridge detachment. Changes in the tilt angle of the cross-bridge heads during stretch (from $\mathcal{V}_1 - \mathcal{V}_2 = \Delta\mathcal{V}$) can be used to estimate the axial movement of the filaments S_1 which would be necessary to induce cross-bridge detachment and bring about sarcomere 'yielding'. This is given by:

$$\begin{aligned} S &= d \cdot \cos \mathcal{V}_1 - d \cdot \cos \mathcal{V}_2 \\ &= d(\cos \mathcal{V}_1 - \cos \mathcal{V}_2) \end{aligned} \quad (7.1)$$

where d = length of cross-bridge head (= 19nm)

and $(\mathcal{V}_1 - \mathcal{V}_2) = \Delta\mathcal{V}$ the full range of angular motion of the attached heads.

The values for S , calculated using the data presented in table 6.1, are listed in table 6.2 for first and second stretches. The mean (\pm S.D.) value for a first stretch is 13.68 ± 1.83 nm and that for a second stretch is 19.9nm. Both are in excellent agreement with direct measurements of sarcomere length changes (by cine photography of diffraction spectra) which gave values of 12.3 ± 0.9 nm and 18.3 ± 1.0 nm, respectively (Flitney & Hirst, 1978a, b).

B. Muscle tension as a function of ΔS and $\Delta\mathcal{V}$. The tension transients can be represented as a function of filament displacement or, alternatively, as a function of the angle of tilt of attached cross-bridge heads.

The analogue form of the tension signal was digitised at a sample frequency of 1kHz, into n discrete values, and since the

sliding motion of the filament is a linear function of time, the extent of the motion as between individual data points, ΔS , is simply $S/n-1$, where S is computed from eqn. 7.1 using start and finish values for γ_1 and γ_2 . The axial displacement of the filaments for the i th. data point is then:

$$S_i = \sum_0^i (s/n-1) = \sum_0^i \Delta S \quad (7.2)$$

The angle of tilt of the cross-bridge heads associated with each tension data point is not a linear function of time and must be calculated from the extent of filament sliding and the starting angle γ_1 . For the i th data point it can be shown that:

$$\gamma_i = \arccos [(d \cdot \cos \gamma_1 - \sum_0^i \Delta S) / d] \quad (7.3)$$

Fig 7.1(A, B) shows muscle tension, P , plotted as a function of γ and fig 7.1(C, D) shows these same values plotted as a function of S . Both first (A, C) and second (B, D) stretches are represented and the data is taken from the double stretch series of experiments using $\lambda = 457.9\text{nm}$.

The most obvious feature to note is that each curve can be divided into a number of straight segments, where P varies linearly with γ or S : the segments are most easily discernible in the plot of P versus γ , where for a first stretch 3 (A_1-B_1 , B_1-C_1 and C_1-D_1) can be recognised and for a second stretch, 5 (A_2-B_2 , B_2-C_2 , C_2-D_2 , D_2-E_2 , E_2-F_2) can be identified.

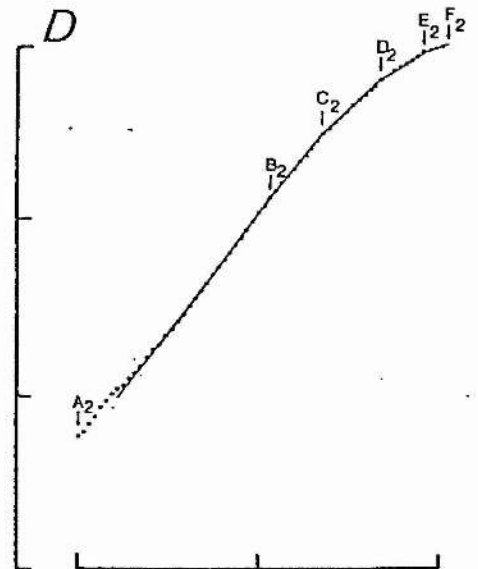
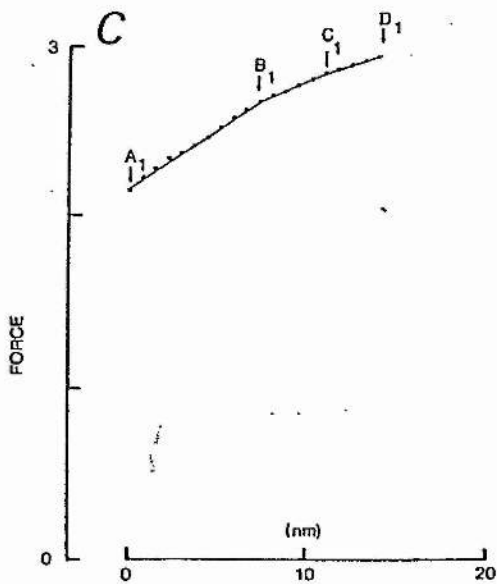
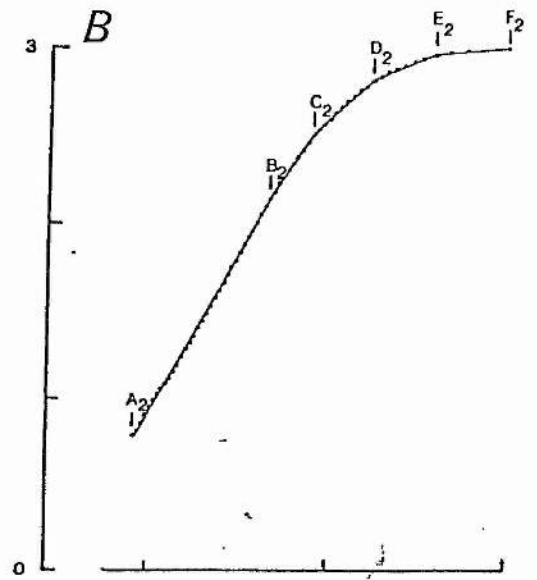
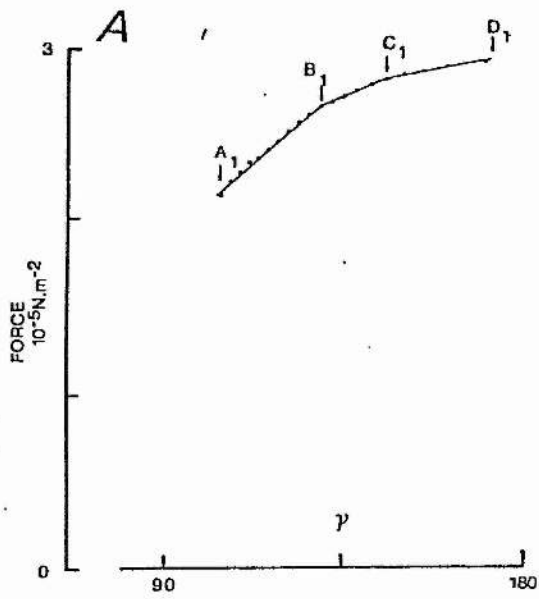
Table 7.1 shows the range of tilt angles ($\Delta\gamma$) and the equivalent amount of filament displacement (ΔS) associated with each of the segments. The tension increments per degree change of tilt ($\Delta P/\Delta S$) are shown for each segment in columns 4 & 5. The data points which define the limits of each segment are listed

FIG. 7.1

A., & B. Tension increment from the plateau of a tetanus to the yield point plotted against γ° .

C., D. The same data but plotted against filament sliding.

Fig 7.1



in column 6 and the total amount of filament sliding up to each of the points $B_1 \dots D_1$ and $B_2 \dots F_2$ appear in column 1.

The important points to notice about the data are the following:

1. The filament sliding required to reach the points C_1 and D_1 is approximately the same as that required to reach B_2 and C_2 .
2. The values for S corresponding to the points B_1 and D_1 and B_2 and F_2 are very nearly integer multiples of 3.4nm. This dimension will be referred to by the letter h . The mean percentage deviation (\bar{x}) from the nearest integer when $h = 3.4\text{nm}$ is $<3.3\%$. The difference becomes larger for $h = 3.3\text{nm}$ ($\bar{x} = 4.7\%$) and $h = 3.5\text{nm}$ ($\bar{x} = 3.5\%$).
3. The angular stiffness ($\Delta P / \Delta \psi$) and the slope stiffness ($\Delta P / \Delta S$) both decrease throughout stretch, in a stepwise fashion, at the points B_1 and C_1 and $B_2 \dots E_2$. This last point is referred to later, since it provides evidence for discrete populations of cross-bridges with different angular orientations.

II. Work absorbed by cross-bridges during stretch.

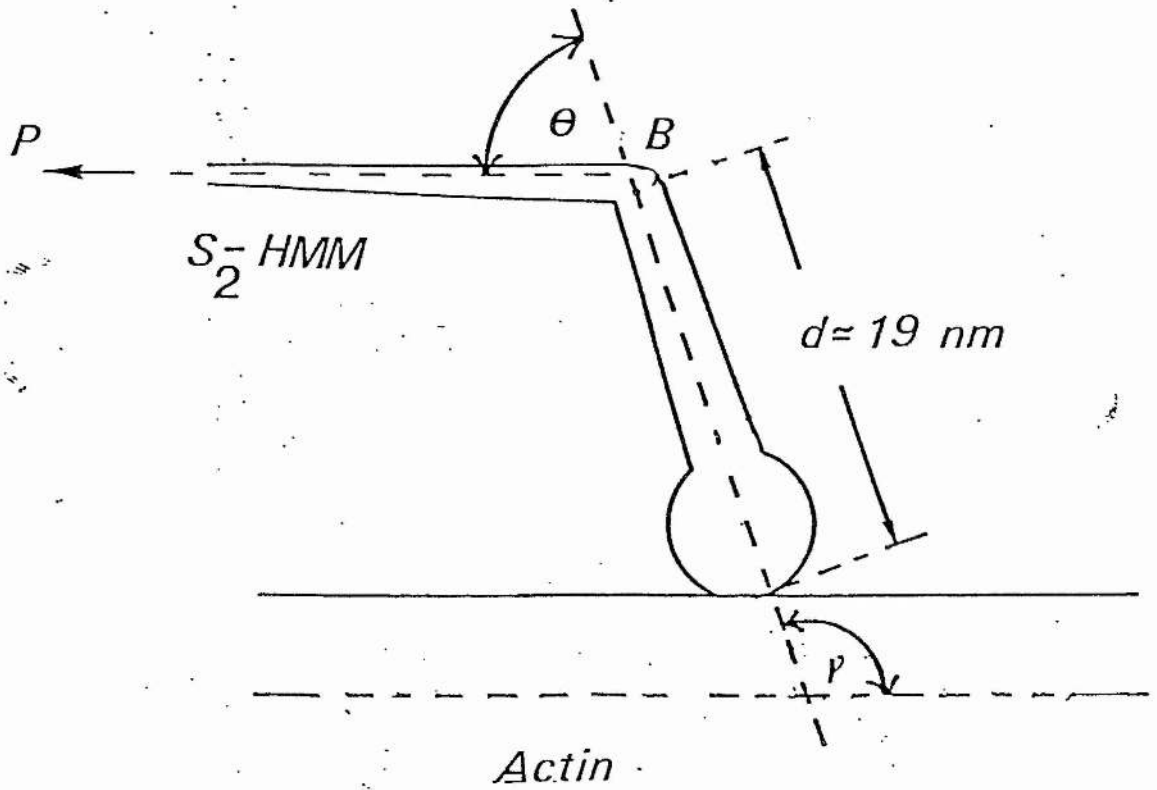
The amount of work, W , done on forcing the heads to change their angle of attachment can be calculated in the following way. Consider fig7.2. This shows a single cross-bridge head making contact with a nearby actin filament and connected to its myosin filament via the S_2 subunit of HMM. The point B is assumed to be a flexible 'hinge' region and the tip of the head is assumed to pivot on the actin filament surface.

The work done during a change of angle is:

FIG 7.2

Diagram illustrating the terms and dimensions of the cross-bridge model used in this chapter.

Fig 7.2



$$W = \Gamma \cdot \Delta\mathcal{V} \quad (7.4)$$

where Γ = moment of force about the actin-myosin contact zone (= torque)

and $\Delta\mathcal{V}$ = change in angle of the cross-bridge head.

The magnitude of Γ is given by:

$$\Gamma = P \cdot \sin\theta \cdot d \quad (7.5)$$

where P = applied force (= instantaneous tension)

d = length of moment arm (= 19nm)

θ = angle between the moment arm and the direction of P .

When the direction of P is parallel to the filament long axis (which it nearly is) then $\sin\theta = \sin\mathcal{V}$ and eqn. 7.5 becomes:

$$\Gamma = P \cdot \sin\mathcal{V} \cdot d \quad (7.6)$$

where \mathcal{V} has its usual meaning.

The work done on moving from \mathcal{V}_1 to \mathcal{V}_2 is:

$$W = \Gamma \cdot (\mathcal{V}_2 - \mathcal{V}_1) = \Gamma \cdot \Delta\mathcal{V} \quad (7.7)$$

where Γ is nearly constant for very small $\Delta\mathcal{V}$'s. However, for larger angular displacements, P varies continuously (and so does Γ) and the total work done is given by the sum of the work terms for many small $\Delta\mathcal{V}$'s, thus:

$$W = (W_1 + W_2 + W_3 + \dots + W_n) \quad (7.8)$$

where:

$$W_1 = (P_1 \cdot \sin\mathcal{V}_1 \cdot d) \cdot \Gamma_1$$

$$W_2 = (P_2 \cdot \sin\mathcal{V}_2 \cdot d) \cdot \Gamma_2$$

or for the i th. point:

$$W_i = (P_i \cdot \sin\mathcal{V}_i \cdot d) \cdot \Gamma_i = \Gamma_i (\mathcal{V}_{i+1} - \mathcal{V}_i) \quad (7.9).$$

Fig 7.3(A, B) shows muscle tension, P , torque, Γ , work absorbed

FIG 7.3

This diagram shows the same data as fig 7.1. Plotted in addition are: torque (Γ), work absorbed per angular displacement (ΔW) and accumulated work (ΣW).

Scales:

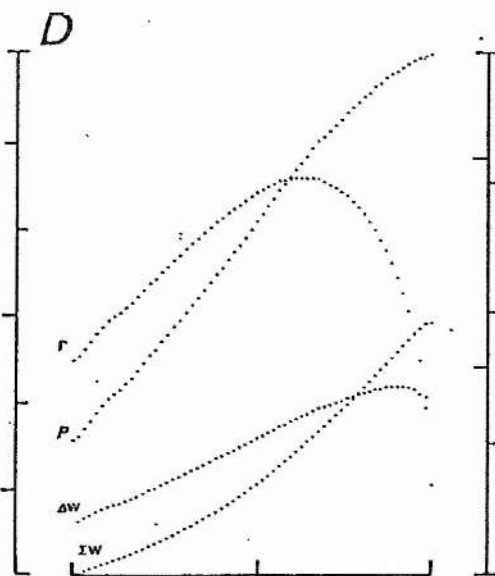
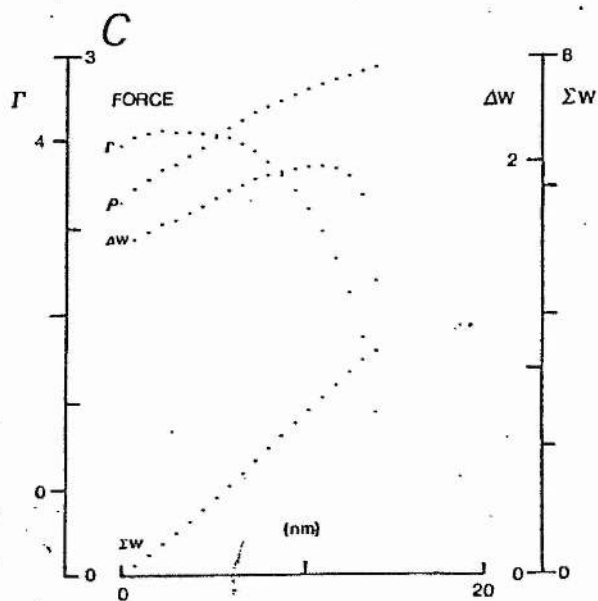
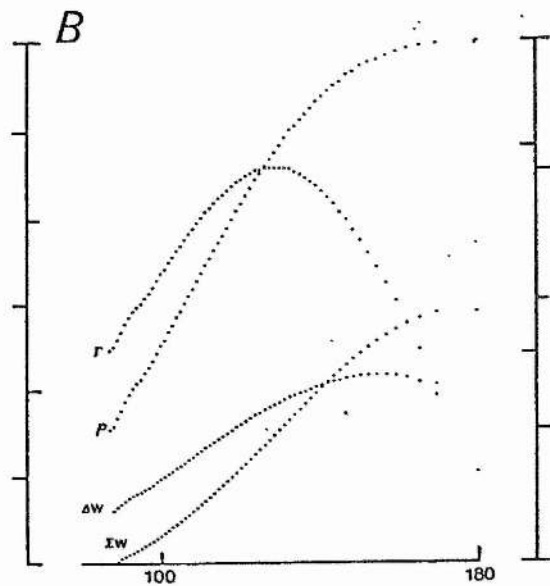
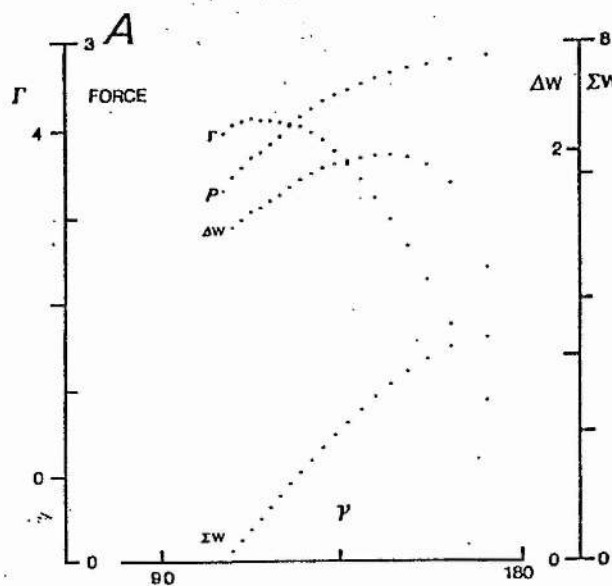
$$(\text{Force}) 0 - 3 \times 10^5 \text{ N.m}^{-2}.$$

$$(\Gamma) 0 - 0.001 - 005 \times 10^5 \text{ N.m}^{-2} \cdot \text{deg}^{-1}.$$

$$(\Delta W) 0 - 2.5^{-4} \text{ J}$$

$$(\Sigma W) 0 - 8 \times 10^{-3} \text{ J}.$$

Fig 7.3



per unit angular displacement, W , and the accumulated work, ΣW , as a function of \mathcal{V} for both first(A) and second(B) stretches. Fig 7.3 C, D shows the same four parameters, but plotted as a function of S .

The tension curves are sub-divided into the same segments as in fig 7.1 and the values for the segment slope and angular stiffness appear in table 7.1. Table 7.2 column 1 lists the work done on the muscle (calculated from eqn. 7.8) for each of the segments $A_1-B_1 \dots C_1-D_1$ and $A_2-B_2 \dots E_2-F_2$ and column 2 shows the accumulated work up to each of the points $B_1 \dots D_1$ and $B_2 \dots F_2$, both estimated graphically from the ΣW curves in Fig 7.3 A,B. The data shows that the total amount of work done on the muscle is greater for a second stretch than for a first: the values obtained are 3.844mJ.m^{-2} and 3.442mJ.m^{-2} respectively. The difference between these values, ΔW amounts to 0.402mJ.m^{-2} . Direct measurements of work absorbed by muscles subjected to a similar pattern of length change, published by Flitney & Hirst (1978b), gave comparable values: 4.29mJ.m^{-2} and 3.18mJ.m^{-2} , with ΔW equal to 1.11mJ.m^{-2} .

The number of cross-projections on the myosin filaments is estimated to be $\sim 5 \times 10^{16} \text{.m}^{-2}$ per half sarcomere (Huxley, 1963) and if they are all involved in forming linkages (which is not certain, however: see later) then ΔW for a second stretch amounts to $3.844/5 \times 10^{19} \text{J} = 7.69 \times 10^{-20} \text{J}$ per cross-bridge, and for a first, $\Delta W = 3.442/5 \times 10^{19} \text{J} = 6.88 \times 10^{-20} \text{J}$ per cross-bridge. The difference between these two estimates is therefore $0.81 \times 10^{-20} \text{J}$ per cross-bridge. This quantity is equal to the potential energy difference between the two preferred cross-bridge distributions and is therefore related, albeit in a

Table 7.1

	1	2	3	4	5	6
SEGMENT	s	Δs	$\Delta \gamma$	$\Delta P/\Delta \gamma$	$\Delta P/\Delta s$	DATA
	(nm)	(nm)	($^{\circ}$)	($\times 10^5 \text{N.m}^{-2} \cdot \text{deg}^{-1}$)	($\times 10^6 \text{N.m}^{-2} \cdot \text{m}^{-1}$)	POINTS
A ₁ -B ₁	7.22	7.22	25.0	0.0207	66.97	0-11
B ₁ -C ₁	10.87	3.65	16.5	0.0101	43.26	11-16
C ₁ -D ₁	13.76	2.89	24.0	0.0037	34.85	16-21
A ₂ -B ₂	10.61	10.61	33.5	0.0408	132.34	0-34
B ₂ -C ₂	13.57	2.96	11.2	0.0342	129.66	34-43
C ₂ -D ₂	16.79	3.22	14.8	0.0225	97.38	43-53
D ₂ -E ₂	19.05	2.26	15.5	0.0092	66.35	53-60
E ₂ -F ₂	20.02	0.97	18.0	0.0014	42.78	60-63

Table 7.2

SEGMENT	1 ΔW (mJ.m ⁻²)	2 ΣW (mJ.m ⁻²)	3 posn.	4 f
A ₁ - B ₁	1.756	1.756	2	0.512
B ₁ - C ₁	0.968	2.724	3	0.309
C ₁ - D ₁	0.718	3.442	4	0.179
A ₂ - B ₂	1.533	1.533	3	0.162
B ₂ - C ₂	0.654	2.187	4	0.287
C ₂ - D ₂	0.849	3.036	5	0.326
D ₂ - E ₂	0.653	3.689	6	0.192
E ₂ - F ₂	0.155	3.844	7	0.033

complex way (see below) to the potential energy difference between consecutive cross-bridge positions. In order to pursue this important question further it is necessary to construct a formal model.

Working hypothesis

The data can be interpreted in terms of the Huxley-Simmons model. Briefly, each cross-bridge has a number (n) of attachment sites through which it interacts with corresponding sites on a nearby actin filament. Attachment through any two consecutive sites constitutes a stable position, of which there are $n-1$. The force is generated, after attachment of the head, in a series of stepping movements, from one stable position to the next, a process made possible because each stable position has a lower potential energy level to the one preceding it. There are thus a number of positions ($n-1$) of discrete orientations which will be referred to as x . The fractional occupancy of each position prior to stretch can be written:

$$l = a+b+c+d\dots\dots m \quad (7.10)$$

where a, b, c, d, \dots, m represents the fraction of heads in positions $1, 2, 3, 4, \dots, X$.

When a muscle is stretched, causing the heads to roll backwards, those cross-bridges in position 1 will become detached first, followed by those in position 2, then 3 and so on, until those in x are finally detached. This will occur for filament displacements equal to integer multiples h , the amount of filament sliding between consecutive head orientations ($\sim 3.4\text{nm}$). The angular distribution of heads is therefore altered sequentially during stretch, as follows:

CHAPTER VII

$$l = a+b+c+d\dots m$$

(initial state before stretch)

$$l-a = b+c+d\dots m$$

(loss of position 1 for filament sliding of h nm)

$$l-(a+b) = c+d\dots m$$

(loss of position 2 for filament sliding of 2h nm)

until

$$l-(a+b+c+d\dots m) = 0$$

(loss of all positions for a filament sliding of x.h nm).

If some of the positions are unoccupied in the initial (pre-stretch) state, say for example, positions 1 & 2, then we have:

$$l = c+d+e\dots m$$

(before stretch)

$$l - c = d+e\dots m$$

(loss of position 3 for sliding of 3h nm)

$$l-(c+d) = e\dots m$$

(loss of position 4 for sliding of 4h nm)

or, in general, the loss of heads will correspond with displacements of hn , $h(n+1)$, $h(n+2)$, $h(n+3)$ $h(n+x)$, where n is an integer = $x-y$ and y is the number of occupied positions.

Stepwise reduction of muscle stiffness. The above sequence of events will result in a stepwise reduction of muscle stiffness, as is observed experimentally (Table 7.1). In principle, it is possible to make use of this experimental data to estimate the fractional occupancy of each of the available x orientations. This requires one additional assumption: that the stiffness of every attached head is the same as that for any other regardless of orientation. Since the cross-bridges are acting in parallel,

their stiffness is additive and so we can write:

$$K_1 = K_a + K_b + K_c \dots K_m \quad (7.11)$$

where k is the stiffness of a single cross-bridge and a, b, c, \dots, m again represent the fraction of the heads in positions $1, 2, 3, \dots, x$. Thus, K_1 in eqn. 7.11 is the stiffness of the first segment (A_1-B_1 or A_2-B_2) since it represents the combined stiffness of the total cross-bridge population.

Then, for segment 2:

$$K_2 = K_1 - K_a = K_b + K_c \dots K_m \quad (7.12)$$

and for segment 3:

$$K_3 = K_1 - (K_a + K_b) = K_c \dots K_m \quad (7.13)$$

etc.

Fig 7.4A shows the angular stiffness of each segment plotted against the segment length for both first (A) and second (B) stretches. This is a graphic representation of the data in columns 2+4 in table 7.1, and shows the stepwise reduction in stiffness for various multiples of $h \sim 3.4\text{nm}$.

For the first stretch, the initial step reduction occurs at a distance $d \sim 2h$, the next at $3h$ and the third at $\sim 4h$. This means that there are heads in positions 2, 3 & 4, but not in 1 or other positions >4 . Similarly, for a second stretch, the first step is at $d \sim 3h$, then $4h$, $5h$ and finally 6 (or 7) h . There is some uncertainty whether or not the last position represents 6 or 7 but it does not materially alter the outcome of the analysis.

Frequency distribution of head orientations. By using the angular stiffnesses, K_1 , K_2 etc. listed in table 7.1 column 4

we can estimate the numerical values for a, b, c...m, in the following way.

Consider, first, segment A_2-B_2 . The value for K_1 ($= 0.0408 \times 10^5 \text{ N.m}^{-2} \cdot \text{deg}^{-1}$) represents the stiffness of heads in positions 3, 4, 5, 6 & 7. K_2 for segment 2 represents the combined stiffness of heads in positions 4, 5, 6 & 7, those in position 3 having been lost, and is equal to $0.034 \times 10^5 \text{ N.m}^{-2} \cdot \text{deg}^{-1}$. The difference $K_1 - K_2 = 0.0066 \times 10^5 \text{ N.m}^{-2} \cdot \text{deg}^{-1}$ represents the contributions from the heads in position 3. This contribution is made by $(K_1 - K_2)/K_1$ of the total population = 0.162.

The same line of reasoning can be applied to all of the segments, generating the frequency distribution in fig 7.5. The fractional occupancies, f , calculated in this manner are also listed in table 7.2 column 4.

Potential energy differences between consecutive cross-bridge orientations. The information in columns 1 & 4 of table 7.2 can now be used to estimate the potential energy difference between consecutive cross-bridge positions. Consider the data for a first stretch. Column 1 shows that the energetic cost of moving the heads in position 4 through 4 consecutive positions = 0.718 mJ.m^{-2} . Column 4 shows that the fraction, f , of heads originally in position 4 = 0.179, so the work done by moving each cross-bridge through 4 positions is simply $0.718/5 \times 0.179 \times 10^{19} \text{ J} = 8.02 \times 10^{-20} \text{ J}$. Similarly, for a second stretch, the work done on moving heads initially in position 7 through 7 positions = $0.155/0.033 \times 5 \times 10^{19} \text{ J} = 9.39 \times 10^{-20} \text{ J}$ per cross-bridge. The difference in the number of steps between first and second stretches is 3 and this is associated with an amount of work =

FIG 7.4

Angular stiffness plotted against displacement for first and second stretches, further details given in text.

Fig 7.4

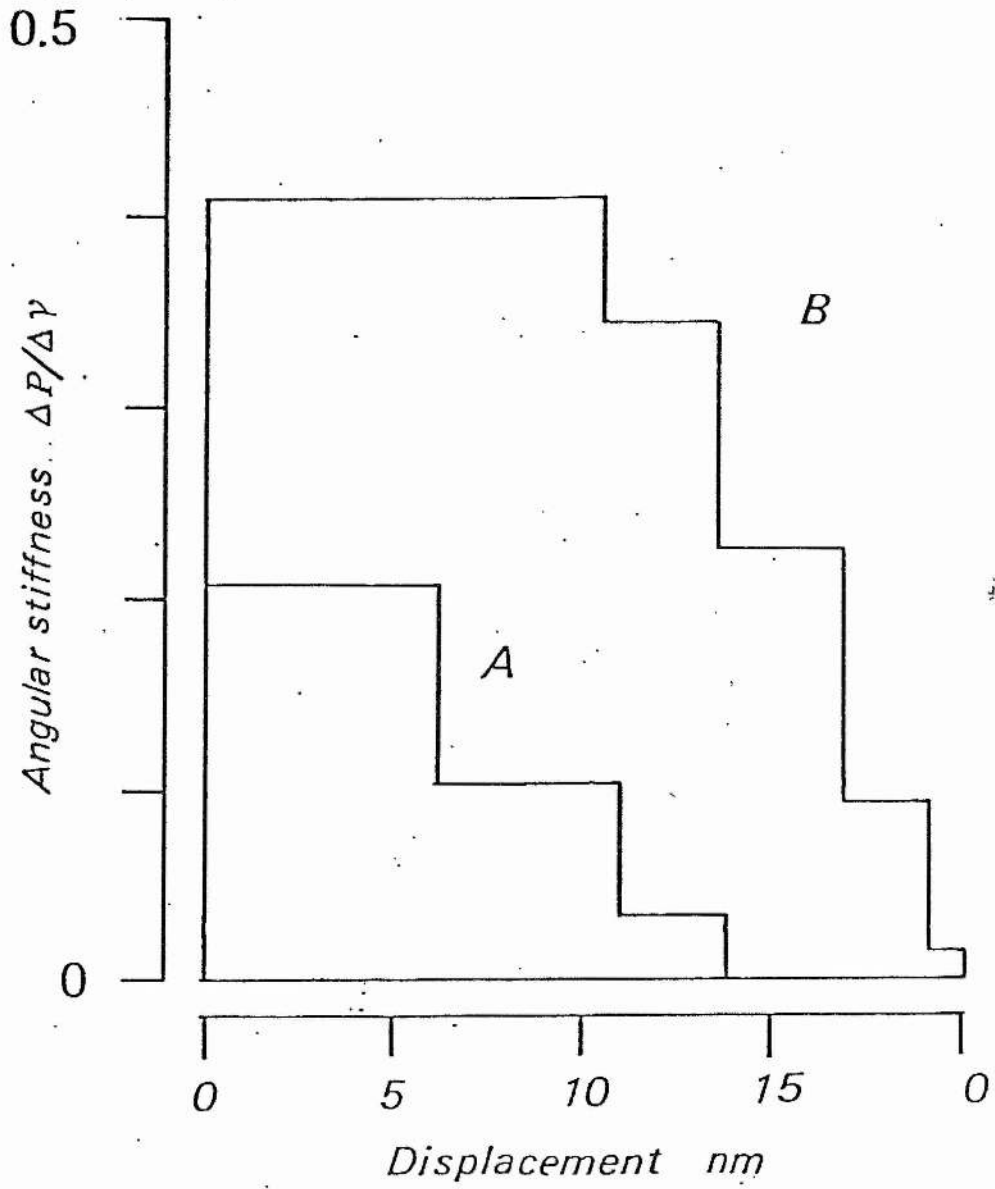


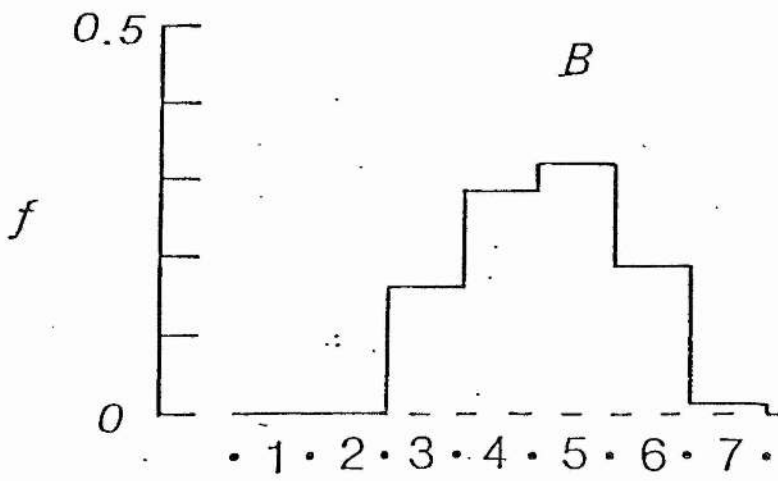
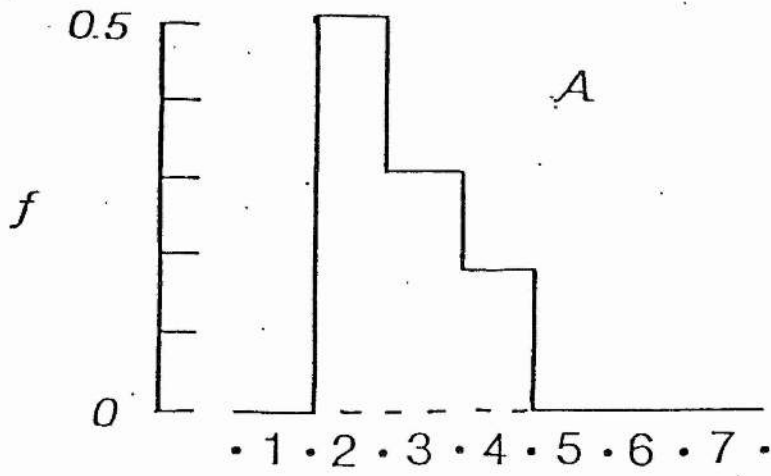
FIG 7.5

Histograms of the fractional occupancy of cross-bridge head positions.

A. First stretch.

B. Second stretch.

Fig 7.5



Position

CHAPTER VII

$9.38 \times 10^{-20} - 8.02 \times 10^{-20} = 1.37 \times 10^{-20} \text{ J}$ per cross-bridge. If we assume that each stable position is separated from its neighbour by an equal potential energy step, U , then this is $1.37 \times 10^{-20} \text{ J} / 3 = 0.457 \times 10^{-20} \text{ J}$.

CHAPTER VIII

CHAPTER VIII

DISCUSSION AND SCOPE FOR FURTHER STUDY.

SUMMARY

The experiments described in this thesis and the major findings can be summarised as follow:

1. A study has been made of the optical transients and associated tension responses generated by stretching active frog's muscle. Sartorius muscles were illuminated with laser light (spectral range 457.9 - 632.8nm), stimulated electrically and then stretched at the plateau of a tetanus. The intensity of the light in the central region of the zero-order line was recorded, together with muscle tension and length. An electro-optical system, incorporating a Pockels cell and sample hold device, oscillated the electric vector through $\pi/2$ radians (between angles (ϕ) of 0° and 90° relative to the muscle long axis) at a frequency of $\sim 7\text{kHz}$, enabling 'simultaneous' recordings of light transmission to be made at orthogonal beam orientations.

2. The rate of rise of tension (slope stiffness) is high initially (phase I) but then decreases abruptly and remains at the lower value during the remainder of the stretch (phase II). Tension persists above but decays towards the original isometric level in the period after stretch (phase III). The transition between phases I-II corresponds with an abrupt lengthening of the sarcomeres caused by cross-bridge detachment.

3. The transmitted light intensity decreases during stretch: this is represented either as a decrease in transparency or an increase in turbidity. The form of the response is complex: it contains length- and tension-dependent components. The latter is

CHAPTER VIII

triphasic and each of its component parts (phases i, ii & iii) corresponds with one of the phases (I, II & III) of the associated tension transient.

4. The amplitude of the decrease in light intensity varies in direct proportion to the tension increment, ΔP , when both parameters are measured at the sarcomere yield point and when ΔP is varied experimentally by varying the starting muscle length. The responses are maximal at maximum filament overlap.

5. Changes of transparency/turbidity are highly anisotropic with respect to ϕ . The amplitudes at any given λ are consistently greater for $\phi = 0^\circ$ than for $\phi = 90^\circ$. The difference between the two signals (0° - 90° responses) increases steeply during the early part of the stretch and is maximal at (or near) the point of sarcomere yielding.

6. Both 0° and 90° signals vary inversely with λ in the range 457.9 - 632.8nm. The wavelength dependence is significantly greater for $\phi = 90^\circ$ ($\lambda^{-3.87}$) than for $\phi = 0^\circ$ ($\lambda^{-2.39}$). These observations suggest that a major component of the optical signals is due to a change of light scattering and that the 90° signal contains a greater contribution from small size ($<\lambda/20$) scattering particles. It is concluded that deformation of the cross-bridges, caused by stretch, contributes to the scattering change.

7. Experiments were made in which muscles were subjected to a pattern of length change comprising a stretch, followed immediately by a release, and then a restretch from a low tension state. Comparisons were drawn between optical and tension responses during stretch from the high (P_0) and low

($0.4P_0$) tension states.

8. The amplitude of the increase in muscle conservative dichroism, $\Delta D (= \Delta\tau_{0^\circ} - \Delta\tau_{90^\circ})$, is inversely related to muscle length. The initial change - that is, up to the point of sarcomere yielding - is independent of λ . The waveform of this component is well fitted by the equation $D = \cos^2\gamma - (1 - \cos^2\gamma/2)$. This describes the expected change in dichroism caused by a change in the axial tilt (γ) of the scattering dipoles, imposed by stretch. Analysis shows (a) that the dimension of the dipole axis is around 17nm, which is close to published values for the long axis of the S-1 HMM sub-unit (= cross-bridge head); and (b) from a statistical curvefit procedure, the mean starting and finishing tilt angles ($\bar{\gamma}_1$ and $\bar{\gamma}_2$) are $106 \pm 4.04^\circ$ to $172.7 \pm 1.33^\circ$ for a first stretch, and 87° to 179° for a stretch commencing from a low tension state.

9. Calculations of the total amount of work done in forcing the heads to rotate backwards until they become detached, using values of $\bar{\gamma}$ derived from the experimental data, show a greater amount of work is absorbed for a second stretch compared to a first: 3.84mJ.m^{-2} as compared to 3.44mJ.m^{-2} . The difference amounts to $\sim 0.8 \text{J} \times 10^{-20}$ per cross-bridge.

10. The tension increment per unit change of tilt angle ($\Delta P/\Delta\gamma$) decrements in a stepwise fashion throughout a stretch. It is thought that this provides evidence for discrete populations of cross-bridges, attached initially with different axial tilts. Points separating consecutive linear segments of the $\Delta P/\Delta\gamma$ curves are separated by whole integer multiples of $\sim 3.4 \text{nm}$.

11. The results are interpreted in terms of a multi-step force

CHAPTER VIII

generating mechanism, similar to the Huxley-Simmons model. The assumption is made that stretch forces the heads to rotate backwards, the reverse of what happens during the working stroke of the cross-bridge. The effective interactive surface between the S-1 sub-unit of HMM and the actin filament is estimated to be 4.8nm , which is just small enough to be accommodated on a single actin monomer. The data suggest that there may be as many as 6 or 7 discrete angular orientations for attached heads, each separated from its neighbour by a potential energy difference of $\sim 0.46 \times 10^{-20}\text{J}$. The average distance between the two attachment sites which specify a particular orientation is calculated to be $\sim 0.7\text{nm}$. The linear sliding motion of the filaments associated with one cross-bridge working stroke is thought to be $\sim 5-6 \times 3.4\text{nm} = 17-20\text{nm}$.

DISCUSSION

Many of the questions raised by this study have been discussed in earlier chapters and will not be referred to in any detail again here. Emphasis will be given instead to some of the uncertainties relating to the interpretation of the data before going on to discuss the possible significance of the conclusions which have been drawn.

Consider, first, the evidence which links the optical transients to structural events occurring in the contractile elements. There is little doubt that the tension increment that accompanies stretch is almost entirely due to deformation of cross-bridges between the actin and myosin filaments: it is known (Flitney & Hirst, 1978a; see their fig 8) that the tension borne by a muscle at the point in a stretch where the slope

stiffness falls varies inversely with muscle length and the amplitude of the fast tension transients produced by abrupt (sub millisecond) length steps also depends upon the extent of the actin-myosin filament overlap (Ford, Huxley & Simmons, 1981; their fig 6). The obvious similarity in the form of the optical transients and that of the tension responses seen in these experiments - it will be recalled that both comprise three distinct phases which are closely related temporally - is therefore fully consistent with the idea that they have a common underlying cause. This interpretation is strengthened by the finding that the amplitudes of the optical signals vary in direct proportion to the tension increment, ΔP .

Much of the analysis depends on Flitney & Hirst's interpretation of the force records and sarcomere length changes which are known to accompany stretch. These authors argue that the sudden transition between the high and low stiffness states (at their point S2) is probably caused by the deformation and eventual detachment of actin-myosin linkages. This interpretation is in keeping with the simultaneous occurrence of an abrupt lengthening of the sarcomeres ('give') which is observed after the filaments have been displaced by ca. 10-12nm. Flitney & Hirst further showed that this latter distance is independent of the starting muscle length and this result supports the idea that sarcomere yielding results from the deformation of a structure which has a finite range of movement and which is located in the region of filament overlap. The evidence, then, clearly favours the idea that the myosin cross-projections are initially deformed by stretch and are ultimately forced to dissociate from actin: it is not considered likely that projections could ever remain attached to actin throughout

phase II of the tension response because the total displacement up to and including 'yielding' is around 33nm. This is considerably greater than any current estimates of the range of movement of a cross-bridge. It is conceivable, however, that inhomogeneities in the behaviour of the sarcomeres in different regions of the muscle might be associated with the transition at S_2 . This possibility was not investigated in any detail by Flitney & Hirst, although the fact that they recorded sarcomere lengths at three different levels in the muscle and obtained nearly identical results (see their fig 6, and fig 1.28 here) should be emphasised as it is the only experimental evidence available. Sarcomere length changes were not recorded in this study and so the possibility that sarcomere inhomogeneities may have played a part in determining the optical responses must be considered. Theoretically, sarcomere yielding in any localised region of the muscle could produce force records such as were obtained in this study. However, if this occurred, and the regions which underwent yielding were not the same as those being illuminated by the laser, then one would not expect to always find a clear temporal relationship between the different phases of the optical and tension responses. It has been repeatedly stressed that this is an invariant finding and this fact argues against local sarcomere inhomogeneities playing a dominant role in determining the optical events. Obviously, it would have been preferable to have made recordings of sarcomere lengths in this study too, but this was not practicable and so the possibility that non-uniform sarcomere length changes might be important cannot be excluded at the present time.

There is also some uncertainty about the physical nature of the optical signals. It was impossible to make directional

recordings as would be required to provide an unequivocal answer. The tentative conclusion, that a change of light scattering makes a major contribution to the signals, is based upon the observation that their amplitudes vary inversely with wavelength: in the case of responses recorded with $\phi = 90^\circ$, the wavelength exponent (-3.87) approaches that expected for a small size ($\lambda/20$) Rayleigh scatterer, whereas the 0° signals have an exponent (-2.39) which is closer to that expected for a system of long thin cylinders (= -3). It was clearly stated earlier (p5.15) that this degree of agreement does not in itself constitute proof that a change in scattering is involved. There are two relevant points to note here. First, the wavelength dependence of the signals does not exclude a contribution (possibly, the major one) from a change of diffraction. Diffraction is simply one extreme example of scattering, from a system of orderly scatterers, and so it maybe that this could have a similar wavelength dependence. The only pointer that diffraction is not likely to be the major factor involved comes from the observation that the form of the optical signals does not resemble the pattern of sarcomere length changes recorded by Flitney & Hirst. Secondly, as noted previously (p5.4), muscle is a relatively condensed optical system and it is not clear to what extent multiple scattering, which is almost certain to occur, would influence the wavelength dependence of the signals.

Finally, the increase in conservative dichroism seen during stretch is interpreted as being due to a change in angular orientation of linear scattering dipoles. It is inferred that these may actually represent attached cross-bridge heads, and while this may turn out to be correct, it has to be admitted that this is an assumption at present. In its favour, it may be

noted that the sign of the effect is in the right direction, because stretch would tend to align cross-bridge heads more closely to the filament long axis.

The above considerations reveal a number of uncertainties relating to the interpretation of the data which cannot yet be resolved satisfactorily. It is still of some interest, however, to explore further some of the consequences of taking the results at face value, because of their potential importance in helping to understand the force generating process more fully.

The most important conclusions are derived from the experiments of chapters 6 + 7 and are based upon the quantitative analysis of the change in muscle conservative dichroism caused by stretch. In this context, it is clear that the origin of the dichroic signal is crucial to the interpretation of the results. Some evidence was presented earlier (chapter VI) to support the idea that it is due to a change in the tilt angle of the attached cross-bridges: calculations based upon the extent of filament sliding required to induce sarcomere 'yielding', from laser diffraction experiments by Flitney & Hirst (1978b), and the estimates of \bar{p}_1 and \bar{p}_2 obtained in this study, show that the dipole axis must be around 17nm in length. This is within the range of estimates for the long dimension of the S-1 HMM sub-unit, based upon a variety of experimental approaches, cited by Squire (1981). Furthermore, a simple argument shows that the magnitude of the dichroic signal is also consistent with the idea that it is generated by the cross-bridges. It can be assumed that the changes in turbidity caused by re-orientating particles would be in proportion to their volume fraction, v . If we evaluate eqn.

6.16 using values for \bar{v}_1 and \bar{v}_2 observed experimentally ($\sim 106^\circ$ and 172° , respectively) then the dichroism changes upon stretch from -0.39 to 0.97, a change of 1.36. The actual change is much less: the values obtained range from 0.0378 - 0.0551, with a mean (\pm S.E) of 0.046 ± 0.008 . This suggests that only a small fraction of the total scattering material behaves in the way envisaged: approximately $0.046/1.36 = 0.0338$. This can be compared to a value for v of 0.028 obtained for the S-1 HMM sub-unit by Irving (1987). The discrepancy is not large, especially since the model used here does not take into account any contribution from the S-2 HMM sub-units, nor does it allow for the possibility that not all of the cross-bridges are necessarily linked to actin at the start of stretch. Finally, one further point to refer to again here is the finding that the waveform of the experimentally obtained dichroic signal is virtually identical to that predicted by the model.

These considerations make it likely that the dichroic signal contains useful information on cross-bridge tilt angles and it is pertinent to ask the question: how do the values for \bar{v}_1 and \bar{v}_2 compare with estimates based on other experimental approaches? Irving (1987, in press) has shown that the transition from the resting to the fully activated state is associated with a drop in fibre birefringence of ~ 0.11 and he argues that if this is solely due to a change in the tilt angle of the S-1 HMM (θ in fig 7.2), then this would be from 30° to 50° . In terms of the angle γ in the present model ($\theta = 180 - \gamma$) this is equivalent to a change from 150° at rest to 115° on activation. The mean starting angle for stretches beginning from the plateau of an isometric tetanus (i.e. first stretch) was found to be $\sim 106^\circ$, which is close (to within 8%) to the figure

CHAPTER VIII

several, histochemical types. It is conceivable, therefore, that each transition point merely signals the complete detachment of all the cross-bridges in different populations of fibres - each with its own characteristic range of tilt angles over which the heads are permitted to rotate - rather than the sequential detachment of cross-bridges with differing starting configurations. There is another, related point to consider here. The analyses are based upon computer averaged responses, often from many records and several muscles, so that small differences in the time of onset of sarcomere yielding could show up as a change of slope or angular stiffness. There are reasons for thinking that neither of these two factors provides a plausible explanation for the present results. First, linear segments can be discerned clearly in individual tension records; and secondly, the occurrence of the transition points separated by intervals of multiples of $\sim 3.4\text{nm}$ would argue against sources of error of a random nature. The situation could be made clearer using identified single fibres in future work, where such variability would not arise.

Finally, the model for the cross-bridge which emerges from this study can be used to predict the amount of work done during its normal cycle. If we take the number of possible configurations as being between 5 and 7 and the potential energy difference between consecutive positions as $\sim 0.46 \times 10^{-20}\text{J}$, then each cross-bridge could generate between $1.84 - 2.76 \times 10^{-20}\text{J}$ per cycle. On the assumption that each cycle is coupled to the hydrolysis of one molecule of ATP, then the work done by a muscle would amount to $1.84 - 2.76 \times 10^{-20} \times 6.02 \times 10^{23}\text{J.mole}^{-1}$ ATP hydrolysed, or $11.1 - 16.6\text{kJ.mole}^{-1}$. The amount of useful work done by real muscles is estimated to be around 4.4kcal.mole^{-1}

calculated from the birefringence data.

The significance of the angle $\bar{\nu}_2$ is more difficult to evaluate. It seems unlikely that it can represent any physiological cross-bridge position, for the following reason. The assumption was made earlier that stretch causes the attached cross-bridge heads to rotate backwards over the actin filament surface: in effect, they are made to undergo a change of tilt, which is the reverse of what happens in a cross-bridge during its normal working stroke. On this hypothesis, $\Delta\gamma$ can be used to estimate the extent of the interactive surface between the myosin head and the actin filament. The dichroic signals indicate that $\bar{\nu}_2$ approaches 180° (for both first and second stretches), showing that the heads are forced into a position where they lie almost parallel to the filament long axis. It is difficult to imagine that this could represent the starting position for a cross-bridge during its normal working stroke - it is much more likely that it commences at some orientation between $\bar{\nu}_1$ and $\bar{\nu}_2$. This would mean that the present estimate of the dimension of the active surface, $\sim 4.8\text{nm}$, is almost certainly an over estimate.

The evidence for the existence of different attached cross-bridge configurations comes from the observation that the tension increment per unit angle of tilt is made up of a series of linear segments and this is crucial to the analysis: the transition between each one is thought to represent the sequential detachment of each sub-population of cross-bridges, brought about by stretch. This interpretation needs to be considered carefully in the light of the preparation being used. The frog sartorius muscle contains hundreds of fibres of

(Huxley & Simmons, 1971) and this is equivalent to 18.39kJ.mole^{-1} , close to the upper limit predicted by the model.

SCOPE FOR FURTHER STUDY

Some of the limitations discussed above could be minimised by using single fibres in any future study. It would be possible then to record dynamic changes in the length of the sarcomeres during stretch - which was not feasible here - and this would have a number of important advantages: it would enable one to study directly the way in which the optical signals appear to depend on filament overlap; individual optical recordings could be related directly to the sliding motion of the filaments; and observations could be made during relaxation, where events similar to those caused by stretch (i.e. cross-bridge tilting and detachment) appear to occur spontaneously in certain fibre segments (Edman & Flitney, 1982). There would be less multiple scattering in single fibres and it would be a relatively easy matter to make 'directional' recordings of optical signals, so as to obtain additional evidence to show that the signals are due to a change in the light scattering properties of the muscle. Experiments along these lines are currently being undertaken.

REFERENCES

- AARONSON, J.F. & MORALES, M.F. (1969). Polarisation of tryptophan fluorescence in muscle. *Biochemistry*, 8, p4517
- AIDLEY, D.J. (1978). *The Physiology of Excitable Cells*. 2nd. Edition, University Press, Cambridge.
- AMOS, L.A.; HUXLEY, H.E.; HOLMES, K.C.; GOODY, R.S. & TAYLOR, K.A. (1982). Structural evidence that myosin heads may interact with two sites on F-actin. *Nature (Lond.)*, 299 p467-469.
- ANSON, M. & BAYLEY, P. (1976). A versatile source ratioing system for fast kinetic spectroscopy. *Rev. Sci. Instrum.* 47, p370-373
- ARMSTRONG, C.M., HUXLEY, A.F., JULIAN, F.J. (1966). Oscillatory responses in frog skeletal muscle fibres. *J. Physiol.* 186, p26P.
- ASAKURA, S. & OOSAWA, F. (1960). Dephosphorylation of ATP in actin solutions at low concentrations of magnesium. *Arch. Biochem. Biophys.*, 87 p273
- BAYLOR, S.M.; CHANDLER, W.K. & MARSHALL, M.W. (1982). Dichroic components of arsenazo III and dichlorophosphonazo III signals in skeletal muscle fibres. *J. Physiol.* 331, p179-210.
- BANGA, I. & SZENT-GYORGYI, A. (1941-42). Preparation and properties of myosin A and B. *Studies from the Institute of medical Chemistry. University of Szeged* 1, p5.

REFERENCES

- BARDEN, J.A. & MASON, P. (1979). Sarcomere shortening and tension development during "Isometric" tetanus of muscle. *Experientia*, 35, pp.1584-1585.
- BARNETT, V.A. & THOMAS, D.D. (1982). STEPR of spin labelled fibers; dependence on sarcomere length. *J. Mol. biol.*
- BASKIN, R.J., ROOS, K.P. & YEH, Y. (1979). Light diffraction study of Single Skeletal Muscle Fibers. *Biophys.J.* 28, pp.45-64
- BOREJDO, J. & MASON, P. (1976). Sarcomere length changes during stimulation of frogs semitenenosis muscle (1976). *J. Mechanochem. Cell. Motil.* 3 p155-161
- BRAGG, W.L. (1913). The structure of some crystals as indicated by their diffraction of X-rays. *Proc. R.Soc. A.* 89, p248-277
- BRENNER, B.; SCHOENBERG, M.; CHALOVICH, J.M.; GREENE, L.E. & EISENBERG, E. (1982). Evidence for cross-bridge attachment in relaxed muscle at low ionic strength. *Proc. Natl. Acad. Sci. U.S.A.* 79 p7288-7291
- BRENNER, B. YU; L.C. & PODOLSKY, R.J. (1984). X-ray diffraction evidence for cross-bridge formation in relaxed muscle fibres at various ionic strengths. *Biophys. J.* 46 p299-306.
- CANTINO, M. & SQUIRE, J.M. (1986). Resting myosin cross-bridge configuration in frog thick filaments. *J. Cell. Biol.* 102, p610-618.
- CARLSEN, F.D. & WILKIE, D.R. (1974). *Muscle Physiology*, pub.

REFERENCES

Prentice-Hall Inc., Englewood Cliffs, NJ, USA.

CHALOVICH, J.M. & EISENBERG, E. (1982). Inhibition of actomyosin ATPase activity in troponin-tropomyosin without blocking the binding of myosin to actin. *J. Biol. Chem.* 252, p2432-2437.

CIVAN, M.M. & PODOLSKY, R.J. (1968). Contraction kinetics of striated muscle fibres following quick changes in load. *J. Physiol.* 184, p511-534.

CLEWORTH, D.R., EDMAN, K.A.P. (1972). Changes in sarcomere length during isometric tension development in frog skeletal muscle. *J. Physiol.* 291, pp143-159.

COOKE, R.; CROWDER, M.S.; THOMAS, D.D. (1982). Orientation of spin labels attached to cross-bridges in contracting muscle fibres. *NATURE (LOND.)*, 300, 776-778.

COOKE, R.; CROWDER, M.S.; WENDT, C.H.; BARNETT, V.A. & THOMAS, D.D. (1984). Muscle cross-bridges: do they rotate. *Contractile mechanisms in muscle*, Eds. Pollack, G.H. & Sugi, H.; pubs. Plenum, N.Y. U.S.A. p413-427

COOKE, R., FRANKS, K.E. (1978). Generation of force by single headed myosin. *J. Mol. Biol.*, 120, pp.361-373.

CURTAIN, N.A., DAVIS, R.E. (1973). ATP breakdown following the activation of muscle. *The Structure and Function of Muscle*, 2nd. edn., vol. III., (ed. Bourne, G.H.), pp.471-515.. pub. Academic Press, New York.

EBASHI, S. (1963). Third component participating in the superprecipitation of "Natural Actomyosin". *Nature (Lond.)*.

REFERENCES

200, pp.1010.

EBASHI, S., EBASHI, F. (1964). A new protein component participating in the super precipitation of Myosin b. J.Biochem, Tokyo, 53, pp.604-613.

EBASHI, S., ENDO, M., NONOMURA, Y., MASAK, T., OHTSUKE, I. (1966). Localization of native tropomyosin in relation to striation patterns. J.Biochem. 60, pp.607-608.

EBASHI, S.; ENDO, M. & OHTSUKI, I. (1969). Control of muscle contraction. Quart. Rev. Biophys. 2, p351-384.

EDMAN, K.A.P., ELZINGA, G. NOBLE, M.I.M. (1981). Critical sarcomere extension required to recruit a decaying component of extra force during stretch in tetanic contractions of frog skeletal muscle fibres. J.Gen.Physiol. 78, pp.365-382.

EDMAN, K.A.P. & FLITNEY, F.W.F. (1982). Laser diffraction studies of sarcomere dynamics during 'isometric' relaxation in isolated muscle fibres of the frog. J. Physiol. 329, pl-20.

EISENBERG, E., MOOS, C. (1968). The interaction of actin and heavy meromyosin in solution at low ionic strength. J.Biol.Chem. 242, p.2945

EISENBERG, E., ZOBEL, C.R., MOOS, C. (1968). Subfragment I of myosin: adenosinetriphosphate activation by actin. Biochemistry(Amer. chem.Soc.), 7, p3186.

ELLIOT, G.F. (1964). X-ray diffraction studies on striated and smooth muscles. Proc.Roy.Soc.B.160, pp.467-472

REFERENCES

ELLIOT, G.F., LOWY, J., MILLMAN, B.M. (1965). X-ray diffraction from living striated muscle during contraction. *Nature*. 206, p.1357.

ELLIOT, G.F., LOWY, J., WORTHINGTON, C.R. (1963). An X-ray and light diffraction study of the filament lattice of striated muscle in the living state and in rigor. *J.molec.Biol.* 6, pp.295-305.

ELLIOT, A., OFFER, G. (1978). Shape and flexibility of the myosin molecule. *J.Mol.Biol.* 123, pp.505-519.

ENGLEHARDT, V.A., LJUBIMOVA, M.N. (1939). Myosin and Adenosinetriphosphotase. *Nature*, 144, p668.

FABIATO, A. & FABIATO, F. (1978). Effects of pH on the myofilaments and the sarcoplasmic reticulum of skinned cells from cardiac and skeletal cells. *J.Physiol.*, 276, p233-255.

FENN, W.O. (1924). The relation between the work performed and the energy liberated in muscular contraction. *J.Physiol.* 58, p373.

FLITNEY, F.W. (1975). Light scattering associated with tension changes in the Short Range Elastic Component of resting Frogs muscle. *J.Physiol.*, 244, pp.1-14

FILTNEY, F.W. & EASTWOOD, J.C. (1982). Transparency changes associated with force enhancement during stretch of active frogs muscle. *Biomedical applications of Laser light Scattering*. eds. Sattelle, D.B.; Lee, W.I. & Ware, B.R. Elsevier Biomedical Press. 271-282.

REFERENCES

- FLITNEY, F.W., HIRST, D.G. (1978a). Cross-bridge detachment and sarcomere "give" during stretch of active frogs muscle. *J. Physiol.* 276, pp.449-465.
- FLITNEY, F.W., HIRST, D.G. (1978b). Filament sliding and energy absorbed by cross-bridges in active muscle subjected to cyclical length changes. *J. Physiol.* 276, pp.467-479.
- FLITNEY, F.W., HIRST, D.G., JONES, D.A. (1976). Effects of temperature and velocity of stretch on the maximum tension borne by the sarcomeres in contracting muscle. *J. Physiol.* 256, pp.127-128P.
- FORD, L.E., HUXLEY, A.F., SIMMONS, R.M. (1977). Tension responses to sudden length changes in stimulated frog muscle fibres near slack length. *J. Physiol.* 269, pp.441-515.
- FORD, L.E., HUXLEY, A.F., SIMMONS, R.M. (1981). The relationship between overlap in stimulated frog muscle. *J. Physiol.* 311, pp.219-249.
- FRANZINI-ARMSTRONG, C. PORTER, K.R. (1964). Sarcolemmal invaginations constituting the T system in fish muscle fibres. *J. Cell. Biol.* 22, pp.675-696.
- FREUNDLICH, A. & SQUIRE, J.M. (1983). Three dimensional structure of insect (*Lethocerus*) flight muscle M-band. *J. Mol. Biol.* 169, p439-453.
- FUJIME, S. (1975). Optical diffraction study of muscle fibres. *Biochim. Biophys. Acta.* 379, pp.227-238.

REFERENCES

FUJIME, S., YOSHINO, S. (1978). Optical diffraction study of muscle fibres. 1. A theoretical basis. *Biophys. Chem.* 8, pp.305-315.

GOLDMAN, Y.E. & SIMMONS, R.M. (1979). A diffraction system for measuring sarcomere length. *J. Physiol.* 292 5-6P.

GORDON, A.M.; HUXLEY, A.F. & JULIAN, F.J. (1966a). Tension development in highly stretched vertebrate muscle fibres. *J. Physiol.*, 184, pl43-169

GORDON, A.M.; HUXLEY, A.F. & JULIAN, F.J. (1966b). The variation in isometric tension with sarcomere length in vertebrate muscle fibres. *J. Physiol.*, 184, pl70-192.

HALL, C.E.; JAKUS, M.A. & SCHMITT, F.D. (1946). An investigation of cross striations and myosin filaments in muscle. *Biol. Bull. Woods Hole*, 90, p32-49.

HANSON, J. & LOWY, J. (1962). Proc. of the 5th. International Congress for Electron Microscopy [09]. Ed. Breese, S.S., Academic Press (N.Y.).

HANSON, J. & LOWY, J. (1963). The structure of F-actin and of actin filaments isolated from muscle. *J. mol. Biol.* 6 p46

HANSON, J. & LOWY, J. (1964). The structure of actin filaments and the origin of the axial periodicity in the I substance of vertebrate striated muscle. *Proc. Roy. Soc. [Biol.]* 160, p523-524

HASELGROVE, J.C. & HUXLEY, H.E. (1973). X-ray evidence for radial cross-bridge movement and for the sliding filament

REFERENCES

- model in actively contracting skeletal muscle. *J. Mol. Biol.* 77, 549-568.
- HASSELBACH, W. (1952). Die Umwandlung von Aktomyosin-ATPase in L-myosin ATPase durch Aktivatoren und die resultierende Activeierungseffekti. *Z. Naturf.* 76, p163
- HAUGEN, P. & STEN-KNUDSEN, O. (1976). Sarcomere lengthening and tension drop in the latent period of isolated frog skeletal muscle. *J. Physiol.* 68, p247-265.
- HELLAM, D.C. & PODOLSKY, R.J. (1969). Force measurements in skinned muscle fibres. *J. Physiol.*, 200, p807-819.
- HILL, A.V. (1938). The heat of shortening and the dynamic constants of muscle. *Proc. Roy. Soc. B.* 136, p195-211
- HILL, A.V. (1970). First and last experiments in muscle mechanics. University Press, Cambridge.
- Hill, D.K. (1953a). The optical properties of resting striated muscle. The effect of rapid stretch on the scattering and diffraction of light. *J. Physiol.* 119, p489-500.
- HILL, D.K. (1953b). The effect of stimulation on the diffraction of light by striated muscle. *J. Physiol.* 119, p501-512.
- HILL, D.K. (1959). The ultra-violet dichroism of living frog muscle. *J. Physiol.* 148, p379-392.
- HILL, D.K. (1968). Tension due to interaction between the sliding filaments in resting striated muscle. The effect of stimulation. *J. Physiol.* 199, p637-684.

REFERENCES

HUXLEY, A.F. (1957). Muscle structure and theories of contraction. Prog. in Biophysics 7.

HUXLEY, A.F. (1974). Muscle structure. J.Physiol. 243, pl-43.

HUXLEY, A.F. & NEIDERGERKE, R. (1954). Interference microscopy of living muscle fibres. Nature (Lond.) 173, p971-973:

HUXLEY, A.F. & PEACHEY, L.D. (1961). The maximum length for contraction in vertebrate skeletal muscle. J. Physiol. 156, pl50-165.

HUXLEY, A.F. & SIMMONS, R.M. (1970). A quick phase in the series elastic component of striated muscle. J. Physiol. 208, p52-53P

HUXLEY, A.F. & SIMMONS, R.M. (1971b). Mechanical transients and origin of muscular force. Cold Spring Harb. Symp. quart. Biol. 37, p669-680.

HUXLEY, A.F. & SIMMONS, R.M. (1971a). Proposed mechanism of force generation in striated muscle. Nature 233, p533-538.

HUXLEY, H.E. (1953b). Electron microscope studies of the organisation of the filaments in striated muscle. Biochem. Biophys. Acta 12, p387-394.

HUXLEY, H.E. (1961). The contractile structure of cardiac and skeletal muscle. Circulation 24, p328.

HUXLEY, H.E. (1963). X-ray analysis and the problem of muscle. Proc. Roy. Soc. B. 141, p59.

REFERENCES

HUXLEY, H.E. (1969). Mechanism of muscle contraction. *Science* 164, p1356-66.

HUXLEY, H.E. & BROWN, W. (1967). Low angle X-ray diffraction of vertebrate striated muscle and its behaviour during contraction and rigor. *J. molec. Biol.* 30, p383-434.

HUXLEY, H.E.; BROWN, W. & HOLMES, K.C. (1965). Constancy of the axial spacings in frog sartorius muscle during contraction. *Nature (Lond.)* 206, p1358.

HUXLEY, H.E.; FARQUI, A.R.; BORDAS, J.; KOCH, M.H.J. & MILCH, J.R. (1980). Use of synchrotron radiation in time resolved X-ray diffraction studies of myosin layer line reflections during muscle contraction. *Nature (Lond.)* 284, 140-143

HUXLEY, H.E. & HANSON, J. (1954). Changes in the cross-striations of muscle during contraction and stretch, their structural interpretation. *Nature (Lond.)* 173, p973-976.

IRVING, M. (1987). The effect on muscle birefringence of orientation parameters in a simple model of the myosin cross-bridge. (In press.)

JULIAN, F.J.; SOLLINS, M.R. & MOSS, R.L. (1978). Sarcomere length non-uniformity in relation to tetanic responses of stretched skeletal muscle fibres. *Proc. Roy. Soc. Lond. B.* 200, p109-116.

JULIAN, F.J.; SOLLINS, K.R. & SOLLINS, M.R. (1973). A model for muscle contraction in which cross-bridge attachment and force generation are distinct. *Cold Spring Harb. Symp. quant. Biol* 37, pp685-688.

REFERENCES

- KERKER, M. (1969). The scattering of light and other electromagnetic radiation. Academic Press, New York, U.S.A.
- KOBAYASHI, S. & TOTSUKA, T. (1975). Electric birefringence of myosin subfragments. *Biochim. Biophys. Acta* 376, p375.
- KUHNE, W. (1864). Untersuchungen uber das Protoplasma und die contractilitat. W. Engelmann, Leipzig.
- LEUNG, A.F. (1983a). Light diffraction by striated muscle fibres in the traverse direction. *J. Mus. Res. & Cell. Motil.* 4, p557-568.
- LEUNG, A.F. (1983b). Light diffractometry for determining the sarcomere length of striated muscle: an evaluation. *J. Mus. Res. & Cell. Motil.* 4, p473-484.
- LEUNG, A.F. (1983c). Sarcomere dynamics in single myocardial cells as revealed by high resolution light diffractometry. *J. Mus. Res. & Cell. Motil.* 4, p485-502.
- LEUNG, A.F.; HIRANG, J.C. & CHEUNG, Y.M. (1983). Determination of myofibrillar diameter by light diffraction. *Pflugers Arch.* 396, p238-242.
- LOWEY, S. (1971). Subunits in Biological systems. pub Marcek Dekker, N.Y. U.S.A..
- LOWEY, S.; GOLDSTEIN, L.; COHEN, C. & LUCK, S. (1967). Proteolytic degradation of myosin and meromyosin by a water soluble polyanionic derivative of trypsin. Properties of helical subunits isolated from heavy meromyosin. *J. molec. Biol.* 23, p287-304.
- LOWEY, S.; SLATER, H.S.; WEEDS, A.G. & BAKER, H. (1969).

REFERENCES

Substructure of the myosin molecule. J. molec. Biol. 42, p1-29.

LUTHER, P.K.; MUNRO, P.M.G. & SQUIRE, J.M. (1981). Three-dimensional structure of the vertebrate muscle A-band. III. M-region structure and myosin filament symmetry. J. Mol. Biol. 151, p703-730.

MATSUBARA, I.; YAGI, N.; MIURA, H.; OZEKI, M. & IZUMI, T. (1984). Intensification of the 5.9nm. actin layer line in contracting muscle. Nature (Lond.) 312, p471-473.

MAW, M.C. & ROWE, A.J. (1980). Fraying of A-filaments into three subfilaments. Nature (Lond.) 286, p412-414.

MENDELSON, R.; MORALES, M.F. & BOTTS, J. (1973). Segmental flexibility of the S-1 moiety of myosin. Biochemistry 12, p2250.

MORIMOTO, K. & HARRINGTON, W.F. (1974). Sub-structure of the thick filament of vertebrate striated muscle. J. molec. Biol. 83, p83-97.

MORNET, D.; BERTRAND, R.; PANTEL, P.; AUDEMOND, E. & KASSAB, R. (1981). Structure of the actin myosin interface. Nature (Lond.) 292, p301-306.

Moss, R.L.; Sollins, M.R. & JULIAN, F.J. (1976). Calcium activation produces a characteristic response to stretch in both skeletal and cardiac muscle. Nature (Lond.) 260, p619-621.

VON MURALT, A. & EDSALL, J.T. (1930). Studies in the physical chemistry of muscle globulin iv. The anisotropy of

REFERENCES

- myosin and double refraction of flow. J. biol. Chem. 89, p315.
- NEEDHAM, D.M. (1971). *Machina Carnis*, University Press, Cambridge.
- NEEDHAM, J.; SHEN, S-C.; NEEDHAM, D. & LAWRENCE, A.S.C. (1941). Myosin birefringence and adenylypyrophosphate. *Nature (Lond.)* 147, p766.
- PAGE, S.G. (1964). Filament length in resting and excited muscle. *Proc. Roy. Soc. B.* 160, p460-466.
- PAGE, S.G. (1968). Fine structure of tortoise skeletal muscle. *J. Physiol.* 197, p709-715.
- PEPE, E.A. (1966). Some aspects of the structural organisation of the myofibril as revealed by antibody staining methods. *J. cell. Biol.* 28, p505-525.
- PODOLSKY, R.J. (1960). Kinetics of muscular contraction; the approach to the steady state. *Nature* 188, p666-668.
- PODOLSKY, R.J. & NOLAN, A.C. (1971). Cross-bridge properties derived from physiological studies of frog muscle fibres. *Contractility of muscle cells*. Prentice Hall, N.J. U.S.A.
- POULSEN, F.R. & LOWY, J. (1983). Small-angle X-ray scattering from myosin heads in relaxed and rigor frog muscle fibers. *Nature (Lond.)* 303, p146-152.
- RAMSEY, R.W. & STREET, S.F. (1940). The isometric length tension diagram of isolated skeletal muscle fibres of the frog. *J. cell. comp. Physiol.* 15, p11-34.

REFERENCES

RANVIER, L. (1874). Du spectre produit par les muscle stries. Arch. Physiol. 6, p775.

REEDY, M.K.; HOLMES, K.C. & TREGEAR, R.T. (1965). Induced changes in the orientation of the cross-bridges of glycerinated insect flight muscle. Nature (Lond.) 207, p1276-80.

REES, M.K. & YOUNG, M. (1967). Studies on the isolation and molecular properties of homogeneous globular actin. J. biol. Chem. 242, p4449.

DOS REMEDIOS, G.G.; MILLIKAN, R.C.G. & MORALES, H.F. (1972). Polarisation of tryptophan fluorescence from single striated muscle fibres. A molecular probe of the contractile state. J. gen. Physiol. 59, p103-120.

RIESER, G.D.; SABBADINI, R.A. & PAOLINI, P.J. (1982). The effects of chemical cross-linking agents on calcium induced structural changes in skinned muscle fibres. Biochem. Biophys. Acta 707, 178-189.

ROOS, K.P.; BASKIN, R.J.; LEIBER, R.L.; CLINE, J.W. & PAOLINI, P.J. (1980). Digital data acquisition and analysis of striated muscle patterns with a direct memory access microprocessor system. Rev. Sci. Instrum. 51.

RUDEL, R. & TAYLOR, S.R. (1969). The influence of stimulus parameters on the contractions of isolated frog muscle fibres. J. Physiol. 205, pp499-513.

RUDEL, R. & ZITE-FERENCZY, F. (1979a). Interpretation of light diffraction by cross-striated muscle as Bragg reflection of light by the lattice of contractile proteins.

REFERENCES

J. Physiol. 290, p317-330.

RUDEL, R. & ZITE-FERENCZY, F. (1979b). Do laser diffraction studies on striated muscle indicate stepwise shortening. Nature (Lond.) 278, p573-576.

SANDOW, A. (1936a). Diffraction patterns of the frog sartorius muscle and sarcomere behaviour during contraction. J. cell. comp. Physiol. 9, p55-75.

SELBY, C.C. & BEAR, R.S. (1956). The structure of the actin-rich filaments of muscles according to X-ray diffraction. J. biophys. Cyt. 2, p71.

SEYMOUR, J. & O'BRIEN, E.J. (1980). The position of tropomyosin in muscle thin filaments. Nature (Lond.) 283, p680-682.

SLATER, H.S. & LOWEY, S. (1967). Substructure of the myosin molecule as visualised by electron microscopy. Proc. natl. Acad. Sci. U.S.A. 58, p1611.

SQUIRE, J.M. (1974). Symmetry and 3-D arrangement of filaments in vertebrate striated muscle. J. mole. Biol. 90, p153-60

STRAUB, F.B. (1942). Actin III. Stud. Inst. med. Chem. Univ. Szeged III, p23.

STRAUB, F.B. & FEUER, G. (1950). Adenosinetriphosphate-the functional group of actin. Biochim. biophys. Acta 4, p455.

SUGI, H. (1972). Tension changes during and after stretch in frog muscle fibres. J. Physiol. 255, p237-253.

SZENTZ-GYORGYI, A.G. (1948). Nature of Life. Academic

REFERENCES

Press, N.Y., U.S.A.

SZENTZ-GYORGYI, A.G. (1951). A new method for the preparation of actin. *J. biol. Chem.* 192, p361.

SZENTZ-GYORGYI, A.G. (1953). Meromyosin, the subunits of myosin. *Arch. Biochem. Biophys.* 42,

TAYLOR, K.A.; REEDY, M.C.; CORDOVA, L. & REEDY, M.K. (1984). Three-dimensional reconstruction of rigor insect flight muscle from tilted thin sections. *Nature (Lond.)* 310, p285-291.

THOMAS, D. & COOKE, R. (1980). Orientation of spin-labelled myosin heads in glycerinated muscle fibres. *Biophys. J.* 32, p891-906.

THOMAS, D.D.; ISHIWATA, S.; SEIDAL, J.C. & GERGELY, J. (1980) Sub-millisecond rotation dynamics of spin labelled myosin heads in myofibrils. *Biophys. J.* 32, p873-890.

WAKABATASHI, T.; HUXLEY, H.E.; AMOS, L.A. & KLUG, P. (1975). Three dimensional image reconstruction of actin-tropomyosin complex and actin-tropomyosin-troponin T troponin I complex. *J. molec. Biol.* 93, p477-97.

WEBER, E. (1846). Muskelbewegung. In *Handwörterbuch der Physiologie*, pl Ed R. Wagner. Braunschweig, F. Bieweg und Sohn.

WORTHINGTON, C.R. (1959). Large axial spacings in striated muscle. *J. mol. Biol.* 1, p398

YEH, Y.; BASKIN, R.J.; LEIBER, R.L. & ROOS, K.P. (1980). Theory of light diffraction by single skeletal muscle

REFERENCES

fibres. Biophys. J. 29, p509-522.

ZITE-FERENCZY, F.; HABERLE, K-D.; RUDEL, R. & WILKE, W. (1986). Correllation between the light diffraction pattern and the structure of a muscle fibre realized using Ewald's construction. J. Mus. res. & Cell. Motil. 7, p197-214.

ZOTH, O. (1890). Versuch uber die beugende struktur der quergestreiften muskelfasern. Wein Akad. der Wissen, Stiz. der Mat-Nat. Classe., Bd 99, S421.